Molecular Mechanisms in the Unconventional Secretion of Insulin-Degrading Enzyme

Dissertation

zur Erlangung des Doktorgrades (Dr. rer. nat.)

der

Mathematisch-Naturwissenschaftlichen Fakultät

der

Rheinischen Friedrich-Wilhelms-Universität Bonn

vorgelegt von

Dipl.-Biochem. Marie Löchner

aus

Berlin

Bonn, Juni 2017

Angefertigt mit Genehmigung der Mathematisch-Naturwissenschaftlichen Fakultät der

Rheinischen Friedrich-Wilhelms Universität Bonn

1. Gutachter: Prof. Dr. rer. nat. Jochen Walter

2. Gutachter: Prof. Dr. rer. nat. Walter Witke

Tag der Abgabe: 19.06.2017

Tag der Promotion: 04.12.2017

Erscheinungsjahr: 2018

An Eides statt versichere ich, dass ich die Dissertation "*Molecular Mechanisms in the Unconventional Secretion of Insulin-degrading Enzyme*" selbst und ohne jede unerlaubte Hilfe angefertigt habe und dass diese oder eine ähnliche Arbeit noch an keiner anderen Stelle als Dissertation eingereicht worden ist.
Auszüge der ausgewiesenen Arbeit wurden im Journal Glia eingereicht und unter folgendem Titel im Jahr 2015 publiziert: „*Serotonin stimulates secretion of exosomes from microglia cells*" (*volume* 63, *issue* 4, *pp.* 626-634).

Promotionsordnung vom 17. Juni 2011 _____

Marie Löchner

Für meine Großeltern

Herlinde und Johannes

Table of Contents

Index I

List of figures I

List of tables II

Abbreviations III

A Introduction 1

1. Insulin-degrading enzyme 1

1.1 IDE structure and mechanism of degrading short polypeptides 1

1.2 IDE in Alzheimer's disease 3

2. Secretion of IDE via exosomes 6

2.1 Conventional and unconventional secretory pathways 7

2.2 Exosomes and the regulation of exosome biogenesis 9

2.3 Unconventional release of IDE 13

3. Microglia 15

3.1 Neuron-microglia communication 16

3.2 Microglia in Aβ degradation and AD 18

4. Rationale and aim of the study 20

B Material and Methods 22

1. Material 22

1.1 Chemicals and Reagents 22

1.2 Media and Solutions 24

1.3 Antibodies 25

1.4 Commercial Kits 27

1.5 Devices and Tools 28

2. Methods 29

2.1 Cell biological techniques 29

2.1.1 Cell culture 29

2.1.2 Preparation of primary hippocampal neurons, astrocytes and microglia from mouse or rat embryonic brain 29
2.1.3 Pharmacological treatment and secretion assay 30
2.1.4 Co-culture of primary mouse hippocampal neurons and BV-2 microglia cells 31
2.1.5 Co-culture of ES-derived serotonergic neurons and BV-2 microglia cells 31
2.1.6 Amyloid-β (Aβ) and insulin degradation assay 31
2.1.7 Calcium measurements 32
2.1.8 Transient protein knockdown by siRNA transfection 32
2.1.9 shRNA-mediated stable protein knockdown in BV-2 microglia cells 33
2.1.10 Immunocytochemistry (ICC) 34
2.2 Protein biochemical techniques 35
2.2.1 Cell lysis and protein extraction 35
2.2.2 Protein precipitation by Trichloroacetic acid (TCA) 36
2.2.3 Protein separation by SDS polyacrylamide gel electrophoresis (SDS-PAGE) / NuPAGE 36
2.2.4 Western immunoblotting (WB) and ECL/Infrared (IR) imaging 37
2.2.5 Coomassie staining of polyacrylamide gel and IR imaging 38
2.2.6 Co-immunoprecipitation (Co-IP) 39
2.2.7 Expression and purification of Maltose-binding protein (MBP) fusion proteins 39
2.2.8 Blue Native (BN) PAGE and subsequent SDS/Urea PAGE in the 2nd dimension 40
2.2.9 Exosome preparation by differential centrifugation and fractionation by density gradient centrifugation 42
2.2.10 Cell fractionation by differential centrifugation 43
2.2.11 Subcellular fractionation of intracellular vesicles by density gradient centrifugation 43
2.3 Molecular biological techniques 44
2.3.1 RNA isolation from eukaryotic cells and cDNA synthesis by reverse transcription (RT) 44
2.3.2 Polymerase chain reaction (PCR) 45
2.3.3 Cloning of expression plasmids 46
2.3.4 Purification of plasmid DNA from E. coli 47
2.3.5 Yeast two-hybrid (Y2H) – protein interaction studies 48
2.4 Statistical analysis 50

C Results 51

1. Stimulation of IDE secretion by serotonin in microglia 51

1.1 Serotonin increases IDE release from microglial cells. 51

1.2 Expression of 5-HT receptors in BV-2 cells and in primary mouse microglia. 52

1.3 Involvement of 5-HT2a, 5-HT2b and 5-HT4 receptors in the regulation of IDE release. 52

1.4 Activation of 5-HT4R promotes the release of IDE via PLC-dependent Ca^{2+} mobilization. 53

1.5 5-HT increases cytosolic Ca^{2+} that stimulates IDE release. 56

1.6 5-HT stimulates the release of exosome-associated IDE. 57

1.7 Neurons can stimulate IDE secretion from BV-2 microglial cells. 59

2. Molecular mechanisms in IDE secretion 62

2.1 Differential effects of nSMase2 and ceramide in the release of exosomal proteins in distinct cell types. 62

2.2 Role of the ESCRT machinery and IDE in the regulation of exosome biogenesis 65

2.2.1 Minor effects of Alix knockdown on the release of IDE in BV-2 cells 65

2.2.2 IDE secretion is significantly increased upon siRNA-mediated knockdown of Vps4B. 66

2.2.3 Generation of BV-2 clones with stable knockdown of Vps4B and IDE by expression of specific shRNA. 68

2.2.4 shRNA-mediated stable knockdown of Vps4B in BV-2 causes changes in IDE and Flotillin-1 but not Alix release. 70

2.2.5 Knockdown of Vps4B in BV-2 microglial cells does not alter the subcellular distribution of IDE. 72

2.2.6 IDE knockdown in BV-2 cells alters subcellular distribution and secretion of Alix. 74

2.2.7 No influence on Alix release and distribution in BV-2 cells with shRNA-mediated stable knockdown of IDE. 76

2.2.8 Differences in the knockdown efficiency of Alix, IDE and Vps4B after longer-lasting siRNA transfection 78

2.2.9 Cell type-dependent differences of Vps4B-mediated regulation of IDE secretion. 80

2.2.10 Modulation of Amyloid-β and insulin degradation in BV-2 microglial cells. ... 82

2.3 Pharmacological inhibition of conventional secretion leads to an increased release of exosomal marker proteins. 84
2.4 Y2H screen to find interaction partners of IDE potentially involved in IDE secretion regulation 85
2.4.1 Y2H screen for IDE 85
2.4.2 Interaction of IDE and Vps4B 90
2.4.3 Interaction of IDE and Vps4B does not affect the usual complex formation of both proteins. 93
D Discussion 96
1. Stimulation of IDE secretion by serotonin in microglia 96
2. Molecular mechanisms in IDE secretion 100
2.1 Inhibition of conventional secretion increases the release of exosomal proteins in BV-2 microglial cells 100
2.2 Differential influence of nSMase2 and ceramide levels on the release of IDE in distinct cell types 102
2.3 ESCRT-dependent effects in IDE secretion and the role of the interaction of IDE and Vps4B 106
2.3.1 Minor effects of Alix in the release of IDE from BV-2 cells 106
2.3.2 Vps4B exerts an inhibitory function in regulation of IDE secretion in BV-2 cells 108
2.3.3 Cell type-dependent differences in Vps4B-mediated regulation of IDE release 114
2.4 Modulation of IDE-mediated Aβ- and insulin degradation by Vps4B in BV-2 microglial cells 115
2.5 Potential role of IDE in the release and intracellular trafficking of exosomal proteins in BV-2 microglial cells 117
3. Conclusions 122
E Outlook 124
F Abstract 126
G References 127
H Acknowledgements 145

Index

List of figures

Figure 1. Structure and functional mechanism of IDE. 2
Figure 2. The origin of exosomes. 10
Figure 3. ESCRT machinery in the sorting of ubiquitinylated cargo into ILVs into the lumen of MVBs. 11
Figure 4. Export of IDE into extracellular space. 14
Figure 5. Principle of Matchmaker™ Gold Y2H System 49
Figure 6. Typical 3-lobed „Mickey mouse“-shaped zygote during mating 49
Figure 7. Serotonin increases the release of IDE from BV-2 and primary microglial cells. 51
Figure 8. Expression analysis of 5-HTRs in BV-2 cells and primary mouse microglia. 52
Figure 9. The 5-HT receptors 2a, 2b and 4 are involved in the regulation of IDE release. 53
Figure 10. Activation of 5-HT4R stimulates IDE release via an increase in intracellular cAMP levels. 54
Figure 11. Activation of Epac and PLC promotes the release of IDE. 55
Figure 12. 5-HT-stimulated increase in $[Ca^{2+}]_i$ triggers IDE release in BV-2 microglial cells. 56
Figure 13. 5-HT stimulates the release of exosomes from BV-2 cells. 58
Figure 14. Neurons can stimulate IDE secretion from BV-2 microglial cells. 60
Figure 15. Inhibition of nSMase2 stimulates release of IDE in the microglia cell lines BV-2 and N9. 63
Figure 16. Inhibition of nSMase2 strongly decreases the release of exosomal marker proteins in primary rat astrocytes. 64
Figure 17. Downregulation of Alix does not significantly influence IDE secretion in BV-2 cells, but does slightly affect IDE expression. 65
Figure 18. Effects of RNAi-mediated knockdown of Vps4A and 4B on the release of IDE and exosomal marker proteins from BV-2 cells. 68
Figure 19. Generation of BV-2 cells stably expressing Vps4B- and IDE-specific shRNA by transduction with lentiviral particles. 69
Figure 20. Influences of stable Vps4B knockdown on the secretion of IDE and Flotillin-1 are rather attributable to the regulation of microvesicle than exosome release. 71
Figure 21. Distribution of IDE, Alix and Flotillin-1 between the cytosolic and the membrane-associated fraction in Vps4B-knockdown cells. 72
Figure 22. Subcellular distribution of IDE, Flotillin-1 and Alix. 73
Figure 23. siRNA-mediated knockdown of IDE leads to an increase in Alix release and influences its subcellular distribution. 75
Figure 24. Stable knockdown of IDE in BV-2 cells increases Flotillin-1 but not Alix secretion from BV-2 cells. 77
Figure 25. Knockdown efficiencies of Alix, IDE and Vps4B and their effects on exosome secretion 72 hours after siRNA transfection. 79

Figure 26. Decreased release of Alix upon knockdown of Vps4B and IDE in primary rat astrocytes. ... **80**
Figure 27. Vps4B knockdown in cos-7 cells causes an increased release of all examined exosome marker proteins, knockdown of IDE influences only Flotillin-1 secretion. . **81**
Figure 28. Involvement of Vps4B in the degradation of Aβ and insulin by IDE. ... **83**
Figure 29. Inhibition of conventional secretion leads to an increase in the release of exosome marker proteins in BV-2 cells. ... **84**
Figure 30. Generation of IDE Bait based on the C-terminal sequence of mouse IDE. ... **86**
Figure 31. Analysis of the potential interaction partners of IDE. ... **89**
Figure 32. Detection of IDE and Vps4B in similar subcellular fractions and in exosomes. ... **90**
Figure 33. Immunocytochemical staining of IDE and Vps4B in cos-7 cells. ... **91**
Figure 34. Co-immunoprecipitation of IDE and Vps4B. ... **92**
Figure 35. Native protein complexes of IDE and Vps4B. ... **94**
Figure 36. Complex formation of neither Vps4B nor IDE is affected by downregulation of both proteins. ... **95**
Figure 37. Proposed signalling pathways regulating 5-HT-stimulated IDE release from microglia cells. ... **97**

List of tables

Table 1. List of chemicals and reagents ... 24
Table 2. List of media and solutions ... 25
Table 3. Primary antibodies ... 26
Table 4. Secondary antibodies and other protein detection reagents ... 27
Table 5. Commercial Kits ... 28
Table 6. Devices and Tools ... 29
Table 7. Pharmacological treatments ... 30
Table 8. FlexiTube siRNAs (Qiagen) ... 33
Table 9. TRC lentiviral shRNA ... 33
Table 10. Composition of SDS-PAGE gels ... 37
Table 11. Composition of BN PAGE gels ... 41
Table 12. Composition of SDS/urea PAGE gels. ... 41
Table 13. Cloning primers and primers for expression analysis ... 46
Table 14. Generated constructs. ... 47
Table 15. Yeast strains and plasmids used in Y2H studies ... 48
Table 16. Potential interaction partners of IDE identified by Y2H cDNA library screen. ... 88

Abbreviations

5-HT	5-Hydroxy-tryptophan, serotonin
5-HTR(s)	5-HT receptor(s)
8-CPT	8-CPT-2ME-cAMP
aa	amino acid
Aβ	amyloid-β
AC	adenylate cyclase
AD	Alzheimer's disease
bp	base pair
BSA	bovine serum albumin
Ca^{2+}	calcium ion
$[Ca^{2+}]_i$	intracellular Ca^{2+} concentration
CALHM1	Calcium homeostasis modulator 1
cAMP	cyclic adenosine monophosphate
CDS	coding sequence
cm	centi meter
CSF	cerebrospinal fluid
DAMPs	damage-associated molecular patterns
DAPI	4′,6-Diamidin-2-phenylindol
DM2	Diabetes mellitus type 2
e.g.	"*exempli gratia*" - for example
EGF	epidermal growth factor
EGFR	EGF receptor
EML	The Eukaryotic Linear Motif Resource
EOAD	early-onset Alzheimer's disease
Epac	exchange protein directly activated by cAMP
ER	endoplasmic reticulum
GEF	guanine exchange factor
Golgi	Golgi apparatus
HLA-DRA	Human leukocyte antigen - antigen D related alpha subunit

HLA-DRB1	HLA-DR beta subunit
HMG-CoA reductase	3-hydroxy-3-methyl-glutaryl-CoA reductase
HRP	horseradish peroxidase
Hrs	hepatocyte growth factor-regulated tyrosine kinase substrate
Hsp	heat shock protein
ICC	immunocytochemistry
i.e.	"*id est*" – that is
IgG	immunglobulin G
ILV	intraluminal vesicle
IP	immunoprecipitation
IP_3	inositol 1,4,5-triphosphate
kb	kilo base pair
kDa	kilo Dalton
LDLR	low-density lipoprotein receptor
LOAD	late-onset Alzheimer's disease
m	milli
3m3FBS	*m*-3m3FBS
µ	micro
M	molar
mAb	monoclonal antibody
MDa	mega Dalton
MHC	major histocompatibility complex
min	minute(s)
mTOR	mammalian target of rapamycin
MVBs	multivesicular bodies
NLS	nuclear localisation sequence
ns	non-significant
NSAIDs	nonsteroidal anti-inflammatory drugs
nSMase2	neutral sphingomyelinase 2
NTC	non-treated control
pAb	polyclonal antibody

PAGE	polyacrylamide gel electrophoresis
PAMPs	pathogen-associated molecular patterns
PBS	phosphate buffered saline
Phalloidin	Fluoresceinyl-aminomethyldithiolano-phalloidin
PLC	Phospholipase C
PNS	post-nuclear supernatant
pp.	pages
Prof.	Professor
PtdIns	phosphatidyl-inositol
PTS	peroxisome targeting signal
PTX	pertussis toxin
OD_{600}	optical density at 600 nm
RT	room temperature
sec	seconds
SD	standard deviation
SEM	standard error of means
UTR	untranslated region
v/v	volume/volume
w/v	weight/volume
WB	Western immunoblotting

A Introduction

1. Insulin-degrading enzyme

The insulin-degrading enzyme (IDE), also called insulysin or insulinase earlier, was discovered as an insulin-degrading protease by Mirsky and Broh-Kahn in several tissue extracts in 1949 (Broh-Kahn & Mirsky, 1949). IDE, a 110 kDa neutral Zn^{2+} metalloprotease, is ubiquitously expressed and most abundant in liver, testis, muscle and the brain (Kuo, et al., 1993; Shen, et al., 2006). Interestingly, the sequence of IDE is highly conserved from bacteria to humans. In eukaryotes homology includes both exon and intron regions, indicating a functional importance of the enzyme in general and, second, that both proteolytic and potential gene expression regulation are conserved as well (Qiu & Folstein, 2006; Fujita, et al., 1994; Affholter, et al., 1988; Kuo, et al., 1990; Shen, et al., 2006). IDE is predominantly localised in the cytosol. In addition, IDE was also detected in mitochondria, the nucleus, rough endoplasmic reticulum (ER) and at the cell surface, as well as in peroxisomes (Qiu, et al., 1998; Duckworth, et al., 1998; Bulloj, et al., 2008; Vekrellis, et al., 2000; Leissring, et al., 2004). Furthermore, IDE was found to be secreted into extracellular fluids by several different cell types (Qiu, et al., 1998; Bulloj, et al., 2010; Zhao, et al., 2009; Glebov, et al., 2011; Son, et al., 2015). The substrates of IDE are highly diverse and share little or no sequence homology. The selectivity of IDE seems to be not determined by a particular sequence, but rather the size of the polypeptides and their secondary structure (Malito, et al., 2008; Guo, et al., 2010). Additionally to insulin, from which it received its name, IDE degrades several small peptides as e.g. glucagon, β-endorphin, transforming growth factor α (TGF α), amylin and somatostatin (Wang, et al., 2006; Ciaccio, et al., 2009; Qiu & Folstein, 2006; Bennett, et al., 2000). In 1994, Kurochkin and colleagues found out that IDE is furthermore cleaving Amyloid-β (Aβ) (Kurochkin & Goto, 1994), which suggested a potential involvement in AD. IDE is able to degrade soluble forms of the main variants, $Aβ_{1-40}$ and $Aβ_{1-42}$, and AICD. AICD is the intracellular cleavage product of γ-secretase processing of APP (Edbauer, et al., 2002; Sastre, et al., 2001; Pérez, et al., 2000).

1.1 IDE structure and mechanism of degrading short polypeptides

A large number of IDE substrates shows the propensity to form β-sheet-containing amyloid fibrils. Examples are Aβ playing a role in the pathogenesis of Alzheimer's disease, and amylin forming islet amyloid deposits in type 2 diabetes mellitus (Bennett, et al., 2000; Kurochkin, 2001). Therefore IDE is assumed to be involved in the catabolic regulation to avoid amyloid deposits through the elimination of its basic components (Qiu & Folstein, 2006).

The enzyme can be subdivided into two parts of around 56 kDa each. The N-terminal part (IDE-N; aa 43-515 in human IDE) and the C-terminal part (IDE-C; aa 542-1016 in human IDE)

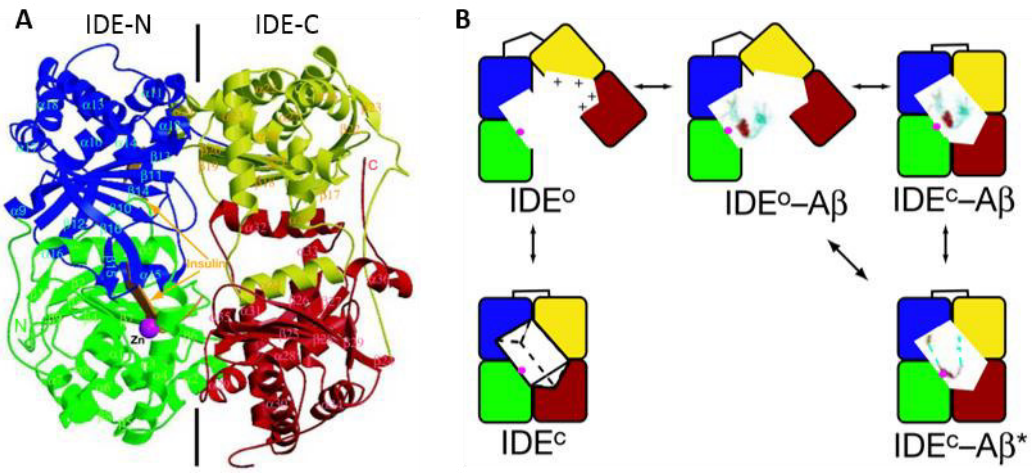

Figure 1. Structure and functional mechanism of IDE. (A) Secondary structure of human IDE-E111Q in complex with the B chain of insulin after X-ray crystallography. The mutation E111Q was integrated to prevent substrate cleavage and enable visualization of an enzyme-substrate complex. The insulin B chain is coloured in orange and the bound Zn^{2+} ion is presented in magenta. (B) Model of the IDE mechanism of substrate binding and recognition including a conformational switch from an open (IDE^o) to a closed (IDE^c) conformation. Binding of Aβ is here shown as an example. The binding of Aβ occurs in the open state, proper recognition, conformational changes in the substrates and cleavage occur in the closed state of IDE. (A) and (B) from *(Shen, et al., 2006)*.

are connected via a 28 amino acid-long loop (see Figure 1A). These two domains form an enclosed chamber that can switch to an open conformation to incorporate the substrate. Due to its dimensions, the catalytic chamber limits the size of the substrates to less than 50 amino acids. After binding the substrate, the enzyme switches to the closed conformation enabling precise recognition and digestion of the peptide and also preventing the binding of a further substrate (see Figure 1B). The peptide undergoes certain conformational changes and can subsequently be cleaved at one or multiple sites. The switch between open and closed conformations of the enzyme is crucial for the proteolytic process. Mutations, that prevent or facilitate the open conformation, inhibit or increase, respectively, the catalytic rate of the enzyme (Shen, et al., 2006).

The active site in IDE-N consists of the amino acid sequence histidine-X-X-glutamate-histidine (HXXEH, aa 108-112 in human IDE), with the X symbolizing a variable amino acid. This sequence is highly conserved. The two histidine residues and an additional glutamate (aa 189 in human IDE) residue coordinate the Zn^{2+} ion. The glutamate residue and a catalytic water molecule is further necessary for the nucleophilic attack on the peptide bond of the peptide substrate (Becker & Roth, 1992; Perlman & Rosner, 1994; Im, et al., 2007). IDE substrates show similarities that are involved in the catalytic process. They possess a 7-13 amino acid sequence that contains a large hydrophobic group and is prone to form a β-sheet. IDE-N is capable to interact with this β-sheet and also with the first 3-5 amino acids of the peptide. The internal chamber for catalysis is formed by both IDE-N and IDE-C. IDE-N holding the active site contributes neutral or negative charges, whereas IDE-C donates predominantly positive

charges and is rather responsible for the substrate recognition (Shen, et al., 2006; Li, et al., 2006).

IDE-C is further involved in the oligomerization of IDE. The enzyme primarily exists as a dimer and can also form tetrameric structures in a concentration-dependent manner. The interaction of two IDE dimers, however, can favour the closed conformation of the enzyme and therefore regulate also the catalytic activity of the enzyme (Safavi, et al., 1996; Song, et al., 2003; Li, et al., 2006; Shen, et al., 2006).

1.2 IDE in Alzheimer's disease

AD is a devastating neurodegenerative disease and the most common cause of dementia. It is characterised by a progressive loss of neuronal cells and synapses especially in brain areas that are responsible for learning and memory. This leads to deficits in memory, orientation and language. There are two forms of AD. The most common, so-called late-onset AD (LOAD) starting after the age of 65 years and the early-onset AD (EOAD) that begins before that age (Alzheimer's association, 2014; Tanzi, 2012). Primarily ageing itself is the most important risk factor for the disease, especially for LOAD. Only 1-5% of all cases are based on dominantly inherited forms of AD, the rest occur sporadically. Pathological hallmarks of AD are intraneuronal neurofibrillary tangles and extracellular senile plaques. The neurofibrillary tangles are formed by hyperphosphorylated and aggregated tau, a tubulin-interacting protein being involved in stabilization of microtubule assemblies (Grundke-Iqbal, et al., 1986; Alonso, et al., 2001). The senile plaques, however, consist mainly of aggregated fibrillar Aβ (Selkoe, 2001). Aβ results from the sequential processing of the transmembrane glycoprotein amyloid precursor protein (APP) by β- and γ-secretase (De Strooper, et al., 1998; Wolfe, et al., 1999; Haass & Steiner, 2002; Vassar & Citron, 2000; Montoliu-Gaya & Villegas, 2015). Several studies underline the strong association of Aβ accumulation to the pathogenesis of AD (Näslund, et al., 2000; Hsiao, et al., 1996; Gandy, 2005; Karran, et al., 2011). The so-called amyloid cascade hypothesis states that cerebral accumulation of Aβ is the first critical step in the pathogenesis of AD that results in the subsequent development of neurofibrillary tangles, neuroinflammation, loss of synapses, neuronal death and in conclusion to the manifestation of the dementia (Montoliu-Gaya & Villegas, 2015; Hardy & Higgins, 1992).

In contrast to the inherited form of AD, where an increase in overall Aβ production or an enhanced aggregation propensity of Aβ play a role, in sporadic AD rather a decreased degradation rate of Aβ is considered to cause the disease (Mawuenyega, et al., 2010; Miners, et al., 2011). Removal and degradation of Aβ in the brain include multiple processes as drainage along perivascular basement membranes, possibly to cervix lymph nodes and the cerebrospinal fluid (CSF), as well as cell surface receptor-mediated transport across vessel walls and the blood brain barrier into the circulation e.g. by low-density lipoprotein receptor

(LDLR)-related protein 1 (LRP1) that is followed by clathrin-mediated endocytosis. In addition, Aβ can be phagocytosed by microglia or proteolytically degraded by several enzymes (Miners, et al., 2011; Bohm, et al., 2015). The neutral endopeptidase IDE was, next to the transmembrane Zn^{2+} metalloprotease neprilysin, discovered as the main protease being involved in the clearance of soluble monomeric Aβ in the brain (Lee & Landreth, 2010; Hickman, et al., 2008; Qiu, et al., 1998; Tamboli, et al., 2010). In the context of an impaired clearance of Aβ that contributes to the pathogenesis of sporadic AD, it is also discussed, if a decline in the expression of Aβ-degrading enzymes or decreased proteolytic activity is causative of an accumulation and aggregation of the peptide (Miners, et al., 2011). Indeed, a decline in IDE expression in brains of both an AD transgenic mouse model and AD patients was reported (Pérez, et al., 2000; Cook, et al., 2003; Zhao, et al., 2004; Miners, et al., 2009; Miners, et al., 2008; Caccamo, et al., 2005). Notably, in the hippocampus, a brain region highly affected during AD, the levels of IDE mRNA and protein are significantly decreased and negatively correlate with the load of Aβ. Additional to the histo- and biochemical observations also a genetic linkage of IDE as a potential susceptibility gene for AD was suggested. Several studies already showed an association between IDE polymorphisms and AD. First, a susceptibility locus linked to an increased risk for sporadic LOAD was identified in a region of chromosome 10 that also harbours the gene of IDE (Bertram, et al., 2000; Ertekin-Taner, et al., 2000; Myers, et al., 2000; Li, et al., 2002; Blacker, et al., 2003). The role of IDE in the degradation of Aβ and the identification of the genetic linkage of the region of chromosome 10 to AD made IDE a strong functional and positional candidate gene for sporadic LOAD (Nowotny, et al., 2005). Several research groups subsequently screened IDE polymorphisms for their association with AD and could confirm an association between specific IDE haplotypes and the clinical diagnosis of sporadic LOAD or an accumulation of $Aβ_{1-42}$ in the plasma (Edland, et al., 2003; Edland, et al., 2004; Prince, et al., 2003; Ertekin-Taner, et al., 2004; Bian, et al., 2004; Björk, et al., 2007). However, other studies did not show a significant association of IDE haplotypes and AD (Abraham, et al., 2001; Boussaha, et al., 2002; Nowotny, et al., 2005).

A further link connecting diminished IDE activity in Aβ degradation and AD is the discovery that patients suffering from type 2 diabetes mellitus (DM2) have an increased risk to develop AD (Arvanitakis, et al., 2004; Grodstein, et al., 2001; Leibson, et al., 1997; Ott, et al., 1999; Peila, et al., 2002; Xu, et al., 2004). IDE as an insulin- and Aβ-degrading enzyme attracted research on both DM2 and AD. A functional link between IDE and these two diseases was additionally supported by IDE-knockout mice that showed characteristic hallmarks of both diseases like decreased Aβ degradation and increased cerebral accumulation of Aβ in the brain, and reduced insulin removal in the liver, hyperinsulinemia, and glucose intolerance (Farris, et al., 2003). An IDE-deficient mouse model, where IDE expression is disrupted by a gene trap insertion (homo- or heterozygous), and a DM2 rat model, the Goto-Kakizaki (GK) rat

carrying a partial loss-of-function mutation in the IDE gene, revealed similar observations (Miller, et al., 2003; Farris, et al., 2004). DM2 is a chronic metabolic disorder. In contrast to type 1 diabetes (DM1) that is caused by a loss of insulin-producing β-cells, DM2 is characterised by an insulin resistance leading to impaired insulin signalling. Its incidence and prevalence increased over the past 25 years and is closely related to the strongly growing prevalence of obesity. To date, the current treatment is based on lifestyle modifications, oral hypoglycaemic agents and insulin sensitizers which show beneficial effects especially at early stages of the disease (Eckel, et al., 2011; Olokoba, et al., 2012; Tang, 2015). Also, IDE was just recently discussed as potential target for DM2 treatment (Tang, 2015; Costes & Butler, 2015). Initially, it was observed that in AD cohorts the percentage of patients with DM2 is significantly higher than in the non-AD control group (Kuusisto, et al., 1997; Ott, et al., 1996; Stewart & Liolitsa, 1999). Subsequent studies suggested a two-fold increased risk of DM2 patients to develop AD (Arvanitakis, et al., 2004; Leibson, et al., 1997; Ott, et al., 1999; Peila, et al., 2002; Gudala, et al., 2013). Leibson and colleagues furthermore discovered that the incidence of AD among DM2 patients that have suffered from the disease for more than 5 years is higher than for patients with a disease duration of less than 5 years. This suggests that the pathogenic effect of DM2 on AD development is a rather gradual process and requires time until its manifestation. It is discussed that the medication to treat DM2, that is often based on β-cell stimulation to increase the insulin secretion and raises insulin serum levels, as for example treatment with sulfonylureas or glinides, might be causative for a higher AD risk. Also other studies showed that an increase in insulin levels is associated with AD (Leibson, et al., 1997; Ott, et al., 1999). Elevated insulin serum levels are characteristics of both diseases, AD (Carantoni, et al., 2000; Kuusisto, et al., 1997; Fujisawa, et al., 1991; Razay & Wilcock, 1994) and DM2 (preclinical syndrome and after onset) (Weyer, et al., 2000; Laakso, 1993; Shanik, et al., 2008). Hyperinsulinemia that establishes in the course of DM2 rather than other consequences of the disease might now be suggested to promote AD pathology. It is discussed that elevated insulin serum levels lead to competitive effects with the degradation of Aβ by IDE. Insulin shows a lower K_M (K_M = 0.1 μM) for IDE than Aβ (K_M >2 μM) and therefore IDE has an approximately 20-fold higher affinity to insulin than Aβ (Qiu & Folstein, 2006). Furthermore, insulin resistance interferes with insulin-mediated signalling which is, inter alia, responsible for the expression regulation of IDE. Thus, the insulin-mediated up-regulation of IDE would be impaired (Zhao, et al., 2004). It was already observed that during AD also insulin signalling is disturbed (Candeias, et al., 2012; De Felice & Ferreira, 2014). A study of Pedersen and colleagues supports this (Pedersen, et al., 2006). They show a reduction of $Aβ_{1-42}$ levels and memory deficits after treatment with rosiglitazone that decreases insulin resistance by activating the peroxisome proliferator-activated receptor γ (PPARγ) which elevates the peripheral insulin sensitivity. The activated PPARγ-mediated signalling by rosiglitazone

increased IDE mRNA levels and IDE activity in the brains of an AD transgenic mouse model causing decreased levels of $A\beta_{1-42}$ and improved learning and memory deficits (Pedersen, et al., 2006).

Taken together, decreased expression and activity of IDE in DM2 and AD might contribute to the pathogenesis of both diseases. Thus, it will be interesting to further examine the role of IDE in AD and DM2, and to assess its potential as a therapeutic target (Tang, 2015; Abdul-Hay, et al., 2015; Moreira, et al., 2013; Haque & Nazir, 2014; Costes & Butler, 2015).

2. Secretion of IDE via exosomes

The discovery of IDE as insulin-degrading enzyme in 1949 (Broh-Kahn & Mirsky, 1949) and as an Aβ-degrading enzyme in 1994 (Kurochkin & Goto, 1994) raised questions regarding the location of IDE interaction with these two substrates. Insulin, for example, was shown to be degraded in endosomal compartments (Duckworth, et al., 1998; Hamel, et al., 1991; Hamel, et al., 1988). Insulin binds to the insulin receptor and the complex is internalized into endosomes where its degradation starts with the cleavage of the insulin B chain by IDE prior to endosomal acidification (Hamel, et al., 1988; Hamel, et al., 1991). For Aβ, however, rather the extracellular compartment is proposed as the site of interaction with IDE and subsequent degradation (Qiu, et al., 1998; Bulloj, et al., 2010). Almost 20 years ago, Qiu and colleagues suggested that additional to an elevated Aβ production a decreased Aβ degradation could contribute to the deposition of Aβ plaques in the brain (Qiu, et al., 1997). It had been established that Aβ is constitutively secreted by several cell types and that an Aβ accumulation promotes its aggregation, but still nothing was known about extracellular degradation of Aβ. Therefore, Qiu et al. screened several neural and non-neural cell lines for their ability to release proteases being able to degrade Aβ. They identified IDE as the major Aβ-degrading protease, that is secreted predominantly by microglial cells (Qiu, et al., 1997; Qiu, et al., 1998). The association of IDE with the outer layer of the plasma membrane further supports the hypothesis of an extracellular degradation of Aβ and possibly also insulin (Yaso, et al., 1987; Bulloj, et al., 2008; Vekrellis, et al., 2000). Until the discovery of Qiu and colleagues in the end of the 1990s nothing was known about potential export pathways for IDE and only 10 years later Zhao and colleagues found out that IDE is not secreted by the classical but via an unconventional secretory pathway (Zhao, et al., 2009). Two parallel studies subsequently discovered that IDE is released from the cell by unconventional secretion via exosomes (Bulloj, et al., 2010; Tamboli, et al., 2010).

2.1 Conventional and unconventional secretory pathways

Many eukaryotic proteins that are released by cells follow the so-called conventional secretory pathway via Golgi and ER (Lodish, et al., 2000; Pollard, et al., 2008; Nickel & Rabouille, 2009). They contain an amino-terminal or internal signal peptide leading to their sorting to the ER after translation at the ribosome. The nascent proteins are directed into the ER by the signal recognition particles. After folding and further modification the protein leaves the ER at so-called ER exit sites in vesicles that are coated by coat protein complex II (COPII) proteins. COPII complexes consist of several subunits and contain, among others, the small GTPase Sar1A. They are responsible for vesicle budding but also mediate cargo selection by specific cargo receptors. The COPII-coated vesicles fuse with the cis-Golgi or form a new stack of the cis-Golgi network and the protein is transported further through the Golgi where it can undergo additional posttranslational modifications. From the trans-Golgi network, proteins are sorted and directed to their final destination. The intra-Golgi transport, also named cisternal migration, is realized via COPI-coated vesicles. COPI-coated vesicles also mediate retrograde movement from Golgi back to ER. COPI complexes comprise among other proteins the small GTPase ADP ribosylation factor 1 (ARF1). ARF1 recruitment to the Golgi is effectively blocked by Brefeldin A, thereby inhibiting formation of COPI vesicles leading to a collapse of the Golgi into the ER and finally preventing conventional protein secretion.

From the trans-Golgi network the proteins destined for secretion are either sorted into vesicles for regulated or constitutive secretion. Vesicles for constitutively secreted proteins directly move to the plasma membrane and the enclosed proteins are released by exocytosis from the cell. In the regulated secretion, however, the so-called secretory vesicles are initially stored intracellularly. Their exocytosis is triggered by a stimulating signal, as, for example, an increase in intracellular Ca^{2+} ($[Ca^{2+}]_i$) in response to hormonal or neural stimulation.

Besides the high efficiency and accuracy of the ER/Golgi system in protein export (Nickel & Rabouille, 2009; Trombetta & Parodi, 2003) a substantial number of proteins not showing a classical ER-signal peptide sequence are released via an unconventional secretory pathway. For these proteins, four different main pathways were proposed (Nickel & Rabouille, 2009; Rabouille, et al., 2012): translocation across the plasma membrane, the autophagosome-dependent pathway, the secretion via microvesicles and the exosome-associated release.

The translocation across the plasma membrane was described in detail for the secretion of the fibroblast growth factor 2 (FGF2). The cytosolic protein is first directed to the inner leaflet of the plasma membrane by binding to phosphoinositide phosphatidyl-inositol-4,5-biphosphate ($PtdIns(4,5)P_2$) (Temmerman, et al., 2008). $PtdIns(4,5)P_2$ induces the oligomerization and subsequent integration of FGF2 into the membrane. Translocation through the membrane is assumed to occur by the formation of a lipidic membrane pore (Steringer, et al., 2012). Heparan sulphate proteoglycans as components of the extracellular matrix were found to be

involved in the unconventional secretion of FGF2, likely by binding the FGF2 molecules after membrane translocation (Zehe, et al., 2006). This proposed process of membrane insertion and translocation as an unconventional secretory pathway is suggested also for other proteins as HIV-1 Tat, annexin A2 and FGF1 (Rabouille, et al., 2012). Another non-vesicular secretory mechanism involving direct translocation across the plasma membrane is the ABC-transporter-based secretion. This pathway seems to be used in particular for the translocation of lipidated proteins and peptides and is ATP-dependent (Rabouille, et al., 2012).

Unconventional secretory pathways that involve intracellular vesicles as "transport intermediates" include not only the formation of secreted microvesicles, but also the secretion via autophagosome-like structures and the release of exosomes (Rabouille, et al., 2012). Secreted so-called microvesicles or shedding vesicles, are produced by direct outward budding of the plasma membrane. Together with apoptotic vesicles, that are released during apoptosis, and exosomes they constitute the group of extracellular vesicles (Raposo & Stoorvogel, 2013; Yáñez-Mó, et al., 2015). In comparison to exosomes, microvesicles lack typical late-endosomal marker proteins (see below), show in the majority a larger size and differ in their lipid composition that indicate their origin from the plasma membrane (Nabhan, et al., 2012; Cocucci, et al., 2009; Record, et al., 2014). The process of outward budding of the plasma membrane is well examined in virus amplification that results in the budding of new virus particles at the plasma membrane. Human immunodeficiency virus (HIV) and some other viruses recruit the host endosomal sorting complex required for transport (ESCRT) machinery from endosomal membranes to the plasma membrane to mediate the budding process (Martin-Serano & Neil, 2011; Nabhan, et al., 2012). Therefore, it has been discussed that also microvesicle budding is dependent on the ESCRT machinery. Nabhan and colleagues then found a virus-independent process of microvesicle production in eukaryotic cells that indeed involves the recruitment of certain members of the ESCRT machinery to the plasma membrane. The arrestin domain-containing protein 1 (ARRDC1) being located to the plasma membrane through its arrestin domain is able to interact with the ESCRT member tumor susceptibility gene 101 (Tsg101, mammalian) and recruit it to the plasma membrane. Tsg101 in turn may recruit further ESCRT proteins which then mediate the budding of microvesicles (Nabhan, et al., 2012).

A new mechanism for the unconventional secretion mediated by autophagosome-like structures, as shown for the mammalian protein acyl-coenzyme A-binding protein A (AcbA, Acb1 in yeast), was proposed approximately five years ago (Bruns, et al., 2011; Rabouille, et al., 2012; Malhotra, 2013). It describes the formation of a specific compartment for unconventional secretion (CUP), a cup-shaped membrane structure, that is generated near ER exit sites in response to starvation (Malhotra, 2013). It has been shown that the formation process of these CUPs and the whole secretion process of AcbA/Acb1 involves several factors

that are required for the biogenesis of autophagic vesicles. Additionally, effectors of endosomal fusion and proteins of the multivesicular body (MVB) pathway as members of the ESCRT machinery do participate, as well as the unconventional secretion-related mammalian proteins GRASP55/65 (Grh1 in yeast and GRASP in Drosophila) (Rabouille, et al., 2012). However, this process is not triggered by rapamycin, which actually induces autophagy by inhibition of the protein kinase mTOR. It is suggested that the CUPs, which contain the proteins destined for secretion, fuse with endosomes which then further develop to MVBs by inward budding, thereby producing the protein-containing intraluminal vesicles (ILVs, see below in 2.2) that are released after fusion with the plasma membrane (Malhotra, 2013).
Also proteins that are secreted via exosomes are sorted to ILVs of MVBs, however, by other mechanisms, dependent or independent of the ESCRT machinery (see in more detail in 2.2 below).

2.2 Exosomes and the regulation of exosome biogenesis

Exosomes are small extracellular vesicles with a size of 30-100 nm that are released by viable cells either constitutively or upon a stimulating signal. Release of exosomes seems to be a general characteristic of all cells and tissues in the body, but could strongly vary in extent (quantitatively) and composition (qualitatively). Exosomes are found in several body fluids like blood, urine and CSF (Record, et al., 2014; Urbanelli, et al., 2013). Exosomes are now attributed to a new class of signal mediators that could regulate cell-to-cell communication (Urbanelli, et al., 2013). Due to their endosomal origin (explained in more detail below), exosomes contain proteins involved in membrane transport and fusion like Rab GTPases, annexins and flotillins. Furthermore, they harbour proteins of MVB biogenesis as Alix and Tsg101 as well as integrins and tetraspanins that are associated to lipid microdomains. Additionally, exosomes enclose proteins that are cell-type-specific like MHC class I or II proteins, proteins linked to the cytoskeleton or to metabolism as well as mediators of signalling pathways (Urbanelli, et al., 2013). Despite its strong cell-type-specific arrangement also the lipid composition of exosomes is in part characteristic. In particular lysobisphosphatidic acid (LBPA, also named BMP) and other lipids associated to lipid rafts like sphingomyelin, cholesterol and ceramides are found in all exosomes.
Exosomes are generated as intraluminal vesicles (ILVs) by inward budding of the limiting membrane of late endosomes which are then named MVBs (see Figure 2), sometimes also multivesicular endosomes (MVEs). The MVB pathway is used primarily for the selective transport of proteins that are destined for lysosomal degradation. Fusion of MVBs with the lysosome releases the cargo-containing ILVs into the lysosomal lumen and both, ILVs and cargo proteins are exposed to the proteolytic function of the lysosomal hydrolases. This serves both the quality control in the cell and the attenuation of receptor-mediated signalling pathways.

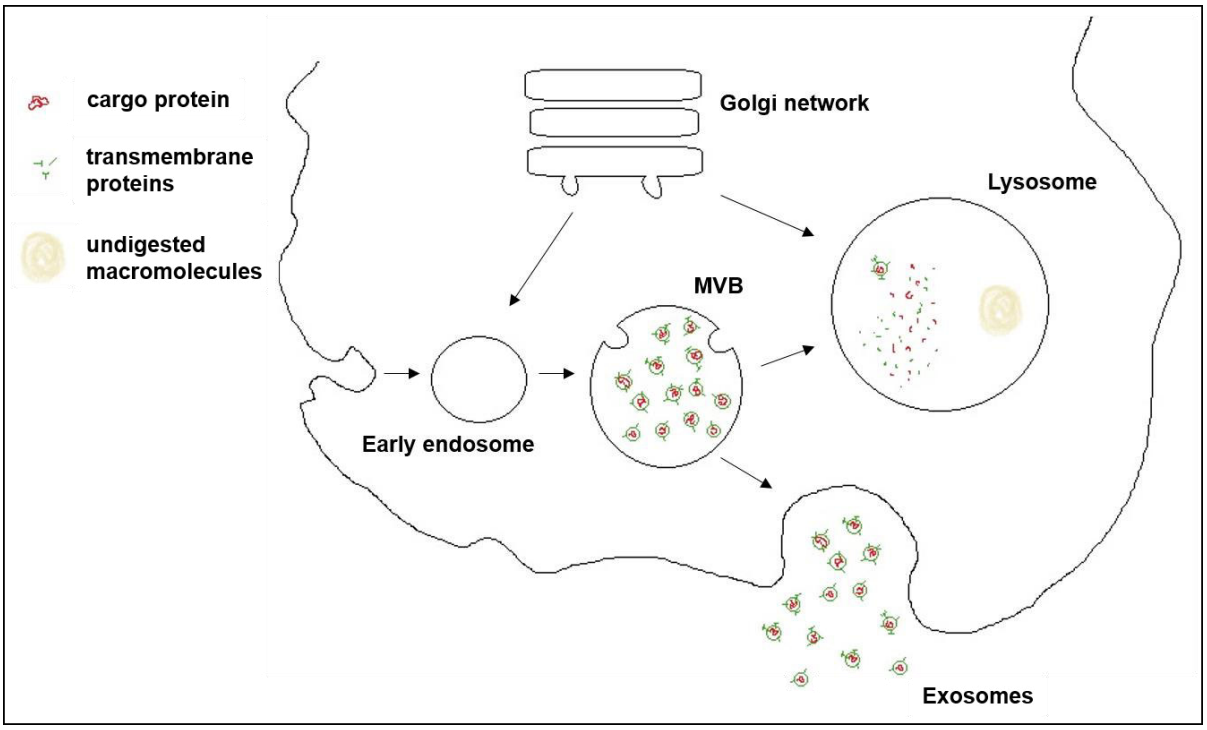

Figure 2. The origin of exosomes. Exosomes are generated as intraluminal vesicles (ILVs) at the limited membrane of endosomes. These endosomes are named multivesicular bodies (MVBs) that can contain hundreds of ILVs. ILVs enclose, among other biomolecules, cytosolic and transmembrane proteins like internalized receptors. MVBs can fuse with lysosomes taking the degradative way leading to the proteolytic degradation of ILVs and their content. Instead they can also fuse with the plasma membrane and release the ILVs as exosomes into the extracellular space. Figure taken and adapted from (Urbanelli, et al., 2013).

Misfolded membrane proteins and excessive membranes as well as activated growth factor, hormone and cytokine receptors are removed from the cell, mainly triggered by a negative feedback loop (Gruenberg & Stenmark, 2004; Katzmann, et al., 2002). First, it was assumed that MVBs exclusively fuse with lysosomes. However, they can also fuse with the plasma membrane resulting in the release of the ILVs to extracellular fluids, then referred to as exosomes (Johnstone, et al., 1987; Simons & Raposo, 2009).

As in the proteasomal degradation pathway ubiquitin tags initiate the proper sorting into the MVB pathway. In comparison to proteasomal degradation cargo proteins are polyubiquitinated via Lys-63-linked instead of Lys-48-linked conjugation or they are monoubiquitinated several times. The ubiquitin tags are recognized by the ESCRT machinery. It also mediates the sorting to invaginations in endosomal membranes, the deformation of the membrane and its inward budding and the abscission of the ILVs into the lumen of the endosome (Raiborg & Stenmark, 2009).

The ESCRT machinery consists of four soluble multiprotein complexes named ESCRT-0, -I, -II and -III that are sequentially recruited to the membrane, suggesting a directional stepwise delivery of cargo from one complex to the other (see Figure 3). Important accessory proteins binding to the ESCRT complexes and being involved in cargo recognition, sorting, and inward budding are e.g. Alix and the ATPase Vps4A/B (mammalian). ESCRT-0 can bind PtdIns(3)P

via its subunit hepatocyte growth factor-regulated tyrosine kinase substrate (Hrs, mammalian), which directs it to the endosomal membrane. Furthermore, ESCRT-0 subunits contain ubiquitin- and clathrin-binding domains that mediate recognition and concentration of ubiquitinated cargo proteins in the endosomal membrane in certain microdomains. In addition, ESCRT-0 ensures recruitment of ESCRT-I complexes by binding its subunit Tsg101. ESCRT-I is also able to recognize ubiquitinated cargo and it recruits ESCRT-II. Most likely, it is also

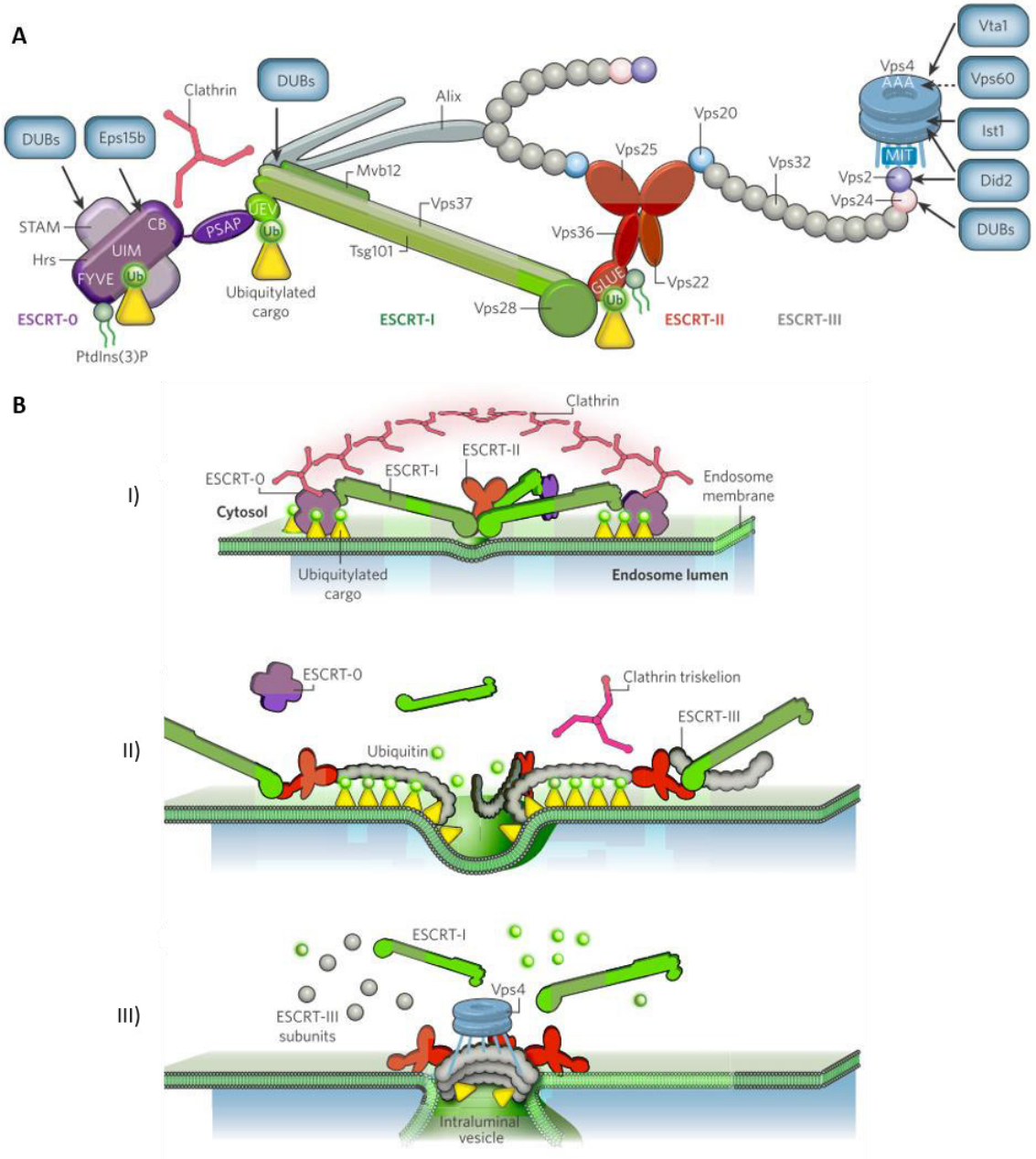

Figure 3. ESCRT machinery in the sorting of ubiquitinylated cargo into ILVs into the lumen of MVBs. (A) Composition and interaction of the four ESCRT complexes 0, I, II, and III. (B) Mechanism of ESCRT machinery: I) Cargo recognition and ESCRT-I recruitment by ESCRT-0. Clathrin mediates cargo recognition and concentration in microdomains. ESCRT-II recruitment and contribution to membrane deformation through ESCRT-I. II) ESCRT-II and Alix (not shown) recruit ESCRT-III for further membrane deformation, gating of cargo into invaginations and recruitment of DUBs. III) Final membrane abscission by ESCRT-III and accessory proteins. The ATPase Vps4 enters the invagination to recycle ESCRT-III subunits for further rounds of budding. DUB – deubiquitylating enzymes. (A) and (B) from (Raiborg & Stenmark, 2009).

involved in the invagination of the endosomal membrane. ESCRT-II then recruits ESCRT-III, which is the most conserved of all four complexes. It is suggested that the accessory protein Alix supports this recruitment or even takes over that function from ESCRT-II. Alix is able to build a bridge between ESCRT-I and ESCRT-III via Tsg101 and the ESCRT-III subunit Vps32 (Raiborg & Stenmark, 2009). ESCRT-III is involved in clustering and gating the cargo into invaginations of the endosomal membrane and the recruitment of deubiquitylating enzymes that remove the ubiquitin tags from the cargo proteins. It further navigates the invagination and the final abscission of the ILVs into the endosomal lumen. ESCRT-III complexes are disassembled by the ATPase Vps4A/B for recycling, which enables further rounds of budding (Raiborg & Stenmark, 2009; Wollert, et al., 2009).

Indeed, for several proteins that are released via exosomes an involvement of the ESCRT machinery could be proven. It could be shown that particular ESCRT members as Hrs, Tsg101, Chmp2A, Chmp4A/B/C and the accessory proteins Alix and Vps4A/B play a role in the release of certain exosomal proteins (Tamai, et al., 2010; Baietti, et al., 2012; Géminard, et al., 2004). For instance, Baietti et al. analysed the function of Alix in the secretion of syntenin-containing exosomes in MCF-7 cells which represent 50% of the total number of exosomes in this cell type and found that Alix by interaction with syntenin and syndecan heparan sulphate proteoglycans is not only involved in sorting cargo, but furthermore needed for exosome formation by recruiting the ESCRT machinery (Baietti, et al., 2012; Hurley & Odorizzi, 2012).

The secretion of other exosome-associated proteins could also occur independent of ESCRT complexes and ubiquitination of cargo proteins (Trajkovic, et al., 2008; van Niel, et al., 2011; Alonso, et al., 2011; Buschow, et al., 2009). Trajkovic and colleagues found a lipid-dependent mechanism that drives the formation of ILVs independent of the ESCRT machinery. The neutral sphingomyelinase generates ceramide that, enriched and clustered in microdomains in the endosomal membrane, due to its polar hydrogen bond-forming headgroup and its cone-shaped structure, promotes and induces the inward budding to ILVs (Trajkovic, et al., 2008; Hurley & Odorizzi, 2012). RNAi-mediated or pharmacological inhibition of neutral sphingomyelinase 2 reduced exosome-associated secretion in an oligodendroglial (Trajkovic, et al., 2008) and in a neuroblastoma cell line (Yuyama, et al., 2012), but did e.g. not influence exosome release in a prostate cancer (Phuyal, et al., 2014) or in a melanoma cell line (van Niel, et al., 2011). Although a detailed mechanism still needs to be investigated also the involvement of tetraspanins, being organised as microdomains in endocytic membranes and found to be enriched in exosomes, in the formation of MVBs represent another ESCRT-independent mechanism for exosome biogenesis (Andreu & Yáñez-Mó, 2014). Most likely, several distinct mechanisms exist depending on the cargo protein and also the cell type.

2.3 Unconventional release of IDE

The discovery to find IDE being secreted by several cell types and representing one of the main, if not the major protease in the extracellular Aβ degradation, especially in microglial cells (Qiu, et al., 1997; Qiu, et al., 1998), marked an important step in the research dealing with proteolytic Aβ degradation in the brain mediated by IDE. As described above, subsequently IDE was discovered to be released by the unconventional secretory pathway via exosomes (Bulloj, et al., 2010; Tamboli, et al., 2010). IDE lacks a classical signal peptide that would lead it to the conventional secretory pathway via ER and Golgi. Furthermore, the release of IDE is not blocked by typical inhibitors of classical secretion as Monensin or Brefeldin A (Bulloj, et al., 2010; Zhao, et al., 2009).

In further examinations dealing with IDE secretion and its regulation, first, Tamboli and colleagues found statins being able to stimulate IDE secretion from microglial cells. Statin treatment triggers IDE release and thereby induces increased degradation of extracellular Aβ (Tamboli, et al., 2010). Statins like lovastatin were already known to have a beneficial effect on the risk to develop AD comparing a group of patients taking statins with patients taking no statins over several years (Haag, et al., 2009). Statins are a class of pharmaceuticals that inhibit the HMG-CoA-reductase, an important enzyme in the cholesterol synthesis, and are used for treatment of high cholesterol levels in the patients. Tamboli and colleagues, however, could show that statins are additionally able to stimulate the release of exosomes, leading to an enhanced IDE secretion that positively affects the degradation of extracellular Aβ (see Figure 4A). This stimulating effect of statins, however, is independent of cellular cholesterol concentrations but assumingly leads to an impairment of the isoprenoid biosynthesis and protein prenylation and might interfere with the isoprenylation of Rab GTPases as Rab11, Rab27a and b that were also shown to be involved in the regulation of docking and fusion of MVBs with the plasma membrane (Tamboli, et al., 2010; Glebov & Walter, 2012).

A further stimulating factor for IDE secretion from microglial cells is somatostatin (Tundo, et al., 2012). Somatostatin is a peptide hormone regulating several processes in the nervous and endocrine system. Its depletion was already associated to the onset of AD (van Uden, et al., 1999) and it was discovered to be an IDE substrate but also a modulator of its activity (Ciaccio, et al., 2009). Tundo and colleagues observed an increasing effect of somatostatin treatment on the secretion and expression of IDE in microglial cells (Tundo, et al., 2012). Another recent study then revealed an intrinsic regulatory element of IDE release in the IDE amino acid sequence itself (Glebov, et al., 2011). Glebov and colleagues found a novel functional domain in the C-terminus of the IDE sequence named SlyX motif (^{853}EKPPHY^{858}; see Figure 4B) that promotes enzyme secretion. Mutagenesis approaches showed that the deletion of this motif and also the deletion of the C-terminus ranging from the SlyX domain to the PTS domain strongly decreased the release of IDE from the fibroblast cell line cos-7. Moreover, addition of

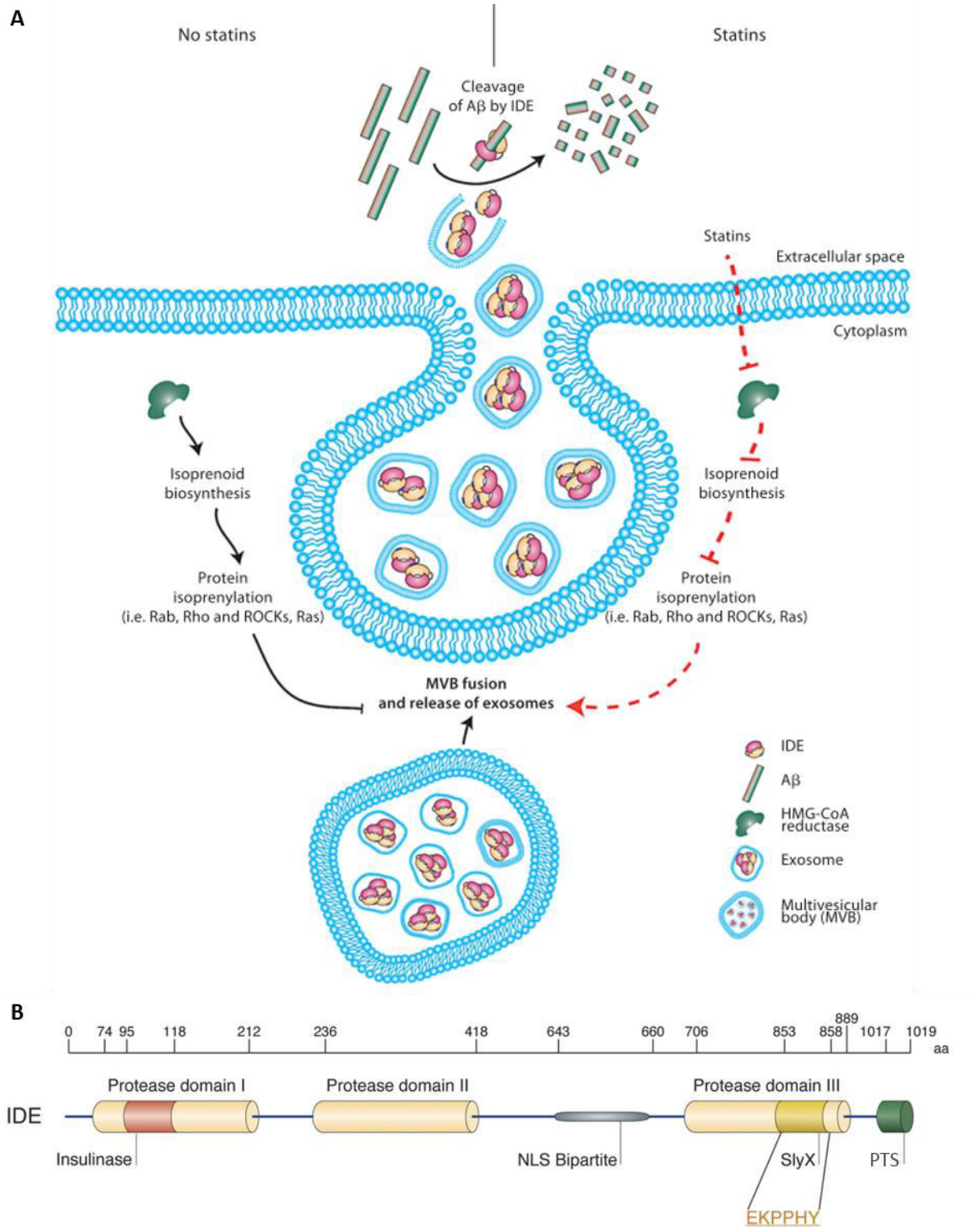

Figure 4. Export of IDE into extracellular space. (A) Suggested mechanism of statin-mediated degradation of Aβ due to an increased release of exosome-associated IDE. Statins impair isoprenoid biosynthesis that prevents protein isoprenylation of e.g. Rab GTPases that are involved in the fusion event of exosome-containing MVBs with the plasma membrane. Decreased protein prenylation leads to an increase in these fusion events and enhances IDE release. From (Glebov & Walter, 2012). (B) Diagram of IDE amino acid sequence. The relative size scale (aa – amino acid) above the diagram shows the position of featured domains. Protease domain I contains the insulinase activity of IDE. Protease domain II and III are inactive. The SlyX motif being involved in the secretion regulation of IDE is located in the protease domain III at aa 853-858. NLS – nuclear localisation domain, PTS – peroxisomal targeting sequence. From (Glebov, et al., 2011).

the SlyX motif to GFP, which is predominantly localised in the cytosol, strongly increased the secretion of GFP into cell supernatants.

3. Microglia

Microglia are the intrinsic phagocytic cells of the CNS and represent the resident endogenous brain defence and immune system to protect the brain against all kinds of pathogenic factors. But they also create and maintain an intact tissue homeostasis to support the neuronal cells (Kettenmann, 2011; Kierdorf & Prinz, 2013). The origin of microglia is still under debate. It was long assumed that microglia are of mesodermal/mesenchymal origin and differentiate from blood-derived monocytes that migrated from the periphery and postnatally immigrated into the brain (Brockhaus, et al., 1993; Haas, et al., 1996; Kettenmann, 2011). Recent studies now indicate that there are embryonic microglia that derive from stem cells that are formed during primitive haematopoiesis in the yolk sac, differentiate to macrophages and seed the brain rudiment already during early fetal development (Ginhoux, et al., 2013; Prinz & Priller, 2014). It is suggested that under certain inflammatory conditions as bone marrow transplantation and neurodegenerative diseases also monocyte-derived progenitors are recruited to the brain and supplement the microglial population to some extent (Ginhoux, et al., 2013). Postnatally, microglia spread evenly over the whole neural tissue and adopt a microglia-specific morphology under physiological conditions named the resting state. It is characterised by a short cell body and multiple thin and branched processes. These processes are highly dynamic and constantly scan the surrounding for neuronal damage, protein aggregates or infectious agents (Kettenmann, 2011). By specific pattern recognition receptors, as for example Toll-like receptors, microglia are able to recognize so-called pathogen-associated molecular patterns (PAMPs), a set of microbial molecules, and damage-associated molecular patterns (DAMPs), endogenous molecules that are released by dead cells. PAMPs alert the organism to intruding pathogens and DAMPs signal tissue and cell damage (Bianchi, 2007; Tang, et al., 2012). Microglia are able to scan the whole brain area by monitoring the extracellular space and their cellular neighbourhood (Nimmerjahn, et al., 2005). Detection of real or potential danger to the CNS induces the activation of the microglia. Activation of microglia is a gradual process that includes changes in cellular phenotype and motility associated with specific alterations in gene expression. This causes the induction and rearrangement of surface proteins for cell-cell and cell-matrix interaction, changes in intracellular enzymes and the release of various proinflammatory and immunoregulatory factors and compounds. During activation, microglia convert from the branched resting phenotype to a so-called amoeboid phenotype which is characterised by thickening and retraction of the processes and an overall more round shape. They can actively move to a lesion or infection along gradients of chemoattractants (Kettenmann, 2011; Davalos, et al., 2005). If it is necessary to fight locally invading germs and

protect and restore tissue homeostasis, some microglia are able to return into a proliferative state to increase the number of microglia for the defence reaction. Furthermore, even other immune cell populations as monocyte-derived cells from the periphery can be recruited to the CNS through microglia by releasing chemoattractive factors (Saijo & Glass, 2011). T cells may be mobilized by antigen presentation to support the adaptive immunity. By activating their phagocytic properties they remove tissue debris, damaged cells or microbes. Additionally to the defence mechanisms microglia produce and release neurotrophic factors and physically associate with endangered neurons to support them (Kettenmann, 2011).

The transformation from the resting to active states serves primarily the protection and support of the structural and functional integrity of the CNS as well as the restoration of the neural tissue homeostasis (Kettenmann, 2011; Kierdorf & Prinz, 2013). The initial signals that modulate microglia activity are not fully understood. They are characterised by a sudden appearance, an abnormal concentration or unusual format of certain factors. It is assumed that the state and function of microglia are controlled by a complex interplay of activating (on) and inactivating (off) signals. Off-signals maintain the persisting receptor signalling to keep the microglia in the resting state. On-signals, on the contrary, change the current receptor signalling and trigger microglial activation (Kettenmann, 2011; Linnartz & Neumann, 2013; Kierdorf & Prinz, 2013). Examples for such signalling molecules are proteins of the bacterial cell walls or viral envelopes, bacterial or viral DNAs or RNAs, factors that are released through tissue damage like high amounts of ATP, cytokines, neuropeptides and growth factors. For recognition of the different signals, microglia express multiple receptors as cytokine receptors, scavenger receptors, pattern recognition receptors and chemokine receptors. In addition, microglia express various neurotransmitter receptors such as glutamate, GABA, cholinergic, adrenergic, dopamine and serotonin receptors and thereby are able to sense a certain change in the release of the respective transmitters (Kettenmann, 2011; Kierdorf & Prinz, 2013). This versatile subset of cell surface molecules on the microglial membrane as well enables a communication of microglia not only with the surrounding glial cells but also with the neighbouring neurons (Kierdorf & Prinz, 2013).

3.1 Neuron-microglia communication

Neurons are able to modulate microglial activity and motility by the release of specific chemokines and neurotransmitters as well as purines and pyrimidines (Eyo & Wu, 2013; Sheridan & Murphy, 2013; Fields & Burnstock, 2006). One example is fractalkine, a chemokine which is expressed on the neuronal surface and sensed by the CX_3CR1 receptor located in plasma membranes of microglia. Expression of fractalkine in neurons increases after neuronal injury, is able to influence microglial intracellular signalling pathways and provides neuroprotection, inter alia by inhibiting excessive microglial activation (Zhang, et al., 2011;

Broderick, et al., 2002; Lyons, et al., 2009). Moreover, effects of neurotransmitters on microglial behaviour started to be investigated in the last years. It can be already suggested that excitatory as well as inhibitory neurotransmission cooperate to regulate microglial activity and motility. However, there are differences between global and local neurotransmitter-mediated regulation of microglia activity. For instance, it could be shown that global inhibition of the inhibitory GABAergic neurotransmission increased the territory surveyed by microglia, displaying an increased activity of microglia in scanning their surroundings (Nimmerjahn, et al., 2005). The global inhibition of excitatory glutamate receptors, in contrast, leads to decreased microglia motility. Conversely, their activation by glutamate receptor agonists enhanced it (Fontainhas, et al., 2011). A regulation of microglial function by local neurotransmission is until now not fully proven. There are controversial results showing no effect of local GABA or glutamate application on microglial motility in mouse brain slices (Wu & Zhuo, 2008; Chen, et al., 2010), but an increased microglial activity upon local glutamate uncaging in zebrafish optical tectum (Li, et al., 2012).

Especially, the interaction between neurons and microglia has been investigated upon neuronal injury. In the 1970s it has been found that the purine nucleotide ATP and its metabolites ADP and adenosine in extracellular fluids can be recognized by certain cell surface receptors. Under physiological conditions their intracellular levels are maintained at high concentration whereas the extracellular levels are kept at relatively low concentration (Burnstock, et al., 2011; Eyo & Wu, 2013). In case of neuronal injury, purines are released from neurons and detected by microglia. Purines then trigger chemotaxis of microglia to the location of the lesion mediated by local concentration gradients. Additional to its role in injury-induced microglial motility, purinergic signalling was also shown to be necessary under physiological conditions, for example to facilitate the formation of direct neuron-microglia contacts (Li, et al., 2012). ATP can be released by neurons, in much lower concentrations than from damaged cells, via activity-dependent opening of pannexin-1 hemichannels. Li et al. showed that this supports the formation of direct contacts between bulbous endings of resting microglia and neuronal soma most probably mediated by ATP/P2 purinergic receptor signalling in microglia (Li, et al., 2012).

By direct physical interaction as well as the release of certain paracrine signals, microglia in turn are able to modulate also neuronal behaviour (Eyo & Wu, 2013). Wake et al., who demonstrated a direct interaction between microglial processes and neuronal dendritic spines, suggest that microglia form these specific contact sites to monitor neuronal function, for example after transient ischaemia (Wake, et al., 2009). On the other hand, Tremblay et al. showed that this physical interaction can also lead to an alteration of number and size of the neuronal spines in the healthy brain (Tremblay, et al., 2010). Additionally to the ability of direct interaction, microglia as well release certain factors that influence neuronal activity and

function. They release neuroprotective factors like neurotrophins or members of the TGFβ and IL-6 families (Suzumura, 2013). Likewise, microglia secrete also pro-inflammatory and rather neurotoxic factors as inflammatory cytokines as IL-1β, TNF-α and nitric oxide (Suzumura, 2013). Moreover, it has been shown that microglia play a role in synaptic pruning during postnatal development and contribute to the build-up of neuronal circuits through different signalling pathways, for instance mediated via the fractalkine receptor, the complement receptor and DAP12 (Eyo & Wu, 2013; Paolicelli, et al., 2011; Schafer, et al., 2012; Wakselman, et al., 2008).

Together, microglia not only react to brain damage or infection, but also play important roles in the regulation of neuronal function under physiological conditions. The bidirectional neuron-microglia interaction can be suggested to represent an essential aspect of the normal function of the brain, including nervous system development and its maintenance (Eyo & Wu, 2013; Sheridan & Murphy, 2013; Suzumura, 2013).

3.2 Microglia in Aβ degradation and AD

Although microglia exert an important and beneficial role in the brain defence, inter alia, by the release of growth and anti-inflammatory factors that have neuroprotective effects, they, on the other hand, might play a double-edged role in the pathogenesis and pathology of AD. Aging itself entails also the loss of efficiency of microglial function, thus, for example, the receptors that promote uptake and clearance of fibrillar Aβ are downregulated (Hickman, et al., 2008). Additionally, aged microglia show enhanced production of pro-inflammatory cytokines as TNF-α and IL-1β and decreased expression of anti-inflammatory cytokines as IL-10 as well as phenotypic changes including dystrophic processes and abnormal clustering (Njie, et al., 2012; Solito & Sastre, 2012; Streit, et al., 2008). Also molecular markers typically found to be up-regulated in activated microglia as MHC-II, Cd11b and Iba1 are increased during aging (Wong, 2013). This suggests an increased activation of microglia, their hypersensitivity in response to stimulation and a decrease in the control mechanisms of microglial activation in the aged brain. Under neurodegenerative conditions microglia were found to be in an hyper-reactive state and it becomes more and more clear that neuroinflammation plays a critical role in AD, although its contribution to the neurodegenerative process is still not fully elucidated (Solito & Sastre, 2012; Suzumura, 2013; Lee & Landreth, 2010). The increased production and release of pro-inflammatory factors, observed in AD patients and AD mouse models (Sastre, et al., 2006; Benzing, et al., 1999; Matsuoka, et al., 2001), does not only exert neurotoxic effects that can cause neuronal damage and death, it has been also shown to suppress the phagocytic response of microglia to fibrillar Aβ (Koenigsknecht-Talboo & Landreth, 2005; Lee & Landreth, 2010). Aβ and APP themselves are assumed to trigger microglial activation (Barger & Harmon, 1997; De Giorgio, et al., 2002; Permanne, et al., 2002). Microglial activation is directly related

to the amyloid load. Furthermore, interaction of microglia with Aβ activates NFκB-mediated pathways and cytokine production (Combs, et al., 2001; Solito & Sastre, 2012). Because neuroinflammation is suspected to exacerbate neurodegenerative processes, the suppression of pro-inflammatory or promotion of anti-inflammatory states of microglia are considered for therapeutical intervention. Recent studies already showed promising results: In an AD mouse model the treatment with rosiglitazone, a PPARγ agonist, suppressed the microglial expression of pro-inflammatory mediators and decreased the amyloid pathology in the mice (Escribano, et al., 2010). Administration of noradrenalin to microglial cells diminished the production of cytokines and chemokines and also promoted phagocytosis of fibrillar Aβ (Heneka, et al., 2010). Moreover, anti-inflammatory cytokines as TGF-β and IL-4 enhanced Aβ clearance from the brain of transgenic AD mice or in primary microglia, respectively (Wyss-Coray, et al., 2001; Shimizu, et al., 2008). Additionally, several epidemiological studies on nonsteroidal anti-inflammatory drugs (NSAIDs) revealed a decreased prevalence of AD upon long-term use of these drugs (McGeer, et al., 1996). Follow-up clinical trials and studies, however, did not reveal a beneficial effect in AD patients, but showed that NSAIDs use started in midlife (prior to 65 years) in comparison to later life prevented cognitive decline during aging (Sastre & Gentleman, 2010).

Additional to the assumed detrimental role of microglia during the pathogenesis of AD, microglia might also exert a beneficial role by contributing to the clearance of Aβ by uptake and removal of Aβ through phagocytosis (Simard, et al., 2006; Lee & Landreth, 2010). Although LRP1-mediated endocytosis might represent an important way of Aβ uptake in neurons, it does not seem to represent the main pathway for the uptake of soluble Aβ in microglia (Harris-White, et al., 2004; Mandrekar, et al., 2009). Mandrekar and colleagues identified another pathway in microglial cells in which soluble Aβ, which encloses monomeric and small oligomeric forms of Aβ, is predominantly taken up through constitutive fluid phase macropinocytosis (Mandrekar, et al., 2009; Lee & Landreth, 2010). Fibrillar, aggregated forms of Aβ, on the other hand, are phagocytosed by another mechanism. They interact with particular fibrillar Aβ recognition receptor complexes and thereby activate intracellular signalling cascades that induce their phagocytosis (Lee & Landreth, 2010). Additionally, fibrillar Aβ may be also ingested through antibody- and complement system-mediated mechanisms (Bard, et al., 2000; Wilcock, et al., 2003; Jiang, et al., 1994; Webster, et al., 1997; Lee & Landreth, 2010).

Internalized soluble Aβ is directly transported to lysosomes for degradation via the endocytic pathway (Mandrekar, et al., 2009). For the degradation of fibrillar Aβ in microglia this is still not fully clear. It was discovered that fibrillar Aβ is taken up and transported to the endosomal-lysosomal compartment in primary microglia, but only a small part is also degraded. Instead it was observed that microglia store fibrillar Aβ for several weeks and, partially, release it again

(Chung, et al., 1999; Paresce, et al., 1997). However, it could be shown that obviously the activation of microglia (see above) may induce their ability to degrade fibrillar Aβ through an acidification of the lysosomes (Lee & Landreth, 2010; Majumdar, et al., 2007; Majumdar, et al., 2011). It can be assumed that Aβ-degrading proteases as cathepsin B and D or endothelin-converting enzyme 2 (ECE-2) with a mildly acidic pH optimum rather than neutral endopeptidases are involved in the lysosomal Aβ proteolysis (Miners, et al., 2011).

Interestingly, also APOE, the strongest known genetic risk factor for the development of LOAD, seems to play a critical role in the clearance of Aβ, e.g. for the microglia-mediated removal. Extracellular soluble APOE primarily secreted by astrocytes stimulates the phagocytosis of Aβ by microglial cells (Terwel, et al., 2011; Giunta, et al., 2008). The APOE lipidation status affects the binding of APOE and Aβ. Moreover, the phagocytosis as well as the intracellular and extracellular degradation of both soluble and fibrillar Aβ in microglia are affected by the lipidation status of APOE, whereby more highly lipidated isoforms cause a more effective clearance of Aβ (Jiang, et al., 2008; Bales, et al., 2009; Lee & Landreth, 2010; Wildsmith, et al., 2013).

In addition to the removal of soluble and fibrillar Aβ through phagocytosis, the extracellular proteolytic degradation of Aβ was shown to be influenced by microglia as well. Microglia express and release Aβ-degrading enzymes that contribute to the extracellular degradation of the peptide and partially also its oligomeric forms and fibrillar deposits (Miners, et al., 2011). IDE was discovered to be released predominantly by microglial cells in the brain and seems to represent the major protease for microglia-mediated degradation of extracellular monomeric Aβ (Qiu, et al., 1998; Tamboli, et al., 2010).

4. Rationale and aim of the study

An imbalance between production and degradation of Aβ leads to its abnormal accumulation and extracellular deposition in senile plaques during the pathogenesis of AD. For sporadic LOAD, the most common form of the disease, it is speculated that rather deficiencies in the clearance of Aβ than an increased production lead to its accumulation and thereby cause the disease (Wildsmith, et al., 2013; Miners, et al., 2011). IDE is one of the major Aβ-degrading enzymes in the brain that contributes to the removal of monomeric Aβ. The enzyme being released by microglial cells or associated to the outer membrane of neurons and endothelial cells in the brain was shown to play a role in the extracellular degradation of Aβ (Qiu, et al., 1998; Tamboli, et al., 2010; Vekrellis, et al., 2000; Lynch, et al., 2006). Two independent studies demonstrated that different cell types can secrete IDE through an unconventional exosome-associated secretory pathway, however, the detailed mechanism of IDE secretion, its regulation and its stimulation in the brain is still not fully understood. IDE secretion from microglial cells could be stimulated by statins leading to an enhanced degradation of

extracellular Aβ. However, natural stimuli for the release of IDE that potentially function within the neuron-microglia communication are not known. Before this study preliminary investigations by Konstantin Glebov revealed a potential role for the neurotransmitter serotonin (5-HT) in the stimulation of IDE secretion.

Therefore the main aim of this project was to examine the molecular mechanisms that underlie the unconventional release of IDE and its regulation in microglia. Here the effects of the neurotransmitter 5-HT on the release of IDE and potential activated signalling pathways being involved should be investigated using cell culture models. Furthermore, the regulation of IDE secretion including its trafficking and sorting into exosomes as well as its subsequent release should be analysed, especially regarding its dependency or independency on the ESCRT function.

To this end, the secretion of IDE using predominantly the cell line BV-2 will be examined both upon serotonin administration and utilizing RNAi as well as pharmacological approaches to analyse signalling pathways and investigate ESCRT-dependent or -independent regulatory mechanisms. Exosome and microvesicle preparation will be applied to gain further inside into certain effects also at the level of extracellular vesicles. In addition, by means of a lentiviral transduction system stable knockdown cell lines for IDE and the ESCRT accessory protein Vps4B shall be established. In parallel a yeast-two hybrid screen utilizing the C-terminal sequence of IDE as bait will be carried out to identify potential interaction partners of IDE that might play a role in its intracellular trafficking or release.

B Material and Methods

1. Material

1.1 Chemicals and Reagents

Chemical/Reagent	Company
Acetic acid	Carl Roth, Karlsruhe, Germany
Adenosine 5`- triphosphate (ATP) disodium salt hydrate	Sigma-Aldrich, Steinheim, Germany
Agar from Red alga Rhodophyceae	MP Biomedicals, CA, USA
Altanserin	Tocris/R&D Systems, Wiesbaden, Germany
6-Aminocaproic Acid	Sigma-Aldrich, Steinheim, Germany
Ammonium persulfate	Sigma-Aldrich, Steinheim, Germany
Ampicillin sodium salt	Carl Roth, Karlsruhe, Germany
Amyloid $\beta_{1\text{-}40}$ (Batch 15/11/14)	Peptide Specialty Laboratories GmbH, Heidelberg, Germany
Bis-Tris	Carl Roth, Karlsruhe, Germany
Boric acid	MP Biomedicals, Eschwege, Germany
Bovine Serum Albumine (Fraction V, BSA)	Carl Roth, Karlsruhe, Germany
Brefeldin A	Tocris/R&D Systems, Wiesbaden, Germany
Bromphenole blue sodium salt	MP Biomedicals, Eschwege, Germany
Calcium chloride	Life Technologies, Darmstadt, Germany
Carbenicillin	Carl Roth, Karlsruhe, Germany
Chloroquine	Sigma-Aldrich, Steinheim, Germany
Choleratoxin B	Sigma-Aldrich, Steinheim, Germany
Coomassie Brilliant Blue G/R 250	Merck, Darmstadt, Germany
p-Coumaric Acid	Sigma-Aldrich, Steinheim, Germany
8-CPT-2ME-cAMP (8-CPT)	Tocris/R&D Systems, Wiesbaden, Germany
Dimethyl sulfoxide	Carl Roth, Karlsruhe, Germany
Disodium phosphate (Na_2HPO_4)	Carl Roth, Karlsruhe, Germany
DTT (1,4-Dithiothreitol)	Carl Roth, Karlsruhe, Germany
EDTA (Ethylene diamine tetraacetic acid)	Carl Roth, Karlsruhe, Germany
EGTA (Ethylene glycol-bis(2-aminoethyether)-N,N,N',N'-tetraacetic acid)	Carl Roth, Karlsruhe, Germany
Ethanol absolute	Merck, Darmstadt, Germany
m-3m3FBS (3m3FBS)	Tocris/R&D Systems, Wiesbaden, Germany

D(+)-Glucose	Sigma-Aldrich, Steinheim, Germany
Glycerine 86%	Carl Roth, Karlsruhe, Germany
Glycin	Carl Roth, Karlsruhe, Germany
GR113808	Tocris/R&D Systems, Wiesbaden, Germany
GW4869	Sigma-Aldrich, Steinheim, Germany
HEPES	Sigma-Aldrich, Steinheim, Germany
Hydrogen peroxide 30%	Carl Roth, Karlsruhe, Germany
5-Hydroxy-L-Tryptophan	Sigma-Aldrich, Steinheim, Germany
Insulin (human, recombinant)	SAFC/Sigma-Aldrich, Steinheim, Germany
Isopropyl β-D-1-thiogalactopyranoside (IPTG)	MP Biomedicals, Eschwege, Germany
Kanamycin sulfate	Sigma-Aldrich, Steinheim, Germany
LB Media (Luria/Miller)	Carl Roth, Karlsruhe, Germany
Luminol	Sigma-Aldrich, Steinheim, Germany
Magnesium Chloride	Carl Roth, Karlsruhe, Germany
2-Mercaptoethanol	Sigma-Aldrich, Steinheim, Germany
Methanol	AppliChem, Darmstadt, Germany
Milk powder	Carl Roth, Karlsruhe, Germany
ML10302	Tocris/R&D Systems, Wiesbaden, Germany
Monensin	Sigma-Aldrich, Steinheim, Germany
Orange G	Santa Cruz, Texas, USA
Polyethylene glycol (3350, 6000)	Sigma-Aldrich, Steinheim, Germany
Poly-L-lysine-hydrobromide	Sigma-Aldrich, Steinheim, Germany
Ponceau S	Carl Roth, Karlsruhe, Germany
Potassium chloride	Carl Roth, Karlsruhe, Germany
Potassium dihydrogen phosphate (KH_2PO_4)	Carl Roth, Karlsruhe, Germany
2-Propanol/Isopropanol	Carl Roth, Karlsruhe, Germany
Protease inhibitor cocktail (cOmplete™)	Roche, Basel, Switzerland
Protein G - Sepharose® 4B	Invitrogen, Karlsruhe, Germany
Protein A - Sepharose® 4B	Invitrogen, Karlsruhe, Germany
Puromycin	InvivoGen, Toulouse, France
RS127445	Tocris/R&D Systems, Wiesbaden, Germany
Serotonin creatinine sulfate monohydrate	Sigma-Aldrich, Steinheim, Germany
Sodium chloride	Carl Roth, Karlsruhe, Germany
Sodium deoxycholat	Carl Roth, Karlsruhe, Germany
Sodium dodecyl sulfate (SDS)	Carl Roth, Karlsruhe, Germany

Sucrose	Carl Roth, Karlsruhe, Germany
TEMED (N,N,N',N'-Tetramethylethane-1,2-diamine)	Carl Roth, Karlsruhe, Germany
Thapsigargin	Invitrogen, Karlsruhe, Germany
Trichloroacetic acid	Carl Roth, Karlsruhe, Germany
Tricine	Carl Roth, Karlsruhe, Germany
Tris	Carl Roth, Karlsruhe, Germany
Triton X-100	Carl Roth, Karlsruhe, Germany
Tween® 20	Sigma-Aldrich, Steinheim, Germany
U73122	Tocris/R&D Systems, Wiesbaden, Germany
Urea	Carl Roth, Karlsruhe, Germany
X-α-Gal	Takara/Clontech Laboratories Inc., CA, USA

Table 1. List of chemicals and reagents

1.2 Media and Solutions

Name	Composition, Company
Amersham ECL Select Western Blotting Reagent	GE Healthcare, Munich, Germany
Aureobasidin A	Takara/Clontech Laboratories Inc., CA, USA
BamHI buffer	Thermo Fisher Scientific, Schwerte, Germany
Bradford Reagent	BioRad, Munich, Germany
DNase I + 10x DNase I reaction buffer	New England BioLabs GmbH, Frankfurt am Main, Germany
Dulbecco's Modified Eagle Medium (DMEM) GlutaMAX™	Thermo Fisher Scientific, Schwerte, Germany
EcoRI buffer	Thermo Fisher Scientific, Schwerte, Germany
Fetal Calf Serum	PAN-Biotech GmbH, Aidenbach, Germany
GelRed™ Nucleic Acid Gel Stains	Biotium Inc., California, USA
GeneRuler 100bp DNA ladder	Thermo Fisher Scientific, Schwerte, Germany
GeneRuler 1kb DNA ladder	Thermo Fisher Scientific, Schwerte, Germany
Gibco® B-27 Supplement	Thermo Fisher Scientific, Schwerte, Germany
Immu-Mount™	Thermo Fisher Scientific, Schwerte, Germany
Neurobasal® Medium	Thermo Fisher Scientific, Schwerte, Germany

NuPAGE® MES SDS Running Buffer	Thermo Fisher Scientific, Schwerte, Germany
NuPAGE® LDS sample buffer (4x)	Thermo Fisher Scientific, Schwerte, Germany
NuPAGE® Antioxidant	Thermo Fisher Scientific, Schwerte, Germany
Odyssey® Blocking Buffer (PBS)	LI-COR Biosciences, Bad Homburg, Germany
Opti-MEM® I Reduced Serum Medium	Thermo Fisher Scientific, Schwerte, Germany
Optiprep™ Density Gradient Medium	Axis Shield, Dundee, Scotland
PageRuler Prestained Protein Ladder	Thermo Fisher Scientific, Schwerte, Germany
PBS for cell culture	Gibco® PBS tablets dissolved in 500ml deionized H_2O, autoclaved Thermo Fisher Scientific, Schwerte, Germany
Penicillin/Streptomycin	Life Technologies, Darmstadt, Germany
Restore™ Western Blot Stripping Buffer	Thermo Fisher Scientific, Schwerte, Germany
Rotiphorese® 30 (37.5:1)	30% aqueous solution, Acrylamide/Bisacrylamide 37.5:1 Carl Roth, Karlsruhe, Germany
See Blue® Pre-stained Protein Standard	Thermo Fisher Scientific, Schwerte, Germany
T4 DNA Ligase + 10x T4 ligase reaction buffer	Thermo Fisher Scientific, Schwerte, Germany
Trypsin	0.05%/EDTA 0.02% in PBS without Ca^{2+} and Mg^{2+}, with Phenol red PAN-Biotech GmbH, Aidenbach, Germany

Table 2. List of media and solutions

1.3 Antibodies

Primary antibodies:

Antibody Name	Company	Dilution
Anti-β-Actin, mouse mAb, A1978	Sigma-Aldrich, Steinheim, Germany	1:3000 - 1:20000
Anti-AIF, rabbit mAb, D39D2 XP®	Cell Signalling/NEB, Frankfurt, Germany	1:1000
Anti-Alix, mouse IgG1 mAb, sc-53540	Santa Cruz, Texas, USA	1:1000
Anti-Amyloid-β (N), mouse IgG mAb 82E1	Immuno-Biological Laboratories Inc. (IBL AMERICA), MN, USA	1:100

Anti-Amyloid-β (N), mouse IgG1 mAb, m3.2	BioLegend, Fell, Germany	1:1000
Anti-Amyloid precursor protein (C), mouse IgG1 mAb, C1/6.1	BioLegend, Fell, Germany	1:1000
Anti-Calnexin, rabbit IgG pAb, sc-11397	Santa Cruz, Texas, USA	1:1000
Anti-EEA1, rabbit pAb, PM062	MBL/Biozol, Eching, Germany	1:1000
Anti-Flotillin-1, mouse IgG1 mAb, 610820	BD Biosciences, Heidelberg, Germany	1:1000
Anti-GAPDH, mouse IgG1 mAb, sc-47724	Santa Cruz, Texas, USA	1:500
Anti-IDE, rabbit pAb, ab25970	abcam, Cambridge, Great Britain	1:1000
Anti-IDE (C), rabbit pAb, ab32216	abcam, Cambridge, Great Britain	1:1000
Anti-IDE, mouse IgG1 mAb, MAB2496	R&D Systems, Wiesbaden, Germany	1:100 (ICC)
Lamp-2, rat IgG2a mAb, ABL-93-c	Developmental Studies Hybridoma Bank, University of Iowa, USA	1:2000
Anti-LC-3, rabbit IgG pAb, PM036	MBL/Biozol, Eching, Germany	1:1000
Anti-MEK 1/2, rabbit mAb, #8727	Cell Signalling/NEB, Frankfurt, Germany	1:1000
myc	(Wahle, et al., 2005)	1:1000
Anti-Vps4A, mouse IgG2a mAb, sc-133122	Santa Cruz, Texas, USA	1:500
Anti-Vps4B, rabbit pAb, NBP1-19119	Novus Biologicals LLC, CO, USA	1:1000 (WB) 1:250 (ICC)
Anti-Vps4B, rabbit pAb, SAB4200023	Sigma-Aldrich, Steinheim, Germany	1:1000 (WB)

Table 3. Primary antibodies

Secondary antibodies and other protein detection reagents:

Antibody/Reagent	Company	Dilution
Anti-mouse Alexa Fluor® 488	Life Technologies, Darmstadt, Germany	1:1000 (ICC)
Anti-mouse-Biotin, goat IgG pAb, B7264	Sigma-Aldrich, Steinheim, Germany	1:5000

Anti-mouse-HRP, rabbit IgG pAb, A9044	Sigma-Aldrich, Steinheim, Germany	1:36000
Anti-mouse-IRDye® 680RD, goat IgG	LI-COR Biosciences, Bad Homburg, Germany	1:10000
Anti-mouse-IRDye® 800CW, goat IgG	LI-COR Biosciences, Bad Homburg, Germany	1:10000
Anti-rabbit Alexa Fluor® 546	Life Technologies, Darmstadt, Germany	1:1000 (ICC)
Anti-rabbit-HRP, goat IgG pAb, A9169	Sigma-Aldrich, Steinheim, Germany	1:36000
Anti-rabbit-Biotin, goat IgG pAb, B8895	Sigma-Aldrich, Steinheim, Germany	1:20000
Anti-rabbit-IRDye® 680RD, goat IgG	LI-COR Biosciences, Bad Homburg, Germany	1:10000
Anti-rabbit-IRDye® 800CW, goat IgG	LI-COR Biosciences, Bad Homburg, Germany	1:10000
Anti-rat-HRP, goat IgG pAb, 612-103-120	Biomol GmbH, Hamburg, Germany	1:36000
Phalloidin Alexa Fluor® 647	Thermo Scientific, Darmstadt, Germany	1:2000 (ICC)
Streptavidin-HRP polymer, ultrasensitive, S2438	Sigma-Aldrich, Steinheim, Germany	1:1000

Table 4. Secondary antibodies and other protein detection reagents

1.4 Commercial Kits

Kit	Company
Easy Yeast Plasmid Isolation Kit	Takara/Clontech Laboratories Inc., CA, USA
GeneJET Plasmid Miniprep Kit	Thermo Fisher Scientific, Schwerte, Germany
HiPerFect Transfection Reagent	Qiagen, Venlo, Netherlands
Matchmaker® Gold Yeast Two-Hybrid System	Takara/Clontech Laboratories Inc., CA, USA
Matchmaker Insert Check PCR Mix 2	Takara/Clontech Laboratories Inc., CA, USA
NucleoBond® Xtra Maxi	Macherey-Nagel, Düren, Germany
NucleoSpin® Plasmid EasyPure	Macherey-Nagel, Düren, Germany
Pfu DNA Polymerase	Promega, Mannheim, Germany
Pierce™ BCA Protein Assay Kit	Thermo Fisher Scientific, Schwerte, Germany
RNeasy® Mini Kit	Qiagen, Venlo, Netherlands
SuperScript® III First-Strand Synthesis System	Thermo Fisher Scientific, Schwerte, Germany

Taq 5x Master Mix	New England BioLabs GmbH, Frankfurt am Main, Germany
WIZARD® SV Gel and PCR Clean-Up System	Promega, Mannheim, Germany
Yeastmaker® Yeast Transformation System 2	Takara/Clontech Laboratories Inc., CA, USA

Table 5. Commercial Kits

1.5 Devices and Tools

Device/Tool	Company
-80°C Freezer	Thermo Scientific
37°C CO_2 Incubator	Binder
37°C Incubator	VWR
Analytical Balance (Labstyle 204)	Mettler Toledo
Autoclave	H+P
Beckman Ultracentrifuge Optima™ XPN-80 Rotor: - SW41Ti - 45Ti	Beckman Coulter
Cell Culture Clean Bench	Thermo Scientific
Centrifuges (5415D, 5415R, 5804, 5804R)	Eppendorf
ChemiDoc™ XRS System with Analysis Software Quantity One® Version 4.6.3.	BioRad
Cooling System (E100)	Lauda
Glass beads acid-washed (425-600μm) G8772	Sigma-Aldrich, Steinheim, Germany
Magnetic stirrer	Velp Scientifica
MultiSkan RC™ Microplate Reader with Ascent™ Software	Thermo Scientific
NanoPhotometer® P-class P330	Implen
Nitrocellulose membrane	Amersham
NuPAGE® 4-12% Bis-Tris Protein Gels	Thermo Fisher Scientific
Odyssey CLx Imager with Analysis Software Image Studio™ Lite 5.2	LI-COR Biosciences
PCR cycler	Eppendorf
pH meter (MP225)	Mettler Toledo
PVDF membrane	GE Healthcare
Roto Shake Genie	Scientific Industries

SE 250 Mini-Vertical Gel Electrophoresis Unit	Hoefer
Sonicator	Merck Eurolabs
TE22 Small Transfer Tank	Hoefer
Thermomixer R 5355	Eppendorf
TransUV illuminator (GVM 20)	Syngene
Vortex (MS2 Minishaker)	IKA
Water bath	Medigen
XCell SureLock™ Mini-Cell Electrophoresis System	Thermo Fisher Scientific
XCell4 SureLock™ Midi-Cell Electrophoresis System	Thermo Fisher Scientific

Table 6. Devices and Tools

2. Methods

2.1 Cell biological techniques

2.1.1 Cell culture

BV-2 microglia, Cos-7, HEK293 (all three obtained from ATCC), HEK293FT (kind gift from Prof. Oliver Brüstle (University of Bonn)) and N9 microglia cells (kind gift from Prof. Michael Heneka (University of Bonn)) were cultured in DMEM GlutaMAX™ supplemented with 10% fetal calf serum (v/v) and 100 U/ml penicillin and 100 μg/ml streptomycin (DMEM +/+). Cells were routinely grown on 10-cm dishes or T75 flasks and incubated at 37°C with 5% CO2 atmosphere.

2.1.2 Preparation of primary hippocampal neurons, astrocytes and microglia from mouse or rat embryonic brain

Primary mouse or rat neurons, microglia and astrocytes were mainly prepared by Janina Gerth and Konstantin Glebov. The cells were obtained by dissection of brains from mouse (C57BL/6) or rat (WISTAR) embryos (E18) in dissection medium. Hippocampi were separated for neuron isolation, incubated with Trypsin/EDTA for 7 min and after removal of Trypsin mechanically dissociated (Pasteur pipette) in chopping medium and centrifuged (1000 g, 5 min). The cells were resuspended in Neurobasal® Medium containing 2% B-27 supplement and 3% fetal calf serum. The medium was changed after 2 hours of settlement to remove cell debris. Cells were seeded to 6-well plates coated with poly-L-lysine and incubated at 37°C with 5% CO_2 atmosphere, changing medium twice a week to Neurobasal® Medium with 2% B-27

supplement (serum free after 3 days and addition of 10 mM AraC to avoid growth of fibroblast and other glial cells like astrocytes). For astrocyte and microglia isolation cortices were mechanically dissociated (Pasteur pipette) and seeded to poly-L-lysine coated T75 flasks. The mixed culture was cultured in DMEM +/+. Primary microglia were received by shaking at 100 rpm for 2 hours and transferred to a new flask. The now mainly astrocytes-containing culture received fresh medium and the procedure of harvesting primary microglia could be repeated after 7 days.

2.1.3 Pharmacological treatment and secretion assay

In order to analyse the secretion of IDE and other exosomal marker proteins an established protocol for a secretion assay was carried out, also described earlier (Glebov, et al., 2015; Tamboli, et al., 2010). For the secretion assay the same number of cells for each replicate was seeded 8 – 24 hours before the assay, cells transfected with siRNA in order to the experimental procedure earlier (see 2.1.8). For the secretion assay, the medium was replaced by serum-free DMEM GlutaMAX™, containing the indicated reagent or equivalent amount of the respective carrier solvent in control cells (see Table 7). Cells were washed once with sterile PBS to remove serum components, which could interfere with the Western blot analysis (see 2.2.4). The medium volume was equal for transfected or treated and control cells as well as for all replicates.

Pharmacological treatments:

compound	concentration
m-3m3-FBS	5 μM
Brefeldin A (BFA)	5 μg/ml
8-CPT-2ME-cAMP (8-CPT)	5 μM
Altanserin	10 nM
GR113808	20 nM
GW4869	1.5 μM; 5 μM
5-Hydroxy-L-tryptophan (5-HTP)	500 μM
ML10302	10 nM
Monensin	10 μM
RS127445	5 μM
Serotonin creatinine sulfate monohydrate (5-HT)	25 μM
Thapsigargin	1 μM
U73122	10 μM

Table 7. Pharmacological treatments

Where indicated, a pharmacological pre-treatment with 5-HT receptor antagonists was carried out for 6 hours before the assay. After 16 hours (shorter time periods are indicated) the

conditioned medium of the cells was collected and centrifuged (1,000xg, 10 min, 4°C) to remove dead and detached cells. After the experiment, cells were lysed (see 2.2.1). Conditioned media and cell lysates were subsequently analysed by immunoblotting (see 2.2.3 and 2.2.4).

2.1.4 Co-culture of primary mouse hippocampal neurons and BV-2 microglia cells

The co-culture for an IDE secretion assay was prepared by preplating primary mouse hippocampal neurons into 6-well plates (see 2.1.2). After two weeks the neuronal culture was pre-treated with 500 µM 5-HT for 6 hours. Separate cultures of BV-2 cells, where indicated, were also pre-treated with 5-HT receptor antagonists for 6 hours. Then BV-2 cells were collected by trypsination and added to the neuronal cultures ($5x10^5$ per well). After 16 hours, conditioned media were collected and cells harvested and subjected to immunoblotting (see 2.2.3 and 2.2.4).

2.1.5 Co-culture of ES-derived serotonergic neurons and BV-2 microglia cells

The co-culture of ES-derived serotonergic neurons and BV-2 microglia cells was carried out by Thorsten Lau and Konstantin Glebov in the laboratories of Prof. Patrick Schloss at the Central Institute of Mental Health in Mannheim. Neuronal stem cell-derived serotonergic neurons were generated as described previously (Lau, et al., 2010). Briefly, prior differentiation neuronal stem cells were cultured for at least two passages in DMEM supplemented with 10% (v/v) ES cell-qualified fetal bovine serum, 1x MEM non-essential amino acids, penicillin (100 U/ml) and streptomycin (100 µg/ml) and LIF (1000 U/ml). The serotonergic differentiation was induced by addition of 1 mM dibutyryl cAMP and 0.05% (v/v) cyclohexane carboxylic acid. For the co-culture experiments, 20,000 neuronal stem cells/μm^2 were plated on 0.1% (v/v) gelatine-coated 24-well dishes and kept in differentiation medium for 7 days to generate stem cell-derived serotonergic neurons. Next, $8x10^4$ BV-2 cells were seeded into the wells with neurons and a secretion assay was performed (see 2.1.3). After 16 hours conditioned medium and cells were harvested. The following analyses by immunoblotting (see 2.2.2 - 2.2.4) were performed by me in the laboratories of Prof. Jochen Walter.

2.1.6 Amyloid-β (Aβ) and insulin degradation assay

In order to analyse the degradation of Aβ and insulin in the presence of BV-2 microglia cells a secretion assay with Aβ - or insulin-containing medium was carried out. Cells were seeded into 24-well plate 40 hours before the assay (10^5 cells per well, in triplicates). After washing the cells once with sterile PBS, the medium was replaced by 800 µl serum-free DMEM GlutaMAX™ containing 1 µM Aβ or 1 µM insulin, respectively. A time point 0 sample was taken

from extra control cells by harvesting the supernatant of the cells directly after adding the medium to the cells. The time point 0 supernatant was centrifuged (1,000xg, 10 min, 4°C) and frozen at -20°C. After 7 hours conditioned medium was collected and centrifuged (1,000xg, 10 min, 4°C). The cells were lysed (see 2.2.1). Supernatant and cell lysates were subjected to immunoblotting (see 2.2.2 - 2.2.4). Conditioned medium was either directly loaded onto a NuPAGE gel for analysis of Aβ or first concentrated by TCA precipitation (2.2.2). Insulin in the medium was detected by loading TCA-precipitated protein (see 2.2.2) onto a NuPAGE gel (see 2.2.3) and subsequently staining it by Coomassie staining (see 2.2.5).

2.1.7 Calcium measurements

Calcium measurements were kindly carried out by Dr. Ronald Jabs from the Institute of Cellular Neurosciences in Bonn, assisted by Olaf Merkel, Dr. Konstantin Glebov and me (Glebov, et al., 2015). If indicated, the cells were pre-treated with particular receptor antagonists for 16 hours overnight. Then cells were bulk labelled with Fluo-4 by incubation with cell culture medium supplied with 3 μM Fluo-4 AM and 2 mM probenecid for 30 min at 37°C, followed by a 30 min washing period. Subsequent time-lapse recordings were performed with a Confocal Laserscan Microscope (Leica DMI 6000, SP8, Leica) at an excitation wavelength of 488 nm (Haberlandt, et al., 2011). Emission was detected between 500 and 650 nm every 15 sec. Changes in $[Ca^{2+}]_i$, measured as change in fluorescence intensity (ΔF), were offline related to the baseline fluorescence (F0) according to $\Delta F/F0 = (F - F0)/F0$. Ratios were determined in separate regions of interest (ROIs) placed in individual BV-2 cells within the field of view. Data were corrected for photobleaching by estimation of the rate from unaffected cells and subsequent linear compensation. Data analysis was performed with LAS Live Data Mode (Leica) and IgorPro 6 software (WaveMetrix Inc.).

2.1.8 Transient protein knockdown by siRNA transfection

For transient RNA interference the indicated cells were transfected with FlexiTube siRNA (see Table 8) and HiPerFect transfection reagent. In general, siRNA transfection was carried out in 24-well format. Control cells were transfected with an AllStars Negative Control siRNA, a non-silencing siRNA with no homology to any known mammalian gene. The siRNA stock solution (10 μM in water) was diluted 1:10 with water and 25 μl per well were pipetted into the middle of the well. A master mix of 5 μl HiPerFect and 95 μl OptiMEM® per well for all transfections was made and 100 μl pipetted onto the siRNA. For complex formation the mix of siRNA and HiPerFect were incubated for 5-10 minutes at RT. In the meantime, cells were trypsinised and counted. $1x10^5$ cells resuspended in 200 μl DMEM +/+ were seeded per well onto the siRNA complexes. Cells were incubated for 3 hours followed by the addition of 500 μl fresh medium.

After incubation overnight the medium was changed and cells were cultured for further 8 or 32 hours before further analyses.

In double transfections same siRNA concentration for each siRNA was applied, the amount of control siRNA was doubled and parallel single transfections were equalized by adding the same amount of negative control siRNA.

The transfection of cos-7 cells was scaled up to 12-well format. $1x10^5$ cells were seeded per well. Primary rat astrocyte siRNA transfection was scaled up to 6-well format and cells were seeded to 90-95% confluency. BV-2 siRNA transfections were scaled up to 10 cm dish in individual experiments (see 2.2.10).

FlexiTube siRNA	Gene	Cell line
AllStars Negative Control	-	BV-2, cos-7, primary rat astrocytes
Mm_Pdcd6ip_2	ALIX/Pdcd6ip	BV-2
Mm_Pdcd6ip_6	ALIX/Pdcd6ip	BV-2
Mm_Ide_6	IDE	BV-2, primary rat astrocytes
Hs_Ide_6	IDE	Cos-7
Mm_Vps4a_1	Vps4A	BV-2
Mm_Vps4b_4	Vps4B	BV-2, primary rat astrocytes
Hs_Vps4b_6	Vps4B	Cos-7

Table 8. FlexiTube siRNAs (Qiagen)

2.1.9 shRNA-mediated stable protein knockdown in BV-2 microglia cells

In order to generate BV-2 cell lines stably expressing IDE- or Vps4B-specific shRNAs to achieve a stable RNA silencing, lentiviral particles containing shRNA-encoding plasmids were generated for transduction of BV-2 cells. The shRNA-encoding plasmids (see Table 9) were generated from The RNAi Consortium (TRC) and purchased from Dharmacon/GE Healthcare (Freiburg, Germany) or Sigma-Aldrich (Steinheim, Germany).

shRNA	Gene	Mature Antisense	Vector
TRCN0000009487	mouse IDE	TTTGTCTCTCTAATAGCAAGC	pLKO.1-puro
TRCN0000009488	mouse IDE	TAATATGTGGTTTCACGAGGG	pLKO.1-puro
TRCN0000009489	mouse IDE	ATAATAGTGCAACTTTCCTGC	pLKO.1-puro
TRCN0000101415	mouse Vps4B	AACCTAGTAATTGTTTGCAGG	pLKO.1-puro
TRCN0000101416	mouse Vps4B	TACAATGCAGTTAGGATCAGC	pLKO.1-puro
TRCN0000101417	mouse Vps4B	ATCCCACATGGAAACAACTGG	pLKO.1-puro
SHC002	non-target shRNA	TTGGTGCTCTTCATCTTGTTG	pLKO.1-puro

Table 9. TRC lentiviral shRNA

Generation of lentiviral particles

$2.5x10^6$ HEK293 FT cells were seeded to poly-ornithine-coated 15 cm dish (2 per lentiviral construct) and cultured for 16 hours. Medium was changed to 13 ml fresh DMEM +/+ containing 25 μM chloroquine and cells were incubated for 5 min. Then cells were co-transfected with the lentiviral plasmid encoding the respective shRNA, the packaging plasmid Pax2 and the envelope plasmid pMD2.G using 25 μM $CaCl_2$ and 2x HBS buffer as transfection reagents. DNA was precipitated by $CaCl_2$ and 2x HBS buffer and then added dropwise onto the cells. After 16 hours of incubation medium was changed to fresh DMEM +/+, 13 ml per dish. After further 24 hours conditioned medium was collected and stored at 4°C until the next day, fresh DMEM +/+ was added to the cells, again 13 ml per dish. After further 24 hours conditioned medium was again collected, combined with the earlier collected medium and cells were discarded. The collected medium was centrifuged (1,100 rpm, 5 min, 4°C) and the supernatant was filtered through a sterile SFCA membrane (pore size: 0.45 μm). The filtered supernatant was added to a polyethylene glycol 6,000 (PEG 6,000) buffer that was prepared according to Kutner et al. (Kutner, et al., 2009). The suspension was incubated for 90 min at 4°C mixing it every 20 min. After centrifugation (4,000xg, 30 min, 4°C) the supernatant was discarded and the pellet composed of the precipitated lentiviral particles was resuspended in 200 μl virus freezing medium and kept at -80°C until further use.

2x HBS buffer:
280 mM NaCl, 10 mM KCL, 1.5 mM Na_2HPO_4, 50 mM HEPES, 12 mM Glucose, pH 7.00
PEG 6000 buffer:
8.5% PEG 6000, 0.3 M NaCl, 7.76% PBS
Virus freezing medium:
2x HBS buffer, 1% BSA

Transduction of BV-2 cells with lentiviral particles and selection

For transduction of BV-2 cells $7.5x10^5$ cells per well were seeded into 6-well plate or to a 3.5-cm dish. After 24 hours the lentiviral particles prepared from two 15-cm dishes (see above) were added to the cells and the cells were incubated with the lentiviral particles for 16 hours. Then medium was discarded, cells were two times washed with DMEM +/+ and supplied with fresh medium. After 5-6 hours selection was started and cells were incubated with DMEM +/+ containing 8 μg/ml puromycin. Cells were further cultured under selection conditions, knockdown was tested by Western immunoblotting (see 2.2.4).

2.1.10 Immunocytochemistry (ICC)

For fluorescence imaging, cells were seeded onto sterile cover slips in respective culture dishes that were coated with poly-L-lysine (poly-L-lysine for 1h at 37°C, three times washed with sterile PBS, one time washed with DMEM). After 24 hours, the cells were washed once

with pre-warmed (37°C) PBS and then fixed using pre-warmed (37°C) 4% paraformaldehyde (PFA) solution for 10 min. Afterwards, the cells were washed two times with PBS to remove residual PFA. The cells were then permeabilized with Triton X-100 solution for 2 min and thereafter incubated with BSA blocking solution for 1 hour at RT. To stain the proteins of interest, the cells were subsequently incubated with the primary antibody (Table 3), which was diluted in antibody solution (100 µl per cover slip), for 1 hour at RT or over-night at 4°C. The cells were washed three times with washing solution and kept in washing solution for 5 min. After repeating the washing step twice the cells were incubated with the secondary antibody conjugated with a fluorescent dye (Table 4, diluted in antibody solution) for 1 hour at RT in the dark. Parallel incubation with DAPI and phalloidin Alexa Fluor® 647 were used to stain the nuclei and F-actin, respectively. Residual antibody was removed by the three washing steps as described above. Then cells were washed three times with PBS, incubated with PBS for 5 min and subsequently washed one time with distilled water. The water was removed and the cover slips were embedded on a microscope slide using Immu-mount™ and afterwards kept in the dark at 4°C. Fluorescence imaging was carried out using a fluorescence microscope (Axio Vert 200, Carl Zeiss) with the ZEN analysis software.

PBS:
137 mM NaCl, 2.7 mM KCl, 10 mM Na_2HPO_4, 1.8 mM KH_2PO_4. pH 7.4
Poly-L-lysine solution:
100 µg/ml sterile poly-L-lysine in PBS
PFA solution:
4% paraformaldehyde in PBS (w/v)
Triton X-100 solution:
0.25% Triton X-100 in PBS
Washing solution:
0.125% Triton X-100 in PBS
BSA blocking solution:
2.5% BSA in washing solution
Antibody solution:
1.25% BSA in washing solution

2.2 Protein biochemical techniques

2.2.1 Cell lysis and protein extraction

Cells were lysed by adding ice-cold RIPA lysis buffer containing 1x-concentrated protease inhibitor (PI) cocktail. After 10-15 min incubation on ice, the lysate was homogenised by pipetting and then transferred to a micro reaction tube. Insoluble and particulate material was removed by centrifugation (13,200xg, 2 min, 4°C). The resulting supernatant was subjected to protein estimation with the Pierce™ BCA Protein Assay Kit according to the manufacturer's instructions. Cell lysates were stored at -20°C until further use. 20-35 µg protein or the same volume of lysate for each condition and replicate was loaded to a polyacrylamide gel for protein separation (see 2.2.3).

RIPA lysis buffer:
50 mM Tris, 150 mM NaCl, 1 mM EDTA, 0.1% SDS, 1% Triton X-100, 1% Na-deoxycholat, pH 7.5
25x Protease inhibitor cocktail:
1 cOmplete™ tablet dissolved in 2 ml deionized H_2O

2.2.2 Protein precipitation by trichloroacetic acid (TCA)

Conditioned media were collected and centrifuged (1,000xg, 10 min, 4°C) to remove dead and detached cells. Then DOC was added to the medium to a final concentration of 0.02% (v/v). The solution was mixed by inverting the tube and incubated for 15 min on ice. Thereafter, TCA solution was added to a final concentration of 10% (v/v). The solution was mixed by inverting the tube and kept on ice. After 60 min the precipitate was pelleted by centrifugation (13,200xg, 10 min, 4°C) and the supernatant discarded. To collect and remove residual TCA from the protein pellet an additional centrifugation step was carried out (13,200xg, 2 min, 4°C). The pellet was dried completely at RT or 37°C, dissolved in Tris/SDS buffer and kept at -20°C until further use or directly loaded to a gel for protein separation (see 2.2.3).

DOC solution:
2% sodium deoxycholic acid in deionized water (w/v)
TCA solution:
100% TCA in deionized water (w/v)
Tris/SDS buffer:
50 mM Tris, 1% SDS in deionized water

2.2.3 Protein separation by SDS polyacrylamide gel electrophoresis (SDS-PAGE) / NuPAGE

SDS-PAGE was used to separate proteins according to their molecular weight. For polyacrylamide gels, a lower separation gel was casted and allowed to polymerize. Then, the upper stacking gel was casted, which is necessary for concentration of the proteins before entering the separation gel. In general, the percentage of the acrylamide/bisacrylamide determining the pore size of the gel was chosen 10% for the separation gel and 4% for the stacking gel (see Table 10). The solution of the separation gel was cast into a gel cassette and covered with a layer of 70% ethanol to remove bubbles and to prevent dehydration. After polymerization the ethanol was removed and the solution of the stacking gel was added. To create wells for later sample loading, a comb was immediately inserted. After complete polymerization, the gel-containing cassette was inserted into a gel electrophoresis chamber. The chamber is filled with running buffer and the comb is carefully removed from the stacking gel and the wells are rinsed with running buffer. Before loading, the samples were denatured by boiling with SDS loading buffer at 95°C for 5 min. Additionally to the protein samples, the protein standard PageRuler Prestained was loaded into one well of the gel. Electrophoresis was performed with constant voltage at 100-120 V.

Alternatively, especially for detection of smaller proteins like Aβ, insulin and proteins in conditioned medium, pre-casted NuPAGE® 4-12% Bis-Tris gradient gels were used. The samples were prepared according to the manufacturer's instructions with 4x LDS buffer and 1 M DTT. As protein standard, here, the SeeBlue® prestained standard was used. Electrophoresis was performed with constant voltage at 150-200 V.

	4% stacking gel	10% separation gel
Deionized H_2O	3.25 ml	8.3 ml
Acrylamide/bisacrylamide 30 (37.5:1)	700 µl	6.7 ml
Upper Tris	1.25 ml	-
Lower Tris	-	5 ml
10% APS	20 µl	50 µl
TEMED	20 µl	50 µl

Table 10. Composition of SDS-PAGE gels

Stacking gel buffer (4 x) (Upper Tris):
500 mM Tris, 0.4% SDS, deionized H_2O, pH 6.8
Separation gel buffer (4 x) (Lower Tris):
1.5 M Tris, 0.4 %SDS, deionized H_2O, pH 8.8
Ammonium persulfate (APS, Sigma):
10% Ammonium persulfate in deionized H_2O
Running buffer:
25 mM Tris, 200 mM Glycine, 0.1% SDS in deionized H_2O
SDS Loading dye (5 x):
25% Upper Tris, 0.34 M SDS, 0.1 M DTT, 50% glycerol, bromphenol blue, with deionized H_2O to 10 ml

2.2.4 Western immunoblotting (WB) and ECL/Infrared (IR) imaging

After protein separation by SDS-PAGE or NuPAGE® the gel was usually subjected to WB for protein detection. Gels and nitrocellulose or PVDF membrane were equilibrated in transfer buffer. PVDF membranes were additionally incubated with methanol. The gel was placed on top of the membrane and both were enclosed by two filter papers on each side. This stack was tightly clamped together and put into a tank blotting chamber connected to a cooling system. The proteins were transferred to the membrane for 1.5-2 hours at constant current of 400 mA. After the transfer, the gel was discarded and the membrane was washed once in deionized water. Transferred proteins were stained with Ponceau S solution for 1 min followed by washing with deionized water. This step was skipped for protein detection by IR imaging.
For protein detection by ECL imaging the membrane was blocked with 5% milk in PBST for 1 hour. After washing the membrane shortly several times with PBST it was incubated in primary antibody diluted in PBST overnight at 4°C or for 2 hours at RT (for primary antibodies and dilution factors see Table 3). Now the membrane was washed three times with PBST for

at least 5 min each time followed by incubation with HRP-conjugated secondary antibody diluted in PBST for 1 hour at RT (for secondary antibodies and dilution factors see Table 4). The membrane was then washed again three times. Where indicated, the incubation with a biotinylated instead of HRP-conjugated secondary antibody was carried out to achieve an additional signal enhancement. After three washing steps the membrane was then incubated with Streptavidin-HRP polymer diluted in PBST for 1 hour at RT, again followed by three washing steps. For protein detection the membrane was incubated with ECL solution for 5 min and chemiluminescence was detected by an ECL imager from BioRad. In case of weak signals the membrane was developed again using ECL SELECT from GE Healthcare according to the manufacturer's instructions to enhance the signal.

Alternatively, proteins were detected by IR imaging. In comparison to ECL imaging the membrane was here blocked with Odyssey® blocking buffer (PBS) 1:1 diluted with PBS and incubated with fluorescently IRDye®-labeled instead of HRP-conjugated secondary antibodies. IR fluorescence was detected by an IR imager of LI-COR.

Protein signals were quantified using densitometric analysis using Quantity One® or Image Studio™ Lite software.

Transfer buffer:
5 mM Tris, 200 mM Glycine, 10% methanol, filled up with deionized H_2O
Ponceau S solution:
2% (w/v) Ponceau S, 30% TCA (w/v) in deionized H_2O
PBS: (2.1.10)
PBST:
0.1% Tween-20 in PBS
Milk blocking solution:
5% milk powder in PBST
ECL solution:
immediately before use mix A and B 1:1
A: 0.1 M Tris pH 8.5, 0.4 mM cumaric acid, 0.25 mM luminol, filled up with deionized H_2O
B: 0.1 M Tris pH 8.5, 0.018 % H_2O_2, filled up with deionized H_2O

2.2.5 Coomassie staining of polyacrylamide gel and IR imaging

Alternatively to WB, proteins could also be detected by direct Coomassie staining of the polyacrylamide gel after SDS-PAGE or NuPAGE®. The gel was incubated with Coomassie staining solution for 30-45 min with gentle shaking. Afterwards the gel was incubated for additional 2-4 hours with destaining solution to remove excess Coomassie from the gel. Coomassie-stained proteins were detected by using the red channel of the IR imager Odyssey® CLx.

Coomassie staining solution:
0.5% Coomassie brilliant-blue R-250 (w/v), 45% isopropanol (v/v), 10% acetic acid (v/v), filled up with deionized H_2O
Destaining solution:
45% methanol (v/v), 10% acetic acid, filled up with deionized H_2O

2.2.6 Co-immunoprecipitation (Co-IP)

After washing once with ice-cold PBS, cells were lysed directly in the cell culture dish with 1 ml IP lysis buffer supplemented with 1x-concentrated protease inhibitor cocktail (see earlier) per 10cm-dish. After 30 min incubation on ice, the cell lysate was homogenised by pipetting and transferred to a micro reaction tube. Using the Pierce™ BCA protein assay kit the protein amount of the cell lysates was determined. An aliquot containing 1 mg protein was incubated with 1-3 µg of the specific antibody and 50 µl of a slurry containing protein A or G sepharose beads overnight at 4°C constantly being inverted. Protein A sepharose was used in combination with rabbit IgG and protein G sepharose in combination with mouse IgG. A control containing only cell lysate and sepharose beads without specific antibody was run in parallel. Subsequently, the beads were pelleted by centrifugation (6,000xg, 2 min, 4°C). The supernatant was discarded and the beads were sucked dry with a syringe needle. The beads were washed by adding 400 µl ice-cold IP lysis buffer and inverting the tube for 5 min at 4°C. Then the beads were pelleted again by centrifugation (6,000xg, 2 min, 4°C) and the supernatant was discarded and the beads sucked dry with a syringe needle. That washing step was repeated twice. The samples were boiled for 10 min with 15 µl of 2x NuPAGE® LDS sample buffer and 1.5 µl 1 M DTT at 70°C and loaded on a NuPAGE® 4-12% Bis-Tris gel for protein separation and subsequent WB analysis (see 2.2.3 and 2.2.4).

IP lysis buffer:
150 mM NaCl, 20 mµ NaF, 10 mM Tris, 1 mM EDTA, 1 mM EGTA, 200 µM Na_3VO_4, 1% Triton X-100, 0.5% Igepal CA-B30, pH 7.4
PBS: (2.1.10)

2.2.7 Expression and purification of Maltose-binding protein (MBP) fusion proteins

For the expression of the Vps4B-MBP fusion protein in E. coli, 400 ml LB medium containing 100 µg/ml ampicillin were inoculated with an 20 ml-overnight culture of bacteria transformed with a Vps4B-MBP construct (see Table 14). The culture was grown at 37°C to an OD_{600} of 0.5-0.6. Before addition of 0.5 mM IPTG to induce the expression of the fusion protein, an aliquot of 200 µl was taken, pelleted and stored at -20°C until further use. After 4 hours of shaking a further aliquot was taken (see above) and the cells were pelleted by centrifugation (3,220xg, 15 min, 4°C). The pellet was resuspended in 10 ml column buffer and incubated for 30 min on ice after addition of lysozyme (5 mg/ml). The suspension was transferred to centrifuge tubes and sonicated 5 times with a pulse at an intensity of 50% for 30 sec. After taking another aliquot (see above) cell debris and insoluble fragments were removed by centrifugation (10,000xg, 30 min, 4°C). The pellet was stored at -20°C and the supernatant containing the fusion protein was transferred to a new tube. Another aliquot was taken (see above) and then the solution was filled up to 45 ml using column buffer. Amylose resin (2 ml

slurry) that binds to MBP was washed 3-4 times with 10 ml column buffer and resuspended in 5 ml fresh column buffer before addition to the protein solution. Both were incubated under constant inversion for 1 hour at 4°C. The amylose resin was pelleted by centrifugation (2,000xg, 5 min, 4°C) and the supernatant was discarded after taking a further aliquot (see above). The amylose resin was resuspended in column buffer and washed 5 times with the just described procedure. The amylose resin was resuspended in 5 ml column buffer and carefully added to a poly-prep chromatography column. The resin was again washed with 5 ml column buffer on the column, taking an aliquot of the flow-through in-between. Finally, the fusion protein was eluted from the resin beads by adding 10 ml elution buffer to the column and collecting 10 fractions of 1 ml each. The protein concentration of the fractions was determined using the Bradford assay (20 µl sample or standard, Bradford Reagent 1:5 diluted – 200 µl per well, extinction at 595 nm) and the purity was controlled by Coomassie staining (see 2.2.5).

Column buffer:
20 mM tris, 200 mM NaCl, 1 mM EDTA, pH 7.4
Elution buffer:
10 mM maltose in column buffer

2.2.8 Blue Native (BN) PAGE and subsequent SDS/Urea PAGE in the 2nd dimension

In order to detect protein complexes, blue native (BN) PAGE was performed to separate proteins according to their molecular weight under non-denaturing and non-reduced conditions. Cells were harvested by trypsination, pelleted and washed once with PBS. Cell pellets were then resuspended in sucrose buffer supplemented with 1x-concentrated PI cocktail adding 2 µl sucrose buffer / mg cells (wet weight). The cells were subjected to ultrasonic for lysis constantly kept on ice: one pulse at an intensity of 50% for 5 sec and two pulses at an intensity of 30% for 5 sec. The lysates were then centrifuged (13,200xg, 30 min, 4°C) and the pellets discarded. After BCA protein estimation, the supernatant was supplemented with ACA buffer and loading buffer and kept on ice or at 4°C. Depending on the sample volume, one volume of ACA buffer is added to two volumes of the sample, completed by addition of one tenth of the final volume of loading buffer. 80 µg of protein were loaded on a BN PAGE described by Wittig and colleagues (Wittig, et al., 2006) consisting of a 4% stacking gel on top of a 5 or 7.5% separation gel. The gels were casted as described earlier (see 2.2.3) with the BN PAGE-specific buffers listed in Table 11. Parallel to the samples 5-8 µl Native Mark Unstained protein standard were loaded. Gel electrophoresis was started with dark blue cathode buffer in the inner chamber and anode buffer in the outer chamber using the following settings: constant 10 mA, 500 V. After the running front had passed the lower edge of the wells and the samples completely entered the separation gel of the stacking gel (circa after 20 min)

the cathode buffer was changed completely to clear cathode buffer without Coomassie G-250 and run further until the blue dye front left the separation gel. Subsequently, the gel was reduced slowly shaking in reducing buffer for 15 min and washed afterwards four times with transfer buffer. Then the gel was subjected to WB (see 2.2.4). For the transfer exclusively PVDF membranes were used. After the transfer the membranes were destained with methanol for 1-2 minutes to get rid of Coomassie. The protein standard can be stained via Ponceau S staining (see 2.2.4). Protein detection was carried out via ECL imaging (see 2.2.4).

	stacking gel	separation gel	
	4%	5%	7.5%
Deionized H_2O	3.23 ml	12.83 ml	10.5 ml
Acrylamide/bisacrylamide 30 (37.5:1)	887 µl	4.67 ml	7 ml
6x Gel buffer	833 µl	3.5 ml	3.5 ml
10% APS	50 µl	80 µl	80 µl
TEMED	5 µl	20 µl	20 µl

Table 11. Composition of BN PAGE gels

Instead of WB additionally a subsequent SDS/Urea PAGE in the 2nd dimension was run from single lanes of the native PAGE. After reducing the gel (see above) it was washed several times with equilibration buffer instead of transfer buffer to remove β-mercapto ethanol. Now single lanes were cut from the gel and marked for their orientation. If not used immediately the gel lane could be frozen at -20°C at this point. The single gel lane was put into a gel cassette in horizontal orientation with decreasing protein size from left to right. A 10% SDS/urea separating gel was cast into the cassette underneath the gel lane. After polymerization a 4% SDS/urea stacking gel was cast around the gel lane also leaving a well to load a protein standard (PageRuler prestained). The gel recipe is given in Table 12. Gel electrophoresis was performed at constant voltage of 100-120 V until the blue running front left the gel and followed by WB (see 2.2.4).

	4% stacking gel	10% separation gel
8 M Urea	3.25 ml	8.3 ml
Acrylamide/bisacrylamide 30 (37.5:1)	700 µl	6.7 ml
Lower Tris	-	5 ml
Upper Tris	1.25 ml	-
10% APS	20 µl	50 µl
TEMED	20 µl	50 µl

Table 12. Composition of SDS/urea PAGE gels.

Sucrose buffer:
250 mM sucrose, 10 mM HEPES, 1.5 mM $MgCl_2$, 10 mM KCl, pH 7.0
25x PI cocktail:
(2.2.1)
ACA buffer:
750 mM ε-amino-caproic acid, 50 mM bis-tris, 0.5 mM EDTA, pH 7.0
Loading buffer:
750 mM ε-amino-caproic acid, 5% Coomassie G-250
6x Gel buffer:
3 M ε-amino-caproic acid, 0.3 M bis-tris
Cathode buffer:
50 mM tricine, 15 mM bis-tris, pH 7.0
Dark blue cathode buffer:
0.2% Coomassie G-250 in cathode buffer
Anode buffer:
50mM bis-tris, pH 7.0
Reducing buffer:
1% SDS (v/v), 1% β-mercapto ethanol (v/v) in deionized H_2O
Transfer buffer:
(2.2.4)
Lower and Upper Tris:
(2.2.3)
Equilibration buffer:
50 mM tris, 1% SDS (w/v), pH 6.8

2.2.9 Exosome preparation by differential centrifugation and fractionation by density gradient centrifugation

Exosomes from conditioned medium of cells were isolated by differential centrifugation, according to Théry and colleagues (Théry, et al., 2006) and Xu and colleagues (Xu, et al., 2015). To remove detached cells the medium was centrifuged at 300xg for 10 min. The supernatant was then centrifuged at 2,000xg and 4°C for 20 min to get rid of dead cells and cell debris. Subsequently the supernatant was centrifuged at 10,000xg for 30 min. The resultant pellet (P10) containing microvesicles was kept and resuspended in RIPA lysis buffer. As a final step the supernatant was now subjected to ultracentrifugation at 100,000xg for 1 hour to sediment exosomes. The resultant pellet (P100) was resuspended in RIPA lysis buffer. All centrifugation steps were carried out at 4°C and after every centrifugation step a 1.4 ml aliquot of the supernatant was taken (S03, S2, S10 and S100) and subjected to TCA precipitation (see 2.2.2). Pellets, medium aliquots and cell lysates were analysed by subsequent WB analysis (see 2.2.3 - 2.2.4).

For further fractionation, the exosome-containing P100 pellet was resuspended in 100 µl 6% OptiPrep™/DMEM GlutaMAX™ and subjected to density gradient centrifugation. The density gradient was prepared using OptiPrep™, a 60% iodixanol solution, and DMEM GlutaMAX™ as diluent. The following solutions were layered one on top of the next with decreasing density from bottom to top, each of 1 ml volume: 6; 9.8; 13.6; 17.4; 21.2; 25; 28.8; 32.6; 36.4; 40.2 (v/v iodixanol). The exosome pellet was loaded on top of the gradient and centrifugation was carried out for 16 hours at 100,000xg at 4°C. Fractions of 1 ml each were collected after

centrifugation and proteins precipitated with TCA (see 2.2.2) before WB analysis (see 2.2.3 - 2.2.4). Centrifugation and ultracentrifugation at 10,000xg and 100,000xg was carried out using an Optima™ XPN-80 with the swinging bucket rotor SW41Ti for volumes till 11 ml and the fixed angle rotor 45Ti for volumes of 35-70 ml.

2.2.10 Cell fractionation by differential centrifugation

Cytosolic, membrane and nuclear fractions were separated by differential centrifugation. Cells were subjected to osmotic lysis by adding 500 µl hypotonic buffer supplemented with 1x-concentrated PI cocktail. After 15-20 min incubation on ice, the cell lysate was transferred to a micro reaction tube and homogenised by passing the lysate 15 times through a 1-ml syringe needle (23G). After centrifugation at 1,000xg and 4°C for 5 min, the pellet containing the nuclear fraction was frozen at -20°C until further use for preparation of the nuclear fraction. The resultant post nuclear supernatant (PNS) was centrifuged at 13,200xg and 4°C for 1 hour to obtain the membrane pellet. The supernatant was transferred to a new tube and kept as the cytosolic fraction. The membrane pellet was resuspended in 50 µl RIPA lysis buffer, incubated on ice for 10 min and then centrifuged at 13,200xg and 4°C for 15 min. The resultant supernatant was kept as the membrane fraction. The nuclear pellet (see above) could now be resuspended in 100 µl buffer C, incubated on ice for 20 min, mixed from time to time, and then centrifuged at 13,200xg and 4°C for 15 min. The resultant supernatant was kept as nuclear fraction. Using the Pierce™ BCA protein assay kit the protein in cytosolic and membrane fraction were determined and 20 µg of each fraction and corresponding volumes of the nuclear fraction were loaded on a SDS PAGE gel and subjected to WB analysis (see 2.2.3 - 2.2.4).

Hypotonic buffer:
10 mM tris (pH 7.5), 10 mM NaCl, 0.1 mM EGTA
25x PI cocktail: (2.2.1)
RIPA lysis buffer: (2.2.1)
Buffer C:
25 % glycerol (v/v), 20 mM HEPES (pH 7.9), 0.5 M NaCl, 1 mM EGTA, 1 mM EDTA (pH 8.0), 25 mM β-glycerophosphate

2.2.11 Subcellular fractionation of intracellular vesicles by density gradient centrifugation

In order to analyse the subcellular distribution of proteins in more detail, the PNS of cell lysates (see above) was subjected to density gradient centrifugation to fractionate intracellular vesicles and organelles. BV-2 cells were lysed with 750 µl hypotonic buffer as described earlier (see 2.2.10). A density gradient was prepared using OptiPrep™, a 60% iodixanol solution, and diluent buffer. The following percentage solutions (%, v/v) were carefully layered one on top of the next with decreasing density from bottom to top, each of 1.2 ml volume:

siRNA experiments:	2.5	5.0	7.5	12.5	15.0	17.5	20.0	30.0	50.0
shRNA experiments:	2.5	5.0	7.5	10.0	12.5	15.0	17.5	20.0	30.0

500 µl of the PNS were loaded on top of the gradient and centrifugation at 100,000xg and 4°C for 16 hours was carried out using an Optima™ XPN-80 with the swing bucket rotor SW41Ti. After centrifugation, 13 fractions of 750 µl each and a 14th last fraction of 1.5 ml were collected from top to bottom of the gradient. Proteins were concentrated via TCA precipitation (see 2.2.2) before the fractions were subjected to WB analysis (see 2.2.3 - 2.2.4).

Diluent buffer:
0.25 mM sucrose, 6 mM EDTA, 60 mM HEPES, pH 7.4

2.3 Molecular biological techniques

2.3.1 RNA isolation from eukaryotic cells and cDNA synthesis by reverse transcription (RT)

Total RNA was extracted from BV-2 cells using the RNeasy® Mini Kit according to the manufacturer´s instructions. The cells were harvested by trypsination or by scraping in PBS using a cell scraper. The pelleted cells were either frozen at -80°C until further use or directly lysed by adding appropriate amount of a guanidine thiocyanate-containing buffer supplemented with β-mercapto ethanol. Homogenisation was carried out by passing the cell suspension 5 times through a syringe needle (20G) and the RNA was isolated using an RNA-binding silica-based membrane. The membrane specifically binds RNA of more than 200 nucleotides in length thereby allowing the enrichment of mRNAs. RNA was eluted with deionized RNAse-free water and stored at -80°C.
Before reverse transcription of RNA samples to get cDNA, endogenous genomic DNA was removed by digestion with DNase I. 2 µg RNA were incubated with 1 U DNase I in 1x-concentrated DNase reaction buffer for 20 min at 37°C. The reaction was stopped by heat inactivation at 75°C for 10 min. Subsequently, the RNA was reverse-transcribed with the SuperScript® III First-Strand Synthesis System using random hexamer primers according to the manufacturer´s instructions in a volume of 25 µl. The RNA was incubated with hexameric primers at 25°C for 10 min. Then mixed deoxyribose nucleoside triphosphates (dNTPs), $MgCl_2$, DTT, RNase inhibitor and the SuperScript III were added and cDNA synthesis reaction was carried out at 50°C for 50 min and terminated by heat inactivation of the reverse transcriptase at 85°C for 5 min. cDNA was stored at -20°C and aliquots of 1 µl cDNA were subjected to PCR as template DNA for cloning or expression analysis (see 2.3.2).

2.3.2 Polymerase chain reaction (PCR)

DNA sequences were amplified by polymerase chain reaction (PCR). In order to subclone certain DNA sequences obtained by reverse transcription of mRNA from eukaryotic cells (see 2.3.1), *Pfu* DNA polymerase was as added together with appropriate primers (see Table 13) that contain the respective restriction sites. A PCR master mix solution containing dNTPs, forward (fw) and reverse (rev) primer, cDNA as template and *Pfu* polymerase was prepared:

10x *Pfu* buffer (with $MgSO_4$)	5 µl	cDNA (~80 ng)	1 µl
dNTPs (0.2 mM each)	5 µl	*Pfu* polymerase (2-3 U/µl)	1 µl
fw primer (0.1 µM)	1 µl	DNase-free H_2O	to 50 µl
rev primer (0.1 µM)	1 µl		

Basic PCR program:

1. Initial denaturation	95°C, 3 min
2. Denaturation	95°C, 30 sec
3. Annealing	variable, 30 sec
4. Elongation	72°C, 2 min/kbp
5. Final elongation	72°C, 5 min
repetition step 2-4	25-30 times

The PCR program varied according to the melting temperature of the primers and the length of the target DNA that is to be amplified. Briefly, the DNA strands were denatured, fw and rev primer were annealed to the DNA according to the annealing temperatures listed in Table 13 and elongated (2 min/kilo base pair (kbp)) by the *Pfu* polymerase to create a new DNA strand. Denaturation, annealing and elongation were repeated for 25-30 times to amplify the DNA fragment.

PCR products were separated by agarose gel electrophoresis. PCR samples were mixed with OrangeG loading dye and loaded on gels (1-1.5% agarose in TBE buffer) containing GelRed™ (2 µl/100 ml). After electrophoresis, DNA was visualised using UV light which induces fluorescence of the DNA-intercalating GelRed™. The fluorescence was detected by an imager from BioRad.

Other PCR applications, including a colony screen after cloning or expression analysis were carried out using *Taq* DNA polymerase and a 5x master mix from NEB. For colony screen PCR, a 12.5 µl PCR master mix was prepared containing 1x-concentrated NEB *Taq* master mix and 0.1 µM of each fw and rev primers. As DNA template 1 µl of bacterial culture for each tested colony (see 2.3.3) was used. The program described above was varied for elongation

time to 1 min/kbp for *Taq* polymerase in comparison to *Pfu* polymerase. For expression analysis a 25 µl PCR master mix was prepared and cDNA transcribed from isolated RNA (see 2.3.1) of BV-2 cells was used as template for the reaction.

TBE buffer:
89 mM tris, 89 mM boric acid, 2 mM EDTA, pH 8.0
6x OrangeG loading dye:
60% glycerin, 0.15 % OrangeG, 60 mM EDTA, 10 mM tris, pH 7.6

Name	Primer Sequence	Annealing temperature
IDE Bait	**fw:** AAA GAA TTC TTC ATC ATC CAG TCA GAA AAA CC **rev:** TTT GGA TCC GAG TTT TGC AGC CAT GAA GTT	59°C
Vps4B-Flag	**fw:** AAA GAA TTC ATG GCG TCC ACG AAC ACC AAC CTG CAG AAA **rev:** TTT GGA TCC TTA CTT ATC GTC ATC GTC TTT GTA ATC GCC TTC CTG GCC AAA	55°C
Vps4B-MBP	**fw:** AAA GAA TTC ATG GCG TCC ACG AAC ACC **rev:** GGA TCC TTA GCC TTC CTG GCC AAA ATC	55°C
Vps4B-mCherry	**fw:** AAA GAA TTC ATG GCG TCC ACG AAC ACC **rev:** TTT GGA TCC TTG CCT TCC TGG CCA AAA TC	60°C

Table 13. Cloning primers and primers for expression analysis

2.3.3 Cloning of expression plasmids

PCR products, further referred to as insert, and the respective vector were digested with the restriction enzymes EcoRI and BamHI for 2 hours at 37°C (2 U each enzyme/1 µg DNA in 1x EcoRI buffer or 2 U BamHI + 4 U EcoRI/1 µg DNA in BamHI buffer). In parallel a positive control digestion was carried out to check for successful restriction. Following restriction, vectors were dephosphorylated by addition of 1 U of FastAP thermosensitive alkaline phosphatase for 10 min at 37°C. Insert, vector and positive control were separated on an agarose gel and visualised by UV light. The restricted vector and insert were cut out of the gel and purified with the WIZARD® SV Gel and PCR Clean Up System according to the manufacturer's instructions. The purified insert and vector were mixed in a molar ratio of 3:1 to 8:1 and ligated by T4 DNA ligase (50-100 ng vector, respective amount of insert, 1x T4 ligase buffer, 2 U T4 ligase) for 30 min at RT. A ligation control was performed in parallel containing only vector (without insert DNA). Directly after ligation, chemically competent *E.coli* (TOP10) cells were transformed. The bacteria were thawed and then incubated with the ligated DNA for 20 min on ice. To allow efficient DNA uptake, a heat shock at 42°C for 45 sec was

performed followed by incubation on ice for 2 min. 950 µl SOC medium was added to the bacteria and they were shaken for 1-1.5 hour at 37°C. After pelleting the bacteria for 1 min at 3,000xg they were resuspended in 30-50 µl SOC medium and spread to an LB agar plate containing the appropriate antibiotics.

The plates were incubated at 37°C overnight and growing colonies were subsequently tested for the particular DNA fragment using colony screen PCR. For this the colonies were picked into 200 µl antibiotics-containing SOC medium and shaken for 3-5 hours at 37°C. 1 µl of these bacterial cultures was used as template for colony screen PCR (see 2.3.2). In parallel a positive and negative control were run. Positive clones showing a signal in the PCR were sequenced by an external company to control for mutations and exact sequence. In some cases, an additional control digestion with the appropriate restriction enzymes was performed before the DNA sequencing.

Name of construct	NCBI accession number	Vector	Restriction enzymes
IDE Bait	NM_031156.3 CDS position (bp): 2568-3083	pGBKT7	EcoRI/BamHI
Vps4B-Flag	NM_009190.2	pcDNA 3.1 (-)	EcoRI/BamHI
Vps4B-MBP	NM_009190.2	pMal-c2	EcoRI/BamHI
Vps4B-mCherry	NM_009190.2	pmCherry-N1	EcoRI/BamHI

Table 14. Generated constructs.

2.3.4 Purification of plasmid DNA from E. coli

Purification of small amounts of plasmid DNA (< 40 µg) from E.coli was carried out using the NucleoSpin® Plasmid EasyPure kit according to the manufacturer's instructions taking bacteria of a 2 ml overnight culture in LB medium with the appropriate antibiotics. For isolation of higher amounts of plasmid DNA (0.5-1.5 mg) the NucleoBond® Xtra Maxi kit was used according to the manufacturer's instructions taking bacteria of a 250 ml overnight culture in LB medium with the appropriate antibiotics. In both kits the pelleted bacteria were resuspended and incubated with lysis and neutralisation buffer. Subsequently, the suspension was cleared from precipitated proteins and cell debris by centrifugation and loaded onto a DNA-binding column. After elution from the column the DNA was either ready to use (NucleoSpin® Plasmid EasyPure kit) or was once again precipitated by isopropanol and washed with 70% ethanol to get a higher purity (NucleoBond® Xtra Maxi kit).

2.3.5 Yeast two-hybrid (Y2H) – protein interaction studies

All Y2H experiments were carried out using Matchmaker™ Gold Yeast Two-Hybrid System, Yeastmaker™ Yeast Transformation System 2 and the Easy Yeast Plasmid Isolation kit. The bacterial and yeast strains as well as plasmids used in this study are listed in Table 15.

Strain or plasmid	relevant characteristics
S. cerevisiae	
Y2H Gold	*HIS3*, *ADE2*, *AUR1-C*, *MEL1*
Y187	*MEL1*, *lacZ*
E. coli	
TOP10	chemically competent cells
Plasmids	
pGBKT7	*Gal4*-DBD, *TRP1*, Kan^r
pGADT7	*Gal4*-AD, *LEU2*, Amp^r
pGBKT7-p53	pGBKT7 derivative containing DBD-p53
pGBKT7-Lam	pGBKT7 derivative containing DBD-Laminin
pGADT7-T	pGADT7 derivative containing AD-SV40 large T-antigen
IDE bait	pGBKT7 derivative containing DBD-IDE bait

Table 15. Yeast strains and plasmids used in Y2H studies

Principle:

The bait protein is expressed as a fusion protein with the Gal4 DNA-binding domain (DNA-BD) by cloning into the plasmid pGBKT7, the prey proteins are fused to the Gal4 activation domain (AD) by cloning into pGADT7. The general principle was described by Stanley Fields and colleagues (Fields & Song, 1989; Chien, et al., 1991). Interaction of bait and prey protein leads to transcription activation of four reporter genes (shown in Figure 5) enabling the yeast to grow in the respective selection medium (see also Figure 5).

AUR1-C AUR1-C expression provides resistance to Aureobasidin A.

HIS3 HIS3 expression enables the cell to synthesize the essential amino acid histidine.

ADE2 Ade2 expression enables the cell to synthesize the essential adenine.

MEL1 Enables the cell to hydrolyse X-α-Gal and produce a blue precipitate.

Furthermore, the used plasmids also encode for *TRP1* (pGBKT7) and *LEU2* (pGADT7) enabling the cell transformed with the respective vector to synthesize tryptophan or leucine and grow in the respective selection medium.

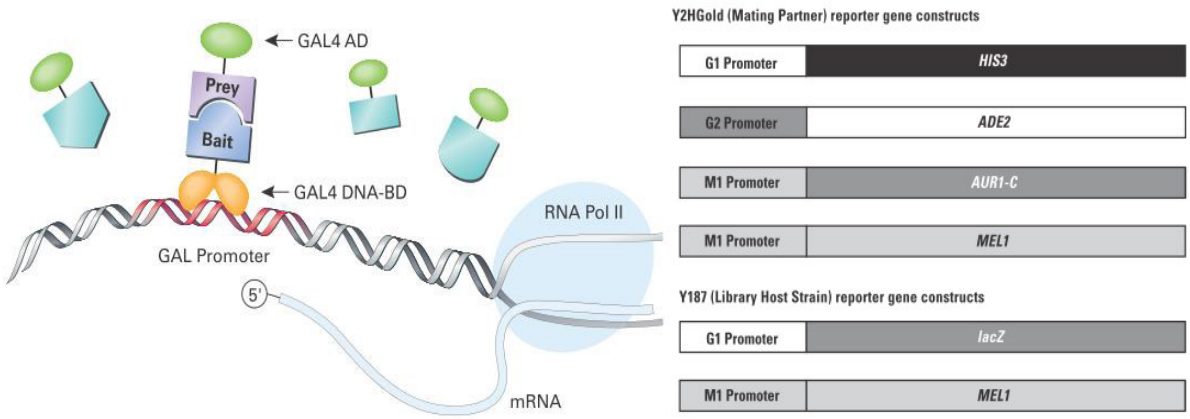

Figure 5. Principle of Matchmaker™ Gold Y2H System: General principle of Y2H (left), reporter gene constructs in Matchmaker yeast strains Y2H Gold and Y187 (right). Source: Matchmaker™ Gold Y2H System User Manual.

cDNA library screen:

A mouse brain Mate & Plate™ cDNA library was purchased from Takara Clontech. The library is cloned into a Gal4 AD vector and transformed into the yeast strain Y187, furthermore, it is normalized by selectively removing transcripts with high frequency to increase the proportion of low abundant transcripts. Y2H Gold transformed with the created IDE bait construct (see Table 14) were generated using the Yeast Transformation System 2 following the manufacturer's instructions. Y187 expressing the cDNA library and the IDE bait-expressing Y2H Gold were mated following the instructions of the Matchmaker™ Y2H Gold kit. Briefly, the IDE bait-containing Y2H Gold and the cDNA library-containing Y187 were cultured together under rich medium condition, which induces spontaneous mating (Merlini, et al., 2013) traceable by the formation of diploid zygotes with a typical 3-lobed shape (see Figure 6). Subsequently a dilution of the mated cells was streaked out on single (SD) and double dropout (DDO) agar plates lacking the essential amino acids leucine and tryptophan, respectively, to determine the mating efficiency. The rest of the mating culture was plated on DDO agar plates additionally containing X-α-Gal and Aureobasidin A (DDO/X/A). Blue colonies were picked, plated on quadruple dropout agar plates (QDO/-Trp/-Leu/-His/-Ade) containing X-α-Gal and Aureobasidin A (QDO/X/A) to select for positive interaction partners. Two screens were carried out. For both a sufficient number of screened diploid clones after the mating procedure could be achieved (screen 1: 4.72×10^6; screen 2: 5.85×10^6), a minimum of 1 million screened clones is recommended for efficient detection of genuine interactions. The calculated mating efficiencies exceeded the minimum value given of 2% (screen 1: 11.7%; screen 2: 15.1%). After growing on QDO/X/A colony PCR was performed using the Matchmaker® Insert Check PCR Mix 2

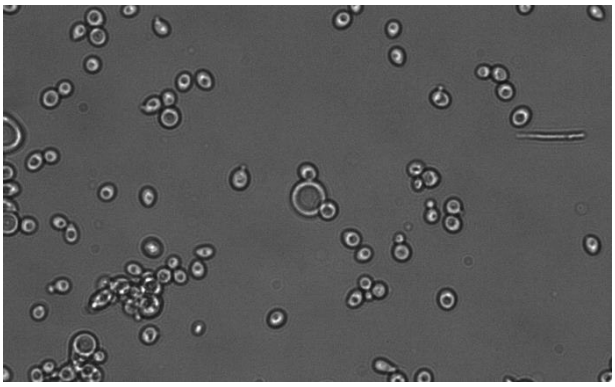

Figure 6. Typical 3-lobed „Mickey mouse"-shaped zygote during mating of the strains Y2H Gold and Y187.

following the manufacturer's instructions. The PCR fragments were sequenced via an external company.

Plasmid rescue and co-transformation:

Plasmids of the respective clones were isolated following the instructions of the Easy Yeast Plasmid Isolation kit. TOP10 competent cells were transformed with these plasmids which then were again sequenced. Co-transformation of bait and the respective prey plasmids were carried out following the instructions of the Matchmaker™ Y2H Gold Kit and the Yeastmaker™ Transformation System 2. This served to distinguish genuine positive which can activate reporter gene expression only by interaction with the bait protein and false positive clones, which can autoactivate it without bait presence.

2.4 Statistical analysis

Statistical analysis of experiments comparing two different individual groups was carried out using the student's t-test (unpaired, two-sided). In experiments comparing more than two individual groups with each other a One-Way ANOVA was carried out (with Dunnett's or Sidak's post hoc test). Confidence level: 95%. The number of independently performed experiments is displayed by n. If not indicated differently the diagrams show the mean value and the corresponding standard deviation (SD). The P values used for classification of statistical significance were the following: $p < 0.05$, *; $p < 0.01$, **; $p < 0.001$, ***. No further indication or the abbreviation ns stands for a statistically non-significant difference.

C Results

1. Stimulation of IDE secretion by serotonin in microglia

1.1 Serotonin increases IDE release from microglial cells.

Previous studies showed that different cell lines, including BV-2 microglial cells (Tamboli, et al., 2010), secrete IDE via an unconventional secretory pathway (Zhao, et al., 2009; Bulloj, et al., 2010). To assess whether serotonin (5-HT) affects the release of IDE, BV-2 cells or primary mouse microglia were incubated for 16 hours with 25 μM 5-HT and IDE was detected in conditioned media and cell lysates by WB. An almost 2-fold increase in IDE levels in conditioned media is detected in comparison to control cells for BV-2 (197.7 ± 92.8% vs. NTC, Figure 7A) and primary mouse microglia (191.5 ± 44.6% vs. NTC, Figure 7B), suggesting that 5-HT can stimulate the release of IDE from microglial cells.

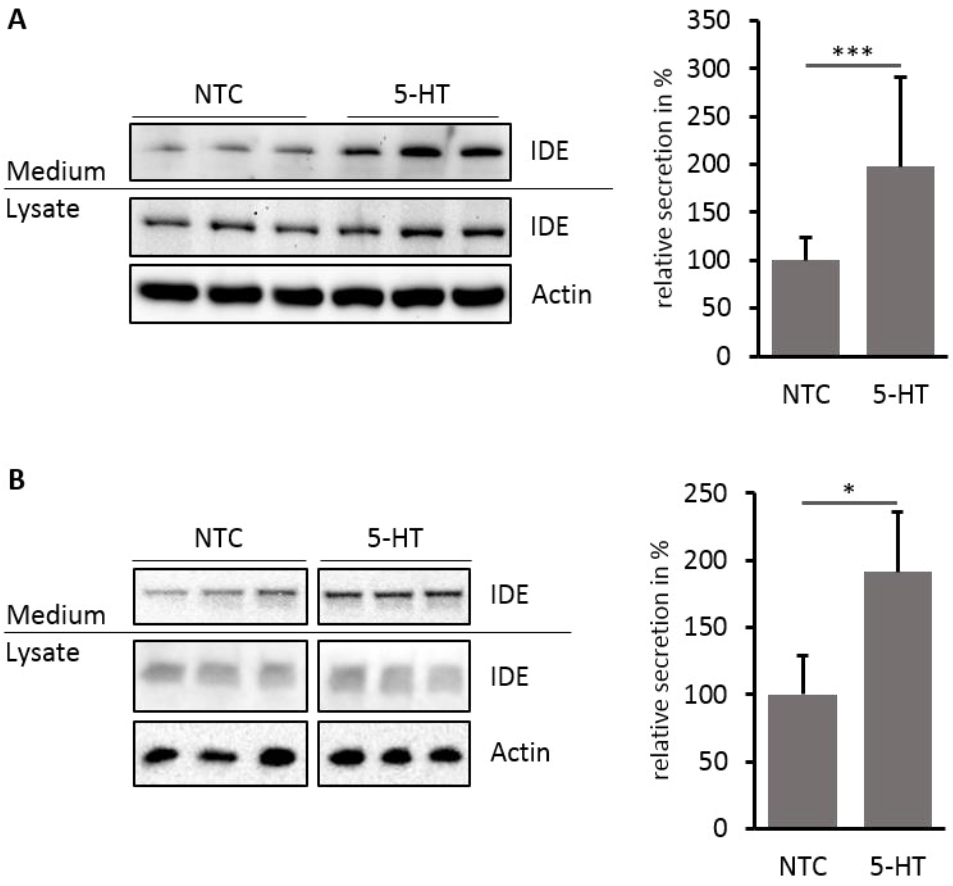

Figure 7. Serotonin increases the release of IDE from BV-2 and primary microglial cells. Western blot analysis of IDE protein levels in conditioned media and lysates of BV-2 cells (A, n=7; 4 in triplicates, 3 in duplicates) and primary mouse microglia (B, n=1 in triplicates) upon administration of 25 μM 5-HT for 16 hours. Relative secretion is expressed as ratio of secreted to intracellular IDE protein levels. Statistical analysis was done using a two-sided unpaired student's t-test (A) and One-Way ANOVA (Dunnett's post hoc test, B, see also Figure 11B+E). Values represent means ± SD.

1.2 Expression of 5-HT receptors in BV-2 cells and in primary mouse microglia.

Since it was shown that some 5-HT receptors (5-HTRs) are found in microglial cells (Krabbe, et al., 2012), it was tested which 5-HTRs were expressed in the microglia cell line BV-2 in comparison to primary mouse microglia. Performing reverse transcription PCR of several 5-HTRs using cDNA synthesized from isolated RNA revealed that BV-2 microglial cells express the 5-HTRs 1b, 2a, 2b, 3 and 4. Primary mouse microglia also express the 5-HTRs 2b, 3 and 4, while the receptors 1b and 2a were not detected. The receptors 2b and 3 show semiquantitatively the highest expression (Figure 8). These results first indicate that BV-2 cells and primary mouse microglia are similar but different in the 5-HTR expression pattern, and second, that 5-HT might activate several G-proteins and related pathways in BV-2 and microglial cells. Furthermore these results are comparable to the expression pattern in primary microglia found by Krabbe and colleagues (Krabbe, et al., 2012).

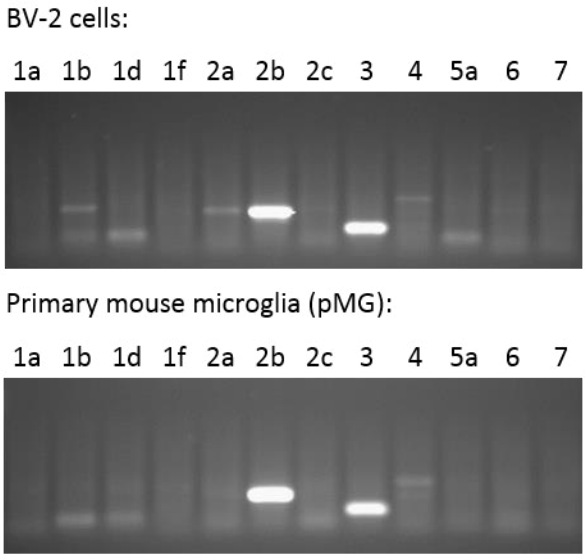

5-HTRs	BV-2	pMG
1a	-	-
1b	+	-
1d	-	-
1f	-	-
2a	+	-
2b	+	+
2c	-	-
3	+	+
4	+	+
5a	-	-
6	-	-
7	-	-

Figure 8. Expression analysis of 5-HTRs in BV-2 cells and primary mouse microglia. Expression analysis by PCR was carried out using specific primers for the 5-HTRs 1a, b, d; 2a, b, c; 3; 4; 5a; 6 and 7 upon RNA isolation and subsequent cDNA synthesis from BV-2 and primary mouse microglial cells. The expression pattern is presented in the table (right).

1.3 Involvement of 5-HT2a, 5-HT2b and 5-HT4 receptors in the regulation of IDE release.

To test if the expressed 5-HTRs 2a, 2b and 4 are involved in the stimulation of IDE release, cells were simultaneously treated with 5-HT and specific antagonists for the three receptors. Altanserine was used as selective 5-HT2aR antagonist, RS127445 as selective antagonist for 5-HT2bR and GR113808 as selective antagonist for the 5-HT4R. While 5-HT alone stimulates the release of IDE, co-treatment with the three antagonists reduces the effect (Figure 9). Altanserine and GR113808 treatment shows a reduction of IDE secretion to the basal level of

control cells (100.13 ± 11.4% and 86.2 ± 42.8% respectively vs. NTC). RS127445 diminishes the release of IDE even stronger to approximately 40% of the basal secretion level (36.7 ± 6.5% vs. NTC). These results suggest the involvement of all three G protein-coupled receptors in triggering IDE release by 5-HT treatment in BV-2 cells.

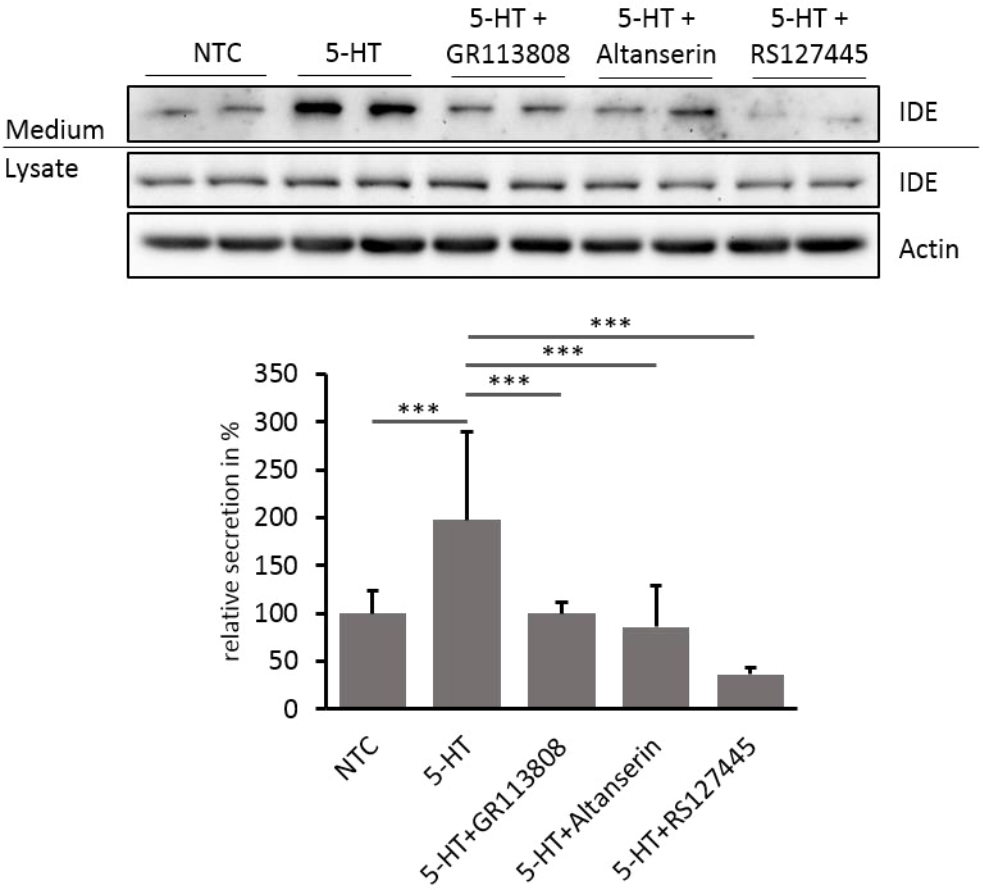

Figure 9. The 5-HT receptors 2a, 2b and 4 are involved in the regulation of IDE release. Western blot analysis of IDE protein levels in conditioned media and lysates of BV-2 cells after treatment with 25 μM 5-HT and the selective 5-HTR antagonists Altanserine (10 nM, 5-HT2aR), RS127445 (5 μM, 5-HT2bR) and GR113808 (20 nM, 5-HT4R) for 16 hours, additional antagonist pre-treatment for 6 hours (n=7 for 5-HT see also Figure 7; n=3 in 2x triplicates, 1x duplicates for 5-HT+antagonists). Relative secretion is expressed as ratio of secreted to intracellular IDE protein levels. Statistical analysis was done using a One-Way ANOVA (Sidak's post hoc test). Values represent means ± SD.

1.4 Activation of 5-HT4R promotes the release of IDE via PLC-dependent Ca^{2+} mobilization.

IDE is released associated to exosomes (Bulloj, et al., 2010; Tamboli, et al., 2010) and several previous studies showed already that exosome secretion is regulated by the level of $[Ca^{2+}]_i$ (Savina, et al., 2003; Raposo, et al., 1997). The 5-HTRs 2a and 2b are $G_{q/11}$ protein-coupled receptors that mediate activation of phospholipase C (PLC) leading to an increase in $[Ca^{2+}]_i$ (Raymond, et al., 2001; Bockaert, et al., 2006; Peroutka, 1995). Only little is known about the role of 5-HT4R in the regulation of $[Ca^{2+}]_i$. Rather, 5-HT4R is known to couple with G_s protein

and to increase intracellular levels of cAMP by activation of the adenylate cyclase (AC) (Fagni, et al., 1992). However, additional studies showed that cAMP can directly activate the guanine-exchange factor (GEF) Epac that can activate PLC via the Rap GTPases Rap1 or Rap2B (de Rooij, et al., 1998; Schmidt, et al., 2001; Oestreich, et al., 2007). Several pharmacological treatments were carried out to test whether these PLC-activating pathways are also triggered by 5-HT4R in BV-2 cells. First, BV-2 cells were treated with the partial 5-HT4R agonist ML10302. Treatment of BV-2 cells with ML10302 significantly increases the release of IDE (151.9 ± 57.9% vs. NTC, Figure 10A). This effect is diminished by the 5-HT4R antagonist GR113808 (133.0 ± 62.4% vs. NTC, Figure 10A).

Treatment of BV-2 cells with the pertussis toxin (PTX) results in an elevated IDE secretion as well, indicating that an increase in intracellular cAMP (Burns, 1988) indeed stimulates release of IDE (Glebov, et al., 2015).

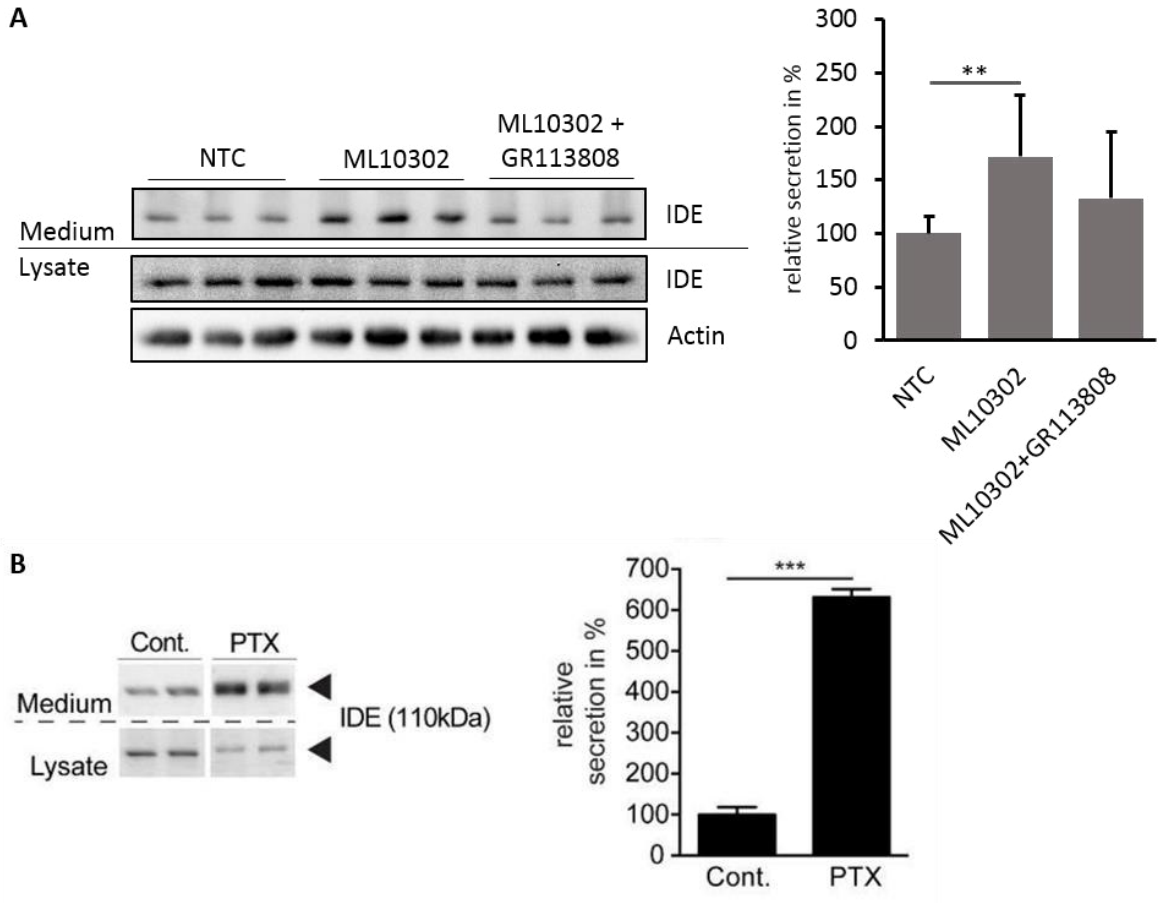

Figure 10. Activation of 5-HT4R stimulates IDE release via an increase in intracellular cAMP levels. (A) Western blot analysis of IDE protein levels in conditioned media and lysates of BV-2 cells upon treatment with ML10302 (10 nM, n=4 in triplicates) and ML10302 + GR113808 (20 nM, n=2 in triplicates) for 16 hours, additional pre-treatment with GR113808 for 6 hours. Relative secretion is expressed as ratio of secreted to intracellular IDE protein levels. Statistical analysis was done using a One-Way ANOVA (Dunnett's post hoc test). Values represent means ± SD. (B) Western blot analysis of IDE protein levels in conditioned media and lysates of BV-2 cells after treatment with Pertussis toxin (PTX) carried out by Olaf Merkel (published in *(Glebov, et al., 2015)*).

8-CPT-2Me-cAMP (8-CPT) is a selective activator of Epac and was used to examine the potential influence of Epac on IDE release without prior stimulation of 5-HT. Administration of

8-CPT results in an increase of IDE release from BV-2 cells (201.4 ± 79.1% vs. NTC, Figure 11A+D) as well as from primary mouse microglia (149.9 ± 13.6% vs. NTC, Figure 11B+E). Also direct stimulation of PLC by treatment of BV-2 cells with the activator *m*-3m3FBS (3m3FBS) leads to an increase in IDE release (126.6 ± 16.6% vs. NTC, Figure 11C+F) and is reduced to almost basal levels of control cells by the PLC inhibitor U73122 (103.2 ± 17.0% vs. NTC, Figure 11C+F).

These results suggest that 5-HT4R might also contribute to the stimulation of IDE release via an increase in cAMP which leads to activation of Epac and PLC.

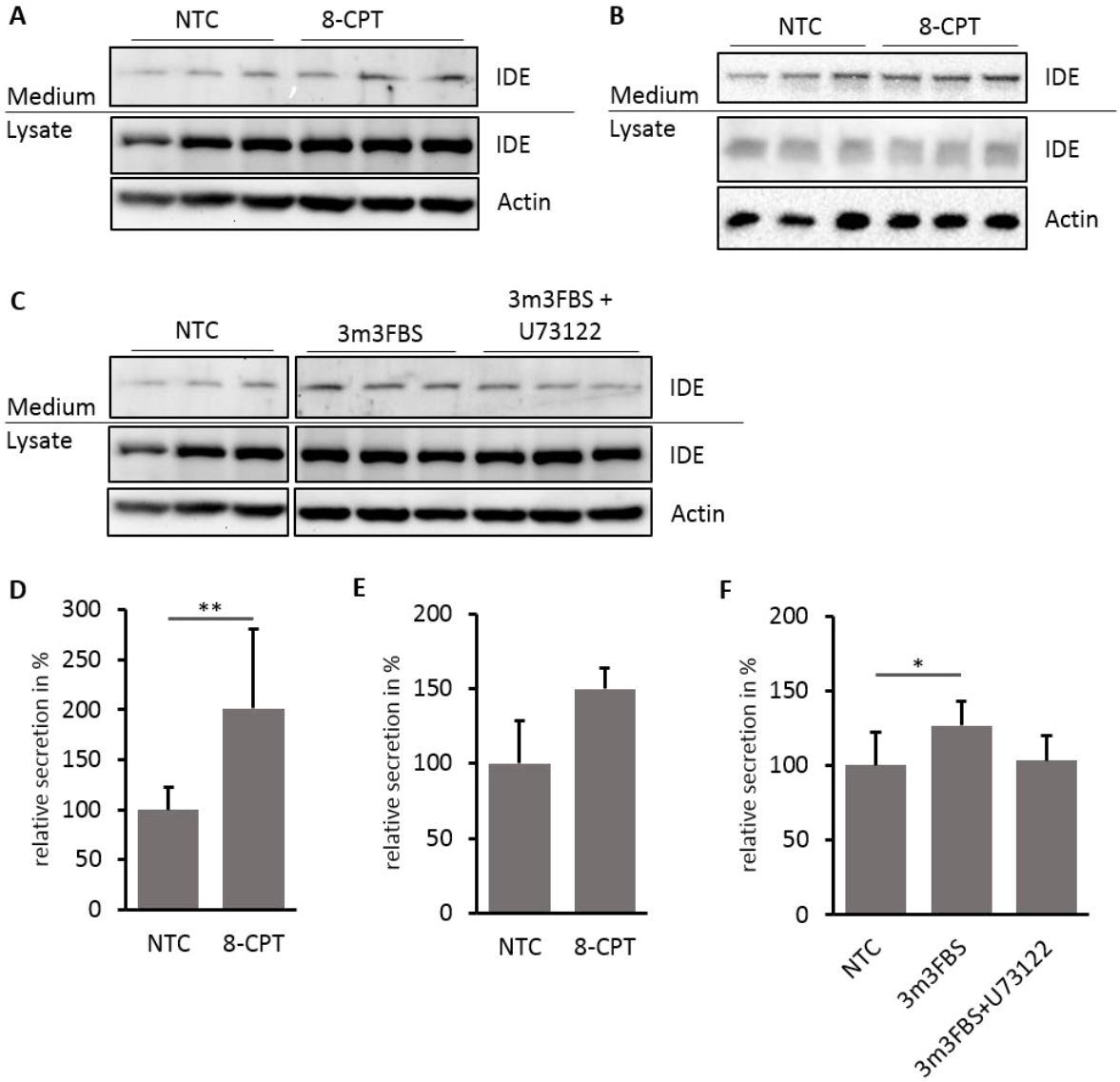

Figure 11. Activation of Epac and PLC promotes the release of IDE. Western blot analysis of IDE protein levels in conditioned media and lysates of BV-2 cells (A+D, n=3 in triplicates) or primary mouse microglia (B+E, n=1 in triplicates) after treatment with the Epac activator 8-CPT (5 µM) for 16 hours. (C+F) IDE protein levels in conditioned media and lysates of BV-2 cells after treatment with 3m3FBS (5 µM) and U73122 (10 µM) for 3 hours (n=2 in triplicates), additional pre-treatment with U73122 for 16 hours. Relative secretion is expressed as ratio of secreted to intracellular IDE protein levels. Statistical analysis was done using a two-sided unpaired student's t-test (D) and a One-Way ANOVA (Dunnett's post hoc test; F; E + Figure 7B). Values represent means ± SD.

1.5 5-HT increases cytosolic Ca^{2+} that stimulates IDE release.

The experiments addressing the stimulatory effect of 5-HT on IDE secretion in BV-2 and primary microglial cells so far revealed the involvement of PLC. PLC induces an increase in $[Ca^{2+}]_i$ by formation of inositol 1,4,5-triphosphate (IP_3). IP_3 activates IP_3 receptors acting as Ca^{2+} channels in the ER and this way opens intracellular calcium stores causing an elevation of $[Ca^{2+}]_i$. This increased $[Ca^{2+}]_i$ can stimulate the fusion of MVBs with the plasma membrane leading to the release of exosomes (Raposo, et al., 1997; Savina, et al., 2003). Several studies already showed that 5-HT leads to an increased formation of IP_3 and elevated $[Ca^{2+}]_i$ mainly attributed to the signalling of 5-HT2Rs (Schmuck, et al., 1994; Saini, et al., 2003; Bonhaus, et al., 1999).

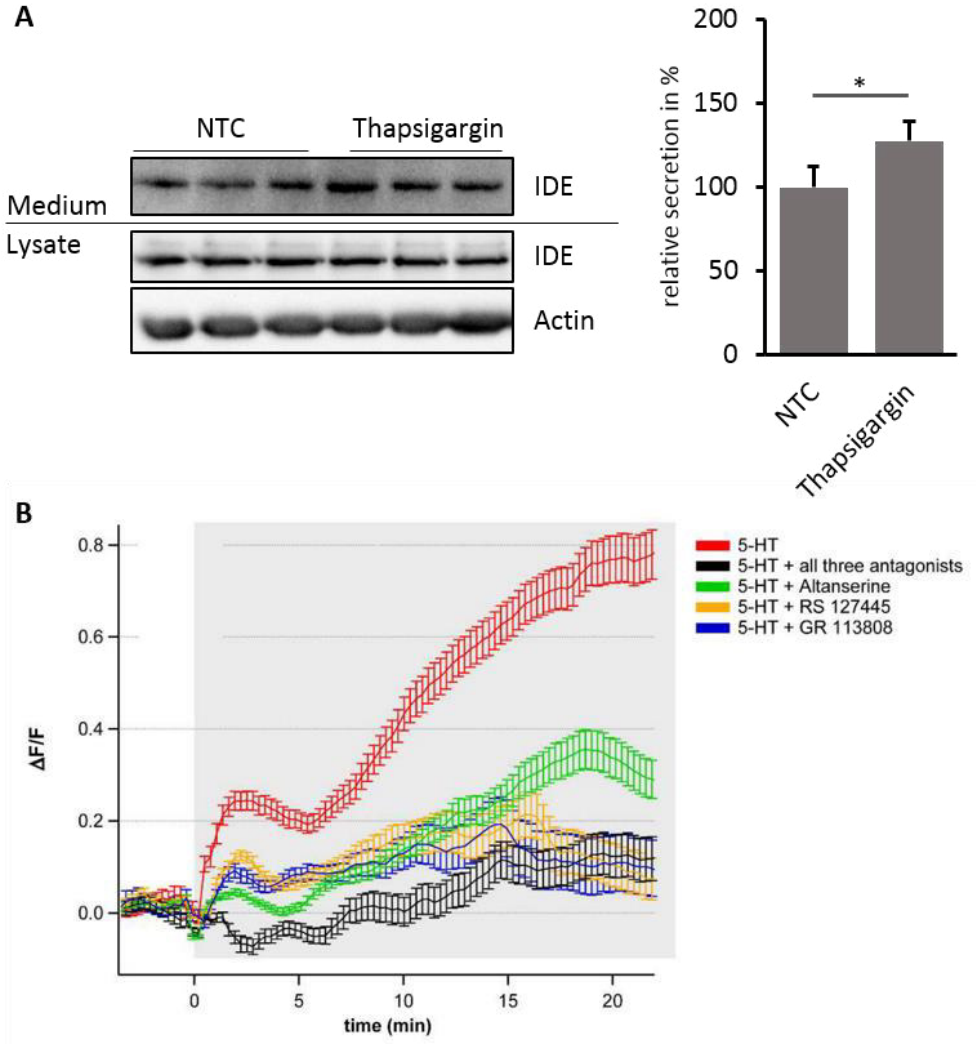

Figure 12. 5-HT-stimulated increase in $[Ca^{2+}]_I$ triggers IDE release in BV-2 microglial cells. (A) Western blot analysis of IDE protein levels in conditioned media and lysates of BV-2 cells after treatment with 1 μM Thapsigargin for 2 hours (n=1 in triplicates). Relative secretion is expressed as ratio of secreted to intracellular IDE protein levels. Statistical analysis was done using a two-sided unpaired student's t-test. Values represent means ± SD. (B) Time lapse recordings of BV-2 cells, that were bulk-labelled with the Ca^{2+} indicator Fluo-4, before and after application of 25 μM 5-HT (grey background) with or without 16 hours pre-treatment of the 5-HTR antagonists Altanserine (10 nM), RS127445 (5 μM) and GR113808 (20 nM) to monitor $[Ca^{2+}]_i$ (source: *(Glebov, et al., 2015)*, Figure 4B).

To test whether 5-HT stimulates the secretion of IDE associated with exosomes via increasing the $[Ca^{2+}]_i$, first, the effect of Thapsigargin that raises the $[Ca^{2+}]_i$ (Lytton, et al., 1991) was examined. IDE secretion slightly elevates upon cell treatment with Thapsigargin (127.5 ± 11.9% vs. NTC, Figure 12A) suggesting that an increase of $[Ca^{2+}]_i$ stimulates the release of IDE. This assumption is further supported by the observation that Monensin also increased IDE release from BV-2 cells (see below, 2.3). Monensin induces an elevation in $[Ca^{2+}]_i$ and this way increases the release of exosomes (Savina, et al., 2003). Next, Ca^{2+} measurements were kindly carried out by Dr. Ronald Jabs to examine the effect of 5-HT and 5-HTR modulators on $[Ca^{2+}]_i$. Application of 5-HT to BV-2 cells significantly increases $[Ca^{2+}]_i$. This effect is attenuated by pre-treatment of cells with the 5-HTR antagonists Altanserine, RS127445 or GR113808 (see Figure 12B). The strongest reduction is observed when cells are pre-treated with all three antagonists simultaneously.
These results indicate that 5-HT stimulates IDE release from BV-2 cells by elevation of $[Ca^{2+}]_i$ which leads to the fusion of MVBs with the plasma membrane and release of IDE-loaded exosomes into the extracellular media.

1.6 5-HT stimulates the release of exosome-associated IDE.

Recent studies showed that statins promote degradation of extracellular Aβ due to the stimulation of exosome-associated secretion of IDE (Tamboli, et al., 2010). To examine if the 5-HT-induced elevation of IDE release is also linked to an increase in exosome secretion, exosomes were isolated from conditioned media of BV-2 cells by differential centrifugation.
Treatment with 5-HT indeed increases IDE levels in the exosome fraction (P100) (142.7 ± 11.6% vs. NTC, Figure 13A). Also other exosomal marker proteins like Flotillin-1 (213.5 ± 6.8% vs. NTC), Alix (120.7 ± 17.6% vs. NTC) and Actin (120.7 ± 17.9% vs. NTC) show a significant (Flotillin-1) or non-significant elevation in the exosome fraction P100 (see Figure 13A). Subsequent density gradient centrifugation of the isolated exosomes by loading the P100 fraction onto a density gradient shows a co-fractionation of IDE with the exosomal markers Alix, Flotillin-1 and Actin. In comparison to the typical exosomal marker proteins, IDE shows a broader distribution across the fractions including also fractions of lower density. However, the majority of IDE co-fractionized with Alix, Flotillin-1 and Actin (see Figure 13B). Furthermore, levels of IDE that co-fractionate with the common exosome marker Alix are elevated upon the treatment with 5-HT (highlighted by the black boxes in Figure 13B). Microvesicle-associated IDE, however, is rather decreased upon treatment with 5-HT. Similar effects are observed for Flotillin-1 and Actin in the microvesicle fraction P10 (Figure 13A).
These findings indeed suggest that the elevation in IDE secretion in BV-2 cells stimulated by 5-HT can be attributed to an increased release of exosomes.

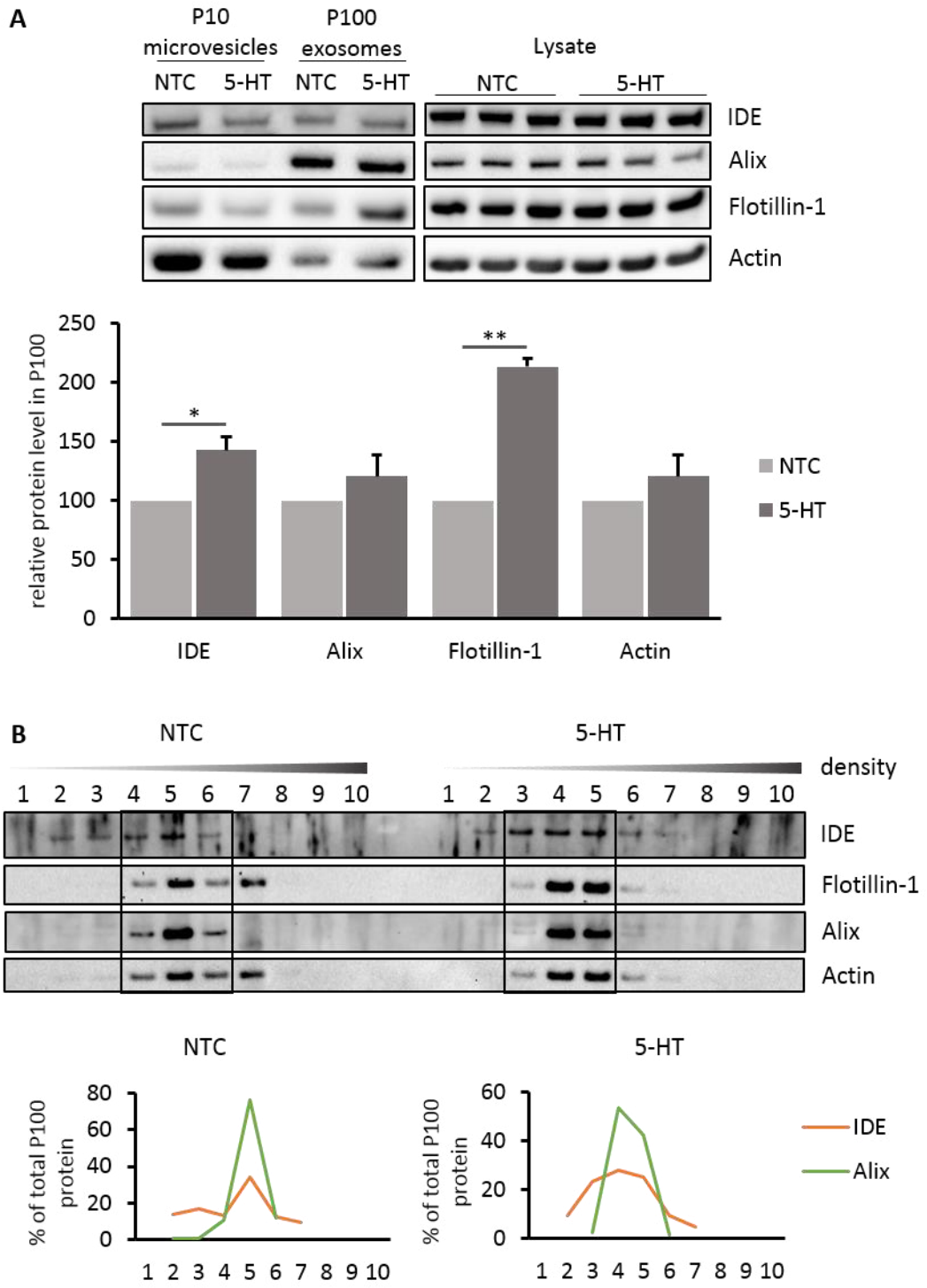

Figure 13. 5-HT stimulates the release of exosomes from BV-2 cells. (A) Western blot analysis of IDE, Flotillin-1, Alix and Actin in P10 and P100 fractions and lysates of BV-2 cells upon treatment with 25 µM 5-HT for 16 hours (n=2 in single replicate for P10 and P100). P10 and P100 were prepared by differential centrifugation from conditioned media. Relative protein levels are expressed as the ratio of signals in the P100 fraction to that in cell lysates. Statistical analysis was carried out using a two-sided unpaired student's t-test. Values (5-HT treatment) represent means ± SD. (B) Western blot analysis of IDE, Flotillin-1, Alix and Actin after fractionation of the exosome fraction P100 through density gradient centrifugation. The density gradient was prepared by OptiPrep® solutions. The exosome fraction is represented by the exosomal marker Alix (black boxes).

1.7 Neurons can stimulate IDE secretion from BV-2 microglial cells.

The communication between neurons and microglia in the brain plays an essential role in neuroinflammation as well as for neurogenesis and neuroprotection (Gemma, et al., 2010). Neuron-derived signals, for example, can regulate microglial activity (Biber, et al., 2007; Eyo & Wu, 2013). Thus, it was tested whether neurons can stimulate the secretion of IDE from microglia by release of 5-HT. Co-culture of BV-2 cells with primary mouse neurons indeed causes a significant increase in IDE release from BV-2 cells (284.2 ± 14.4% vs. BV-2 alone, 233.3 ± 42.3% in the presence of the 5-HT precursor 5-hydroxy tryptophan (5-HTP), Figure 14A+B). The neurons themselves secrete only low quantities of IDE (Figure 14A). Addition of 5-HTP should assure neuronal 5-HT production in case neurons would not express the tryptophan hydroxylase. 5-HTP addition shows a moderate decrease in the effect observed for IDE secretion which, however, is not significant.

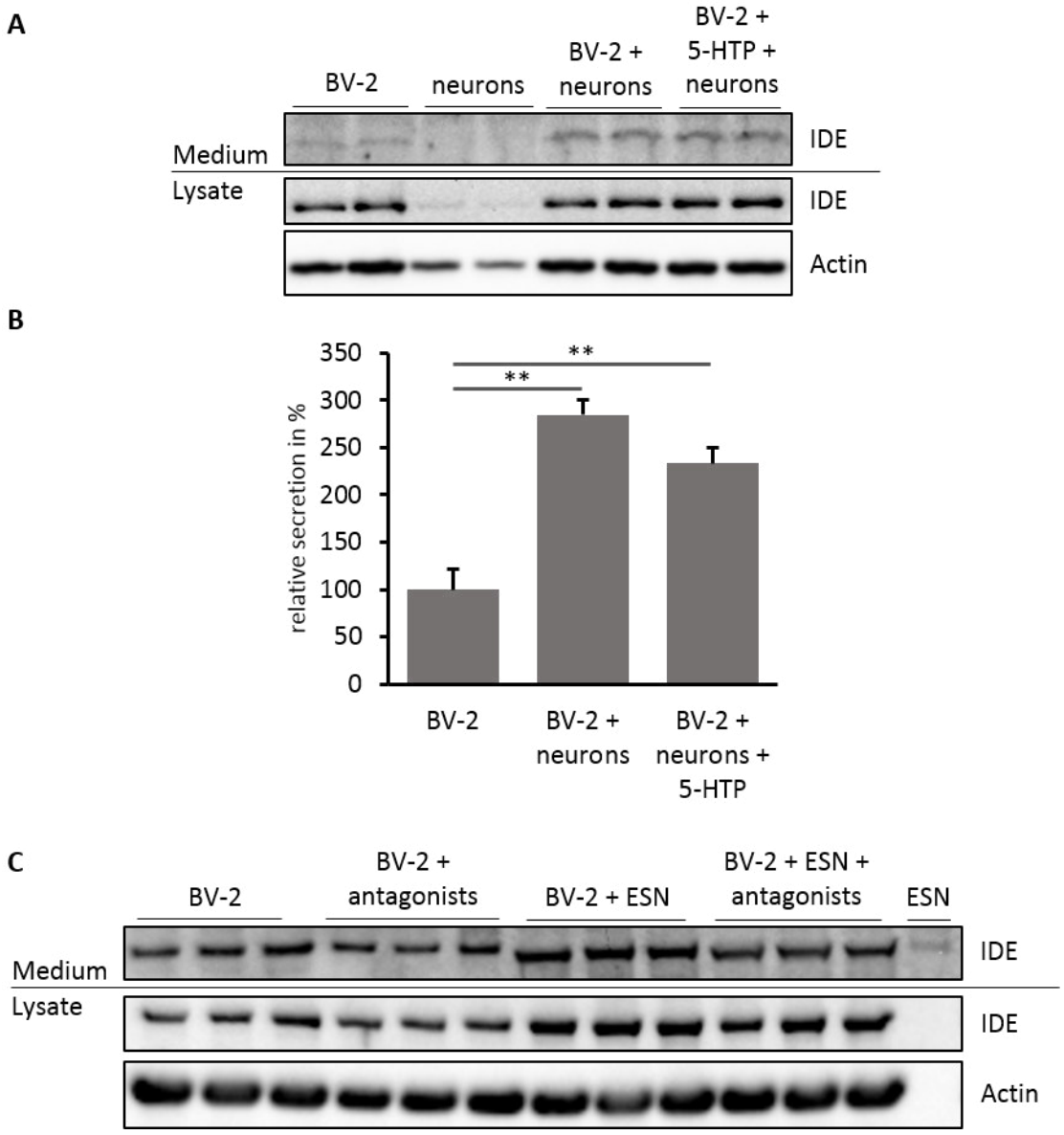

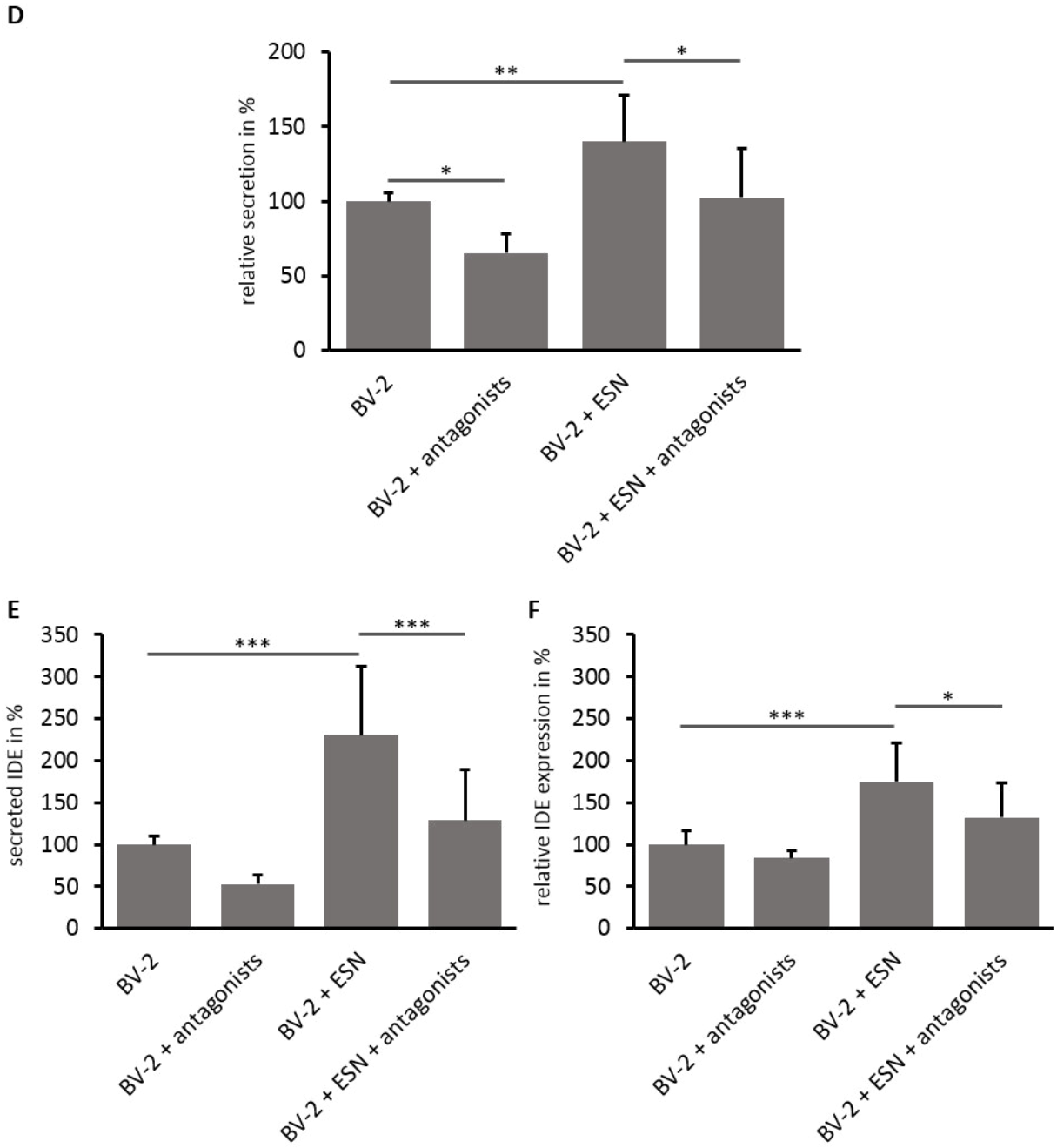

Figure 14. Neurons can stimulate IDE secretion from BV-2 microglial cells. Western blot analysis of IDE protein levels in conditioned media and lysates of BV-2 cells upon co-culture with primary mouse neurons (A+B, n=1, BV-2 in triplicate, neurons in duplicate, BV-2 + neurons in duplicate, BV-2 + 5-HTP + neurons in septuplicate) or co-culture with ES-derived serotonergic neurons (ESN) (C-F, n=3 in triplicate). IDE secretion from BV-2 cells is increased in the presence of neuronal cells (B+D). Co-treatment of co-cultured BV-2 and ESN with the 5-HTR antagonists Altanserine (10 nM), RS127445 (5 µM) and GR113808 (20 nM) leads to a significant diminished effect but also decreases IDE secretion in BV-2 cells alone (C+D). Upon co-culture with ESN absolute levels of secreted IDE from BV-2 cells (E) are stronger increased than relative IDE secretion (D) and accompanied by an elevated IDE expression (F). Relative secretion is expressed as ratio of secreted to intracellular IDE protein levels, relative expression as normalization of intracellular IDE to Actin protein level. Statistical analysis was done using a One-Way ANOVA (Sidak's post hoc test). Values represent means ± SD.

To determine in more detail if neuronal 5-HT release stimulates IDE release, a co-culture approach of BV-2 cells with ES-derived serotonergic neurons (ESN) was carried out. 90% of the ES-derived neurons exhibit a serotonergic phenotype and release 0.24 ± 0.03 pmol

5-HT/well/min (Lau, et al., 2010). Co-culture of BV-2 cells with these ESN results in an increased IDE release by BV-2 cells (140.1 ± 31.2% vs. BV-2 alone, Figure 14C+D). This effect is reduced to basal levels of BV-2 cells alone by co-treatment with the 5-HTR antagonists Altanserine, RS127445 and GR113808 (102.6 ± 33.1% vs. BV-2 alone, Figure 14C+D). ESN themselves secrete only low quantities of IDE (see Figure 14C). However, also treatment of BV-2 cells alone with the three antagonists leads to a significant decrease of IDE release (65.3 ± 12.7% vs. BV-2 alone), similar in magnitude as observed for co-cultured BV-2 cells and ESN. This rather suggests an at least partial independency of 5-HT stimulation for the observed effect.

The absolute amount of secreted IDE by BV-2 cells is even more elevated by co-culture with ESN (230.4 ± 81.3% vs. BV-2 alone, Figure 14E) in comparison to the approximately 1.5-fold increase in relative IDE secretion (secreted/intracellular IDE). Also here a significant reduction by co-treatment with the three antagonists can be detected (128.6 ± 61.0% vs. BV-2 alone, Figure 14E). The increase of secreted IDE is accompanied by an increased IDE expression in BV-2 cells after co-culture with ESN (174.1 ± 47.5% vs. BV-2 alone, Figure 14F), which is partially diminished in the presence of the three 5-HTR antagonists (131.9 ± 41.2% vs. BV-2 alone, Figure 14F).

These results suggest that serotonergic neurons not only stimulate the secretion of IDE from BV-2 microglial cells, but also induce an increase in IDE expression. The underlying mechanisms leading to an increase in IDE expression need to be elucidated. Also the actual proportion of neuronal 5-HT-mediated stimulation of IDE secretion in BV-2 cells needs further examinations.

2. Molecular mechanisms in IDE secretion

2.1 Differential effects of nSMase2 and ceramide in the release of exosomal proteins in distinct cell types

The mechanisms for protein sorting to MVBs during inward budding of intraluminal vesicles are not fully understood. ESCRT- dependent (Babst, et al., 1998; Baietti, et al., 2012; Gan & Gould, 2011) and ESCRT-independent (Trajkovic, et al., 2008; van Niel, et al., 2011; Alonso, et al., 2011) mechanisms have been identified. Trajkovic and colleagues showed that inward budding is triggered by raft-based microdomains enriched in ceramides. To decrease ceramide levels they treated cells with GW4869, an inhibitor for the neutral sphingomyelinase 2 (nSMase2), that catalyses the conversion of sphingomyelin to ceramide.

In order to examine the effect of nSMase2 inhibition on exosome release, and in particular on the secretion of IDE, BV-2 cells were treated with 1.5 and 5 µM GW4869. Inhibition of nSMase2 with GW4869 causes a significant increase in IDE release in BV-2 microglial cells (1.5 µM: 173.8 ± 34.4% vs. NTC; 5 µM: 256.6 ± 50.2% vs. NTC; Figure 15A).

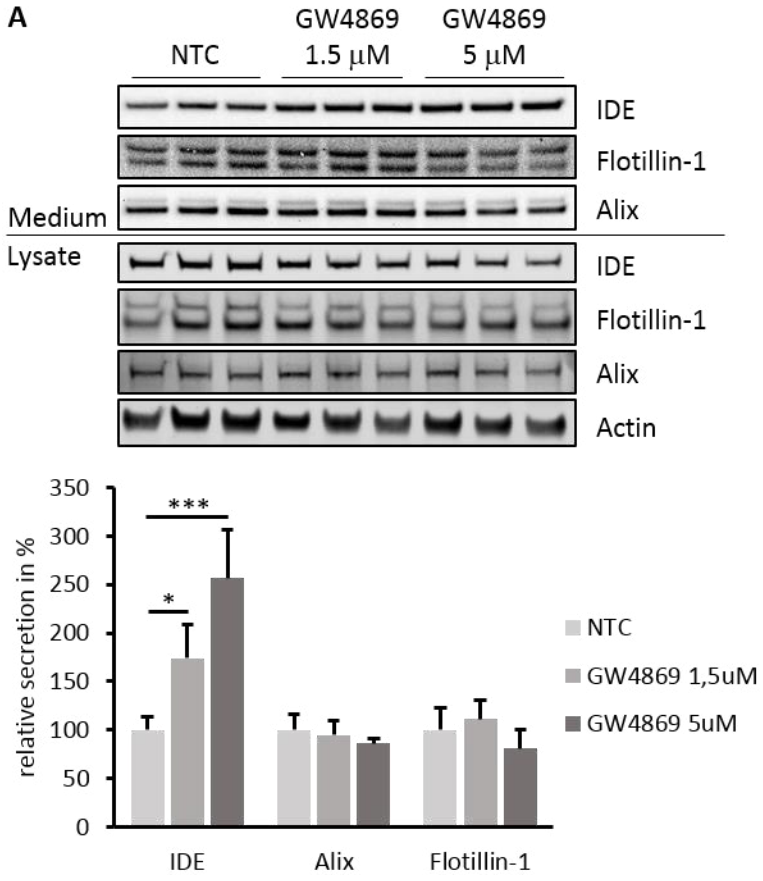

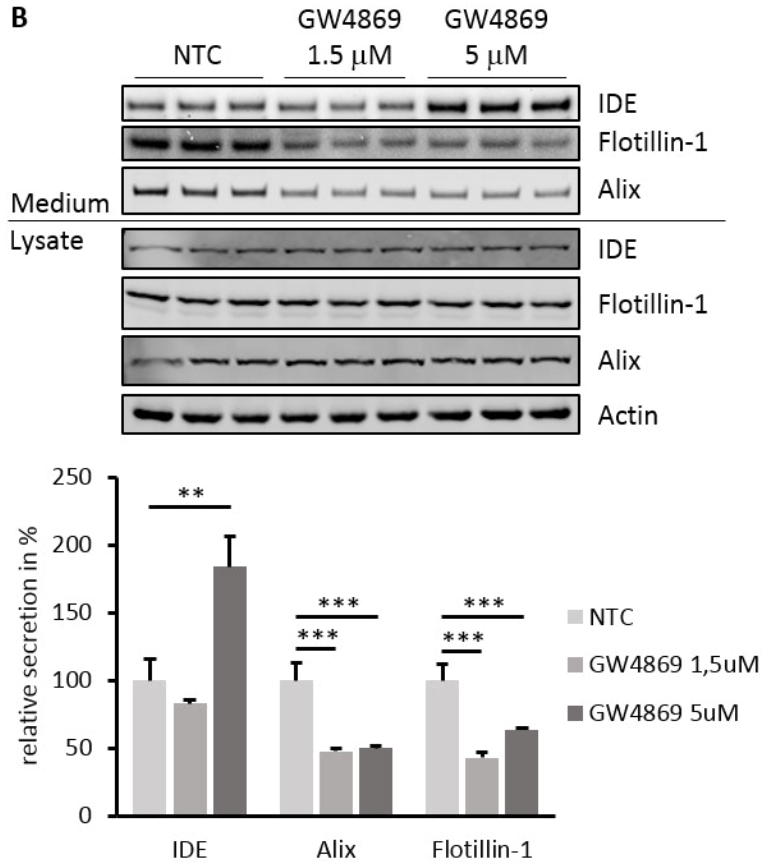

Figure 15. Inhibition of nSMase2 stimulates release of IDE in the microglia cell lines BV-2 and N9. Western blot analysis of IDE, Alix and Flotillin-1 protein levels in conditioned media and lysates of BV2 (A) and N9 cells (B) upon treatment with 1.5 μM (n=1 in triplicates) and 5 μM GW4869 (n=2 in triplicates for BV-2, n=1 in triplicates for N9) for 16 hours. Relative secretion is expressed as ratio of secreted to intracellular protein levels. Statistical analysis was done using a One-Way ANOVA (Dunnett's post hoc test). Values represent means ± SD.

In comparison, the secretion of the exosome markers Alix (1.5 μM: 94.9 ± 14.4% vs. NTC; 5 μM: 86.1 ± 5.1% vs. NTC) and Flotillin-1 (1.5 μM: 111.5 ± 19.9% vs. NTC; 5 μM: 81.0 ± 19.8% vs. NTC) are rather unaffected by GW4869 treatment (Figure 15A). These results contradict the findings by Trajkovic and colleagues showing a decreased release of the exosome-associated proteins PLP and CD63 in Oli-neu cells upon GW4869 treatment (Trajkovic, et al., 2008). In addition to BV-2 cells, another mouse microglial cell line, N9, was analysed. GW4869 treatment also here increases IDE secretion in N9 cells at 5 μM (183.7 ± 22.9% vs. NTC, Figure 15B), whereas 1.5 μM shows no significant effect (82.7 ± 2.7% vs. NTC, Figure 15B). However, secretion of Alix and Flotillin-1 is significantly decreased after inhibition of nSMase2 (1.5 μM: Alix 47.3 ± 1.9% vs. NTC, Flotillin-1 42.6 ± 4.6% vs. NTC; 5 μM: Alix 49.8 ± 1.3% vs. NTC, Flotillin-1 63.5 ± 0.8% vs. NTC). These results demonstrate differential effects of GW4869 on different exosomal proteins in microglial cells, suggesting the involvement of ESCRT-dependent and -independent mechanisms in the release of the different exosomal proteins.

A recent study showed involvement of astrocyte-derived exosomes in the aggregation of Aβ. Inhibition of nSMase2 by GW4869 treatment significantly decreased exosome release by primary astrocytes of a transgenic mouse model and reduced Aβ plaque formation (Dinkins, et al., 2014). Thus, the study on IDE secretion was extended to primary rat astrocytes.
Inhibition of nSMase2 by GW4869 strongly decreases the release of Alix (1.5 μM: 8.1 ± 2.4% vs. NTC; 5 μM: 1.0 ± 1.3% vs. NTC; Figure 16) and Flotillin-1 (1.5 μM: 14.7 ± 6.7% vs. NTC; 5 μM: 13.8 ± 7.5% vs. NTC; Figure 16). Also IDE secretion is strongly decreased by GW4869 treatment in primary rat astrocytes (1.5 μM: 16.8 ± 5.2% vs. NTC; 5 μM: 18.5 ± 7.7% vs. NTC; Figure 16) suggesting a cell type-specific regulation of IDE secretion in microglia and astrocytes.

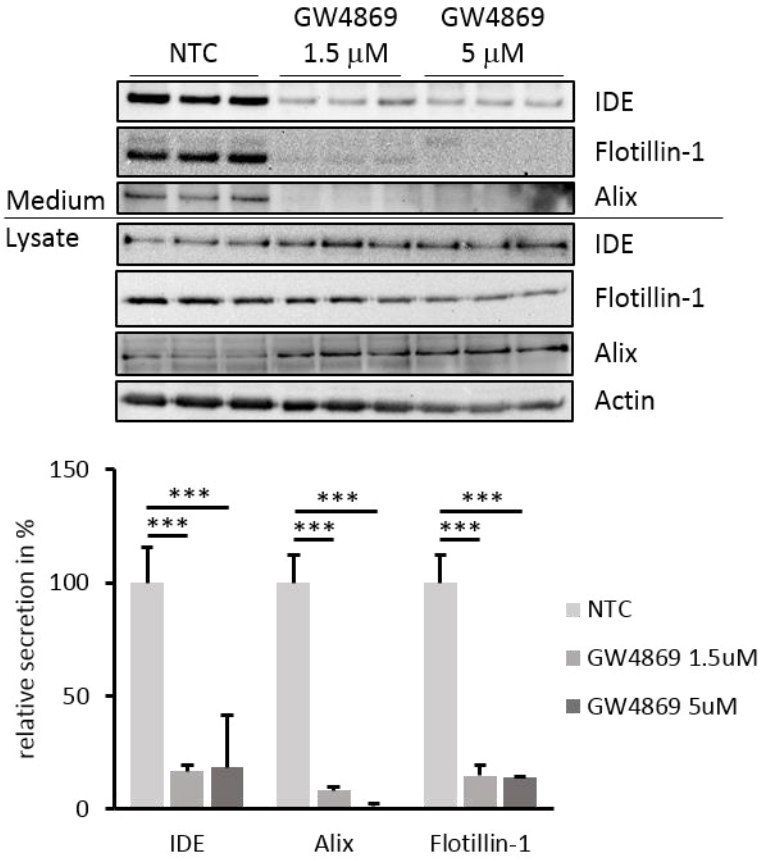

Figure 16. Inhibition of nSMase2 strongly decreases the release of exosomal marker proteins in primary rat astrocytes. Western blot analysis of IDE, Alix and Flotillin-1 protein levels in conditioned media and lysates of primary rat astrocytes upon treatment with 1.5 μM and 5 μM GW4869 for 16 hours (n=2 in triplicates). Relative secretion is expressed as ratio of secreted to intracellular protein levels. Statistical analysis was done using a One-Way ANOVA (Dunnett's post hoc test). Values represent means ± SD.

These results again emphasise that the regulation of exosome release, which might be also coupled to the composition of exosomes, seems to vary not only for different exosome cargo proteins but also between different cell types.

2.2 Role of the ESCRT machinery and IDE in the regulation of exosome biogenesis

2.2.1 Minor effects of Alix knockdown on the release of IDE in BV-2 cells

Alix is an accessory protein of the ESCRT machinery and modulates vesicle budding and cytokinesis (Odorizzi, 2006; Morita, et al., 2007). The involvement of Alix in the sorting and secretion of exosomal cargo and possibly also the formation process of exosomes as ILVs at endosomal membranes was demonstrated recently by Baietti and colleagues (Baietti, et al., 2012). They showed a strong decrease in the release of exosomal marker proteins after knockdown of Alix by RNAi. To test whether Alix is functionally involved in IDE release, BV-2 cells were transfected with Alix-specific siRNA. Two independent siRNAs efficiently decrease protein levels of Alix by ~90% (Alix: 10.3 ± 7.3% for siRNA 2 and 4.7 ± 4.3% for siRNA 6 vs. neg. ctrl. siRNA; Figure 17), but do not significantly change the secretion of IDE (121.1 ± 24.1% for siRNA 2 and 117.9 ± 36.5% for siRNA 6 both vs. neg. ctrl. siRNA; Figure 17). The amount of secreted IDE tends to be increased, in particular for siRNA 2, which is associated with a moderate increase in IDE expression, being significant only for siRNA 2 (122.7 ± 7.9% for siRNA 2 and 109.6 ± 13.5% for siRNA 6 vs. neg. ctrl. siRNA; Figure 17).

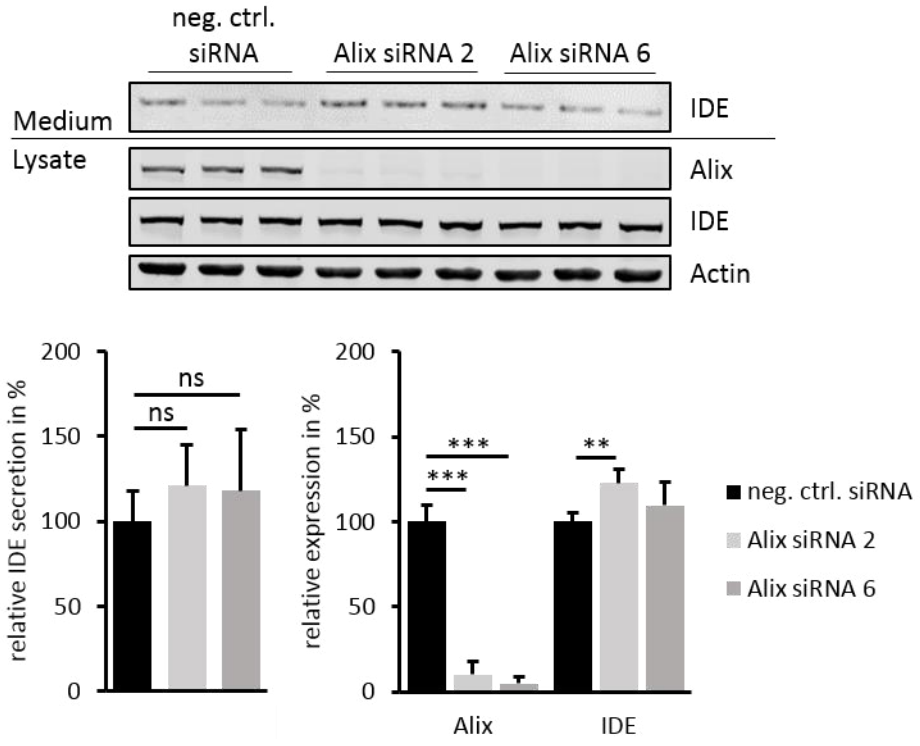

Figure 17. Downregulation of Alix does not significantly influence IDE secretion in BV-2 cells, but does slightly affect IDE expression. Western blot analysis of IDE protein levels in conditioned media and lysates of BV-2 cells after siRNA-mediated knockdown of Alix 48 hours after transfection (n=2 in triplicates). Relative secretion is expressed as ratio of secreted to intracellular IDE protein levels, relative expression as normalization of intracellular IDE to Actin protein level. Statistical analysis was done using a One-Way ANOVA (Dunnett's post hoc test). Values represent means ± SD.

These observations suggest that Alix could affect IDE secretion, but rather cellular IDE expression or metabolism. Whether sorting of IDE into exosomes is affected by Alix remains to be determined in more detail.

2.2.2 IDE secretion is significantly increased upon siRNA-mediated knockdown of Vps4B.

The AAA ATPase Vps4B is also an ESCRT-accessory protein (Hanson & Cashikar, 2012; Babst, et al., 1998). It plays a role in the formation of ILVs that are released as exosomes upon fusion of MVBs with the plasma membrane (Baietti, et al., 2012; Kunadt, et al., 2015; Colombo, et al., 2013), although that role of Vps4B is controversial (Trajkovic, et al., 2008). To assess whether IDE secretion is dependent on Vps4B, its expression was knocked down by transient transfection with Vps4B-specific siRNA in BV-2 cells.

The yielded knockdown is 55% on average (Vps4B: 44.9 ± 17.0% vs. neg. ctrl siRNA, Figure 18A) and varies from 32-77% between the different experiments. Knockdown of Vps4B significantly increases the release of IDE (244.3 ± 120.3% vs. neg. ctrl. siRNA, Figure 18A). The high standard deviation values result from a varying effect strength between the individual experiments, while the variations between biological replicates within one experiment are rather small. The effect of siRNA-mediated Vps4B knockdown on IDE secretion in BV-2 cells ranges from 53 to 313% increase.

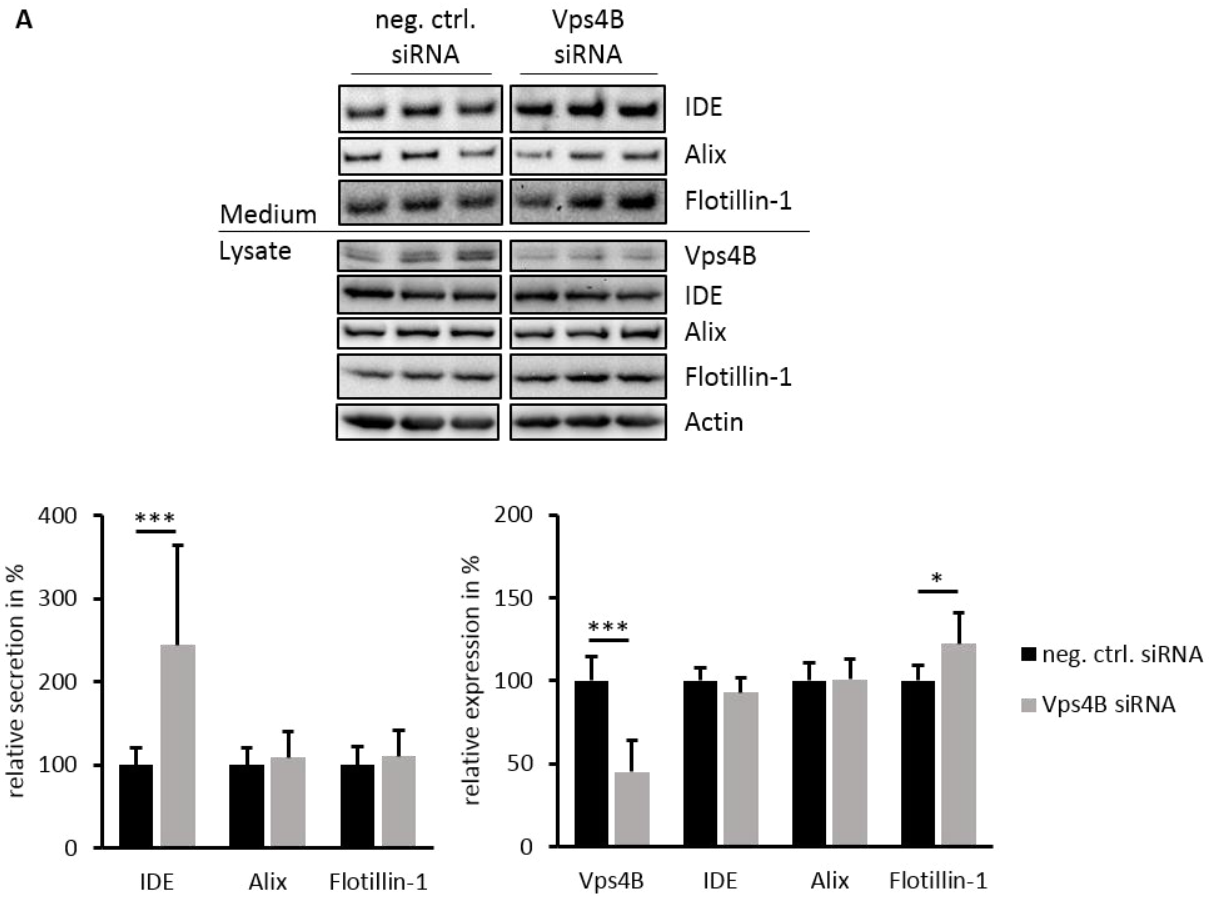

B

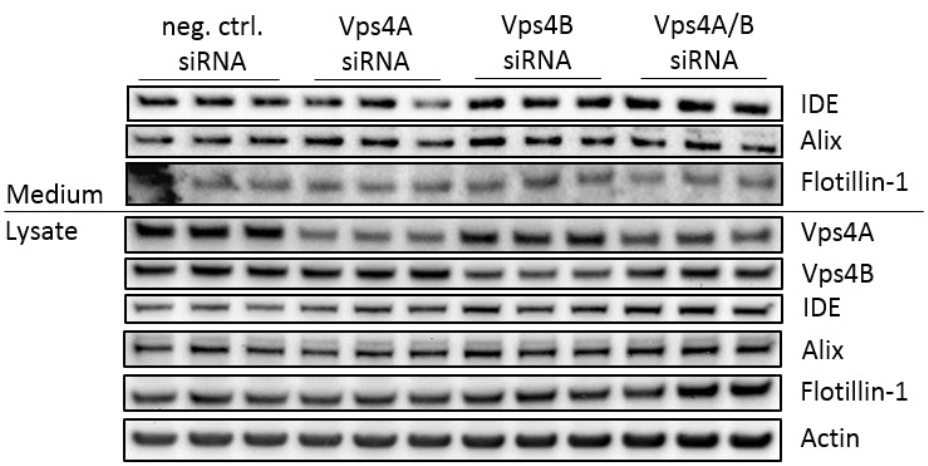
neg. ctrl. siRNA
Vps4A siRNA
Vps4B siRNA
Vps4A/B siRNA
IDE
Alix
Flotillin-1
Medium
Lysate
Vps4A
Vps4B
IDE
Alix
Flotillin-1
Actin

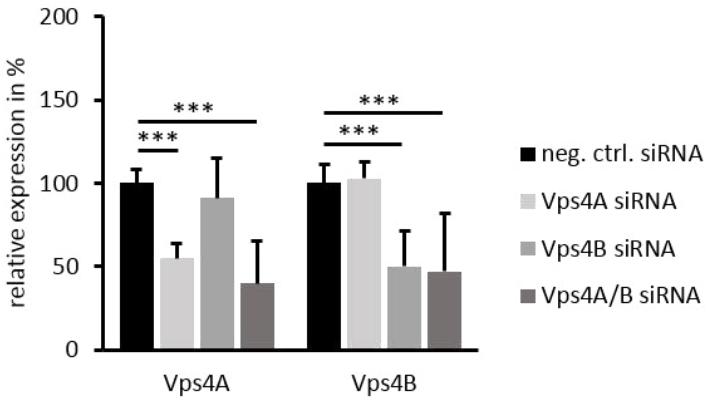
relative expression in %
200
150
100
50
0
***
***
***
***
Vps4A
Vps4B
neg. ctrl. siRNA
Vps4A siRNA
Vps4B siRNA
Vps4A/B siRNA

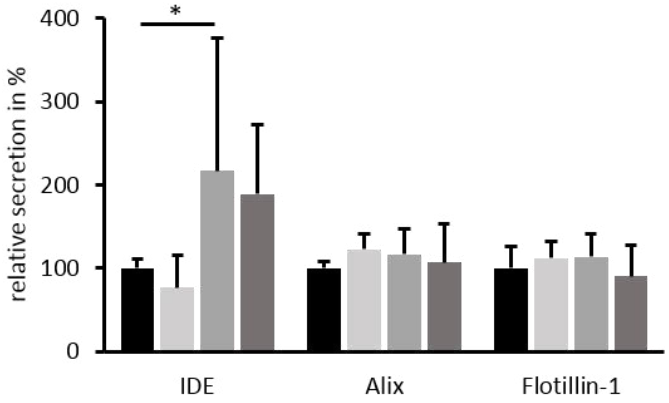
relative secretion in %
400
300
200
100
0
*
IDE
Alix
Flotillin-1

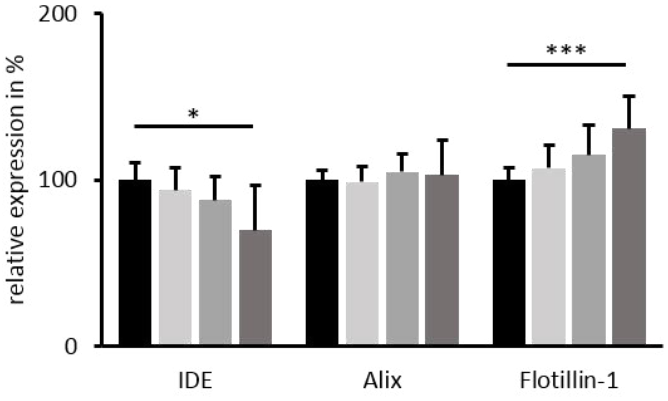
relative expression in %
200
100
0
*
***
IDE
Alix
Flotillin-1

Figure 18. Effects of RNAi-mediated knockdown of Vps4A and 4B on the release of IDE and exosomal marker proteins from BV-2 cells. Western blot analysis of IDE, Alix, Flotillin-1, Vps4A and Vps4B protein levels in conditioned media and/or lysates of BV-2 cells after siRNA-mediated knockdown of Vps4B alone (A, n=4 in triplicates, Flotillin-1: n=3 in triplicates) or Vps4A and 4B (B, n=3 in triplicates) 48 hours after transfection. Relative secretion is expressed as ratio of secreted to intracellular protein levels, relative expression as normalization of intracellular IDE, Alix, Flotillin-1, Vps4A or Vps4B to Actin levels. Statistical analysis was done using a One-Way ANOVA (Dunnett's post hoc test, for A see also Figure 23A). Values represent means ± SD.

In comparison to IDE release the secretion of the exosomal marker proteins Alix (109.4 ± 30.7% vs. neg. ctrl. siRNA, Figure 18A) and Flotillin-1 (110.0 ± 30.1% vs. neg. ctrl. siRNA, Figure 18A) is not significantly affected but shows interexperimental variations as well. To test potential compensating effects of the Vps4B paralogue Vps4A, both paralogues were targeted by RNAi. However, combined knockdown of Vps4A and Vps4B does not further stimulate IDE secretion (189.2 ± 84.3% vs. neg. ctrl. siRNA, Figure 18B) as compared to the knockdown of Vps4B alone (216.5 ± 158.7% vs. neg. ctrl. siRNA, Figure 18B). The knockdown of Vps4A alone has no significant effect on IDE secretion. As observed before for Vps4B alone, neither single nor double knockdown of both paralogues affects the release of the exosomal marker proteins Alix and Flotillin-1 (see Figure 18B). These data suggest that Vps4A could not compensate the suppression of Vps4B. In line with this, the protein levels of Vps4A are not changed upon knockdown of Vps4B.

Interestingly, Vps4A and 4B double knockdown cells show slight changes in intracellular levels of IDE and Flotillin-1. Whereas intracellular Flotillin-1 is slightly increased (131.3 ± 18.5% vs. neg. ctrl. siRNA, Figure 18B), IDE levels appear to be decreased (70.2 ± 27.3% vs. neg. ctrl. siRNA, Figure 18B) indicating an influence of the double knockdown on the expression or metabolism of both proteins, which, however, was not further determined.

The combined data indicate that the release of IDE from BV-2 cells is negatively regulated by Vps4B. However, the secretion of the exosome marker proteins Alix and Flotillin-1 is not significantly affected by Vps4B knockdown. The findings support that there is a "heterogeneity of extracellular vesicles" (Colombo, et al., 2013), and also suggest the existence of different exosome pools harbouring a distinct set of cargo proteins.

2.2.3 Generation of BV-2 clones with stable knockdown of Vps4B and IDE by expression of specific shRNA

To achieve a stable knockdown for Vps4B and IDE for further biochemical analyses at larger scale, BV-2 cells with stable expression of shRNA should be generated. Approaches to transfect BV-2 cells with DNA plasmids were inefficient. Inefficient transfection of microglial cells or the related macrophages in general was already observed in several other studies (Balcaitis, et al., 2005; Smolny, et al., 2014; Burke, et al., 2002). Therefore BV-2 cells were transduced with lentiviral particles containing constructs with a Vps4B- or IDE-specific shRNA or non-targeting shRNA (referred to as neg. ctrl. shRNA from now on), respectively (see Figure

19A+B). Selection of transduced clones was achieved by treatment with 8 µg/ml puromycin. Successful knockdown of IDE or Vps4B, respectively, was tested by Western immunoblotting. Different passages of the cells were analysed to test for potential loss of knockdown efficiency (see Figure 19C). An efficient and persistent IDE knockdown for all three used shRNA constructs is detected. shRNA 9488 shows weaker suppression of IDE as compared to shRNAs 9487 and 9489 (see Figure 19C). For further experiments, cells expressing shRNA 9489 are used.

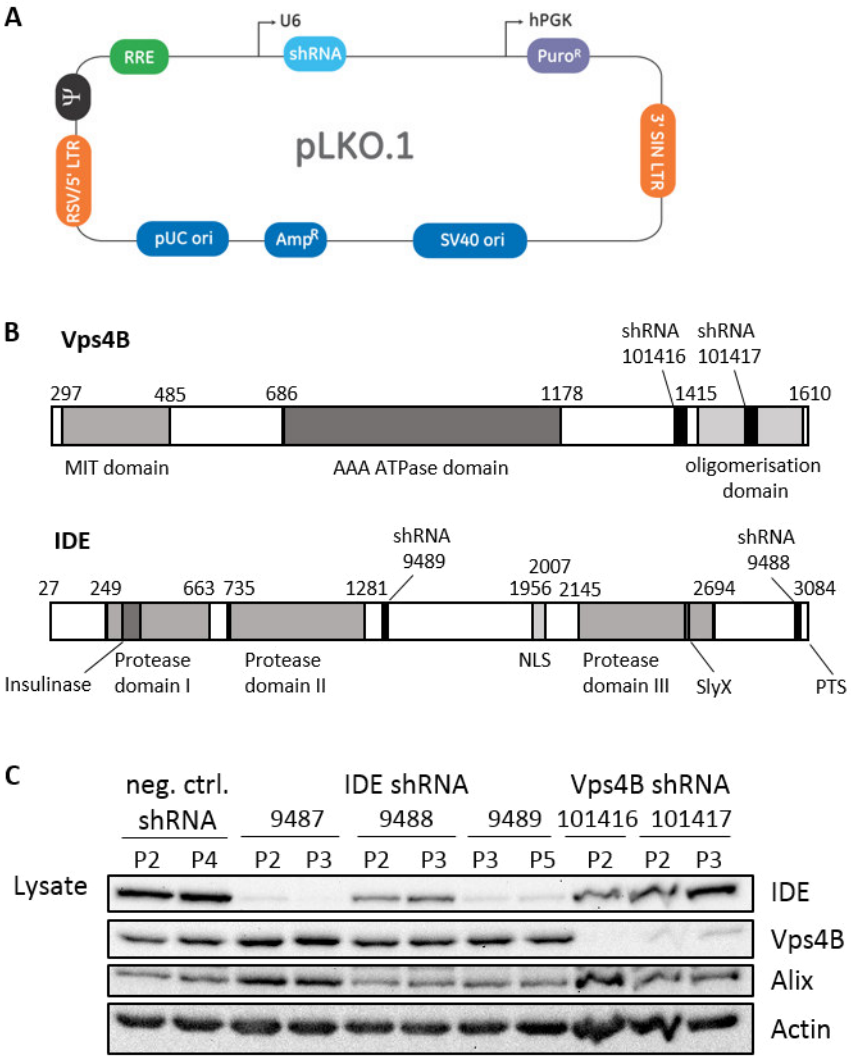

Figure 19. Generation of BV-2 cells stably expressing Vps4B- and IDE-specific shRNA by transduction with lentiviral particles. (A) shRNA constructs with the vector backbone of pLKO.1-puro containing Vps4B- and IDE-specific shRNAs or a non-target shRNA generated by The RNAi Consortium (TRC) were purchased from Dharmacon and Sigma. Scheme from TRC manual. (B) mRNA domain map and nucleotide numbering scheme for mouse Vps4B and IDE. The location of shRNA sequences inside the coding sequences (CDS) are indicated by black boxes. IDE-specific shRNA 9487 is encoded in the 3'UTR and not marked here. Map of Vps4B is based on *(Scott, et al., 2005)*. MIT – microtubule interacting and trafficking. Map of IDE is based on *(Glebov, et al., 2011)*. NLS – nuclear localisation sequence, PTS – peroxisome target signal (C) Western blot analysis of IDE, Vps4B, Alix, and Actin protein levels in cell lysates of transduced BV-2 cells after selection procedure with puromycin. Different passages (P) were analysed to test for potential loss of knockdown efficiency.

Vps4B is also efficiently knocked-down by shRNAs 101416 and 101417 in BV-2 cells (see Figure 19C). Here 101417-expressing cells are used for further experiments. shRNA 101416-expressing cells show reduced growth/proliferation rates in comparison to the other shRNA-transduced BV-2 cells.

2.2.4 shRNA-mediated stable knockdown of Vps4B in BV-2 causes changes in IDE and Flotillin-1 but not Alix release.

Stable expression of the Vps4B-specific shRNA 101417 decreases Vps4B expression by 75% (Vps4B: 24.8 ± 8.7% vs. neg. ctrl. shRNA cells, Figure 20A). In contrast to the siRNA-transfected cells here only a rather small variation of the knockdown efficiency between the experiments could be observed ranging from 62-82%. Nevertheless also here strong interexperimental fluctuations are detected regarding the analysis of the release of exosome-associated proteins. Despite high variations in the effect size, an increased IDE secretion upon stable knockdown of Vps4B in BV-2 cells can be determined (238.3 ± 222.2% vs. neg. ctrl. shRNA cells, Figure 20A) supporting the earlier observations after transient siRNA transfection (see 2.2.2). In two experiments also Flotillin-1 release is significantly enhanced, but two further experiments show no effect (182.9 ± 144.9% vs. neg. ctrl. shRNA cells, Figure 20A). The release of Alix appears to be unaffected by knockdown of Vps4B also underlining the observations made with siRNA transfection (see 2.2.2).

Subsequently, microvesicles and exosomes were isolated from conditioned media using differential centrifugation. In the microvesicle fraction, IDE, Alix and Flotillin-1 tend to be increased. However, this effect varies in three independent experiments, and is not statistically significant. The levels of these proteins in the exosome fraction are rather unchanged upon knockdown of Vps4B (see Figure 20B).

These results suggest a potential role for Vps4B in the formation or release of microvesicles rather than of exosomes. Thus, the observed increase in the secretion of IDE and partly of Flotillin-1 into conditioned medium (see Figure 20A) seems to be rather attributable to an increased release of microvesicles than of exosomes. Only a small proportion of Alix is released via microvesicles in comparison to that in exosomes, why the elevated Alix levels in the microvesicle fraction upon Vps4B knockdown have no impact on its overall secretion. By contrast, a much higher proportion of IDE and Flotillin-1 are also found in the microvesicle fraction. However, additional experiments would be required to substantiate the conclusions.

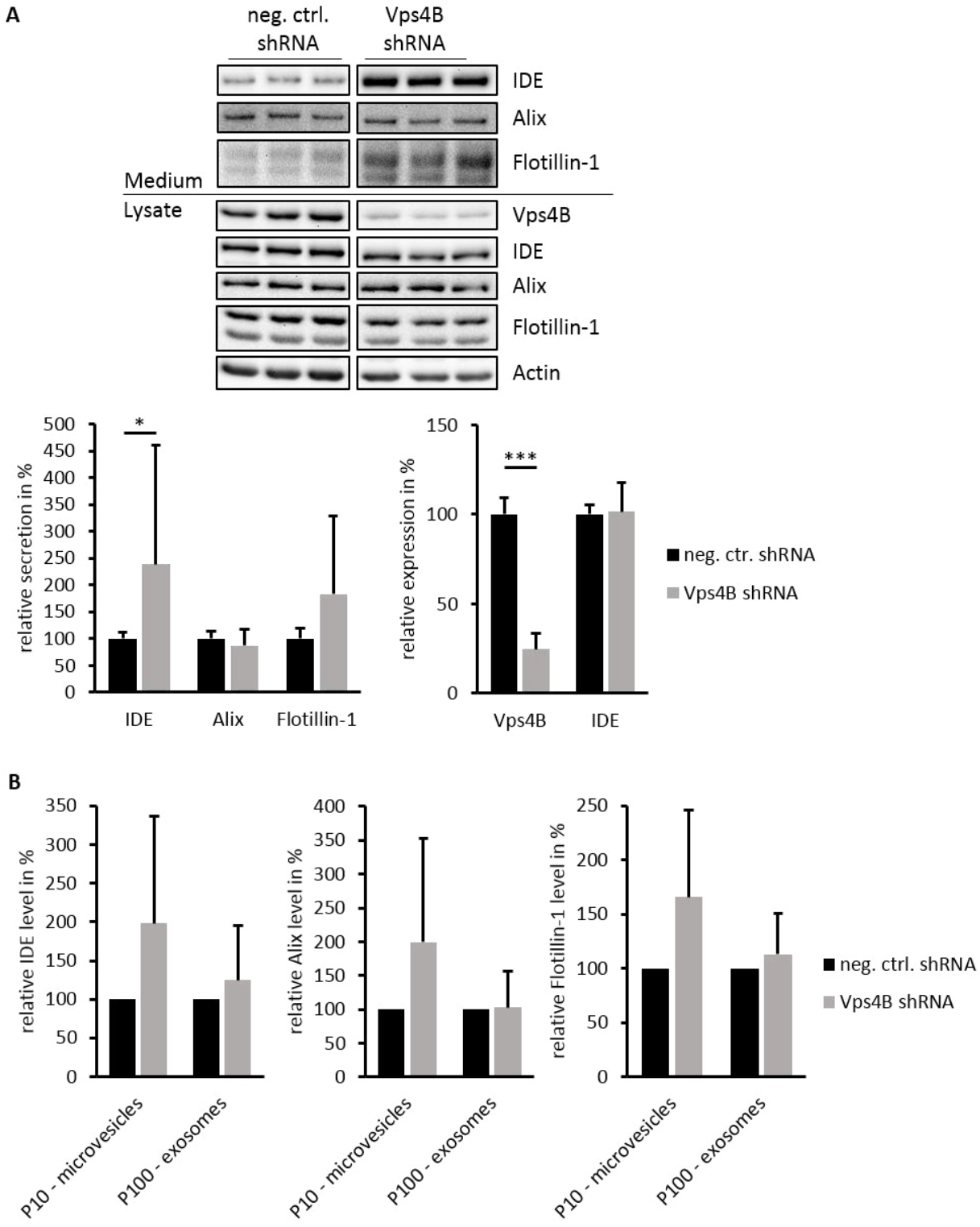

Figure 20. Influences of stable Vps4B knockdown on the secretion of IDE and Flotillin-1 are rather attributable to the regulation of microvesicle than exosome release. (A) Western blot analysis of IDE, Alix, Flotillin-1 and Vps4B protein levels in conditioned media and/or cell lysates of BV-2 cells after shRNA-mediated stable knockdown of Vps4B (n=4 in triplicates). Relative secretion is expressed as ratio of secreted to intracellular protein levels, relative expression as normalization of intracellular IDE/Vps4B to Actin levels. Statistical analysis was done using a One-Way ANOVA (Dunnett's post hoc test, see also Figure 24A). Values represent means ± SD. (B) Preparation of microvesicles (P10) and exosomes (P100) by differential centrifugation from conditioned media of BV-2 cells (n=3 in single replicates for P10 and P100). Relative protein levels are expressed as ratio of P10/P100 protein to intracellular protein levels.

2.2.5 Knockdown of Vps4B in BV-2 microglial cells does not alter the subcellular distribution of IDE.

As a member of the ESCRT machinery Vps4B was already shown to play a role in endocytic protein trafficking (Bishop & Woodman, 2000; Lin, et al., 2012; Hislop, et al., 2004). Thus, the subcellular distribution of IDE was analysed upon siRNA- and shRNA-mediated knockdown of Vps4B. Subcellular fractionation reveals predominant localisation of IDE in the cytosol,

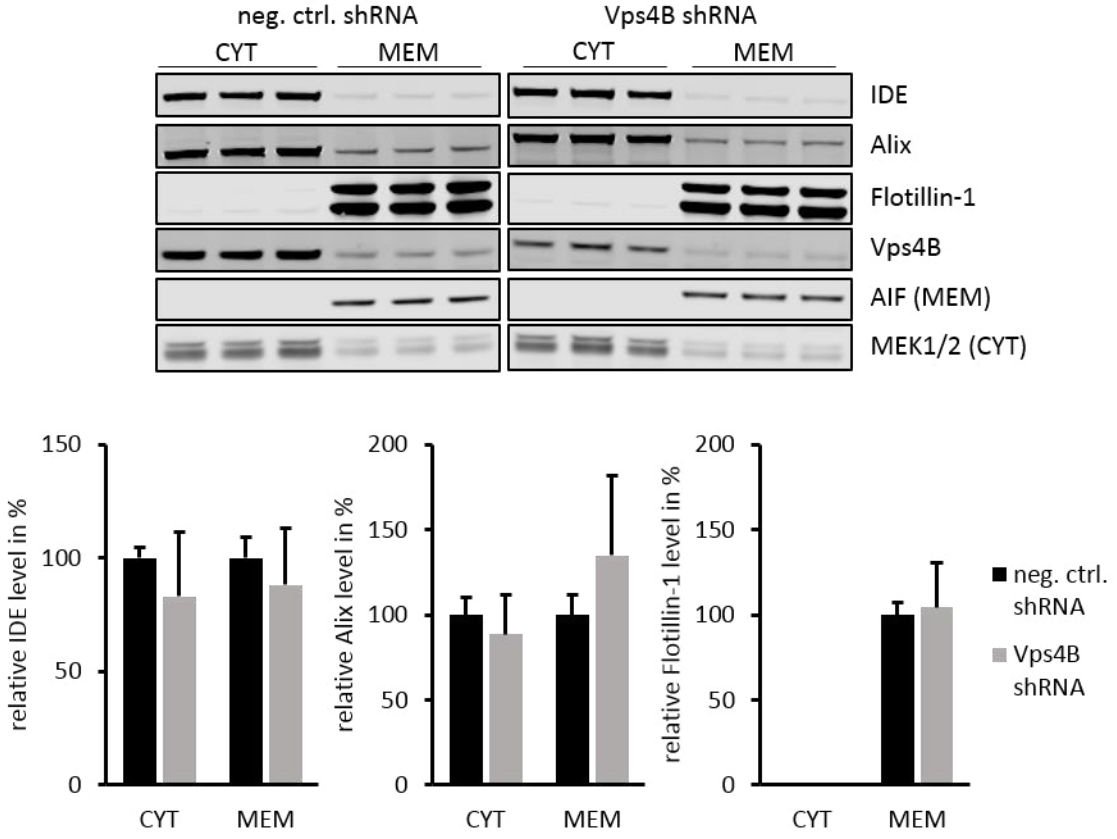

Figure 21. Distribution of IDE, Alix and Flotillin-1 between the cytosolic and the membrane-associated fraction in Vps4B-knockdown cells. Western Blot analysis of IDE, Alix, Flotillin-1, AIF and MEK1/2 protein in the cytosolic (CYT) and the membrane (MEM) fraction of BV-2 cell lysates after cell fractionation (n=3 in triplicates). Cytosolic MEK1/2 (mitogen-activated kinase kinases) and mitochondrial-intermembrane space-localised AIF (apoptosis-inducing factor) are used as marker proteins for successful separation of cytosolic and membrane fraction. Relative protein levels are expressed as ratio to Actin protein level. Statistical analysis using One-Way ANOVA (Dunnett's post hoc test) does not show statistical difference. Values represent means ± SD.

although readily detectable association of IDE with the cellular membranes is evident. A similar distribution is also found for Alix. Flotillin-1, as expected for an integral membrane protein (Otto & Nichols, 2011), is detected in the membrane fraction. Stable knockdown of Vps4B does not cause obvious changes in the distribution of all three proteins (Figure 21).

To gain further insight into the vesicular distribution of IDE, a density gradient centrifugation of the post nuclear supernatant (PNS) was performed. Individual fractions were characterised by the detection of marker proteins for distinct vesicular compartments. Alix, a known exosome cargo protein (Théry, et al., 2001; Géminard, et al., 2004), can be expected in MVBs, apart from its predominantly cytosolic localisation.

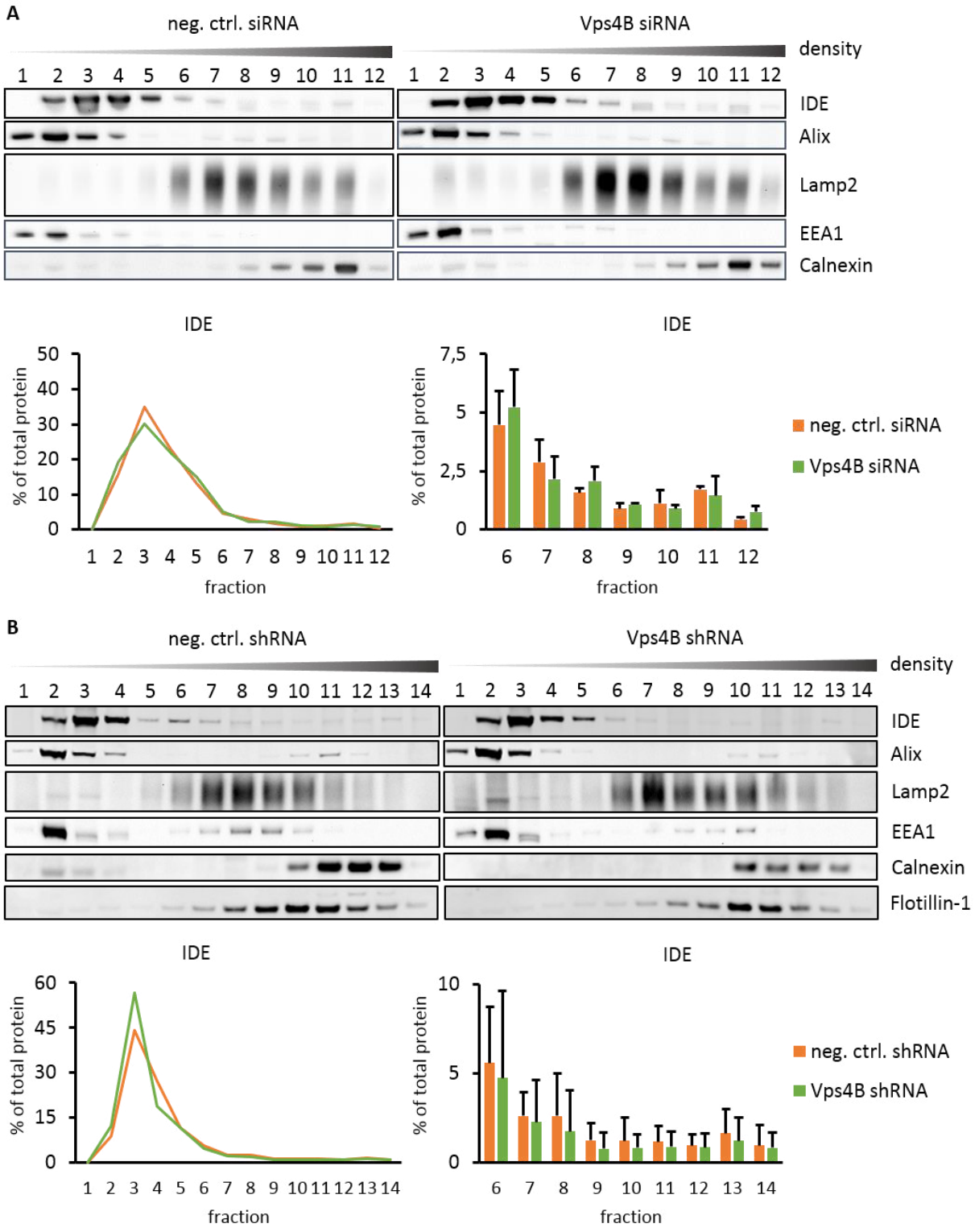

Figure 22. Subcellular distribution of IDE, Flotillin-1 and Alix. Detection of IDE and other proteins by Western immunoblotting after fractionation of intracellular vesicles and organelles by density gradient centrifugation of PNS from BV-2 cells. After centrifugation, the gradient was divided by taking off 12 (siRNA experiments, A) or 14 (shRNA experiments, B) fractions of increasing density. Specific marker proteins were used to discriminate endosomal (EEA1), lysosomal (Lamp2), MVB (Alix) and ER (Calnexin) fractions. Neither transient Vps4B knockdown by siRNA (A, n=2) nor stable knockdown by shRNA (B, n=3) does affect the subcellular distribution of IDE especially concerning its localisation to the MVB fractions (A: 7-10; B: 10-12). Statistical analysis using a One-Way ANOVA (Dunnett's post hoc test, A) and an unpaired two-sided t-test (B) does not show significant differences in the distribution of the tested marker proteins. All values represent means, partly ± SD.

It can be assumed that MVBs show a similar density as lysosomes and thus co-migrate with lysosomal marker proteins in the applied gradient. Co-fractionation of MVBs and lysosomes was already shown by Alonso and colleagues using Percoll density gradient centrifugation (Alonso, et al., 2011). Therefore Alix found in fractions of higher density is likely associated with MVBs and can be used as MVB marker in these gradients (gradient in siRNA experiments: fraction 7-10; gradient in shRNA experiments: fraction 10-12, see Figure 22). IDE is predominantly found in fractions of lower density representing cytosol and early endosomes and only a small proportion is found in fractions of higher density that are associated to compartments surrounded by membranes (fraction 6-12/14, see Figure 22). Knockdown of Vps4B does not significantly change the subcellular distribution of IDE, especially its association with MVB containing fractions is unaffected (see Figure 22). This indicates that neither transient nor stable knockdown of Vps4B does influence the trafficking of IDE.
Taken together the results do not support a major role of Vps4B in sorting of IDE to MVBs. All in all within the framework of the performed techniques it can be assumed that the observed changes in IDE secretion upon knockdown of Vps4B are not a consequence of an altered IDE intracellular transport or a shift from cytosolic to membrane-associated IDE.

2.2.6 IDE knockdown in BV-2 cells alters subcellular distribution and secretion of Alix.

Several previous studies showed that IDE is released via unconventional secretion associated to exosomes (Bulloj, et al., 2010; Tamboli, et al., 2010; Glebov, et al., 2015). To test whether IDE could also exert a functional role in the biogenesis and secretion of exosomes IDE was downregulated by transient transfection with IDE-specific siRNA in BV-2 cells.
In the individual experiments expression of IDE is decreased by 45 to 78% upon RNAi (IDE: 43.2 ± 16.5% vs. neg. ctrl. siRNA, Figure 23A). Interestingly, knockdown of IDE causes a significant increase of Alix release (146.3 ± 48.8% vs. neg. ctrl. siRNA, Figure 23A) in BV-2 cells whereas Flotillin-1 secretion is not significantly affected (106.2 ± 10.0% vs. neg. ctrl. siRNA, Figure 23A). Also here, like already observed analysing secretion upon knockdown of Vps4B (2.2.2) the interexperimental fluctuations are high and the increasing effect on Alix release by knockdown of IDE is detectable only in 3 out of 4 experiments.
Density gradient centrifugation revealed that the main proportion of Alix protein (about 90%) is found in fractions of lower density containing cytosolic (LC3-I) and early endosome-associated proteins (EEA1) (fraction 1-4/5, Figure 23B). Only a small proportion of Alix is detectable in fractions of higher density containing Lamp2-positive compartments (fraction 7-10, Figure 23B). The knockdown of IDE causes a slight but significant change of Alix distribution. In comparison to control cells IDE knockdown shows an increase in MVB-associated Alix protein

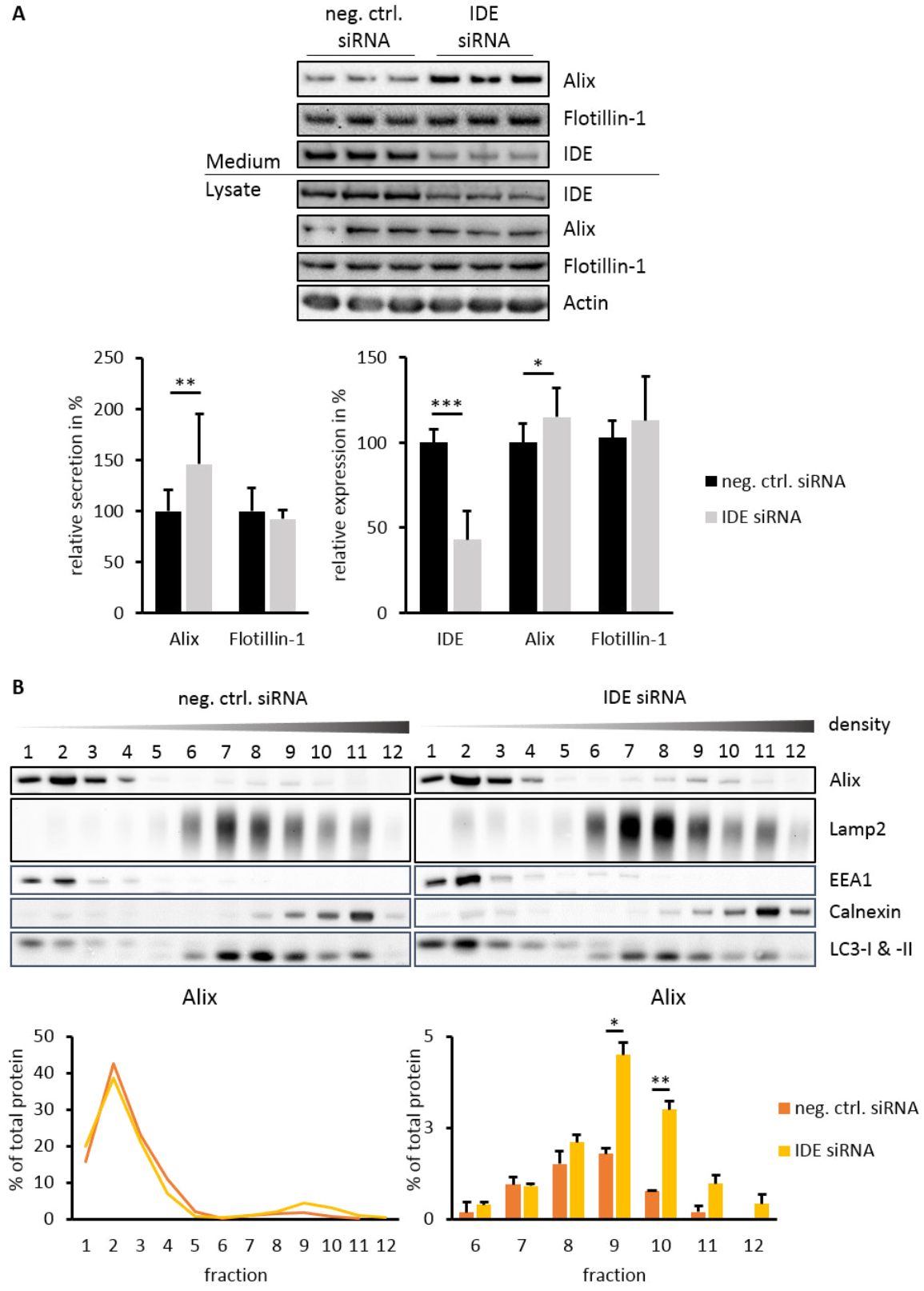

Figure 23. siRNA-mediated knockdown of IDE leads to an increase in Alix release and influences its subcellular distribution. Western blot analysis of IDE, Alix and Flotillin-1 protein levels in conditioned media and lysates of BV-2 cells after siRNA-mediated knockdown of IDE, 48 hours after transfection (A, n=4 in triplicates). An increased release of Alix is accompanied by a significant increase of Alix in the MVB fractions (9 +10) after density gradient centrifugation of PNS (B, n=2). Relative secretion is expressed as ratio of secreted to intracellular protein levels, relative expression as normalization of intracellular IDE and Alix to Actin levels. Statistical analysis was done using a One-Way ANOVA (Dunnett's post hoc test, for A see also Figure 18A, for B also Figure 22A). Values represent means ± SD.

in the fractions 9 and 10 (9: 4.50 ± 0.35% vs. 1.79 ± 0.14% for neg. ctrl. siRNA cells; 10: 3.00 ± 0.24% vs. 0.76 ± 0.03% in neg. ctrl. siRNA cells; Figure 23B).
These results show an influence of IDE knockdown not only on the secretion but also on the subcellular distribution of Alix. They, moreover, indicate a role of IDE itself in the regulation of exosome formation (possibly the budding of ILVs) or sorting of exosomal cargo to MVBs. Thus, it can be suggested that knockdown of IDE leads to an enhanced transport or association of Alix to MVBs and exosomes. The data indicate that IDE could selectively inhibit the sorting to and secretion of Alix with exosomes.

2.2.7 No influence on Alix release and distribution in BV-2 cells with shRNA-mediated stable knockdown of IDE

In contrast to the effects of siRNA-mediated knockdown of IDE in BV-2 cells on Alix distribution and secretion, examinations of stable IDE knockdown in shRNA-expressing BV-2 cells (see 2.2.3) show different observations. Stable knockdown of IDE in BV-2 cells (IDE: 16.3 ± 9.4% vs. neg. ctrl. shRNA cells) has no significant effect on Alix secretion in comparison to control cells (see Figure 24A). The IDE knockdown efficiency ranges between 70 and 94% in the individual experiments. In addition, stable IDE knockdown does not change the subcellular distribution of Alix especially concerning its localisation to MVBs showing comparable levels as in control cells (fraction 10-12, see Figure 24B).
Stable knockdown of IDE, however, enhances the release of Flotillin-1 (182.9 ± 144.9% vs. neg. ctrl. shRNA cells, Figure 24A). It is significantly increased in 2 out of 4 experiments whereas the other two show no effect, leading to the high standard deviation. Furthermore, a significant but moderate increase in cellular Flotillin-1 levels is detected (129.9 ± 26.2% vs. neg. ctrl. shRNA cells, Figure 24A). However, the cellular accumulation of Flotillin-1 is only observed in the two experiments that do not show enhanced Flotillin-1 release. Subcellular fractionation does not reveal altered distribution of Flotillin-1 upon knockdown of IDE (see Figure 24B). Flotillin-1 is known as a marker for lipid rafts and is localised at the plasma membrane, late endosomes or lysosomes, and to a lesser extent in early endosomes and exosomes (Kim, et al., 2006; Bickel, et al., 1997; Otto & Nichols, 2011). Therefore this technique most likely reaches its limits in assessing shifts in Flotillin-1 distribution due to a very probable overlapping of its localisation in raft domains of plasma membrane, lysosomes and MVBs. Therefore a potential influence of decreased IDE presence on the intracellular distribution of Flotillin-1 cannot be excluded, but would not be detectable here.

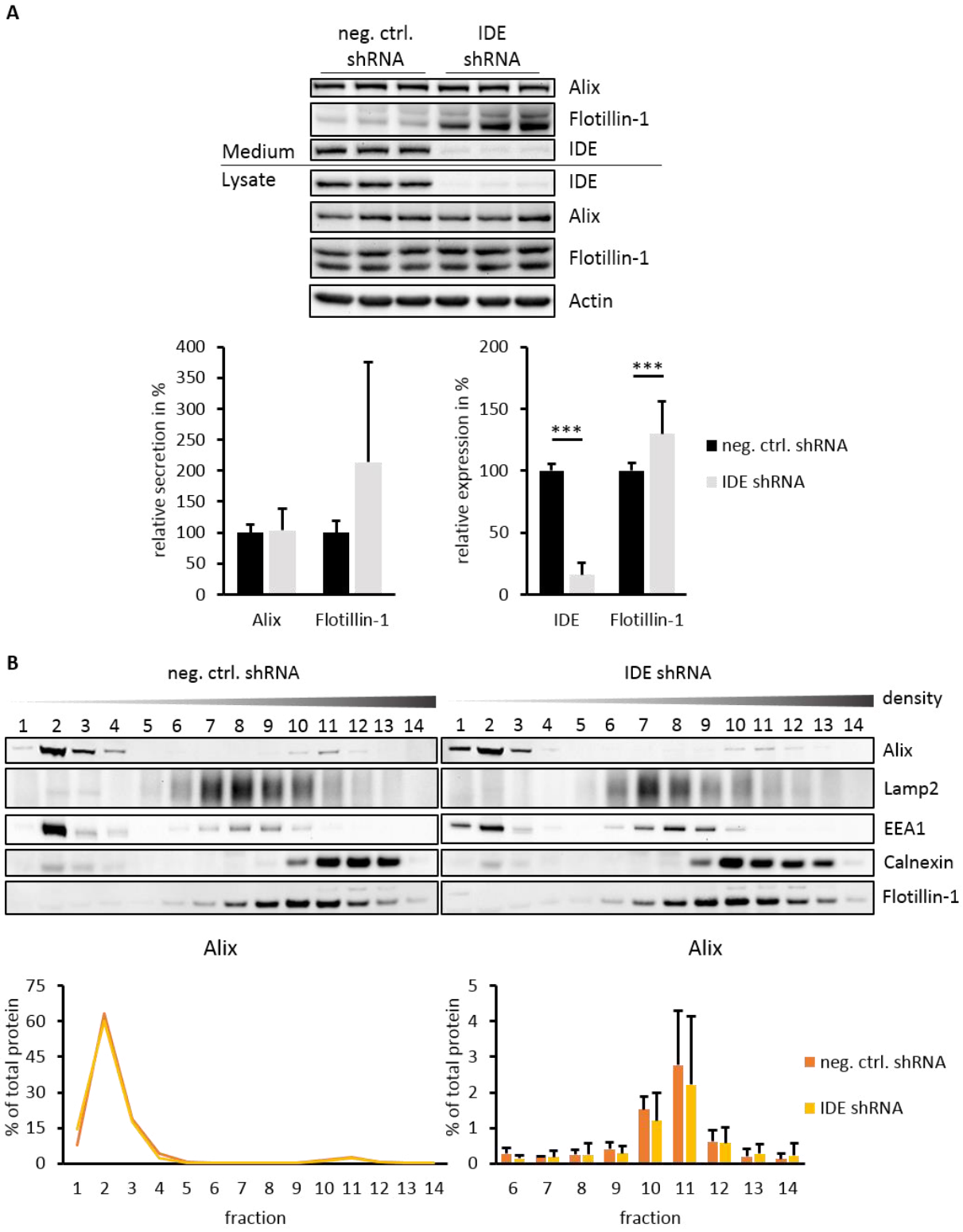

Figure 24. Stable knockdown of IDE in BV-2 cells increases Flotillin-1 but not Alix secretion from BV-2 cells. Western blot analysis of IDE, Alix and Flotillin-1 protein levels in conditioned media and lysates of BV-2 cells after shRNA-mediated stable knockdown of IDE (A, n=4 in triplicates). Nor Alix neither Flotillin-1 distribution is significantly changed upon knockdown of IDE illustrated by fractionation of intracellular vesicles and organelles by density gradient centrifugation of PNS (B, n=3). Relative secretion is expressed as ratio of secreted to intracellular protein levels, relative expression as normalization of intracellular IDE/Flotillin-1 to Actin levels. Statistical analysis was done using a One-Way ANOVA (Dunnett's post hoc test; for A see also Figure 20A) or unpaired two-sided t-test (B). Values represent means, partly ± SD.

In conclusion it can be stated that seemingly the observed effect on Alix distribution and secretion upon transient knockdown of IDE in BV-2 cells (see 2.2.6) is attributed to an ad hoc reaction on the changed IDE levels. This effect would then not be detectable during stable knockdown of IDE. Additional mechanisms might compensate the deficits in the sorting and secretion of Alix upon stable knockdown of IDE. In contrast to the release of Alix, the release of Flotillin-1 is only significantly affected upon constant knockdown of IDE and not during transient fluctuations in IDE levels.

2.2.8 Differences in the knockdown efficiency of Alix, IDE and Vps4B after longer-lasting siRNA transfection

Differential effects of transient and stable knockdown in BV-2 cells on the secretion and subcellular distribution of different exosomal cargo proteins (see 2.2.2 - 2.2.7) lead to the assumption that there are processes concerning exosome formation and sorting that are influenced differently by “short-term” and “long-term” changes in IDE and Vps4B intracellular levels. Furthermore, secretion assays carried out 72 instead of 48 hours after siRNA transfection show obvious differences in the knockdown efficiency of IDE and Vps4B but not of Alix.

72 hours after siRNA transfection of BV-2 cells levels of Vps4B are almost similar in control and in Vps4B-specific siRNA-treated cells (86.0 ± 8.3% vs. neg. ctrl. siRNA cells). In cells transfected with IDE-specific siRNA levels of cellular IDE are even slightly increased (137.2 ± 7.6% vs. neg. ctrl. siRNA cells). In contrast, cellular levels of Alix are strongly decreased 72 hours after transfection with Alix-specific siRNA (see Figure 25).

Notably, despite the slightly elevated levels of IDE in cell lysates of cells treated with IDE-specific siRNA after 72 hours of RNAi, IDE secretion is significantly decreased (37.4 ± 4.3% vs. neg. ctrl. siRNA cells, Figure 25). This suggests an efficient IDE knockdown earlier. Furthermore, an enhanced secretion of Alix from these cells, also observable after 48 hours (see 2.2.6), can be detected (263.8 ± 93.6% vs. neg. ctrl. siRNA cells, Figure 25). In Vps4B-siRNA cells, however, no increase in IDE release, that was observed after 48 hours (2.2.2), is found. IDE secretion is even slightly but not significantly decreased (70.9 ± 13.1% vs. neg. ctrl. siRNA cells, Figure 25). The complete knockdown of Alix does not result in any significant effect on IDE (79.7 ± 15.8% vs. neg. ctrl. siRNA cells) and Flotillin-1 secretion (83.6 ± 6.8% vs. net. ctrl. siRNA, Figure 25).

These observations, first, suggest different regulatory mechanisms for Alix and for IDE and Vps4B in case of potential expression changes. Obviously, processes to compensate or reactivate expression are activated after siRNA-mediated downregulation especially for IDE but also Vps4B. For Alix, however, these mechanisms are, possibly still, not in place after 72 hours. Furthermore, the observable stimulated Alix release in IDE siRNA-transfected cells

despite missing IDE knockdown let assume that possible effects of IDE expression changes still have an influence, even though IDE levels turned back to normal again. This possibly also suggests that formation of exosomes is a longer-lasting process. In comparison to that, secretion of IDE is, probably no more, affected in cells transfected with Vps4B siRNA.

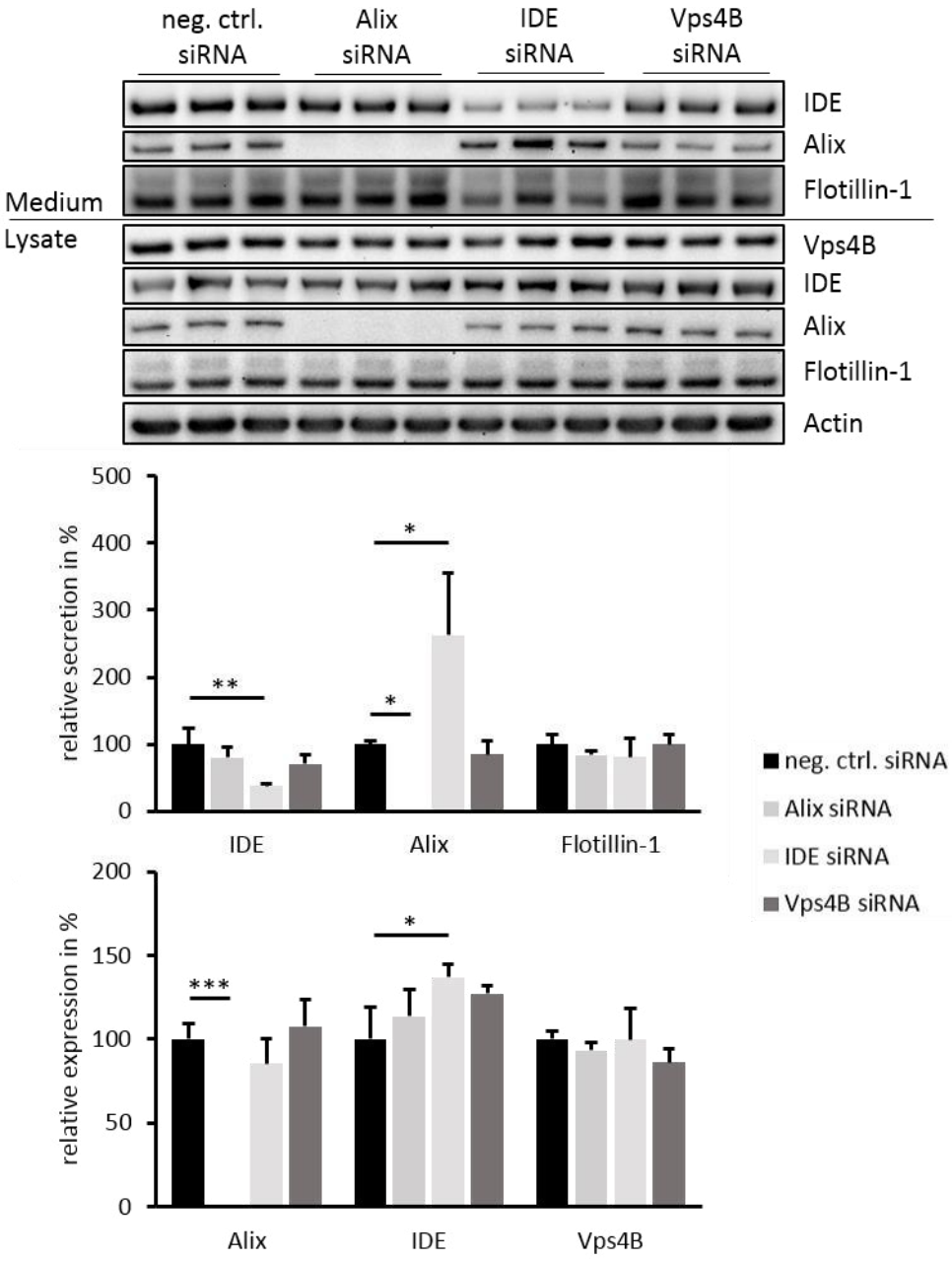

Figure 25. Knockdown efficiencies of Alix, IDE and Vps4B and their effects on exosome secretion 72 hours after siRNA transfection. Western blot analysis of IDE, Alix, Flotillin-1 and Vps4B protein levels in conditioned media and/or lysates of BV-2 cells 72 hours after siRNA transfection (n=1 in triplicates). Relative secretion is expressed as ratio of secreted to intracellular protein levels, relative expression as normalization of intracellular Alix/IDE/Vps4B to Actin levels. Statistical analysis was done using a One-Way ANOVA (Dunnett's post hoc test). Values represent means ± SD.

2.2.9 Cell type-dependent differences of Vps4B-mediated regulation of IDE secretion

Several studies already addressed the involvement of ESCRT-dependent and -independent mechanisms in exosome release and also showed differences not only between different exosome cargo proteins but also between different cell types (van Niel, et al., 2011; Phuyal, et al., 2014; Trajkovic, et al., 2008). Similar observations have also been made for the involvement of Vps4B (Kunadt, et al., 2015; Baietti, et al., 2012; Trajkovic, et al., 2008; Colombo, et al., 2013). To assess the role of Vps4B and IDE on the secretion of exosomal proteins in distinct cell lines, primary rat astrocytes and cos-7 fibroblasts were transfected with mouse or human Vps4B- and IDE-specific siRNAs, respectively, for a transient knockdown of both proteins. The results indeed show apparent variations between BV-2 microglial cells (see 2.2.2 and 2.2.6), primary rat astrocytes and cos-7 fibroblast cells.

In primary rat astrocytes a knockdown of Vps4B of approximately 70% on average (Vps4B: 32.2 ± 4.1% vs. neg. ctrl. siRNA cells, Figure 26) does not significantly influence IDE secretion but significantly decreases intracellular IDE levels (64.4 ± 5.9% vs. neg. ctrl. siRNA cells). On contrary to BV-2 cells, Vps4B knockdown significantly reduces Alix secretion (58.6 ± 22.2% vs. neg. ctrl. siRNA cells, Figure 26). Also Flotillin-1 secretion might be affected by Vps4B knockdown, but shows high variation in the effect size between the individual experiments.

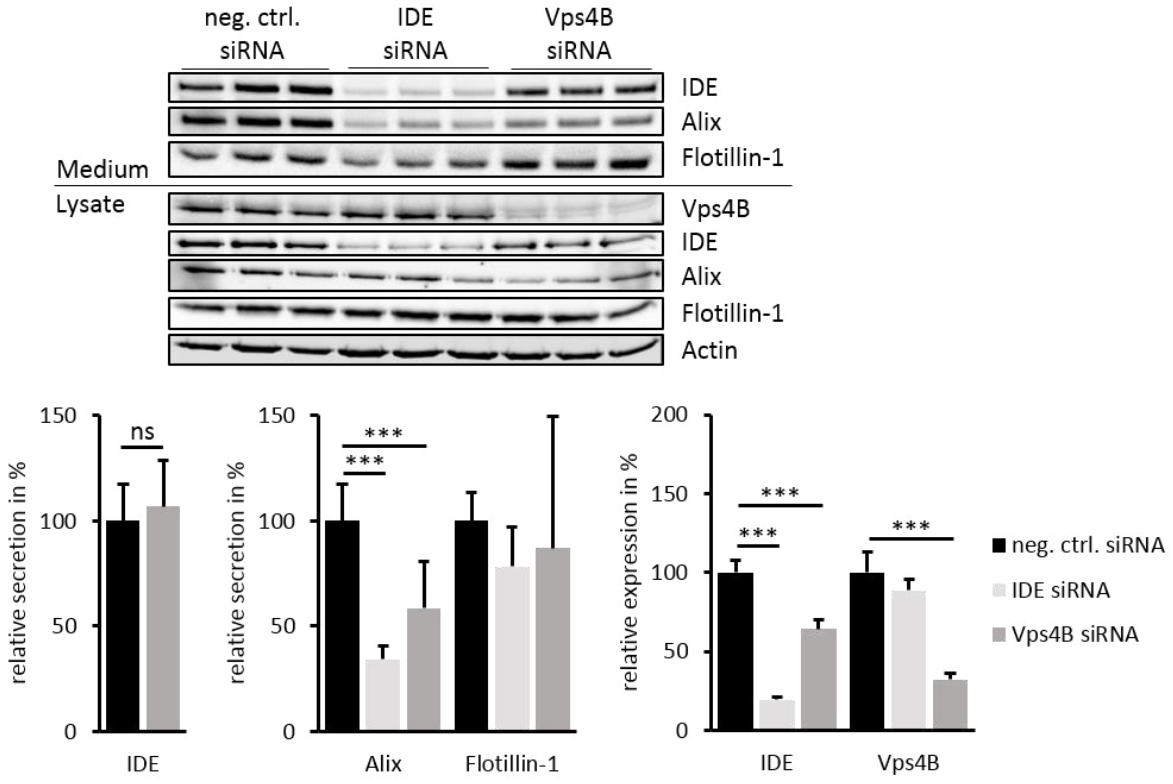

Figure 26. Decreased release of Alix upon knockdown of Vps4B and IDE in primary rat astrocytes. Western blot analysis of IDE, Alix, Flotillin-1 and Vps4B protein levels in conditioned media and/or lysates of primary rat astrocytes after siRNA-mediated knockdown of Vps4B and IDE 48 hours after transfection (n=2 in triplicates). Relative secretion is expressed as ratio of secreted to intracellular protein levels, relative expression as normalization of cellular IDE/Vps4B to Actin levels. Statistical analysis was done using a One-Way ANOVA (Dunnett's post hoc test). Values represent means ± SD.

Surprisingly, the knockdown of IDE by 80% on average (IDE: 19.5 ± 1.4% vs. neg. ctrl. siRNA, Figure 26) significantly decreases the release of Alix (34.2 ± 6.5% vs. neg. ctrl. siRNA cells, Figure 26). Levels of Flotillin-1 in the supernatant are slightly but not significantly decreased upon knockdown of IDE.

In cos-7 cells, a fibroblast cell line (Gluzman, 1981), the knockdown of Vps4B (Vps4B: 21.7 ± 2.5% vs. neg. ctrl. siRNA cells, Figure 27A) reveals a significant increase of all

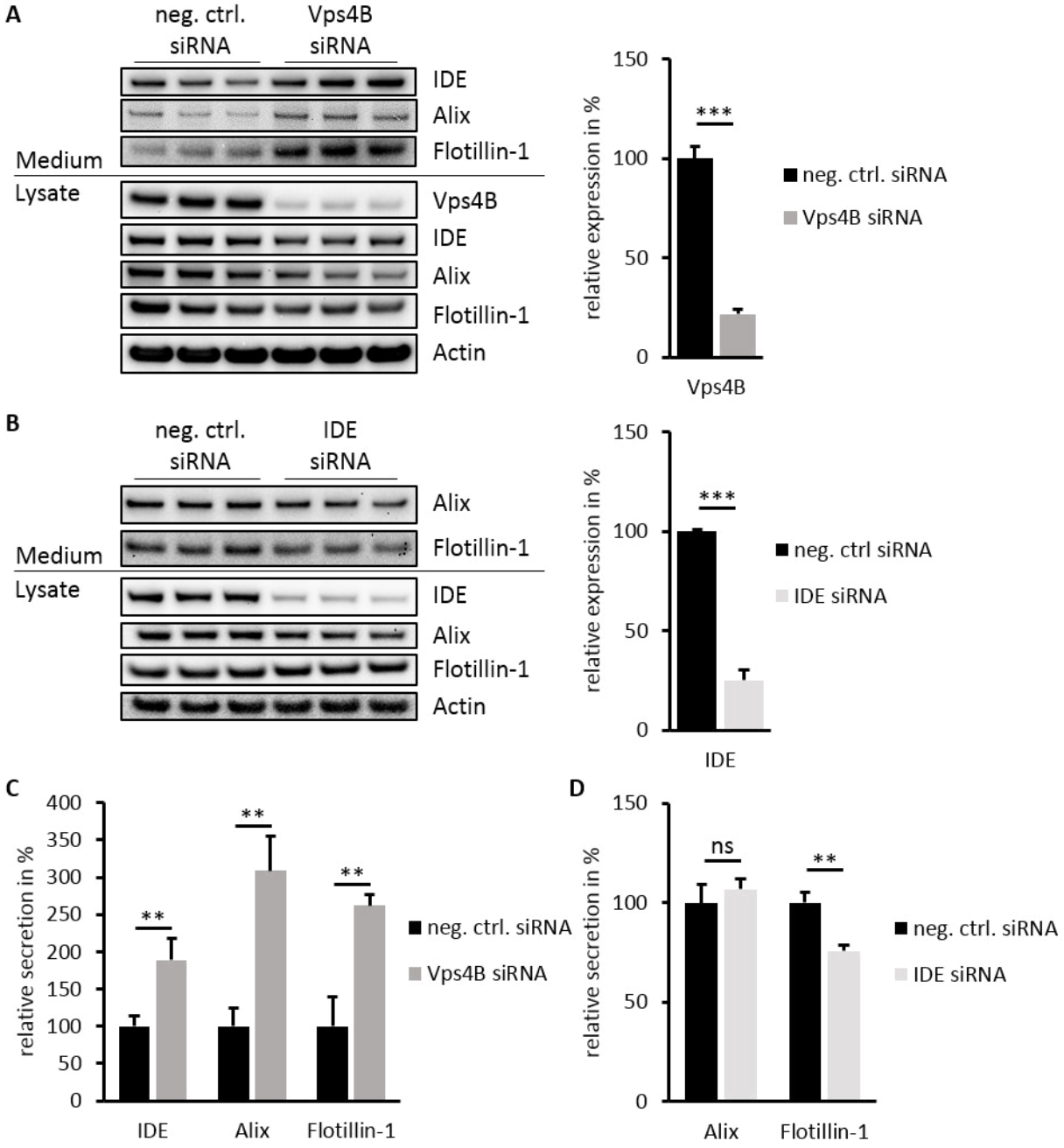

Figure 27. Vps4B knockdown in cos-7 cells causes an increased release of all examined exosome marker proteins, knockdown of IDE influences only Flotillin-1 secretion. Western blot analysis of IDE, Alix, Flotillin-1 and Vps4B protein levels in conditioned media and/or lysates of cos-7 cells after siRNA-mediated knockdown of Vps4B (A+C, n=1 in triplicates) and IDE (B+D, n=1 in triplicates) 48 hours after transfection. Relative secretion is expressed as ratio of secreted to intracellular protein levels, relative expression as normalization of intracellular IDE/Vps4B to Actin levels. Statistical analysis was done using a One-Way ANOVA (Dunnett's post hoc test). Values represent means ± SD.

examined exosome markers in the supernatant (IDE: 189.0 ± 29.6%; Alix: 308.7 ± 46.3%; Flotillin-1: 261.9 ± 15.1%; all vs. neg. ctrl. siRNA cells; Figure 27A+C). Knockdown of IDE (IDE: 25.1 ± 5.0% vs. neg. ctrl siRNA cells, Figure 27B) has no effect on Alix, but slightly and significantly reduces the release of Flotillin-1 (75.8 ± 3.0% vs. neg. ctrl. siRNA, Figure 27B+D). In conclusion it can be stated that the secretion of IDE and the other exosomal cargo proteins Alix and Flotillin-1 is differently influenced by knockdown of IDE and Vps4B in the different cell lines analysed in this work. This indicates that the release of IDE, Alix and Flotillin-1 is differently regulated in distinct cell types. Interestingly, both Vps4B and IDE seem to play a functional role in the secretion of exosome-associated proteins in all examined cell types, although exerting differential effects on individual exosomal proteins.

2.2.10 Modulation of Amyloid-β and insulin degradation in BV-2 microglial cells

Several studies already showed the involvement of secreted IDE in degradation of extracellular Aβ in BV-2 microglial cells (Tamboli, et al., 2010; Farris, et al., 2003). Therefore the involvement of Vps4B in the IDE-dependent degradation of Aβ and insulin was examined with BV-2 cells. BV-2 cells stably expressing Vps4B-specific shRNA were subjected to a degradation assay for Aβ and insulin adding 1 μM Aβ or insulin, respectively, to the medium. IDE knockdown cells served as control.

Extracellular Aβ and insulin are efficiently degraded in the conditioned media of neg. ctrl. shRNA cells (Aβ: 46.9 ± 7.3%; insulin: 63.5 ± 3.3%; both vs. time point 0 set to 100%; Figure 28A+B). The knockdown of IDE completely inhibits the degradation of both peptides, indicating that IDE is the major protease involved in the degradation of Aβ and insulin in this cell model (Aβ: 103.2 ± 9.0%; insulin: 102.2 ± 5.1%; both vs. time point 0; Figure 28A+B). Interestingly, knockdown of Vps4B leads to even more decreased levels of extracellular Aβ and insulin in comparison to control cells (Aβ: 32.6 ± 4.0%; insulin: 43.5 ± 2.4%; both vs. time point 0; Figure 28A+B). In line with an increased degradation the levels of secreted IDE in the conditioned media are significantly increased upon Vps4B knockdown in the presence of insulin (155.5 ± 9.5% vs. neg. ctrl. shRNA cells, Figure 28B), however, only slightly enhanced in the presence of Aβ (112.5 ± 10.9% vs. neg. ctrl. shRNA cells, Figure 28A).

Levels of cell-associated Aβ (cell-associated insulin was not detectable) are strongly increased in IDE knockdown cells (263.4 ± 134.0% vs. neg. ctrl. shRNA set to 100%, Figure 28A), also indicating decreased degradation. Furthermore, levels of cell-associated Aβ levels are decreased in Vps4B knockdown cells in comparison to control cells (51.6 ± 22.1% vs. neg. ctrl. shRNA cells, Figure 28A), as it is also found for extracellular Aβ levels. The ratio of both extracellular and cell-associated Aβ between Vps4B knockdown and control cells is similar. Therefore it can be assumed, that the observed decrease in extracellular Aβ is not caused by increased uptake and intracellular degradation upon knockdown of Vps4B.

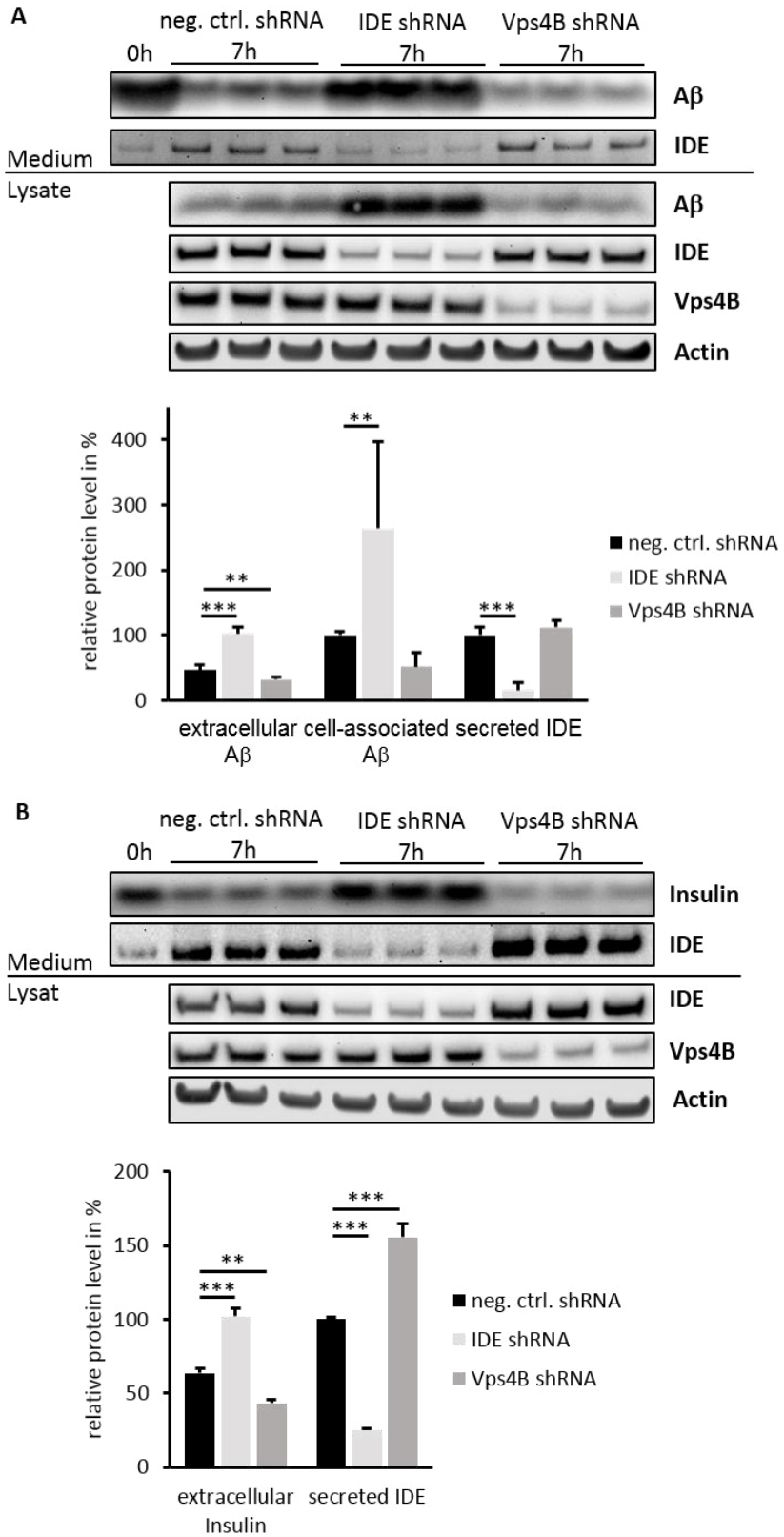

Figure 28. Involvement of Vps4B in the degradation of Aβ and insulin by IDE. Western blot analysis of IDE, Aβ and Vps4B protein levels in conditioned media and/or lysates of BV-2 cells upon stable knockdown of Vps4B and IDE in the presence of Aβ (A, n=2 in triplicates) and insulin (B, n=1 in triplicates) for 7 hours. Insulin was detected by Coomassie blue staining after SDS-PAGE. Time point 0 sample was taken immediately after the start of the assay from neg. ctrl. shRNA cells. Relative protein levels of extracellular Aβ and insulin were normalized on time point 0 protein levels, set to 100%. Relative protein levels of secreted IDE or cell-associated Aβ were normalized on neg. ctrl. shRNA cells. Statistical analysis was done using a One-Way ANOVA (Dunnett's post hoc test). Values represent means ± SD. Aβ – monomeric Aβ.

These results demonstrate a major involvement of IDE in the degradation of both Aβ and insulin by BV-2 microglial cells. Furthermore, the data also indicate a role of Vps4B in the IDE-mediated degradation of both peptides. In the presence of insulin an increased IDE secretion upon knockdown of Vps4B is detectable. Thus, the stimulated degradation of insulin by Vps4B knockdown cells might be attributed to an increase in secreted IDE. Interestingly, this effect seems to be weakened in the presence of Aβ. Hence the enhanced Aβ degradation upon Vps4B knockdown is rather related to other effects that were not examined.

2.3 Pharmacological inhibition of conventional secretion leads to an increased release of exosomal marker proteins.

IDE is released in association with exosomes and its secretion is not blocked by inhibition of the conventional secretory pathway (Bulloj, et al., 2010; Zhao, et al., 2009). To test this with BV-2 cells, Brefeldin A and Monensin, two known inhibitors of conventional secretion that block the transport of secretory vesicles from ER to Golgi or in the Golgi system, respectively, were used (Donaldson, et al., 1992; Griffiths, et al., 1983).

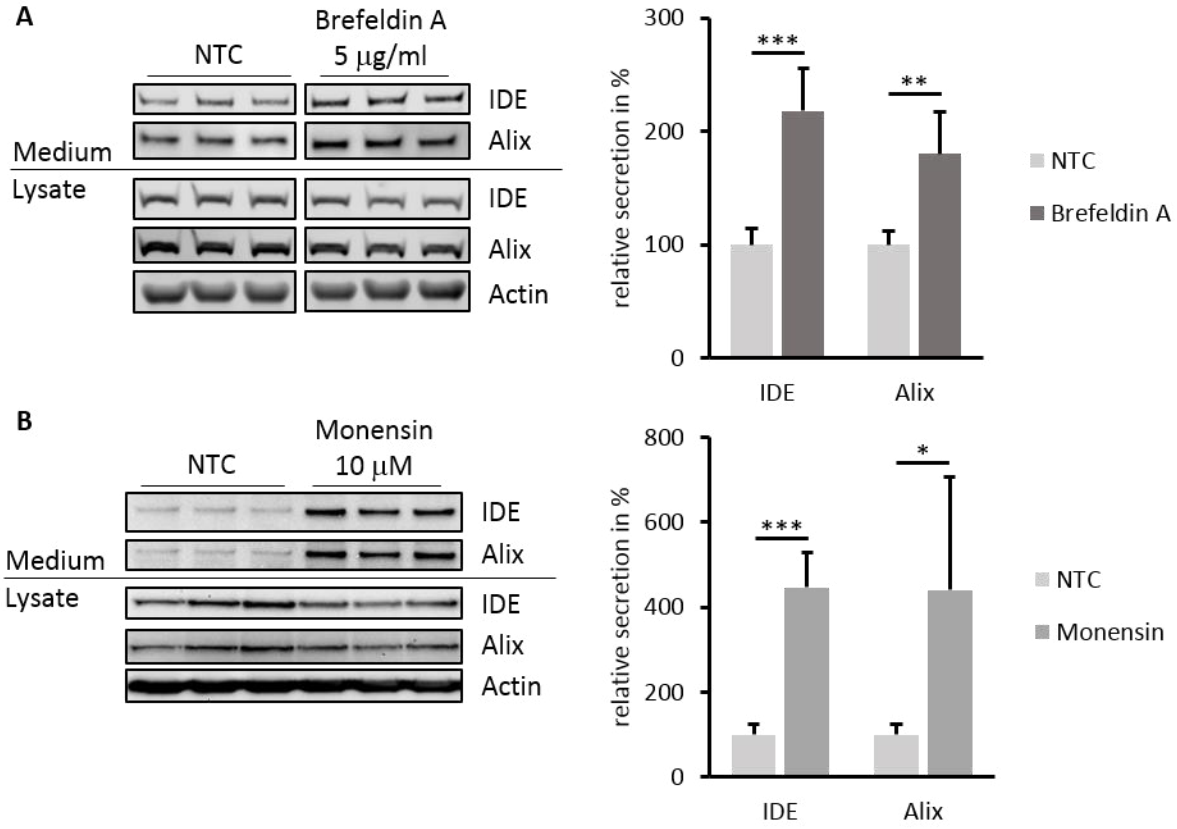

Figure 29. Inhibition of conventional secretion leads to an increase in the release of exosome marker proteins in BV-2 cells. Western blot analysis of IDE and Alix protein levels in conditioned media and/or lysates of BV-2 cells upon treatment with 5 µg/ml Brefeldin A (A, n=2 in triplicates) or 10 µM Monensin (B, n=2 in triplicates) for 5 hours. Relative secretion is expressed as ratio of secreted to intracellular protein levels. Statistical analysis was done using an unpaired, two-sided student's t-test. Values represent means ± SD.

Both inhibitors strongly stimulate the secretion of IDE from BV-2 cells (Brefeldin A: 218.2 ± 37.3% vs. NTC; Monensin: 446.2 ± 81.8% vs. NTC; Figure 29). Also the release of Alix is significantly increased by both compounds (Brefeldin A: 180.4 ± 37.3% vs. NTC; Monensin: 440.5 ± 267.5% vs. NTC; Figure 29).

These data suggest that inhibition of the conventional secretory pathway in BV-2 cells leads to stimulation of the unconventional protein secretion via exosomes. The comparable effect on the two different exosome-associated proteins IDE and Alix further suggests that Brefeldin A and Monensin directly affect the release process of exosomes rather than their intracellular formation or sorting of protein cargo to exosomes.

2.4 Y2H screen to find interaction partners of IDE potentially involved in IDE secretion regulation

Only a few proteins like ubiquitin, the androgen and glucocorticoid receptors (AR and GR) as well as the intermediate filament proteins vimentin and nestin are known to interact with IDE. Some of them were demonstrated to modulate the catalytic activity of the enzyme in the degradation of insulin and other substrates (Chou, et al., 2009; Kupfer, et al., 1994; Saric, et al., 2003). The interaction with IDE enhances the DNA binding of AR and GR (Kupfer, et al., 1994). However, little is known about interaction partners of IDE that might regulate its trafficking and secretion. To further understand the mechanism of unconventional IDE release, the yeast two-hybrid (Y2H) system was used to identify new interaction partners of IDE that might play a role in the intracellular transport of IDE and its release via exosomes.

2.4.1 Y2H screen for IDE

Truncation of the IDE C-terminus significantly decreased the release of the enzyme. A so-called SlyX domain in the C-terminal region of IDE was found to modulate the unconventional secretion of IDE (Glebov, et al., 2011) suggesting a functional role of this domain in the intracellular trafficking and exosome-associated secretion of this protein. Furthermore, in-silico analysis, using *The Eukaryotic Linear Motif Resource* (EML) (Dinkel, et al., 2014), predicted several protein interaction or modification domains additional to the SlyX domain in the C-terminal sequence of IDE. For example, SH2 and SH3 domain binding motifs, a MAPK docking domain and a SUMO interaction site. Therefore a C-terminal sequence (aa 848 - 1019) was used as bait protein to identify IDE interacting proteins with the Y2H system (see Figure 30). To confine the screen to interaction partners that might be important for brain-specific functions of IDE a mouse brain cDNA library was utilized.

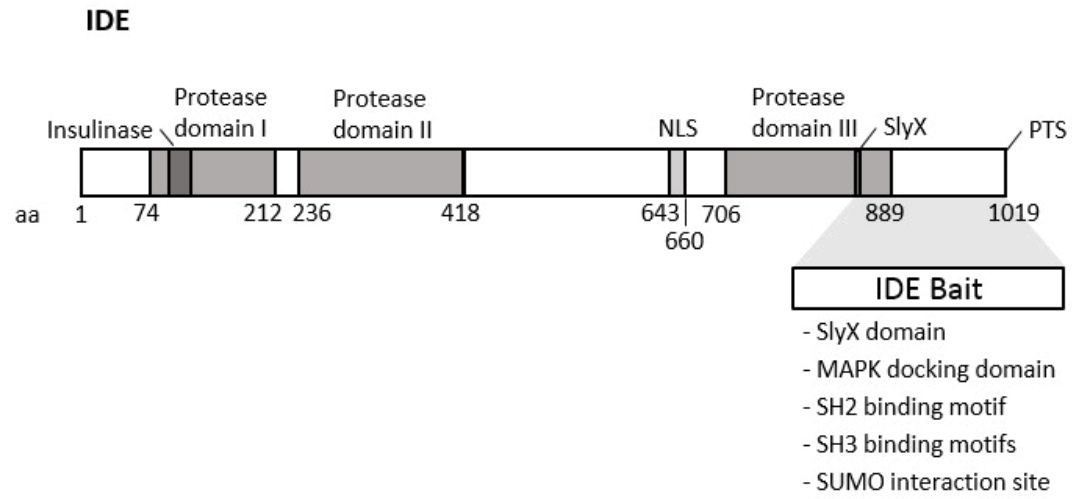

Figure 30. Generation of IDE Bait based on the C-terminal sequence of mouse IDE. Domain map and amino acid (aa) numbering scheme for mouse IDE, based on *(Glebov, et al., 2011)*. Sequence homology of IDE Bait with the C-terminal part of IDE (aa 848-1019) is indicated by grey pattern. EML analysis of this sequence predicted several protein interaction and modification sites. NLS – nuclear localisation sequence, PTS – peroxisome targeting signal.

A first screen has resulted in 7 putative IDE interacting proteins. In a second screen 19 new potential interacting proteins have been identified (see Table 16). However, only three proteins have been detected in both screens, i.e. malate dehydrogenase 1, the electron transferring flavoprotein α polypeptide and the prolin-rich coiled-coil protein 2b. In the second screen the proteins lactate dehydrogenase A and the Zn^{2+} finger protein 365 are found in two and four replications, respectively.

Potential IDE interaction partner	Cellular compartment	Characteristics
Vacuolar protein sorting-associated protein 4B (Vps4B)	cytosol, endosome membrane	involved in the late steps of the endosomal MVB pathway
Rab GTPase activating protein 1-like (RabGAP1l)	Golgi, endosomes, nucleus	regulation of protein localisation, activation of Rab GTPases
Carboxypeptidase E (CPE)	cytoplasmic vesicles, secretory vesicle membrane, secreted	binding and processing of regulated secretory pathway proteins
Secretory carrier membrane protein 5 (SCAMP5)	cell membrane, Golgi, endosomes, secretory and synaptic vesicles	required for Ca^{2+}-triggered exocytosis of signal sequence-containing cytokines
Tripeptidyl peptidase 2 (TPP2)	cytoplasm	acting downstream of 26S proteasome in ubiquitin-proteasome pathway

Ubiquitin-like containing PHD and RING finger domains (Uhrf2)	nucleus	E3 ubiquitin ligase, important for G1/S transition
Kelch-like 13 (Klhl13)	cytoplasm, nucleus?	adaptor of Cullin 3-based E3 ubiquitin ligase complex, important for chromosome segregation
E1A binding protein p400 (EP400)	nucleus	belongs to the chromatin remodelling complex, cell cycle control, apoptosis
COMM domain containing protein 8 (COMMd8)	cytoplasm	mediates degradation of IκBα and increases NFκB activity by binding Cullin 1-based E3 ubiquitin ligase complex
F-Box protein 38 (Fbxo38)	cytoplasm, nucleus	probably ubiquitination and degradation of phosphorylated proteins, transcriptional co-activator of Krueppel-like factor 7
Neuroblastoma apoptosis-related RNA binding protein (NAPOR)	nucleus, cytoplasm	region-specific alternative splicing in the nervous system
Zn^{2+} finger RAN binding domain containing protein 2 (ZranB2)	nucleus	alternative splicing, suppression of BMP-signalling via Smad-binding
Zn^{2+} finger protein 365 (ZFP365)	cytoplasm	centrosome-associated, essential for cell division, high expression levels in brain
Heat shock protein 90 beta member 1 (Hsp90b1)/ Grp94	ER	molecular chaperone, paralogue of Hsp90, processing and transport of secreted proteins, involved in ER stress signalling
Aminoadipate-semialdehyd dehydrogenase-phospho-pantheteinyl transferase (Aasdhppt)	cytoplasm	catalyses the post-translational modification of target proteins by phosphopantetheine
Sirtuin 3 (SIRT3)	mitochondrion matrix, nucleus?	role in dietary restriction, controlling metabolism at transcriptional level
Electron transferring flavoprotein α polypeptide (ETFA)	mitochondrion membrane	part of the respiratory chain (complex II)
Aldo-keto reductase 1 (Akr1a1)	cytosol, apical plasma membrane	NADPH-dependent reduction of a variety of aromatic and aliphatic aldehydes

Tissue specific transplantation antigen P35B (Tsta3)	cytoplasm	NADPH-binding protein, role in GDP-D-mannose metabolism
$GABA_A$ receptor subunit β2 (Gabrb2)	cell membrane	activation of $GABA_A$ receptors provides an inhibitory effect on neurotransmission
Lactate dehydrogenase A (LDH A)	cytosol, mitochondrion	pyruvate fermentation to lactate
Enolase 1	cytoplasm, cell membrane	role in glycolysis
Malate dehydrogenase 1 (Mdh1)	cytoplasm, mitochondrion	role in gluconeogenesis and other processes like malate and oxalacetate metabolism
Asparaginase like 1 (Asrgl 1)	cytoplasm	role in asparagine catabolism
Prolin-rich coiled-coil protein 2b (prrcb2)	cytoplasm	unknown function
RIKEN cDNA D030056L22	unknown	unknown function

Table 16. Potential interaction partners of IDE identified by Y2H cDNA library screen. Two Y2H cDNA library screens with IDE Bait utilizing a mouse brain cDNA library reveal 26 putative IDE-interacting proteins. Eight have to be excluded (highlighted in grey). Their protein sequence interacting with IDE Bait is coded by a part of their mRNA sequence that is located in the 3' untranslated region outside their coding sequence (CDS). This generates protein sequences which are normally not expressed.

Eight IDE putative interaction partners are considered false positive, because their protein sequence interacting with IDE Bait is coded by a part of their 3' untranslated mRNA region. The other 18 putative interaction partners can be related to energy metabolism, cell cycle regulation, ubiquitination and the proteasomal protein degradation pathway. The majority (83%) of these proteins are associated to energy and protein metabolism (see Figure 31A). Most interestingly, Vps4B being examined in parallel for its regulatory role in the exosome-associated release of IDE, is identified as potential interaction partner of IDE as well. The fragment of Vps4B that is able to interact with IDE Bait corresponds to a protein sequence of Vps4B of 237 aa including almost the whole AAA ATPase domain as well as a small part of the MIT domain (microtubule interacting and trafficking domain), that is responsible for binding the ESCRT III complex (Scott, et al., 2005), (see Figure 31B). Furthermore, another interesting protein, Carboxypeptidase E (CPE), involved in sorting of conventionally secreted proteins in the brain and rather part of the conventional secretory pathway (Cawley, et al., 2012) is found. Interaction of Vps4B and IDE Bait could be confirmed by an additional Y2H candidate co-transformation assay, while CPE has to be excluded due to autoactivation in this system.

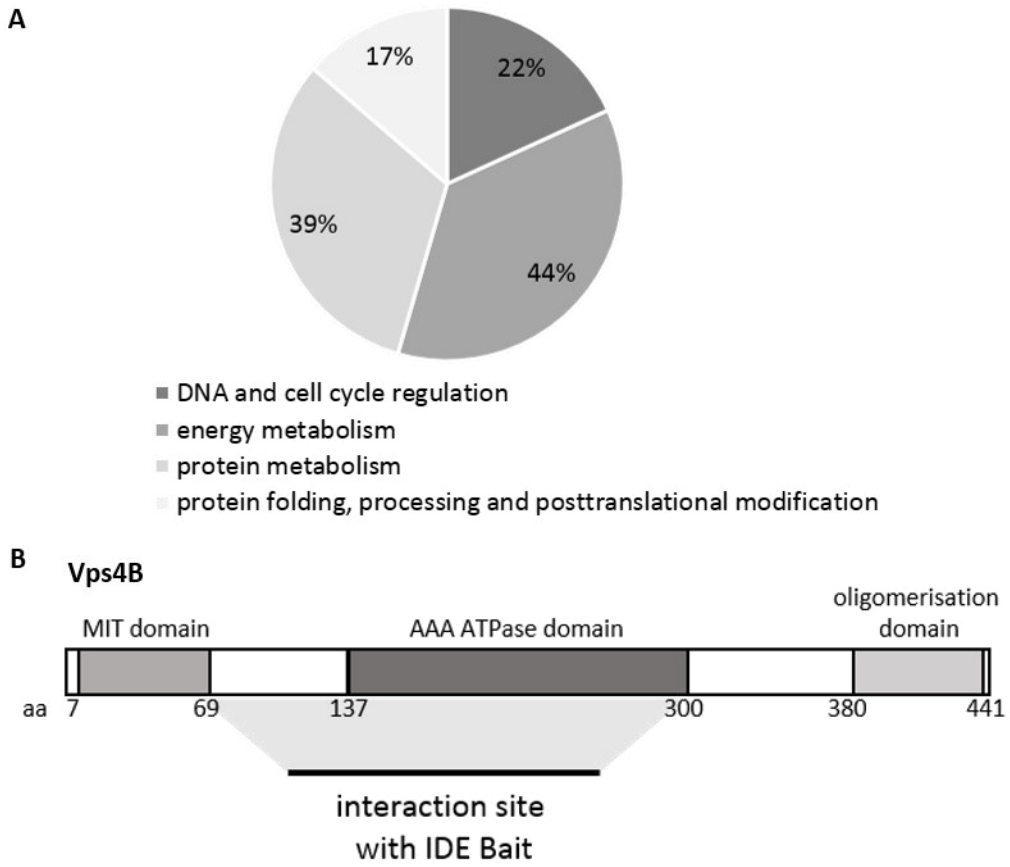

Figure 31. Analysis of the potential interaction partners of IDE. (A) Pie chart of biological functions of putative interaction partners of IDE, see Table 16 above. (B) Domain map and amino acid (aa) numbering scheme for mouse Vps4B, based on *(Scott, et al., 2005)*, indicated: interaction site of the Vps4B fragment (62-298 aa) interacting with IDE Bait. MIT – microtubule interacting and trafficking.

2.4.2 Interaction of IDE and Vps4B

IDE and Vps4B are mainly localised to the cytosol (Duckworth, et al., 1998; Bishop & Woodman, 2000). The results presented in 2.2.5 (see Figure 21) also demonstrate predominant localisation of both proteins in the cytosol in BV-2 cells. Hence, the main proportion of IDE and Vps4B are present in the same compartment, which topologically could allow an interaction. Additionally, IDE as cargo of exosomes (Bulloj, et al., 2010; Tamboli, et al., 2010) and Vps4B as regulatory protein for the MVB pathway (Hanson & Cashikar, 2012; Babst, et al., 1998), can both be associated with intracellular vesicles like endosomes or MVBs.

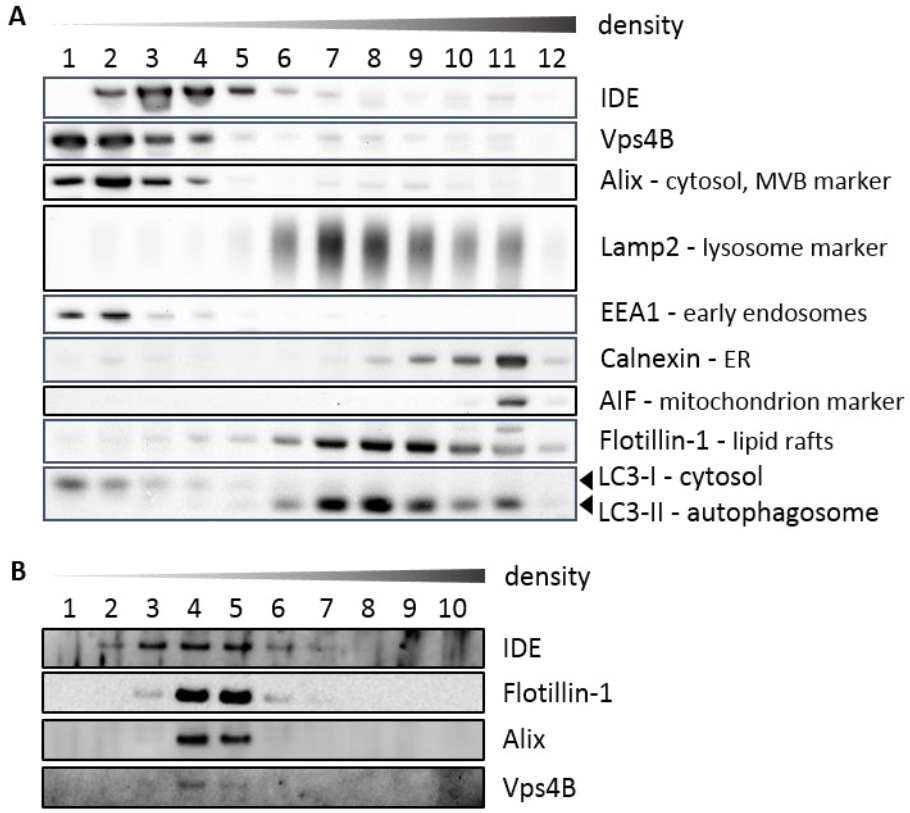

Figure 32. Detection of IDE and Vps4B in similar subcellular fractions and in exosomes. Western blot analysis of IDE, Vps4B and other proteins after fractionation of intracellular vesicles and organelles or exosomes, respectively, by density gradient centrifugation of PNS (A) or the exosome fraction P100 from conditioned medium (B) of BV-2 cells. A partial overlap of IDE and Vps4B in subcellular vesicle fractions and a strong co-migration with other exosomal markers in exosome vesicles of the same density is detectable.

Density gradient centrifugation reveals an overlap of both proteins, predominantly in fractions 2-4 (see Figure 32A). Interestingly, IDE is not detected in fraction one, representing most likely the main cytosolic fraction, and peaks in fraction three. Vps4B, however, shows an almost complete overlap with Alix in fractions 1-4 that also contain LC3-I. IDE and Vps4B also show co-fractionation with the endosomal marker EEA1. Only about 11-13% of both proteins are detected in fractions of higher density that contain larger compartments surrounded by membranes (fraction 6-12), where markers as Lamp2, LC3-II and Calnexin are found. Thus, smaller proportions of IDE and Vps4B can be detected in fractions potentially containing MVBs

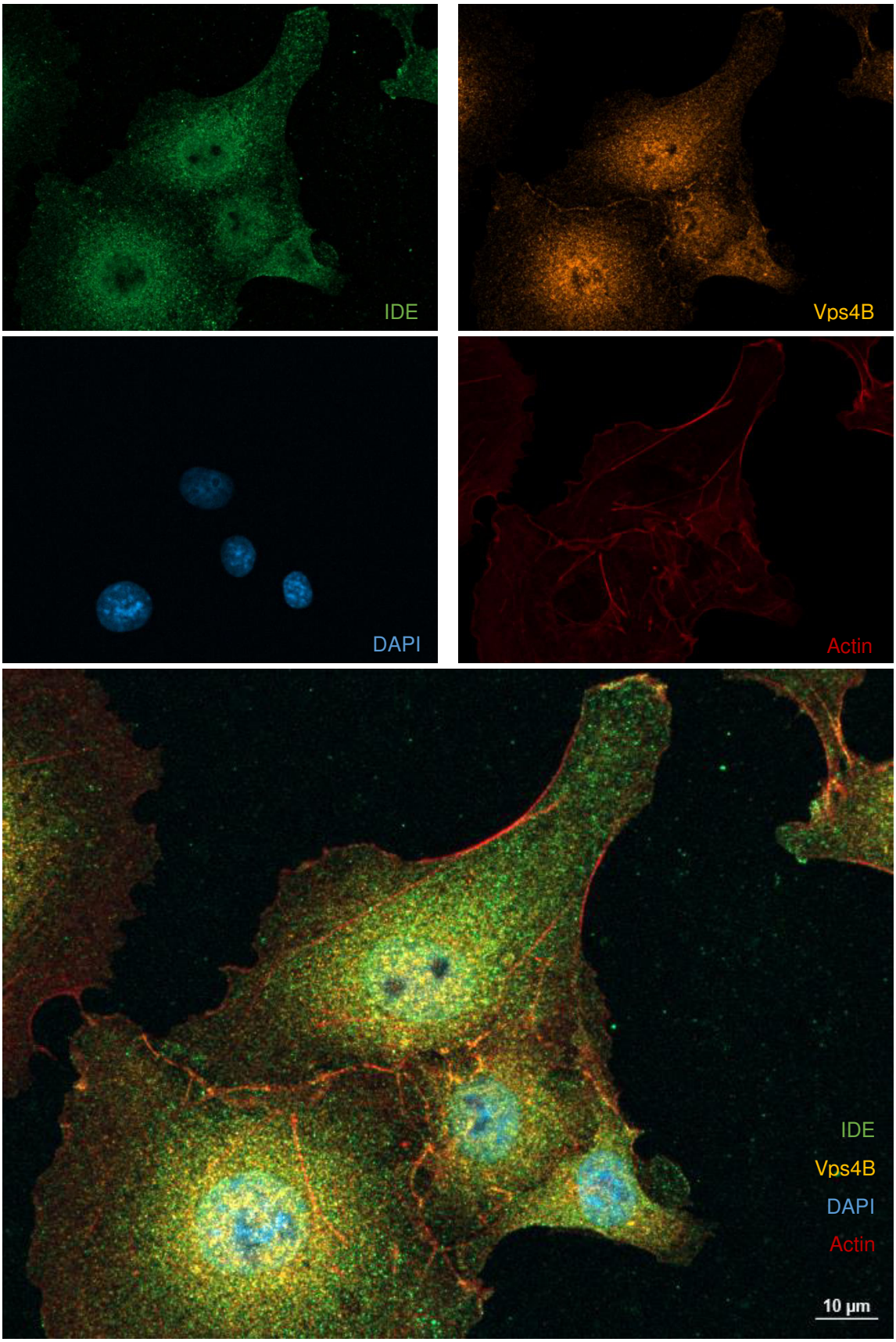

Figure 33. Immunocytochemical staining of IDE and Vps4B in cos-7 cells. Immunofluorescence staining of IDE, Vps4B and Actin in cos-7 cells. IDE was detected using a monoclonal mouse antibody (MAB2496) and an Alexa Fluor® 488-coupled anti-mouse antibody and Vps4B was stained by a polyclonal rabbit antibody (NBP1-19119) and an Alexa Fluor® 546-coupled anti-rabbit antibody. Phalloidin coupled to Alexa Fluor® 647 served to detect F-Actin. Nuclei were visualized by DAPI staining.

(fraction 7-10, Figure 32A). A strong overlap of IDE and Vps4B is also observed upon isolation and fractionation of exosomes by density gradient centrifugation, together with the other exosomal marker proteins Alix and Flotillin-1 (fraction 4 and 5; Figure 32B).

Immunocytochemical staining of endogenous IDE and Vps4B in cos-7 cells shows a similar, mainly cytosolic distribution of both proteins. In addition, both proteins show punctate pattern in the cytoplasm slightly concentrated around the nuclear region. Vps4B also displays a partial co-localisation with the Actin cytoskeleton (see Figure 33).

To further examine the interaction of IDE and Vps4B a co-immunoprecipitation (Co-IP) approach was carried out. However, little if any specific co-IP with the endogenous proteins is detected. In contrast, overexpression of both proteins reveals co-immunoprecipitation of myc-tagged IDE and Vps4B (lane 2, Figure 34A and B).

Since the high size similarity of Vps4B (49.4 kDa) and the heavy chain of the IP antibody (~50 kDa) prevented an adequate Vps4B detection and IP-suitable IDE and Vps4B antibodies had the same host organism, an alternative approach was carried out using the fusion protein Vps4B-MBP with the size of approximately 100 kDa. Here, IDE-myc co-immunoprecipitates Vps4B-MBP (lane 2, Figure 34C) and vice versa (lane 3, Figure 34C).

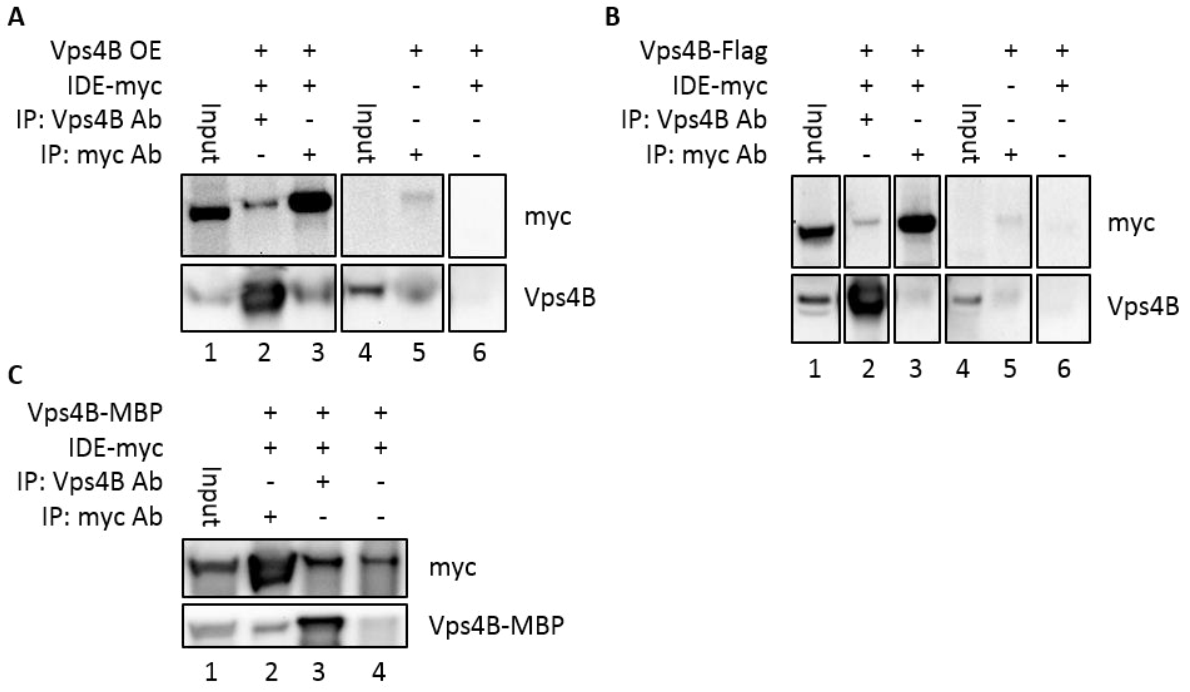

Figure 34. Co-immunoprecipitation of IDE and Vps4B. (A+B) Western blot analysis of IDE-myc and Vps4B after immunoprecipitation (IP) of IDE-myc or Vps4B/Vps4B-Flag, respectively, from lysates of Vps4B/IDE-myc-overexpressing HEK293. A control IP using lysates of only Vps4B-overexpressing cells + the myc antibody for IP (lane 4+5, respectively) and a bead control without addition of IP antibody (lane 6, respectively) were carried out. Co-IP of Vps4B with IDE-myc (lane 3, A+B) is not possible to distinguish significantly from the control IP without IDE-myc overexpression showing a weak signal at the size of Vps4B as well (lane 5, A+B). (C) Modified Co-IP approach: Detection of Vps4B-MBP after IP of IDE-myc from lysates of IDE-myc-overexpressing HEK293 cells complemented with the fusion protein Vps4B-MBP. OE – overexpression, Ab – antibody

The combined results indicate an interaction of IDE and Vps4B. However, this interaction might be weak or transient.

2.4.3 Interaction of IDE and Vps4B does not affect the usual complex formation of both proteins.

Vps4B exists in monomeric and dimeric states. In addition, higher order dodecameric assemblies have been described in the presence of ATP (Scott, et al., 2005; Babst, et al., 1998). IDE was shown to exist primarily as a dimer (Safavi, et al., 1996; Shen, et al., 2006; Song, et al., 2003). Native gel electrophoresis should provide an insight into the complex formation of IDE and Vps4B. Blue Native PAGE (BN-PAGE) (Wittig, et al., 2006) enables the electrophoretic separation of protein complexes. A subsequent SDS/Urea PAGE results in dissociation and separation of these protein complexes.

BV-2 cells were lysed without detergent or with different concentrations of the mild nonionic detergent Digitonin and resultant lysates subjected to BN-PAGE. IDE is prominently detected at approximately 242 kDa (see Figure 35A) consistent with the expected size of a dimer. In contrast, Vps4B is predominantly detected at around 1.2 MDa and a smear of lower size than 242 kDa (see Figure 35A). The high molecular weight form (1.2 MDa) could represent the ATPase complex formed by Vps4A and Vps4B, and probably additional proteins (Scott, et al., 2005). The smear at lower molecular mass (below 242 kDa) likely represents monomeric and dimeric forms of Vps4B. Cell lysis with Digitonin decreases the detection of the high molecular weight form (1.2 MDa), suggesting the Vps4B ATPase complex is sensitive and partly or almost completely dissociates with 0.5% or 1% Digitonin, respectively.

Complexes reactive for both IDE and Vps4B are not detectable. Nevertheless, an interaction of IDE and Vps4B is not excluded since lower amounts of such a complex might not be detectable with this method. Furthermore, epitopes of the respective antibodies used for detection might be masked in potential complexes. Subsequent separation by SDS/Urea PAGE reveals two strong signals for IDE in the 2nd dimension (see Figure 35B) which most likely represent the dimer (left) and monomer (right) forms. The two signals partly overlap, a characteristic observation for 2D-separations. Detection of Vps4B demonstrates a weak signal (left) that can be attributed to the 1.2 MDa ATPase complex and an intense smear (right) most likely representing the monomer and/or dimeric assemblies.

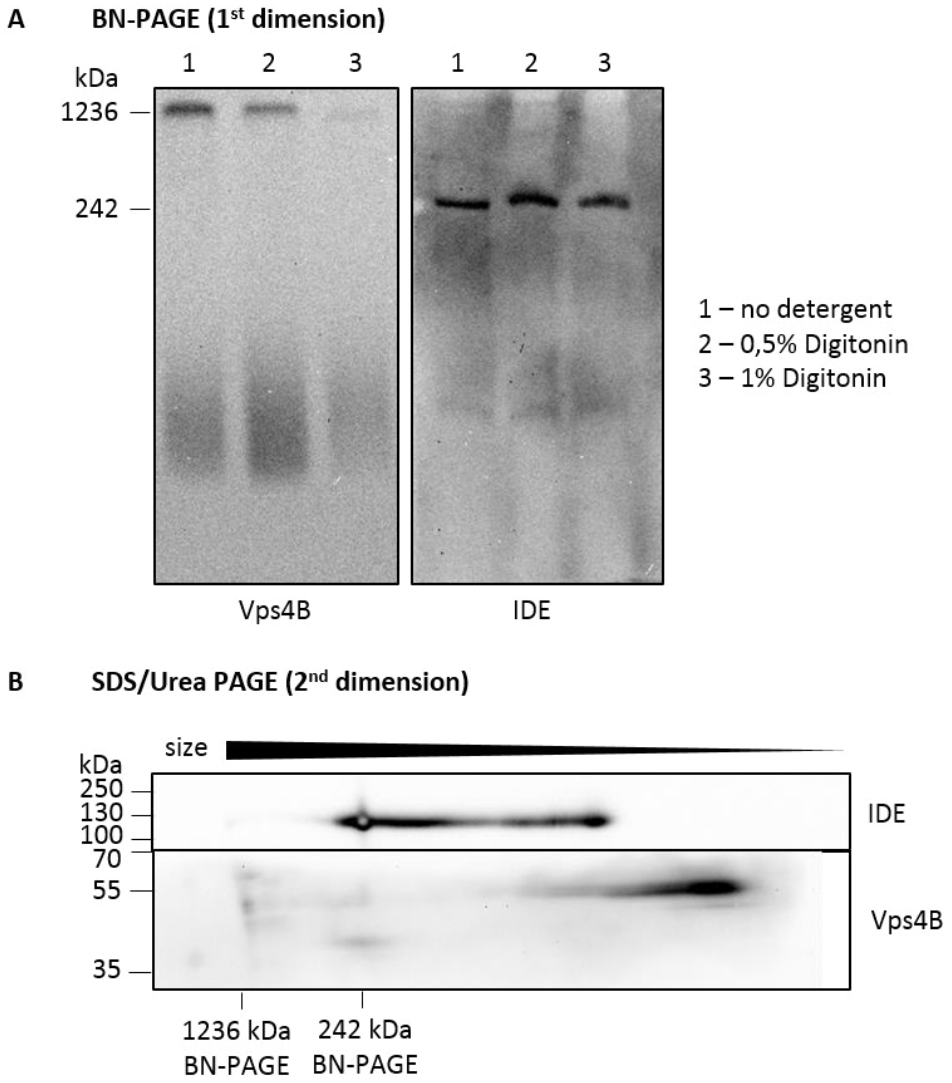

Figure 35. Native protein complexes of IDE and Vps4B. (A) Western blot analysis of Vps4B and IDE upon BN-PAGE of BV-2 cell lysates in the presence/absence of Digitonin. (B) Subsequent SDS/Urea PAGE in the 2nd dimension and detection of IDE and Vps4B by Western immunoblotting.

To further examine a potential role of IDE or Vps4B in the complex formation of both proteins BV-2 cells stably expressing IDE- or Vps4B-shRNAs (see 2.2.3) were also analysed. Neither knockdown of Vps4B nor of IDE does cause overt changes in the migration of the individual complexes (see Figure 36A and B). Notably, knockdown of one of the two proteins increased the signal of the other protein (see Figure 36A). Separation in the 2nd dimension by SDS/Urea PAGE reveals a similar pattern for IDE and Vps4B under both, knockdown and control conditions. As expected the signal intensity for the downregulated protein is decreased.

In conclusion, complex formation of IDE with Vps4B could not be detected unambiguously using native gel electrophoresis and subsequent SDS/Urea PAGE. However, the observed changes in the amounts of higher molecular weight complexes containing IDE and Vps4B upon the knockdown of the other, respectively, could hind to a potential functional interaction of both proteins.

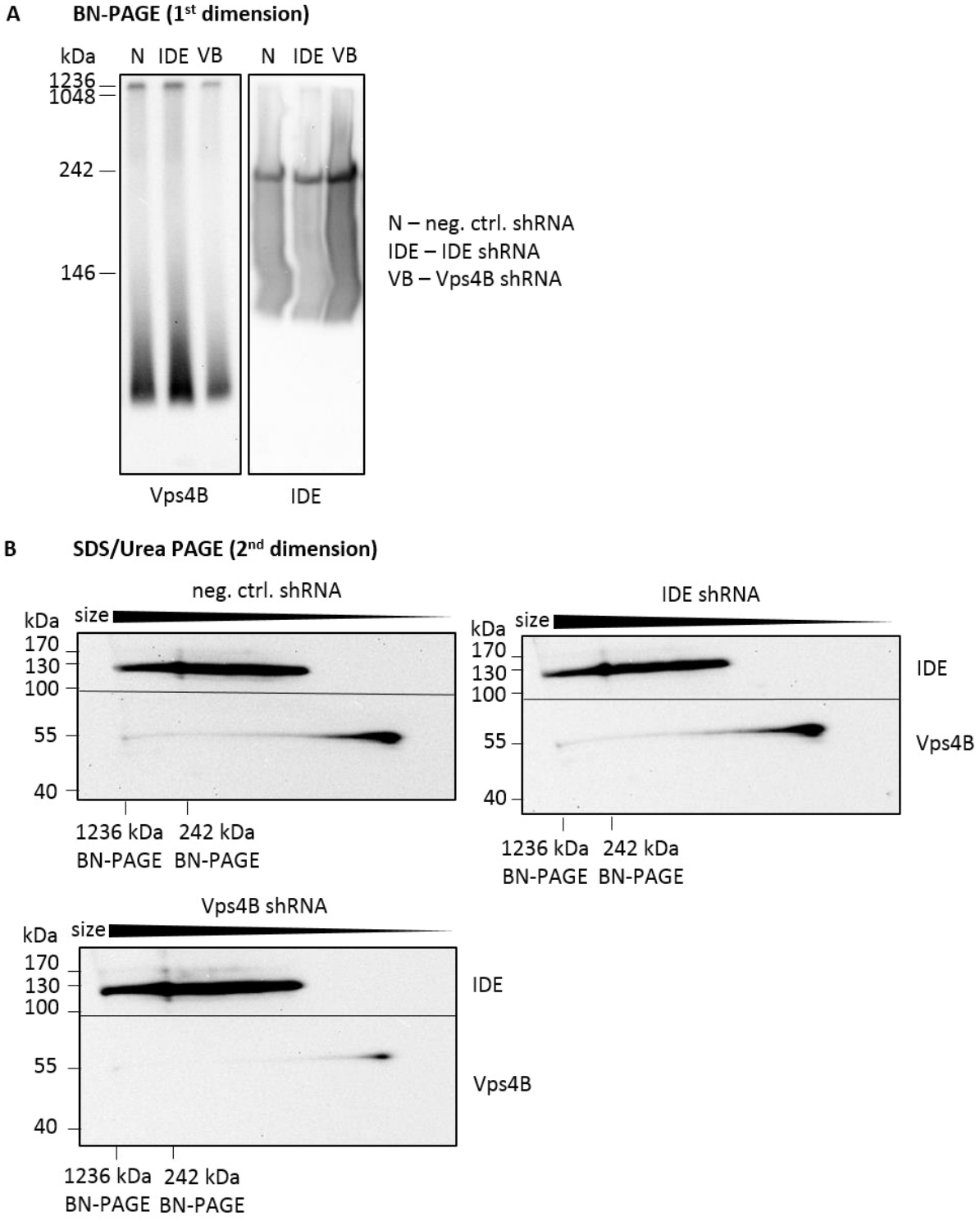

Figure 36. Complex formation of neither Vps4B nor IDE is affected by downregulation of both proteins. BN-PAGE (A) and subsequent SDS/Urea PAGE in the 2nd dimension (B) of BV-2 cell lysates upon stable knockdown of IDE and Vps4B and detection of IDE and Vps4B by Western immunoblotting.

D Discussion

1. Stimulation of IDE secretion by serotonin in microglia

Since the discovery that IDE can degrade Aβ and thereby could contribute to Aβ clearance in the brain, it became an interesting enzyme to be investigated in Alzheimer's research. It was shown that the expression of IDE is significantly decreased in familial and late-onset AD (Cook, et al., 2003; Pérez, et al., 2000; Zhao, et al., 2004; Miners, et al., 2009). The IDE-mediated clearance of Aβ occurs mainly extracellularly, but the exact mechanisms and possible stimuli that promote the release of IDE are not fully understood. In this study, it could be demonstrated that 5-HT stimulates the release of IDE from microglia cells via activation of several 5-HTRs (see Figure 7 and Figure 9). As shown recently by Tamboli and colleagues an increased release of IDE results in decreased extracellular levels of Aβ (Tamboli, et al., 2010).

The serotonergic system in the brain is affected already in the early stages of AD pathogenesis (Benton, et al., 1982; Reynolds, et al., 1995; Cross, 1990; Geldenhuys & Schyf, 2011). The functional relationship between the serotonergic system and AD aetiology, however, is not fully understood. It has also been shown that antidepressants based on 5-HT or inducing an increased serotonergic neurotransmission via inhibition of 5-HT reuptake can shift APP processing towards increased non-amyloidogenic cleavage by the α-secretase, which increases the secretion of the neuroprotective sAPPα and leads to decreased levels of Aβ (Lezoualc'h & Robert, 2003; Cirrito, et al., 2011; Hashimoto, et al., 2012; Nitsch, et al., 1996; Robert, et al., 2005; Cochet, et al., 2013; Tesseur, et al., 2013). In this context, Nitsch et al. showed an involvement of the 5-HT2aR and 5-HT2bR-mediated signalling, independent on PKC activation (Nitsch, et al., 1996). Furthermore, the activation of ERK signalling upon inhibition of 5-HT reuptake has been demonstrated to increase the α-secretase activity, likely by post-translational modification (Cirrito, et al., 2011). 5-HT4R-mediated signalling may promote the α-cleavage of APP also via activation of AC and increased levels of cAMP but appears to be independent of PKA activation (Lezoualc'h & Robert, 2003; Maillet, et al., 2003; Robert, et al., 2005; Cochet, et al., 2013; Tesseur, et al., 2013). Cochet and colleagues further suggest an additional effect of 5-HT4R by constitutively inducing α-cleavage of APP through a physical interaction with the α-secretase ADAM10 (Cochet, et al., 2013). The present study revealed that 5-HT, in addition to its effect on the proteolytic generation, can also promote the degradation of extracellular Aβ.

The results obtained in this study indicate that the activation of the 5-HTRs 2a, 2b and 4 stimulates IDE release via a PLC-dependent elevation of $[Ca^{2+}]_i$ (see Figure 37). The $G\alpha_q$-dependent activation of PLC is the classical and exclusive signalling pathway mediated by 5-HT2Rs that increases $[Ca^{2+}]_i$ by IP_3 formation and IP_3-mediated Ca^{2+} release from the ER (Raymond, et al., 2001; Bockaert, et al., 2006; Peroutka, 1995). 5-HT4R is known to induce

an AC-dependent increase of cAMP levels via $G\alpha_s$ (Fagni, et al., 1992). Recently it was shown that increased cAMP levels can switch on the Epac-Rap1/2B pathway that can activate PLCε (de Rooij, et al., 1998; Schmidt, et al., 2001; Oestreich, et al., 2007; Maillet, et al., 2003; Robert, et al., 2005). In this context, Maillet and Robert et al. also found that 5-HT4R-induced signal transduction increases sAPPα secretion attributed to a modulation of α-secretase activity. They show that cAMP activates the Epac-Rap1 signalling pathway that results in the activation of the small GTPase Rac that may increase α-secretase activity, possibly by its phosphorylation (Maillet, et al., 2003; Robert, et al., 2005). In the present study, by using specific activators of 5-HT4R (ML10302), Epac (8-CPT) and PLC (3m3FBS) and the

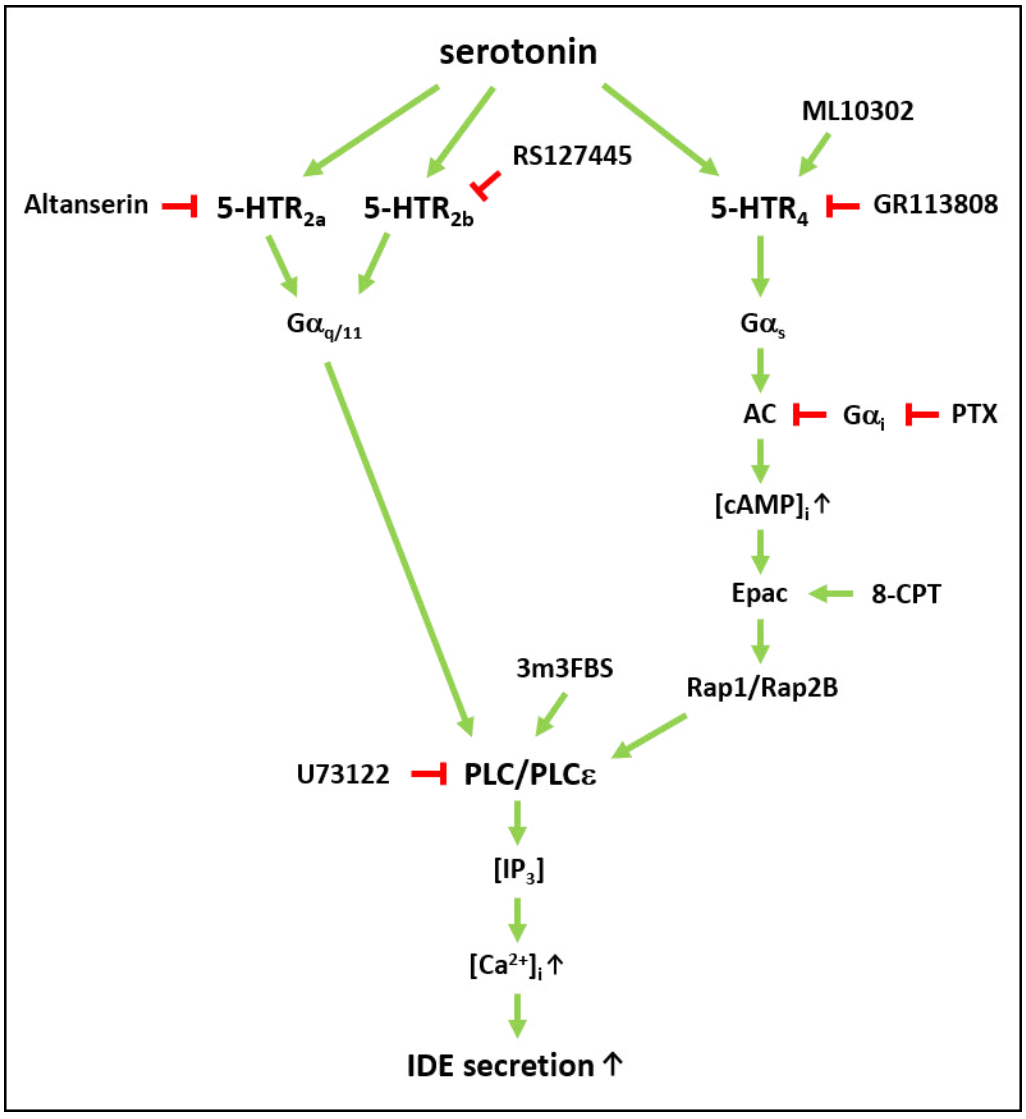

Figure 37. Proposed signalling pathways regulating 5-HT-stimulated IDE release from microglia cells. Adapted from *(Glebov, et al., 2015)*. Serotonin/5-HT activates 5-HT2a, 2b and 4 receptors in microglia/BV-2 cells. The selective 5-HTR antagonists RS127445, Altanserine and GR113808 block the receptor activation. 5-HT2a and 2b receptor activation leads to activation of $G\alpha_q$ mediating an increase of $[Ca^{2+}]_i$ upon PLC-dependent formation of IP_3. Activation of 5-HT4R stimulates an elevation of $[cAMP]_i$ dependent on AC activation by $G\alpha_s$, which can be also obtained by treatment with PTX that blocks $G\alpha_i$-mediated AC inhibition. cAMP activates the GEF Epac leading to a Rap1/2B-dependent activation of PLCε and a subsequent $[Ca^{2+}]_i$ increase. Elevated $[Ca^{2+}]_i$ promotes the secretion of IDE.

PLC inhibitor U73122, it could be shown that, at least in part, 5-HT-dependent stimulation of IDE secretion involves 5-HT4R and Epac-Rap1/2B-dependent activation of PLCε (see Figure 10 and Figure 11). The findings presented here therefore indicate that 5-HT4R-mediated signalling could contribute to the degradation of extracellular Aβ and thereby exert beneficial effects of 5-HT in the protection against AD.

Additionally, this work demonstrated that 5-HT elevates $[Ca^{2+}]_i$ in BV-2 cells and that a rise of $[Ca^{2+}]_i$ is associated with the stimulated release of IDE (see Figure 12). Earlier studies already demonstrated that increased $[Ca^{2+}]_i$ stimulates the secretion of exosomes by promoting the fusion of MVBs with the plasma membrane (Savina, et al., 2003; Savina, et al., 2005; Emmanouilidou, et al., 2010). In line with this, very recent investigations of Vingtdeux and colleagues showed a CALHM1-mediated increase in IDE secretion in N2A cells (Vingtdeux, et al., 2015). CALHM1 (calcium homeostasis modulator 1) is a plasma membrane ion channel permeable for Ca^{2+} and has been found to be a genetic risk factor for AD (Ma, et al., 2012; Dreses-Werringloer, et al., 2008). The expression and activation of the CALHM1 ion channel in N2A cells induces an influx of extracellular Ca^{2+} and elevates the $[Ca^{2+}]_i$ which most probably, although the authors do not directly refer to it, triggers the elevated release of IDE through fusion of MVBs with the plasma membrane (Vingtdeux, et al., 2015).

It could be furthermore shown, that the increased release of IDE is linked to an increased release of other exosomal markers like Alix, Flotillin-1 and Actin (see Figure 13), indicating that this stimulation is not selective for IDE but rather leads to a general increase of exosome release. However, the extent of secretion of the individual exosome-associated proteins differed. For example the release of IDE and Flotillin-1 is significantly increased by more than 40 and even 100%, respectively, whereas release of Alix and Actin shows only a weaker rise of 20% upon treatment with 5-HT in the exosome fraction (see Figure 13A). Here the question arises whether this might indicate the presence of distinct exosome pools, possibly whole MVBs, that exhibit a distinct composition of proteins. This is also discussed in literature. First, previous data suggested specific populations of MVBs that could either fuse with lysosomes or with the plasma membrane (Colombo, et al., 2013; Raposo & Stoorvogel, 2013). It could be established that MVBs destined for lysosomal degradation in contrast to secretory MVBs contain the MVB marker LBPA, but much less cholesterol (Möbius, et al., 2002; Wubbolts, et al., 2003; White, et al., 2006). Colombo and colleagues found by using a capture-based assay specific for particular exosome marker proteins to prepare exosomes, that cells secrete a heterogeneous population of exosomes not only differing in size, but also in the protein composition. Thereby they also support the concept that cells could contain different subpopulations of MVBs (Colombo, et al., 2013).

Co-culture experiments of BV-2 microglial cells with primary hippocampal or ES-derived serotonergic neurons (ESN), respectively, showed that neurons can stimulate the release of

IDE in microglial cells (see Figure 14). Pretreatment and simultaneous administration of selective antagonists for the 5-HTRs 2a, 2b and 4 during co-culture attenuated IDE release. These data further support that the neuronal release of 5-HT might promote the secretion of IDE from microglial cells. On the other hand, it was observed that antagonist treatment of BV-2 cells in the absence of ESN as well causes a decrease in IDE secretion. This rather suggests a 5-HT-independent effect. Further investigations could address whether the three 5-HTRs probably exhibit a constitutive activity in microglial cells, what has not been described so far. The constitutive activity of the 5-HTRs 1A, 1B, 1D, 2A, 2C, 3, 4 and 6 was already found in other cell types (Seifert, et al., 2005; Spencer, 2015; Claeysen, et al., 2000; Berg, et al., 2008). It is observed under specific conditions, e.g. low receptor density, or in certain tissues. Selective antagonists may exert distinct effects on constitutively active receptors in comparison to non-activated receptors and may act for example as inverse agonists. If considered antagonists behave as inverse agonists they not only block the effects of binding agonists but also inhibit the basal activity of constitutive active receptors (Chidiac, et al., 1994; Greasley & Clapham, 2006). That was observed already for 5-HT4R antagonists in 5-HT4R-transfected cells (Claeysen, et al., 2000) and for 5-HT3- and -4R antagonists in investigations of gut motility *in vivo* (Spencer, 2015). GR113808, however, could be proven as neutral antagonist that has no activity in the absence of an agonist in case of a constitutive active 5-HT4R (Claeysen, et al., 2000). Possibly Altanserin acts as an inverse agonist, in case the 5-HT2aR would exhibit a constitutive activity. The same might be suggested for the 5-HT2bR and its selective antagonist RS127445. However, this needs to be investigated.

Additionally to the increased IDE release also a more than 1.5-fold elevated IDE protein level can be detected in BV-2 cells upon co-culture with ESN (see Figure 14F). This increased expression is only slightly reduced upon simultaneous antagonist treatment suggesting a minor importance of 5-HT-mediated signalling in that effect. This is supported by the fact that 5-HT treatment of BV-2 cells does not cause an increase in IDE expression. The absolute amount of secreted IDE from BV-2 cells shows, as expected, an increase upon co-culture with ESN (see Figure 14E). It needs to be determined whether the increased cellular levels of IDE upon co-culture with neurons contributes to the increased IDE secretion. However, what catches the eye is the fact that in BV-2 cells co-cultured with ESN the amount of secreted IDE rises of larger magnitude than the expression of IDE (2.3-fold in comparison to 1.7-fold). Interestingly this effect can be observed in the same extent in BV-2 cells that were treated with 5-HTR antagonists (2.4-fold in comparison to 1.6-fold). These observations could, first, indicate that the secretion of IDE is influenced by other mechanisms than the increased expression in BV-2 cells upon co-culture with ESN. On the other hand, this could also point to differences in the intra- and extracellular metabolism of IDE. However, the fact that the amount of secreted IDE is increased to the same extent also in BV-2 cells under the influence of 5-HTR antagonists

rather suggests no effect of neuronal 5-HT in the stimulation of IDE release from BV-2 cells. Other mechanisms of neuron-glia interaction, as for example direct physical interaction or probably the release of other signalling molecules, seem to play a role and a more detailed investigation of these communication pathways is required.

Together, the present results indicate that 5-HTR-mediated signalling in microglia, either by constitutive active or stimulated receptors, plays an important role in the secretion of IDE via exosomes. This suggests an important and beneficial function of the communication between neurons and microglia also for the extracellular degradation of Aβ. A probable disturbance of these communication pathways might contribute to the pathogenesis and progression of Alzheimer's disease.

2. Molecular mechanisms in IDE secretion

2.1 Inhibition of conventional secretion increases the release of exosomal proteins in BV-2 microglial cells.

Several years ago it was proven that IDE secretion occurs independent of the conventional secretory pathway (Zhao, et al., 2009; Bulloj, et al., 2010). In hepatocytes, HeLa cells and the neuroblastoma cell line N2A known inhibitors of the conventional protein secretion revealed no or even an increasing effect on IDE release. In the present study, an increasing effect could be observed in microglial BV2 cells. Two inhibitors of the conventional secretory pathway, Brefeldin A and Monensin, do not block, but significantly elevate the release of IDE, accompanied by a simultaneous increase in the secretion of the exosome marker Alix (see Figure 29). Due to the comparable effect on two distinct exosome-associated proteins it can be assumed that the inhibition of the conventional secretory pathway promotes the secretion of exosomes in general, especially as the sorting of both proteins to MVBs seems to be regulated differently (discussed below). Therefore it might be suggested that Brefeldin A- and Monensin-mediated inhibition stimulates the fusion of MVBs with the plasma membrane rather than exosome biogenesis.

It has already been shown that Monensin increases the $[Ca^{2+}]_i$ by inducing a reversed activity of the Na^+/Ca^{2+} exchanger, which leads to a Ca^{2+} entry into the cell, and this way also stimulates the secretion of exosomes (Savina, et al., 2003). Interestingly Savina and colleagues found that Monensin treatment leads to formation of enlarged MVBs in K562 cells, a human myelogenous leukemia cell line. Most probable this is induced by its function as Na^+/H^+ antiporter that promotes swelling of acidic compartments, including endosomes and lysosomes. MVBs also accumulate Ca^{2+} intraluminally which is indicated to play a role for the secretory process as well. Savina et al discuss the requirement of released luminal Ca^{2+} to induce the docking and fusion process of MVBs with the plasma membrane (Savina, et al.,

2003). Bulloj and colleagues observed an almost 3-fold enhanced release of IDE and its localisation in the enlarged MVBs upon Monensin treatment also in N2A cells (Bulloj, et al., 2010). They also found enlarged MVBs upon administration of the calcium ionophor A23187, supporting an involvement of intracellular Ca^{2+}. Thus, a similar effect of Monensin on the secretion of IDE can be suggested for BV-2 cells as well. It can be further assumed that the Monensin-induced increase in IDE secretion is not mediated by blocking the ER-Golgi transport, although it cannot be completely excluded. In addition, this supports the conclusion that 5-HT-stimulated IDE secretion is triggered by an 5-HTR-induced increase in $[Ca^{2+}]_i$. Additional experiments, i.e. immunocytochemistry or subcellular fractionation, with BV-2 cells should provide further insight in the localisation of IDE and formation of enlarged MVBs upon Monensin treatment. However, a specific MVB marker still remains to be identified, because LBPA staining, used for example by Bulloj et al., was not possible in BV-2 cells (data not shown).

For Brefeldin A, distinct observations in affecting secretion of exosome-associated proteins are found in literature. McCready and colleagues observed that inhibition of the conventional secretory pathway through Brefeldin A leads to an increased release of Hsp90α that is secreted via exosomes in the breast cancer cell line MDA-MB231 (McCready, et al., 2010). On the contrary, two groups, examining exosome release in J77 T cells and the lung cancer cell line A549, respectively, observed a strong decrease in the release of the exosome-associated proteins CD81 and CD63 (Mittelbrunn, et al., 2011; Wilson, et al., 2014). The release of the exosomal Hsp70, in contrast, was not influenced by inhibition of Brefeldin A in the monocytic cell line THP1, and in peripheral blood mononuclear cells (Lancaster & Febbraio, 2005; Tulapurkar, et al., 2015). Notably, the release of IDE was not affected by BFA in hepatocytes and HeLa cells (Zhao, et al., 2009). Brefeldin A blocks the transport of secretory vesicles from ER to Golgi by inhibiting ARFs - GTP-binding protein ADP-ribosylation factors - leading to the disassembly of the Golgi apparatus (Donaldson, et al., 1992; Sciaky, et al., 1997; Schekman & Orci, 1996). Thus, Brefeldin A seems to influence the release of exosomes by a distinct mechanism than described above for Monensin. Possibly, Brefeldin A rather affects the sorting of cargo into exosomes or the budding of ILVs into MVBs. So far, MVBs are described as a part of the endosomal compartment and the endocytic pathway and thus, are not directly connected to vesicular transport to and from the trans-Golgi. However, it is imaginable that MVBs also originate from the trans-Golgi, at least indirectly. So, for example a sorting of proteins from the trans-Golgi to the endosomal/lysosomal system via vesicular transport is not unlikely. First, typical exosomal marker as the tetraspanins CD63 and CD81 are found in the Golgi network (Laulagniera, et al., 2005; Mori, et al., 2008; Shoham, et al., 2006). Furthermore, a maturation of MVBs from the trans-Golgi network was proven already in plants. In plants, however, the trans-Golgi network and the early endosome compartments

are not comparably separated as in mammalian cells (Scheuring, et al., 2011). Thus, at least some exosomal cargo might originate from Golgi compartments. Due to the assumed distinct subpopulations of exosomes (discussed above) the effect of Brefeldin A might vary for different exosomal proteins and also between different cell types.

Findings by Lippincott-Schwartz et al. revealed moreover that upon Brefeldin A treatment the trans-Golgi network, which is separated from the rest of the Golgi system that is redistributed into the ER, may fuse with the endosomal recycling system, whereas the transport between endosomes and lysosomes is impaired (Lippincott-Schwartz, et al., 1991). They could show that the typical trans-Golgi network marker TGN38 mixes with the endosomal recycling system upon treatment with Brefeldin A and could cycle to and from the cell surface. Probably this could give another explanation how under the influence of Brefeldin A also exosomal proteins, that might originate from the trans-Golgi network, could reach the plasma membrane and could be secreted.

In conclusion the observed increase in IDE and general exosome release from BV-2 cells upon inhibition of conventional secretion shows a rather unexpected effect, in particular for Brefeldin A because it was shown not to alter IDE secretion in other cell types (Bulloj, et al., 2010; Zhao, et al., 2009). It needs further investigation especially concerning its influence on the formation of MVBs, e.g. by immunofluorescence staining and subcellular fractionation of intracellular vesicles. This could help to elucidate, if the increase in IDE release might be caused by a disassembly of the Golgi system by partial redistribution of the Golgi into the ER. Possibly also preparation of microvesicles and exosomes from Monensin- and Brefeldin A-treated cells could provide more detailed insight into their effect on IDE secretion. The findings, either way, indicate a closer relation between conventional and the unconventional exosome-mediated secretory pathway than previously assumed.

2.2 Differential influence of nSMase2 and ceramide levels on the release of IDE in distinct cell types

Exosomes originate from intraluminal vesicles that are generated by inward budding of the endosomal membrane. However, the regulation of their biogenesis is controversial until now. The ESCRT machinery was soon presumed to play an important role in this budding process and there are several studies that could confirm its involvement in exosome formation and release (Babst, et al., 1998; Tamai, et al., 2010; Gan & Gould, 2011; Baietti, et al., 2012; Colombo, et al., 2013). However, the release of certain exosome-associated proteins can occur independently from ESCRT function. One striking example was the discovery that exosome formation is triggered by raft-based microdomains enriched in ceramides (Trajkovic, et al., 2008). Trajkovic et al. proposed that due to its cone-shaped structure, ceramide promotes the inward budding of unilamellar vesicles. To decrease ceramide levels they treated

cells with GW4869, an inhibitor for the neutral sphingomyelinase 2 (nSMase2) that catalyses the conversion of sphingomyelin to ceramide, or downregulated nSmase2 by RNAi. Thereupon they observed a significant decrease in exosome secretion, indicated by the release of the proteolipid protein (PLP) that is secreted via exosomes from the oligodendrocyte cell line Oli-neu and partly also by the release of CD63 in Oli-neu and PC-3 cells, a prostate cancer cell line. By additionally investigating EGFR degradation, a characteristic example of lysosomal degradation mediated by transport via the MVB pathway, they propose that the ESCRT machinery is only needed for ILV formation for the lysosomal degradation pathway whereas ILV formation of later exosomes requires ceramide (Trajkovic, et al., 2008; Heinrichs, 2008).

Examining the effect of nSMase2 inhibition on exosome secretion in microglial cell lines and primary rat astrocytes the present study revealed differences not only between different cell types, but also between different exosome-associated proteins (see Figure 15 and Figure 16). In the microglial BV-2 and N9 cells, the release of IDE is significantly increased upon inhibition of nSMase2 by GW4869 whereas the secretion of the exosomal proteins Alix and Flotillin-1 is significantly decreased in N9 cells by approximately 50% and tendencially rather decreased also in BV-2 cells. In primary rat astrocytes, however, nSMase2 inhibition displays an entirely different effect especially on the secretion of IDE. Here, the release of all three examined exosomal marker proteins - IDE, Alix and Flotillin-1 - was almost completely blocked upon treatment with GW4869. This indicates that exosome secretion seems to be differentially regulated in microglial cells and astrocytes. While formation and the subsequent release of exosomes in astrocytes seems to be strongly dependent on ceramide levels, they appear to be rather independent on nSMase2 function in microglial cells, as indicated by the differential susceptibility of both cell types to inhibition of nSMase2. Not only IDE showed opposite effects upon nSMase2 inhibition in the two cell types. Also the secretion of Alix and Flotillin-1 is much stronger affected by nSMase2 inhibition in primary rat astrocytes than in N9 and especially in BV-2 cells. It needs to be tested, however, whether this might also be attributed to a distinct sensitivity to GW4869 in the two different cell types.

These findings reflect the varying observations of several studies on the regulation of exosome release and protein sorting into MVBs by nSMase2 (Phuyal, et al., 2014; van Niel, et al., 2011; Yuyama, et al., 2012), and underline existing differences between different exosome-associated proteins and between different cell types. So, for example van Niel and colleagues found no influence of GW4869-mediated inhibition of nSMase2 on the sorting of PMEL (premelanosome protein) into ILVs of MVBs for melanosome generation. Instead, CD63, a common exosomal marker protein was discovered to play a role in ILV biogenesis (van Niel, et al., 2011). Yuyama and colleagues demonstrated a significant decrease of exosome release upon treatment with GW4869 or downregulation of nSMase2 in N2A neuroblastoma cells and primary neurons, indicated by the exosomal proteins Alix, Tsg101 and GM1 (Yuyama, et al.,

2012). On the other hand, in the cell line PC-3 inhibition of nSmase2 or its RNAi-mediated downregulation did not affect the release of the exosomal proteins Caveolin-1 and Annexin A2 (Phuyal, et al., 2014). In the study by Trajkovic, however, GW4869 treatment decreased the release of the exosome marker protein CD63 in PC-3 cells (Trajkovic, et al., 2008), also suggesting differently regulated secretion or MVB sorting for distinct exosomal proteins in the same cell line.

Nevertheless, no study has described an increased release of an exosome-associated protein upon inhibition of nSMase2 leading to decreased ceramide levels as it was observed for IDE in BV-2 and N9 cells. The fact that secretion of other exosomal proteins is rather unaffected or even decreased raises the question, if the inhibition of the nSMase2 indeed affects the release of IDE via exosomes. Bulloj and colleagues suggested that only about 50-60% of secreted IDE is released via exosomes in N2A cells (Bulloj, et al., 2010). Possibly the decreased ceramide levels rather influence another pathway that is involved in the secretion of IDE. Several studies already described a localisation of IDE at the cell surface in various cell types (Vekrellis, et al., 2000; Seta & Roth, 1997; Lynch, et al., 2006; Yaso, et al., 1987), but until now the exact mechanism of membrane attachment and translocation is unknown. Furthermore, the amino acid sequence of IDE has no canonical motif for secretion or association with the cellular membrane. The present study revealed by using cell fractionation that only a small proportion of IDE is associated with intracellular membrane systems as well as the plasma membrane of BV-2 cells (see Figure 21). Also immunocytochemical staining of endogenous IDE in BV-2 cells (data not shown) did not show a prominent localisation of IDE at the plasma membrane. This might be further examined using for example cell surface biotinylation. Nevertheless also in BV-2 cells, a fraction of IDE might be exposed at the cell surface, which would require an uncharacterised non-vesicular export mechanism for IDE. This potential mechanism might be affected by ceramide.

As an example, a secretory process which could be influenced by ceramide is membrane translocation via ABC transporters. ABC transporters have been implicated in the unconventional secretion of proteins (compare introduction 2.3) and might represent a further possibility of IDE membrane translocation. The functionality of ABC transporters depends also on the surrounding lipid composition (Aye, et al., 2009). For instance, the ABCA1-mediated cholesterol efflux is affected by the ceramide content in the plasma membrane (Ghering & Davidson, 2006). Furthermore, accumulation of cell surface ceramide during keratinocyte differentiation appears to increase ABCA7 expression (Kielar, et al., 2003; Aye, et al., 2009). Accordingly, an elevated expression of the respective ABC transporter through increased ceramide levels might then also enhance the protein transport via the membrane. Thus, in case IDE might additionally be secreted by an ABC transporter this could be influenced by ceramide levels in the plasma membrane. However, the observation by Zhao and colleagues

that the broad-spectrum ABC transporter inhibitor glyburide did not affect IDE secretion in HeLa cells (Zhao, et al., 2009) would speak against an IDE export by ABC transporters. On the other hand, Brefeldin A and Monensin displayed distinct effects on IDE secretion in HeLa cells (Zhao, et al., 2009) and BV-2 cells (see Figure 29) as well. Thus, it would be important to test an influence of ABC transporter inhibitors on the release of IDE also in BV-2 and other cell types.

Another example is the influence of ceramide on the release of hyaluronan, a part of the extracellular matrix. A recent study described that decreased levels of ceramide in the plasma membrane increase the secretion of hyaluronan. Decreased ceramide in the plasma membrane activates the Akt pathway that in turn stimulates transcription of certain genes. Thereby the secretion of hyaluronan is increased due to an upregulation of hyaluronan synthase leading to an enhanced hyaluronan production at lipid rafts in the plasma membrane (Qin, et al., 2012). Another study dealing with hyaluronan synthesis and microvesicle release observed an increased release of microvesicles in hyaluronan synthase-overexpressing cells (Rilla, et al., 2013). Rilla et al. found that the increased release of microvesicles in these cells was associated with the hyaluronan synthesis rate and that the released microvesicles were coated with hyaluronan. Therefore, another mode of unconventional secretion for IDE, which might be affected by ceramide levels in the plasma membrane, is the release via microvesicles. Microvesicles bud from the plasma membrane and are directly pinched off to the extracellular space. They display an expected size of 100-500 nm whereas they most probably can be separated from exosomes by differential centrifugation (compare Material and Methods 2.2.9) (Cocucci & Meldolesi, 2015). As also found in this work, IDE is, additionally to the exosome fraction, as well found in the microvesicle fraction from BV-2 cells (see Figure 13A). As described above, decreased ceramide levels in the plasma membrane may activate the Akt pathway which activates hyaluronan synthase expression leading to an increased hyaluronan synthesis at the plasma membrane (Qin, et al., 2012). Thus, it could be speculated, if decreased ceramide levels in the plasma membrane through nSMase2 inhibition might increase hyaluronan synthesis at the plasma membrane and thereby also enhance microvesicle release. Therefore it would be interesting to assess, if GW4869 is able to affect the Akt pathway, the hyaluronan synthase expression and hyaluronan synthesis in microglial cells. In addition, it should be tested first if hyaluronan synthase isoforms are expressed in microglia. So far only the expression and activation of hyaluronan receptors in microglia is described (Wang, et al., 2006; Austin, et al., 2012). In particular the influence of GW4869 treatment on microvesicle-associated IDE should be examined in BV-2 cells.

The present results, firstly, show that the secretion and the sorting of distinct exosomal proteins into MVBs may be regulated differently in the same cell type. In addition, the release/sorting of the same protein may be regulated differently in distinct cell types, as shown here for IDE.

This could also indicate that IDE is secreted by different secretory mechanisms in these cells. To conclude, this study shows that nSMase2 inhibition and therewith probably associated lower ceramide levels stimulate IDE release in microglial cells. It furthermore might indicate a potentially higher importance of the microvesicle-associated or the existence of another new IDE secretory mechanism distinct from exosome release in particular in microglial cells.

2.3 ESCRT-dependent effects in IDE secretion and the role of the interaction of IDE and Vps4B

As described earlier, the ESCRT machinery has been suspected to be involved in the biogenesis of exosomes due to its function in MVB generation, and a functional role for several proteins of the individual ESCRT complexes in the release of exosome-associated proteins could already be proven. For example, RNAi-mediated downregulation and knockout of Hrs, a member of ESCRT-0, in dendritic cells led to a significant decrease of typical exosome marker proteins as Tsg101 and Hsp70 in isolated exosomes, and also decreased the amount of ubiquitinated and total protein in the exosome fraction (Tamai, et al., 2010). Furthermore, RNAi-mediated knockdown of Tsg101 and CHMP4A/B/C, members of ESCRT-I and -III, respectively, caused strongly decreased levels of exosomal proteins like CD63 and syntenin in isolated exosomes of MCF-7 cells, a breast cancer cell line, shown recently by a detailed study on ESCRT function in exosome release of Baietti et al. (Baietti, et al., 2012). Downregulation of Hrs, Tsg101 and the further ESCRT-I member Stam1 by stable shRNA-expression in HeLa cells also led to a decreased release of exosomes positive for CD63 and CD81 in another large-scale study on ESCRT function (Colombo, et al., 2013). In addition to the ESCRT proteins, the ESCRT accessory proteins Alix and the ATPase Vps4B, that mediate ESCRT-III recruitment or the final step of membrane abscission by disassembly of the ESCRT-III members, respectively, are interesting proteins to investigate the involvement of the ESCRT machinery in exosome biogenesis. Baietti and colleagues could furthermore prove a function of Alix in sorting and release of exosomal cargo, including syntenin, syndecan, CD63, Tsg101 and Hsp70 in MCF-7 cells (Baietti, et al., 2012). Combined RNAi-mediated knockdown of Vps4A and B inhibited the secretion of the exosomal marker CD63, syntenin and syndecan (Baietti, et al., 2012; Hurley & Odorizzi, 2012). An influence of both ESCRT accessory proteins on the secretion of exosomes could be verified also by previous and following studies (Gan & Gould, 2011; Colombo, et al., 2013; Kunadt, et al., 2015). Therefore it was important to examine the ESCRT function in the secretion of IDE from BV-2 cells.

2.3.1 Minor effects of Alix in the release of IDE from BV-2 cells

RNAi-mediated knockdown of Alix in MCF-7 cells strongly decreased the secretion of several exosomal marker proteins and the sorting of syntenin and syndecan into exosomes (Baietti, et

al., 2012). In contrast, the siRNA-mediated downregulation of Alix showed only minor effects on the release of IDE in BV-2 cells (see Figure 17). IDE secretion slightly and not significantly increased upon knockdown of Alix which indicates a minor role for Alix in the sorting or release of IDE in BV-2 cells. Knockdown of Alix resulted in a slight but significant increase also in cellular IDE levels, probably causing the elevated amount of secreted IDE. However, this effect was detected only for one of the used siRNAs, which indicates potential off-target effects. Colombo and colleagues discovered increased expression levels of MHC II in MHC II-overexpressing HeLa cells upon RNAi-mediated downregulation of Alix (Colombo, et al., 2013). They also found an increased number in released CD63-positive exosomes and an increased exosomal secretion of MHC II upon downregulation of Alix, in contrast to the results of Baietti mentioned above (Baietti, et al., 2012). The accumulation of MHC II could be attributed to an increase in the HLA-DRB1 and HLA-DRA mRNAs, encoding MHC II, revealing an unexpected effect of Alix on mRNA expression or stability (Colombo, et al., 2013). Thus, it would be interesting to further analyse whether IDE expression is affected by Alix knockdown in a similar manner, for example by analysing IDE mRNA level. Nevertheless, the effects observed after downregulation of Alix are rather small considering the knockdown efficiency of 90-95% at the protein level. Thus, the functional relevance of Alix for IDE secretion or potentially compensatory mechanisms remains unclear. That the effect of downregulation of Alix might be compensated is indicated by an experiment analysing secretion and expression of exosomal proteins upon siRNA-mediated knockdown of Alix, IDE and Vps4B for longer time periods (72 hours) (see Figure 25). In cells treated with Alix-specific siRNA a very efficient and prolonged knockdown was detectable. In IDE- and Vps4B-knockdown cells, however, protein expression of IDE or Vps4B, respectively, turned back to control levels or even higher after 72 hours. This suggests the existence of rather rapid mechanisms to reestablish the protein levels of IDE and Vps4B in comparison to Alix protein levels. Possibly there are compensatory mechanisms for the loss of Alix function or Alix has only little contribution to the regulation of exosome secretion in BV-2 cells. In its capacity as ESCRT accessory protein, the function of Alix could possibly be taken over by ESCRT-II, as it was suggested that both exert a similar function in the recruitment of ESCRT-III (compare introduction 2.2). It is proposed that Alix potentially replaces the ESCRT-II function in cytokinesis and virus budding, where the ESCRT machinery is involved as well (Raiborg & Stenmark, 2009; Christ, et al., 2016). Downregulation of Alix for 72 hours in BV-2 cells, moreover, did not affect IDE secretion or expression anymore. This together with the observed slightly increased IDE expression in IDE-siRNA cells after 72 hours (see Figure 25) suggests that the maintenance of a certain IDE protein level seems to be important.

Thus, Alix appears of limited importance in the regulation of IDE secretion, but might be involved in control of IDE expression.

2.3.2 Vps4B exerts an inhibitory function in regulation of IDE secretion in BV-2 cells.

The role of the ATPase Vps4B was examined in detail in this study. A siRNA-mediated downregulation of Vps4B protein by more than 50% in BV-2 cells induced a significant 2-fold increase in secretion of IDE, whereas the release of Alix and Flotillin-1, other exosomal proteins, is unaffected (see Figure 18). It should be noted here that the effect size for the increased IDE release highly varied between the individual experiments. High variation of the effect size between different experiments was also observed upon stable expression of Vps4B-specific shRNA in BV-2 cells yielding a stronger and stable Vps4B knockdown of 70-80% (see Figure 20). Also here a significantly enhanced IDE release is detectable upon depletion of Vps4B. As in siRNA-treated cells Alix secretion remains unaffected, but a trend to an increased release of Flotillin-1 is observed. The high interexperimental variations appear to be characteristic for secretion and exosome analyses upon knockdown of Vps4B. Higher interexperimental fluctuations were also observed in other studies on exosome secretion. High standard deviations of up to 100-150% (n=3-5) (Baietti, et al., 2012) and sometimes even opposite effects in different experiments are also described previously (Colombo, et al., 2013). Colombo et al. showed for shRNA-mediated knockdown of Vps4B interexperimental variations in the effect size on exosome secretion of about 100-200% for CD63, 100-400% for MHC II and even 6000% for Hsc70, which are comparable and partly even higher values as observed in the present study on IDE secretion. As all experiments were carried out under apparently similar technical conditions, using also a similar passage number of the cells, the higher variations might indicate a dependency on the state of the cell, as for example metabolic state or the stage of the cell cycle. It is discussed and also proposed for multicellular organisms that a population of actually identical cells still maintains a diversity of cell phenotypes to be able to respond to novel environments (Dueck, et al., 2016). It is further argued that the rapid response of small subsets of cells on perturbations and emitted signals may coordinate the whole population behaviour. That was already observed for example for inflammatory responses (Dueck, et al., 2016). Possibly, mechanisms that compensate functional consequences of the Vps4B downregulation are activated only in a subset of the cells and depending on their presence or strength this affects the behaviour of the whole cell population more or less leading to variations in the observed effect strength.

In the context of the known function of Vps4B in the formation of ILVs and potentially exosomes in the MVB pathway, the increased release of IDE upon Vps4B downregulation is a rather unexpected finding. Considering that depletion of Vps4B might result in disruption of the final step in ILV formation, a reverse effect would be expected, provided that IDE release depends on ESCRT-mediated exosome biogenesis. The findings eventually indicate that Vps4B rather suppresses the secretion of IDE. On the other hand, also Colombo and colleagues found an increased release for all examined exosomal marker proteins as MHC II, CD63 and Hsc70

upon RNAi-mediated downregulation of Vps4B (Colombo, et al., 2013). However, potential mechanisms underlying these observed results were not discussed. Another study on an ESCRT-independent pathway of exosome secretion shows in the supplementary data a statistically non-significant increased release (~1.5-fold) of CD63-positive exosomes upon overexpression of a Vps4 variant that is deficient in ATP-binding. Also here a high standard deviation indicates high interexperimental variations (Trajkovic, et al., 2008). However, Baietti, as described earlier, observed a decrease in the release of exosomal proteins upon RNAi-mediated downregulation of Vps4B (Baietti, et al., 2012) which contradicts the observations of Colombo and in this work. Besides the studies by Baietti and Colombo all other studies addressing the function of ESCRT in exosome biogenesis and release used only overexpression of ATPase-deficient variants for analysing Vps4B function, but used RNAi approaches for all other ESCRT members. Possibly overexpression of an ATP-binding- or ATPase-deficient Vps4B variant exhibits a different effect on exosome secretion as its RNAi-mediated protein downregulation. For IDE secretion in N2A cells, Bulloj and colleagues observed a slight decrease upon overexpression of the ATPase-deficient variant of Vps4B in comparison to empty vector-transfected cells indicating a minor role of Vps4B and its ATPase function (Bulloj, et al., 2010). In this work, stable expression of the wild type Vps4B and the ATPase-deficient variant Vps4B-E235Q in BV-2 cells using a lentiviral transduction system was tried (compare Material and Methods 2.1.9). However, stable expression of these variants could not be achieved, likely by downregulation or silencing of the transgene after transduction (data not shown). Also the attempt to transiently overexpress Vps4B and its ATPase-deficient variant in cos-7 cells was not successful due to toxic effects and induced cell death. An explanation for distinct effects of the Vps4B ATPase-deficient variant and a depletion of the whole protein might be, as proposed recently already from Hurley and Odorizzi (Hurley & Odorizzi, 2012), an additional non-catalytic function of Vps4B in the exosome formation or release pathway which, however, is not examined until now.

Interestingly, analysis of separated exosome and microvesicle fractions from the media of stable Vps4B-depleted cells revealed that Vps4B knockdown might rather affect the secretion of IDE, as well as Flotillin-1 and Alix, via microvesicles, whereas their release via exosomes is only slightly or not influenced (see Figure 20B). This is consistent with the observation that Alix levels in the supernatant of the cells are rather unaffected upon downregulation of Vps4B, because Alix is predominantly present in the exosome fraction and to a much lesser extent in the microvesicle fraction. Flotillin-1 showing as IDE similar proportions in the exosome and microvesicle fraction, however, was influenced by Vps4B-depletion in 50% of the experiments. This finding supports the idea, as discussed earlier, that microvesicles might contribute stronger to the release of IDE than exosomes in microglial cells (compare 2.2). A function of Vps4B and also other ESCRT members in the formation of microvesicles, that bud from the

plasma membrane and are directly pinched off to the extracellular space, was recently proven (Nabhan, et al., 2012; Cocucci & Meldolesi, 2015). A role of the ESCRT machinery in shedding of microvesicles is further supported by its involvement in other processes at the plasma membrane as virus budding and membrane abscission during cytokinesis (Raposo & Stoorvogel, 2013; Cocucci & Meldolesi, 2015). However, involvement of the ESCRT machinery in the release of microvesicles is much less investigated as it is for exosomes. The protein composition of microvesicles appears to be even more heterogeneous than that of exosomes, and no representative marker proteins exclusively found in microvesicles have been identified (Turola, et al., 2012). However, also characteristic exosomal marker proteins are detected in microvesicles, as for example Alix and Hsp70 (Bernimoulin, et al., 2009). Possibly, Vps4B affects additionally to its ATPase-dependent function in vesicle abscission also the sorting of proteins into microvesicles. Such a function for Vps4B was already described in sorting of the viral protein Gag during virus budding at the plasma membrane and sorting of CD63 and CD81 into extracellular vesicles (Gan & Gould, 2011). The procedure by Gan and Gould to isolate extracellular vesicles slightly differed to the common protocol for exosome isolation also used in this work (compare Material and Methods 2.2.9), and therefore could rather result in a fraction containing both microvesicles and exosomes. Nevertheless, the study of Gan and Gould suggests a sorting function of Vps4B by direct interaction with cargo proteins of microvesicles, and probably also exosomes. As mentioned above, in case Vps4B might be implicated in the sorting of IDE, Alix and Flotillin-1 into microvesicles in BV-2 cells, the present results would suggest an inhibitory function of Vps4B. This would contrast with the findings of Gan and Gould, that indicate a promoting effect of Vps4B in sorting of CD63 and CD81 (Gan & Gould, 2011).

Interestingly, Vps4B was identified in the Y2H screen performed during this project to identify interaction partners of IDE (see Table 16). This interaction could be confirmed by co-immunoprecipitation approaches in extracts of IDE- and Vps4B-overexpressing cells (see Figure 34). However, co-immunoprecipitation of these proteins was of low efficiency, probably indicating weak or transient interactions. In extracts with endogenous levels of IDE and Vps4B an interaction was not detectable. Nevertheless, both proteins show a very similar subcellular localisation that is predominantly cytosolic as indicated by density gradient fractionation of subcellular compartments and by immunocytochemical stainings of the endogenous proteins (see Figure 32A and Figure 33). Moreover, Vps4B and IDE are both found in exosomes of the same density indicating their presence in the same exosome pool (see Figure 32B). Thus, the topological conditions in the cells would allow an interaction of both proteins. However, using native gel electrophoresis and subsequent denaturing gel electrophoresis in the second dimension a protein complex which contains both proteins IDE and Vps4B could not be detected (see Figure 35). This again indicates a rather weak interaction or a low prevalence of

this complex below the detection limit of the used method. It is also conceivable, that method-dependent limitations as for example epitope masking in the complex prevent the efficient precipitation or detection of the complex by the used antibodies.

The question that now arises is whether the interaction with Vps4B is functionally involved in IDE sorting into exosomes or microvesicles and if, which mechanisms might contribute. A potential influence on the complex formation of Vps4B and IDE, respectively, appears rather unlikely. Neither IDE depletion affected the formation of the Vps4B ATPase complex in BV-2 cells, nor Vps4B downregulation disturbed dimerization of IDE (see Figure 36). The Vps4B ATPase complex consists of two hexameric rings of Vps4A and B subunits, that assemble in the presence of ATP by interactions between their C-terminal oligomerisation domains and additionally bind LIP5 proteins (Scott, et al., 2005). IDE predominantly exists as a dimer and the C-terminal part (IDE-C, compare Figure 1) is responsible for IDE oligomerisation (Li, et al., 2006). The Y2H screen was carried out using a C-terminal sequence of IDE (IDE Bait, compare Figure 30). The respective encoded amino acid sequence of Vps4B found to interact with IDE Bait in the Y2H screen encloses a small part of the N-terminal MIT domain (microtubule interacting and trafficking domain) and almost the whole AAA ATPase domain (compare Figure 31B). Therefore an interruption of IDE dimerization or ATPase function of Vps4B by the interaction of both proteins might be possible. Further characterization of the exact interaction domains of IDE and Vps4B would enable functional analyses using interaction mutants. The current results of this study do not allow a definite statement on the function of the interaction. Therefore, a potential effect of the IDE-Vps4B interaction on IDE release needs further examination.

Moreover, it should be assessed how known stimuli of microvesicle release affect IDE release, as for example the impact of PKC-activating phorbol esters that stimulate microvesicle release or ATP treatment triggering microvesicle release by activating $P2X_7$ receptors also in microglia (Cocucci, et al., 2009; Cocucci & Meldolesi, 2015). In addition, the obtained results showing increased (but not statistical significant) protein levels in the microvesicle fraction upon Vps4B knockdown need further verification to consolidate the made conclusions that Vps4B rather influences microvesicle than exosome release.

Furthermore, it should be examined, as mentioned earlier (see 2.2) if hyaluronan synthesis and activation of the Akt pathway may influence IDE release via microvesicles. Fractionation of microvesicle and exosome fraction by gradient centrifugation (compare Material and Methods 2.2.9) could then give an insight into the distribution of IDE to microvesicles and exosomes, possibly even to their subpopulations. Bobrie and other scientists, who have investigated exosomes and their secretion for years, published a joint study on subpopulations of secreted vesicles. They discuss that the exosome preparations obtained by the common differential ultracentrifugation also used in this work might contain subpopulations of vesicles

secreted by different intracellular mechanisms and not only exosomes originating from endosomes/MVBs. This way they contain also microvesicles that budded from the plasma membrane (Bobrie, et al., 2012). Therefore, density gradient fractionation of prepared extracellular vesicles might provide more precise information on the distribution of IDE to exosomes and microvesicles.

Due to the known function of Vps4B in intracellular trafficking (Scheuring, et al., 2001; Yoshimori, et al., 2000; Fujita, et al., 2003), the influence of Vps4B depletion on the subcellular distribution of IDE was analysed. A well-studied example of Vps4B-dependent intracellular trafficking is the EGFR. Upon binding of EGF, the EGFR undergoes endocytosis and is targeted for lysosomal degradation via the ESCRT-mediated MVB pathway (Fader & Colombo, 2009; Katzmann, et al., 2002; Saksena, et al., 2009). Recent studies indicate that loss of Vps4B or inhibition of its enzymatic activity disturbs EGFR degradation and thereby prolongs EGF-induced signalling (Yoshimori, et al., 2000; Lin, et al., 2012; Fujita, et al., 2003). Yoshimori and colleagues additionally found that the structure of endosomal compartments and endosomal trafficking from and to the plasma membrane as well as to the lysosome depend on the ATPase function of Vps4B (Yoshimori, et al., 2000). Also the retrograde transport of endosomes from the plasma membrane to the trans-Golgi network is abrogated through a deficient ATPase function of Vps4B as shown by Fujita and colleagues (Fujita, et al., 2003). However, neither transient nor stable knockdown of Vps4B significantly affected the subcellular distribution of IDE in BV-2 cells as demonstrated in the present study (see Figure 21 and Figure 22): 95% of IDE is found in the cytosolic fraction of the Vps4B knockdown cells, as it is observed in control cells. Only a small fraction of IDE is associated with cellular membranes. Downregulation of Vps4B did not significantly affect the distribution of IDE between individual subcellular compartments as cytosol, the endosomal and the lysosomal compartment. In addition, the amount of IDE as well as the exosomal marker Alix in the MVB fractions is not changed (see Figure 22) indicating no effect of Vps4B depletion on the sorting of exosomal proteins to MVBs. This might also explain the observation that Alix secretion is unaffected by knockdown of Vps4B (see Figure 18 and Figure 20). In addition, this again supports the notion that the increase in IDE in conditioned media upon knockdown of Vps4B is rather caused by stimulated shedding of microvesicles, than secretion of exosomes.

The effect of Vps4B depletion on IDE secretion could also be independent from alterations in sorting of IDE to microvesicles or another mechanism of regulated membrane translocation. Several studies showed the formation of aberrant endosomes upon overexpression of the ATPase-deficient variant Vps4B-E235Q, also sometimes called E235Q compartments, in which several proteins, that are transported in the endosomal system, accumulate. Examples are the EGFR destined for lysosomal degradation, the protein TGN38 destined for recycling to the trans-Golgi network from the plasma membrane, and the transferrin receptor destined for

recycling or distribution to the plasma membrane after synthesis (Scheuring, et al., 2001; Yoshimori, et al., 2000; Fujita, et al., 2003). Fujita and colleagues furthermore found accumulation of immature forms of lysosomal hydrolases as Cathepsin D in these aberrant endosomes. Moreover, these immature forms of Cathepsin D are secreted to a much higher extent than in control cells indicating a fusion of these aberrant endosomes with the plasma membrane (Fujita, et al., 2003). This process is called hyper-secretion and was described already earlier by Babst et al. upon overexpression of a Tsg101 mutant and in class E vps mutants in yeast (Babst, et al., 2000; Babst, et al., 1997). Class E vps proteins are yeast homologues of the mammalian ESCRT proteins. Hyper-secretion might serve to remove proteins that accumulated in these aberrant endosomes. It would be interesting to analyse whether also downregulation of Vps4B could result in the formation of aberrant endosomal compartments and thereby increase the secretion of certain proteins, including IDE. This might represent a mechanism which is influenced by the downregulation of Vps4B, but independently of the release via exosomes or microvesicles. IDE could reach these compartments by the endocytosis of cell surface IDE which is also discussed by Bulloj and colleagues as a possible mechanism of IDE localisation to MVBs (Bulloj, et al., 2010). A luminal endosomal localisation and activity of IDE was already shown (Hamel, et al., 1988; Hamel, et al., 1991; Duckworth, et al., 1998).

Endosomal hyper-secretion could also contribute to increased release of Flotillin-1, which was observed in some of the experiments upon stable knockdown of Vps4B. Flotillins also play a role in endocytic processes and are suggested to recruit transmembrane cargo proteins as for example the EGFR into Flotillin microdomains in the plasma membrane for pre-endocytic cluster formation. Flotillins do not seem to be directly involved in the endocytic process, but function in sorting of cargo to endosomes for recycling to the plasma membrane or retrograde transport to the Golgi and ER (Meister & Tikkanen, 2014). Of course, these assumptions would urgently need further examinations. Aberrant endosomes in BV-2 cells upon RNAi-mediated downregulation of Vps4B might be characterised by detecting EGFR, TGN38 and transferrin receptor by immunocytochemical staining or biochemical subcellular fractionation (compare Material and Methods 2.1.10 and 2.2.11 and Results 2.2.5 and 2.4.2). Furthermore, the potential hyper-secretion of immature Cathepsin D could be investigated. An initial analysis of EGFR degradation in cells with a transient Vps4B knockdown gave a first hint to an increased stability of the receptor (data not shown), but would need further verification.

In conclusion, the present results of this work indicate complex functional implications of Vps4B in different secretory pathways in BV-2 cells and suggest that depletion of Vps4B might cause an imbalance of these pathways and additional compensating mechanisms. Vps4B seems to be of limited relevance for the secretion of IDE via exosomes, but might be rather important in the regulation of IDE release via microvesicles, possibly by affecting IDE sorting by direct

interaction. Furthermore, if it could be confirmed that Vps4B depletion also leads to the formation of aberrant endosomes causing hyper-secretion of their content into the extracellular space, a potential pool of IDE in these compartments could be hyper-secreted and thereby contribute to elevated levels of IDE in the conditioned media upon downregulation of Vps4B. The present results further support the presence of different subpopulations of exosomes and MVBs, and that IDE, Flotillin-1 and Alix might be sorted into distinct subsets of extracellular vesicles which might contribute to the differential release of these proteins.

2.3.3 Cell type-dependent differences in Vps4B-mediated regulation of IDE release

The influence of Vps4B depletion on the secretion of IDE and other exosomal proteins was also studied using primary rat astrocytes and cos-7 cells (see Figure 26 and Figure 27). The results indicated not only cell type-, but also cargo-dependent differences in the Vps4B-mediated regulation of exosome, possibly microvesicle, release which was discovered and discussed in several other studies (Baietti, et al., 2012; Colombo, et al., 2013; Trajkovic, et al., 2008).

Knockdown of Vps4B in primary rat astrocytes did not change IDE relative secretion, but significantly decreased its cellular level, indicating a potential new function of Vps4B in IDE metabolism or transcription regulation. Thus, it would be interesting to assess IDE mRNA expression or IDE protein turnover including, for example, analysis of lysosomal and proteasomal degradation pathways upon knockdown of Vps4B. Vps4B depletion in primary rat astrocytes, moreover, significantly decreased the secretion of Alix to almost 50% indicating a functional involvement of Vps4B in the release and possibly sorting of Alix into exosomes or other extracellular vesicles. Earlier discussed results concerning the strong influence of ceramide levels in Alix and in general exosome release in astrocytes (see 2.2) could also indicate that both, ESCRT-dependent and ceramide-driven mechanisms contribute to the secretion of Alix. For Flotillin-1 release, no clear statement on Vps4B-mediated influence can be made due to varying effects observed in independent experiments. In conclusion this indicates, first, that in astrocytes IDE and Alix might occur in distinct subpopulations of exosomes or other extracellular vesicles, which are generated independently of the ESCRT machinery or at least independent of Vps4B. Second, the observed effect of nSMase2 inhibition causing an almost completely blocked IDE, Alix and Flotillin-1 secretion (see Figure 16) rather indicates a downstream of Vps4B function located effect of ceramide levels on the release of exosomes or other extracellular vesicles. In any case these results suggest that IDE secretion might involve distinct secretory pathways or at least that it is differently regulated in microglia and astrocytes.

In cos-7 cells, depletion of Vps4B affects the release of all three examined exosomal proteins similarly. The secretion of IDE, Alix and Flotillin-1 is increased indicating a general inhibitory

function of Vps4B in exosome formation and release as in BV-2 cells. However, the secretion of all three proteins is affected in the same tendency, suggesting that all three proteins might be located in the same subpopulation of exosomes or other extracellular vesicles, and that their biogenesis might be regulated the same way. An initial experiment examining the influence of ceramide on the secretion of the three proteins in cos-7 cells displayed no effect of nSMase2 inhibition (data not shown) which would support the latter assumption.
Although the present results need further validation for verification and also further investigations (as undertaken in BV-2 cells), they underline that the mechanism, that is involved in the regulation of cargo sorting and secretion of exosomes, may change depending on cell types as well as the cargos associated with different exosome subpopulations (Colombo, et al., 2013).

2.4 Modulation of IDE-mediated Aβ- and insulin degradation by Vps4B in BV-2 microglial cells

The importance of extracellular IDE for the degradation of Aβ in the brain was demonstrated already by several studies, and referred to both secreted and cell surface-associated pools of the enzyme (Qiu, et al., 1998; Vekrellis, et al., 2000; Lynch, et al., 2006; Zhao, et al., 2009; Bulloj, et al., 2010; Tamboli, et al., 2010). Especially microglial cells were in the focus in degradation of extracellular Aβ, because they not only internalize Aβ for lysosome-mediated removal of the peptide, but also degrade extracellular Aβ by secreted IDE (Qiu, et al., 1997; Qiu, et al., 1998; Mandrekar, et al., 2009). So for example, Tamboli and colleagues could prove that stimulation of IDE release from BV-2 cells promotes the degradation of extracellular Aβ (Tamboli, et al., 2010). Thus, it was interesting to study the influence of Vps4B in IDE-mediated degradation of extracellular Aβ and insulin.
The stable knockdown of IDE strongly inhibited degradation of extracellular Aβ (see Figure 28A). This finding is consistent with previous studies, showing that IDE is a major protease in the degradation of extracellular Aβ by microglia (Qiu, et al., 1998; Tamboli, et al., 2010). Depletion of IDE decreased not only removal of extracellular Aβ (and insulin) but also the degradation of cell-associated and potentially internalized Aβ indicating also an important role for the IDE-mediated intracellular and potentially cell-surface Aβ degradation. Interestingly, depletion of Vps4B increased the degradation of extracellular Aβ (and insulin) as well as cell-associated Aβ in comparison to control conditions by additional 30% (see Figure 28). The same magnitude of enhancement in Aβ and insulin degradation suggests the same mechanism mediated by the depletion of Vps4B. First, it could be assumed that an increased secretion of IDE caused by the knockdown of Vps4B might be responsible for the enhanced removal of Aβ and insulin. Whereas in insulin-administered cells the amount of secreted IDE is increased, Aβ-treated cells only show a slightly enhanced release of IDE (see Figure 28).

This might be attributed to a particular effect of Aβ preventing an increase in IDE release. An effect of insulin or Aβ exposure on the secretion of IDE has not been described yet, but both peptides were shown to enhance IDE expression (Zhao, et al., 2004; Leal, et al., 2006). The increased degradation of insulin might be attributed to the increased release of IDE upon knockdown of Vps4B, whereas then the enhanced removal of extracellular Aβ would involve another mechanism which is not known and rather unlikely. However, in both cases the equally decreased levels of Aβ and insulin, respectively, could also indicate an effect of Vps4B downregulation on the enzymatic activity of IDE, for example by direct interaction. As determined in earlier studies several interaction partners of IDE were already found to modulate the degradation of its substrates. Chou and colleagues found that interaction with the intermediate filament proteins nestin and especially phosphorylated vimentin decreased the insulin-degrading activity of IDE, but increased its ability to degrade a bradykinin-mimetic (Chou, et al., 2009). Furthermore, ubiquitin was found to interact in a non-covalent manner with IDE and inhibit its insulin-degrading activity by preventing insulin-binding to the enzyme (Saric, et al., 2003). Also somatostatin, a substrate of IDE itself, enhanced IDE degrading activity for synthetic $A\beta_{10-25}$ by an allosteric mechanism (Ciaccio, et al., 2009). Thus, possibly the interaction with Vps4B (see Table 16 and Figure 34) might inhibit IDE enzymatic activity and the degradation for Aβ and insulin, but further investigations would be necessary to clarify this. A possible approach would be to test the ability of IDE to degrade insulin and Aβ upon addition of Vps4B in vitro (e.g. the Vps4B-MBP fusion protein used in the interaction study, compare Material and Methods 2.2.7 and Figure 34C).

Another point that should be considered is, if depletion of Vps4B might influence the internalization and subsequent lysosomal degradation of Aβ, which could also affect the amount of extracellular Aβ. The internalization of soluble monomeric Aβ via macropinocytosis by BV-2 cells and an immediate further transport to the lysosome could already be proven (Mandrekar, et al., 2009). However, dysfunction of Vps4B leads to a disturbance of endosomal transport, especially the transport of proteins destined for lysosomal degradation (Scheuring, et al., 2001; Yoshimori, et al., 2000; Fujita, et al., 2003; Lin, et al., 2012) (also mentioned above). Therefore, an increased lysosomal degradation of Aβ upon knockdown of Vps4B is very unlikely. Nevertheless, additional experiments would be important that specifically address potential effects of Vps4B depletion on Aβ uptake and intracellular degradation. In this context also the actual role of IDE in intracellular degradation of Aβ would need further investigation. If Vps4B indeed could modulate the enzymatic activity of IDE, this might also influence the IDE-mediated intracellular Aβ degradation.

Another possibility would include the earlier discussed presumption (see 2.3.2) that Vps4B depletion might cause the formation of aberrant endosomes that harbour also IDE.

Macropinocytosed Aβ could be transported to these compartments and meet IDE or potentially also other Aβ-degrading enzymes.
In conclusion the work further demonstrates the importance of IDE for Aβ degradation in BV-2 cells. Moreover, Vps4B influences Aβ and insulin degradation potentially through a modulation of the catalytic activity of IDE which might be mediated by the direct interaction of both proteins. To get a better understanding of this, further investigations are necessary as activity assays to test e.g. the insulin-degrading activity of IDE upon knockdown of Vps4B and cell-free experiments on the degradation of Aβ in conditioned media of control and Vps4B-depleted cells.

2.5 Potential role of IDE in the release and intracellular trafficking of exosomal proteins in BV-2 microglial cells

Due to its function in insulin and Aβ degradation, IDE is considered to play a role in the pathogenesis of DM2 and AD. In addition, IDE is involved in several cellular processes by cleaving various other substrates as TGF α, β-endorphin, glucagon and other bioactive peptides (Wang, et al., 2006; Ciaccio, et al., 2009; Qiu & Folstein, 2006; Bennett, et al., 2000). Moreover, IDE has been shown to interact with non-substrate proteins, for example the steroid receptors GR and AR (glucocorticoid and androgen receptor), the 26S proteasome, ubiquitin and the intermediate filaments nestin and vimentin (Authier, et al., 1996; Kupfer, et al., 1994; Bennett, et al., 2000; Fawcett, et al., 2007; Chou, et al., 2009; Udrisar, et al., 2005; Saric, et al., 2003; Leissring, et al., 2004; Vieira, et al., 2011). This suggests that IDE is a multifunctional protein that could not only regulate biological processes by its enzymatic function, but might also affect the biological activity of other proteins independently. In line with multiple functions, IDE is found in different subcellular localisations. It was detected in the cytosol and in association with mitochondria, peroxisomes, ER, nucleus and endosomes, and also at the cell surface and in extracellular fluids (compare also introduction 1.). In this study, a Y2H screen revealed novel potential interaction partners of IDE which could indicate additional functions of this protein (see Table 16 and Figure 31A). The interaction with Uhrf2, Klhl13 and EP400 could indicate a function of IDE in the regulation of cell cycle, with Fbxo38 in transcriptional regulation, suggesting a role of IDE in the nucleus. Little is known about the nuclear functions of IDE. Only Kupfer and colleagues showed about 20 years ago that IDE may modulate the DNA-binding of the steroid receptors GR and AR (Kupfer, et al., 1994), probably independent from its catalytic activity. Interestingly, additional data indicate that IDE might not possess insulin-degrading activity in the nucleus (Kupfer, et al., 1994; Udrisar, et al., 2005), further supporting a protease-independent function.
Another interesting observation from the Y2H screen is that most of the potential interaction partners (44%) are related to the cellular energy metabolism. Due to its role in the degradation

of insulin and glucagon, IDE is considered to regulate energy metabolism mainly through its protease function. However, the present results suggest that IDE might also participate in cellular energy metabolism by direct interaction with enzymes like enolase 1 or lactate dehydrogenase A. Thus, it would be interesting to investigate the physiological relevance of the identified interaction of IDE with other metabolic proteins.

Proteins as Fbxo38, the E3 ubiquitin ligase Uhrf2, Klhl13 and COMMd8, adaptor proteins of E3 ubiquitin ligase complexes, and TPP2 acting downstream of the 26S proteasome further support a role for IDE in ubiquitination and proteasomal protein degradation. It was shown previously, that IDE directly interacts with the 20S and 26S proteasome and inhibits proteasomal degradation (Bennett, et al., 2000; Tundo, et al., 2013; Fawcett, et al., 2007; Sbardella, et al., 2015). IDE also binds to ubiquitin and might regulate poly-ubiquitination of proteins (Saric, et al., 2003; Ralat, et al., 2011; Tundo, et al., 2013).

Other identified potential interaction partners of IDE show an involvement in protein folding and posttranslational modification in ER and cytoplasm (Hsp90b1/Grp94, Aasdhppt). An interesting connection opens up by the finding of Tundo and colleagues that IDE seems to represent a heat shock-like protein being upregulated in a Hsp-like fashion upon cell stress as heat and exposure to H_2O_2 (Tundo, et al., 2013). In the present work, Grp94 was identified as a potential binding partner for IDE. Grp94 is a paralogue of Hsp90β, localised in the ER, and involved in processing and transport of proteins destined for secretion (Marzec, et al., 2012). This might indicate a role for IDE in protein folding under both physiological conditions and cellular stress and suggests a specialized function for IDE in the ER.

Functional studies on the role of IDE in the release of exosomes and sorting of exosomal cargos performed during this project showed that transient knockdown of IDE in BV-2 cells resulted in a significant increase in the release of Alix (see Figure 23A). This same effect was still detectable after IDE expression turned back to even increased levels (see Figure 25). Furthermore, IDE depletion resulted in an increased localisation of Alix in MVB fractions suggesting a regulatory function of IDE in the sorting of Alix into ILVs of MVBs (see Figure 23B). This might indicate a longer-lasting process that influences sorting of Alix into MVBs and exosomes. Nevertheless, this would need further investigation. Shorter time periods in the experimental set-up should be examined to be able to analyse Alix secretion levels in direct comparison to the normalising IDE cellular levels. Possibly Alix secretion turns back to normal after the gradual increase in IDE expression. A surprising finding was that stable downregulation of IDE by shRNA expression in BV-2 cells did not affect Alix secretion and sorting into exosomes, which contrasts to the results obtained upon transient knockdown of IDE. This suggests that it might be an ad-hoc reaction of the cells on sudden fluctuations in IDE expression, which seems to be balanced upon constantly low IDE levels. In stable IDE-depleted cells, furthermore, the release of Flotillin-1 was found to be increased, as well in

contrast to cells with transient IDE knockdown (see Figure 24). Downregulation of IDE did not influence Flotillin-1 subcellular distribution. However, minor differences in the distribution of Flotillin-1 might not be detected by the used method, as mentioned before (compare Results 2.2.7). Thus, the molecular mechanisms underlying these complex effects remain to be identified in more detail.

How might IDE exert a function in exosome biogenesis and secretion? Based on the identified interaction with Vps4B, a potential influence of IDE on the ATPase activity and function of Vps4B in exosome release was tested. As mentioned above, the Vps4 ATPase complex is described as a dodecamer formed by two hexameric rings formed of Vps4A and B subunits that additionally bind ATP and LIP5 proteins (Scott, et al., 2005). The rationale was, first, that IDE might affect the formation of this ATPase complex. However, native gel electrophoresis did not reveal an effect of IDE-depletion on Vps4B complexes (see Figure 36). IDE might also inhibit Vps4B ATPase activity by direct interaction. In the Y2H screen the Vps4B fragment interacting with IDE Bait indeed contained parts of its ATPase domain. Furthermore, as mentioned above, there are preliminary results that Vps4B depletion stabilized EGFR (data not shown). The downregulation of IDE, however, here induced a slight decrease in EGFR levels (data not shown), probably indicating a rather increased EGFR degradation, which in turn might suggest a decrease in the ATPase activity of Vps4B by IDE indeed. An alternative approach to investigate potential effects of IDE on the ATPase activity of Vps4B would be to analyse the release of HIV-1 and its infectivity which requires ATP binding and hydrolysis of Vps4B (Scott, et al., 2005; Garrus, et al., 2001; von Schwedler, et al., 2003). On the other hand, the finding that Vps4B depletion, which would also result in decreased Vps4B ATPase activity, does neither affect Alix subcellular distribution and localisation to MVB fractions (see Figure 22) nor its secretion (see Figure 18 and Figure 20) rather speaks against the hypothesis that the decreased secretion of Alix upon IDE knockdown involves the inhibition of Vps4B activity.

Nevertheless, other functions already examined for the “multifunctional” protein IDE (Vieira, et al., 2011) could give a hint on its potential role in the regulation of exosome biogenesis. First, it should be mentioned that Axl1p, a yeast orthologue of IDE, was found to be involved in vesicular budding as a key determinant for the bud site selection in haploid cells during mitosis. Its expression leads to the axial budding usually observed for haploid cells instead of the bipolar budding that is typical for diploid cells in yeast (Fujita, et al., 1994). Axl1p assembles with other proteins to form a “landmark” complex. This complex is recognized by GTPases that in turn influence the polarization of the actin cytoskeleton, which then is involved in endocytic or exocytic processes (Gao, et al., 2007). Spiliotis compared these by the “landmark” determined areas for axial budding in the yeast membrane with distinct regions for exocytosis in the plasma membrane of other eukaryotic cells that are restricted by certain cytoskeleton-

membrane domains (Spiliotis & Nelson, 2003). Distinct membrane microdomains in membranes of endosomes might also modulate formation of ILVs, indicated by results of Trajkovic et al. on the effect of ceramide on inward budding (Trajkovic, et al., 2008). It is intriguing to speculate that IDE might play a role in such a “landmark”-like protein complex in mammalian cells determining particular regions for ILV budding in MVBs.

Interestingly, Axl1p is also involved in the maturation of the yeast mating pheromone a-factor that is secreted via an unconventional pathway through the ABC transporter Ste6p. The Axl1p-mediated processing of the a-factor is the last step before secretion and most probably performed at the membrane due to the fact that the last precursors of the a-factor are prenylated and membrane-bound (Michaelis, 1993; Chen, et al., 1997). Mutants of Axl1p block the secretion of the a-factor (Adames, et al., 1995) indicating a role of Axl1p also in regulation of an unconventional secretory pathway. If this could be transferred to the mammalian orthologue IDE, this might, first, indicate a functional association of the protein to the membrane, which secondly, might be expanded to a potential influence of IDE on the unconventional protein secretion. Either way, this would indicate a possibility of IDE membrane association.

A further mechanism in IDE-dependent exosome biogenesis, potentially connected to the former, would be the modulation of protein ubiquitination that might also regulate exosome sorting and biogenesis. Polyubiquitination or multiple monoubiquitination of cargo proteins regulates their sorting into invaginations at the endosomal membrane which precedes ILV formation into MVBs. As mentioned above, IDE not only shows a non-covalent interaction with ubiquitin, which leads to an inhibition of its insulin-degrading activity (Saric, et al., 2003), it is also able to proteolytically cleave ubiquitin itself (Ralat, et al., 2011), although Ralat and colleagues did not describe if IDE might also degrade ubiquitin in poly-ubiquitin protein tags. Furthermore, the findings of the present study indicate an interaction of IDE with E3 ubiquitin ligases or adaptor proteins which might additionally hint to a potential role of IDE in regulating ubiquitination of proteins. Interestingly, Tundo and colleagues detected a decrease in the total amount of poly-ubiquitinated proteins upon siRNA-mediated knockdown of IDE 48-36 hours after transfection (Tundo, et al., 2013; Sbardella, et al., 2015). They rather attributed this effect to an increased proteasomal activity upon knockdown of IDE leading to an enhanced turnover of poly-ubiquitinated proteins. However, ubiquitination of proteins as a posttranslational modification not only regulates their degradation, but also the subcellular targeting and their function (Moreno-Gonzalo, et al., 2014; d'Azzo, et al., 2005). Polyubiquitination or multiple monoubiquitination, as described above, regulates protein sorting into MVBs, and is recognized by the ESCRT machinery, specifically ESCRT-0 and -I (compare also Introduction 2.2). Although some cargo for ILVs is deubiquitylated before vesicle abscission also ubiquitinated proteins were detected in isolated exosomes (Moreno-Gonzalo, et al., 2014),

indicating a role of ubiquitination in cargo sorting into exosomes as well. However, exosomal protein sorting can occur also independent on ubiquitination (Buschow, et al., 2009; Villarroya-Beltri, et al., 2014), further demonstrating the complexity in the molecular mechanisms that regulate exosomal protein targeting, and also defining distinct subpopulations of exosomes (Colombo, et al., 2013).

Monoubiquitination can also regulate protein activity. Monoubiquitination was found for ESCRT-0 subunits and might regulate the directional flow of cargo to additional complexes (Moreno-Gonzalo, et al., 2014; d'Azzo, et al., 2005). Also Alix was described to be monoubiquitinated regulating its activity (Sette, et al., 2010; Dores, et al., 2015). Furthermore, Sette and colleagues by analysing the release of HIV, revealed that Alix is able to recruit an E3 ubiquitin ligase (Nedd4-1) which facilitates virus budding from the plasma membrane (Sette, et al., 2010). In general, E3 ubiquitin ligases, in particular members of the Nedd4 family or their adaptors, are involved in several vesicle budding processes, including virus budding, endocytosis, microvesicle shedding from the plasma membrane and also exosome biogenesis in MVBs (d'Azzo, et al., 2005; Sette, et al., 2010; Chung, et al., 2008; Moreno-Gonzalo, et al., 2014; Putz, et al., 2008; Nabhan, et al., 2012).

It could now be speculated that IDE might influence protein ubiquitination through ubiquitin degradation and thereby modulate either the polyubiquitination of exosome cargo or the monoubiquitination of proteins that are involved in exosome biogenesis. Moreover, IDE might recruit an E3 ubiquitin ligase and thereby drive vesicle budding or prevent it by an inhibitory ubiquitination of certain target proteins. Concerning the secretion of Alix, IDE might rather exert an inhibitory effect. A possible connection might be that IDE influences the monoubiquitination of Alix thereby negatively regulating its activity. This would interfere with its function in exosome release and also inhibit its own sorting into exosomes, which involves syndecans and syntenin (Baietti, et al., 2012). The mechanisms underlying the effect of IDE on protein ubiquitination possibly affecting the sorting of Alix and other proteins as Flotillin-1 would require further investigation. In this regard, an inducible shRNA-based RNAi system would be more appropriate than the used stably shRNA-expressing cells.

The examination of IDE depletion in other cell types, namely primary rat astrocytes and cos-7 cells, revealed, as observed already for the downregulation of Vps4B (discussed above in 2.3.3), different and partly opposite effects than detected in BV-2 microglial cells (see Figure 26 and Figure 27). In rat astrocytes, in contrast to BV-2 cells, IDE transient depletion caused a decrease in the release of Alix by more than 65% whereas Flotillin-1 secretion is not significantly affected. In cos-7 cells, however, IDE knockdown did not influence Alix secretion, but slightly and significantly decreased the release of Flotillin-1 by approximately 25%. This once again supports that exosome biogenesis might be regulated differently in distinct cell types. On the other hand it underlines again that Alix and Flotillin-1, most probably, are located

in different exosome subpopulations in astrocytes as well as in cos-7 and BV-2 cells. Together, these combined observations also indicate a regulatory function of IDE in the biogenesis of exosomes or sorting of exosomal cargo proteins not only in BV-2 cells.

3. Conclusions

The present investigations on molecular mechanisms of IDE secretion, predominantly in BV-2 cells, showed that not only the release of distinct exosomal marker proteins is regulated differently, but also the exosome secretion in distinct cell types.

First, this study revealed that IDE secretion in microglial cells is stimulated by 5-HT and indicates an important function of 5-HTR-mediated signalling in the release of IDE. Moreover, the present results suggest that communication between neurons and microglia might play a beneficial role for the microglia-mediated degradation of extracellular monomeric Aβ in the brain.

The findings of the study further suggest that the regulation of IDE release from microglial cells seems to be multi-facetted due to the possible involvement of several distinct secretory pathways. The modulation of ceramide metabolism indicated that this lipid plays a minor role in exosome biogenesis in BV-2 cells, but promotes this process in primary rat astrocytes. Interestingly, ceramide appears to even inhibit the secretion of IDE in microglial cells, leading to the assumption that in microglial cells a pool of IDE is possibly released by an additional secretory pathway distinct from exosome-mediated export. The study also showed an interaction of IDE with the ESCRT accessory ATPase Vps4B. Even though the functional implication remains to be determined in much more detail, Vps4B unexpectedly exerts an inhibitory effect on IDE release in BV-2 cells. Although Vps4B is known for an influence on exosome biogenesis and endosomal transport of proteins mediated by its ATPase function in the MVB pathway, its contribution to the sorting and intracellular trafficking of IDE appears to be limited. The present findings indicate that Vps4B rather affects the release of IDE via microvesicles than via exosomes, which might be attributed to an ATPase-independent function. On the other hand, the loss of Vps4B might also cause a hyper-secretion of several proteins accumulated in aberrant endosomes involving also IDE. Furthermore, depletion of Vps4B stimulated the IDE-mediated degradation of insulin and Aβ in BV-2 cells.

The most surprising finding of this study is probably that IDE itself plays a functional role in unconventional release of certain exosome cargo proteins and possibly selected exosome pools, potentially mediated by a modulated exosome biogenesis or modulated sorting of exosomal cargo.

All in all, the combined results of this work reflect the controversial and sometimes opposing results on the regulation of exosome biogenesis and release described in the literature. The present data support the existence of several distinct subpopulations of exosomes varying not

only in their protein composition, but also in their existence in distinct cell types. Moreover, also regulatory mechanisms for exosome (and probably microvesicle) biogenesis and the presence or absence of these same mechanisms are varying between the cell types. Furthermore, most exosomal proteins are not exclusively found in exosomes, but as well in microvesicles. Also other unconventional pathways as export via ABC transporter are conceivable. But even inhibition of the conventional secretory pathway, especially by interrupting the vesicular transport inside the Golgi network, seems to stimulate the exosomal release in general, indicating a closer but also very complex relation and conjunction of the distinct secretory pathways in the cell than possibly expected at the moment.

E Outlook

The regulation of exosome biogenesis and release in mammalian cells is not fully understood and an involvement of the ESCRT machinery in this process is controversial. The underlying regulatory mechanisms could differ between individual cargo proteins and cell types. The present work on molecular mechanisms of IDE secretion supports the existence of different subpopulations of exosomes. Until now it is difficult to determine these subpopulations. In addition, there are mainly no uniform methods for the isolation of exosomes. For example, a common procedure of exosome preparation by differential centrifugation (Théry, et al., 2006), which is utilized also in this study, seems to be susceptible to variation especially concerning the separation of microvesicles and exosomes (Bobrie, et al., 2012). Therefore, an important focus should be placed on the development of improved isolation procedures to separate microvesicles and exosomes and, furthermore, a standardisation of these used methods should happen to enable more comparability between distinct studies on exosome regulation. Then, it would be important to further characterise the molecular details of unconventional secretion of IDE. In particular, given that the present study indicates additional secretory mechanisms to the known exosome-associated pathway. An involvement of the ESCRT-accessory Vps4B in IDE secretion could be determined in this study, thereby supporting previous studies on a role of Vps4B in the release of exosome-associated proteins (Baietti, et al., 2012; Colombo, et al., 2013; Kunadt, et al., 2015; Gan & Gould, 2011). Further analyses of Vps4B function in the exosome and microvesicle but also other unconventional secretory pathways could elucidate the partly contradictory effects obtained by the different studies. It would be also interesting to further characterise the interaction of IDE and Vps4B by determining the precise sequences of the interaction domain in both proteins and subsequent mutation analyses.

Interestingly, ESCRT dysfunction is associated to AD (Lee & Gao, 2012). Already in early stages of the disease a disturbed endosomal-lysosomal system leads to an impaired maturation of autophagic vacuoles (AVs) to lysosomes and thereby the accumulation of such AVs in dystrophic neurites, most likely promoting neuronal cell death and contributing to disease progression (Funk, et al., 2011; Lee, et al., 2011; Nixon & Yang, 2012). Therefore, altered Vps4B function and thereby induced aberrant endosomes and hyper-secretion (Scheuring, et al., 2001; Yoshimori, et al., 2000; Fujita, et al., 2003) might contribute to the pathogenesis of AD. It would be crucial to investigate the formation of aberrant endosomes that are observed during Vps4B ATPase-deficiency mainly in its potential consequences for protein secretion, which might affect not only IDE release, but also other unconventionally secreted proteins. Moreover, an effect of Vps4B deficiency on Aβ clearance would represent

an important point to be analysed in more detail, especially after the unexpected finding of this work that Vps4B depletion causes an 30% increased degradation of Aβ in microglial cells.
Finally, this study strongly suggests a regulatory function of IDE in the exosome biogenesis and release. It would be interesting to assess if this potential new role of IDE might be associated with its assumed function in protein ubiquitination and the possible recruitment of E3 ubiquitin ligases that might influence membrane budding, as it is described for example for Alix (Sette, et al., 2010) or whether IDE might be part of a membrane “landmark” complex, marking particular membrane domains for vesicle budding. In this context, it might be furthermore interesting to examine the consequences of IDE deficiency in AD given the fact that increased exosome secretion was shown to have both beneficial and detrimental effects on the progression of the disease affecting mainly Aβ clearance and its aggregation (Dinkins, et al., 2014; Rajendran, et al., 2006; Perez-Gonzalez, et al., 2012; Yuyama, et al., 2014).

F Abstract

Extracellular deposition of amyloid-β (Aβ) plaques in the brain, a hallmark of Alzheimer's disease (AD), results from an imbalance between production and clearance of the peptide. Insulin-degrading enzyme (IDE) is one of the major proteases that degrade monomeric Aβ in the brain and is suggested to be mainly involved in the removal of extracellular Aβ. Recent studies demonstrated that the enzyme is released by microglial cells via the unconventional exosome secretory pathway, but little is known about the regulation of IDE secretion and sorting into extracellular vesicles.

This work revealed that serotonin (5-HT) stimulates the secretion of exosome associated IDE from microglial cells. Activation of the 5-HT receptors 2a, 2b and 4 induces an elevation of intracellular Ca^{2+} which is likely to promote the release of IDE. Co-culture experiments showed that the presence of neurons stimulates secretion from and expression of IDE in microglial cells.

Further experiments revealed that inhibition of nSMase2 that decreases ceramide production unexpectedly increased IDE release from microglial cells, whereas the secretion of other exosomal proteins rather decreased or remained unaffected. RNAi-mediated knockdown of the ESCRT-associated ATPase Vps4B elevated secretion of IDE without affecting the trafficking of IDE to MVBs or its secretion via exosomes. Vps4B depletion promoted IDE release by increasing microvesicle shedding. Interestingly, Vps4B was identified as potential interaction partner of IDE in a yeast two-hybrid screen and confirmed by co-immunoprecipitation. Depletion of IDE or Vps4B, respectively, did not influence the usual complex formation of both proteins. But because knockdown of Vps4B in BV-2 microglial cells also increased IDE-mediated degradation of extracellular Aβ and insulin, it could be assumed that the interaction of IDE and Vps4B might modulate IDE protease activity.

Moreover, transient knockdown of IDE increased the release of Alix from microglial cells by enhancing its subcellular transport to MVBs suggesting a role for IDE itself in the regulation of exosome secretion. Secretion analyses in primary rat astrocytes and fibroblast cos-7 cells revealed cell type- and cargo-dependent differences in the ceramide-, Vps4B- and IDE-mediated regulation of exosome release. This suggests not only the existence of distinct exosome subpopulations but also distinct mechanisms of exosome biogenesis dependent on cell type and the particular cargo protein.

Together these results indicate a complex interaction of several regulatory mechanisms for IDE secretion in microglial cells and suggest the potential involvement of further pathways for IDE export regulated by Vps4B and nSMase2.

G References

Abdul-Hay, S. et al., 2015. Selective Targeting of Extracellular Insulin-Degrading Enzyme by Quasi-Irreversible Thiol-Modifying Inhibitors. *ACS Chem Biol.*, 10(12), p. 2716–2724.

Abraham, R. et al., 2001. Substantial linkage disequilibrium across the insulin-degrading enzyme locus but no association with late-onset Alzheimer's disease. *Hum Genet.*, 109(6), pp. 646-652.

Adames, N., Blundell, K., Ashby, M. N. & Boone, C., 1995. Role of yeast insulin-degrading enzyme homologs in propheromone processing and bud site selection. *Science*, 270(5235), pp. 464-467.

Affholter, J., Fried, V. & Roth, R., 1988. Human insulin-degrading enzyme shares structural and functional homologies with E. coli protease III. *Science*, 242(4884), pp. 1415-1418.

Akiyama, H. et al., 1988. Cellular localization of insulin-degrading enzyme in rat liver using monoclonal antibodies specific for this enzyme. *Biochem Biophys Res Commun.*, 155(2), pp. 914-922.

Alonso, A. d. C. et al., 2001. Hyperphosphorylation induces self-assembly of τ into tangles of paired helical filaments/straight filaments. *Proc Natl Acad Sci USA.*, 98(12), p. 6923–6928.

Alonso, R. et al., 2011. Diacylglycerol kinase α regulates the formation and polarisation of mature multivesicular bodies involved in the secretion of Fas ligand-containing exosomes in T lymphocytes. *Cell Death Differ.*, 18(7), pp. 1161-1173.

Alzheimer's association, 2014. *alz.org | Alzheimer's and dementia.* [Online]
Available at: http://www.alz.org/

Andreu, Z. & Yáñez-Mó, M., 2014. Tetraspanins in Extracellular Vesicle Formation and Function. *Front Immunol.*, Volume 5, p. 442.

Arvanitakis, Z. et al., 2004. Diabetes mellitus and risk of Alzheimer disease and decline in cognitive function. *Arch Neurol.*, 61(5), pp. 661-666.

Austin, J. W., Gilchrist, C. & Fehlings, M. G., 2012. High molecular weight hyaluronan reduces lipopolysaccharide mediated microglial activation. *J Neurochem.*, 122(2), p. 344–355.

Authier, F., Posner, B. & Bergeron, J., 1996. Insulin-degrading enzyme. *Clin Invest Med.*, 19(3), pp. 149-160.

Aye, I. L., Singh, A. T. & Keelan, J. A., 2009. Transport of lipids by ABC proteins: interactions and implications for cellular toxicity, viability and functio. *Chem Biol Interact.*, 180(3), p. 327–339.

Babst, M., Odorizzi, G., Estepa, E. J. & Emr, S. D., 2000. Mammalian tumor susceptibility gene 101 (TSG101) and the yeast homologue, Vps23p, both function in late endosomal trafficking. *Traffic*, 1(3), p. 248–258.

Babst, M., Sato, T. K., Banta, L. M. & Emr, S. D., 1997. Endosomal transport function in yeast requires a novel AAA-type ATPase, Vps4p. *EMBO J.*, 16(8), pp. 1820-1831.

Babst, M., Wendland, B., Estepa, E. J. & Emr, S. D., 1998. The Vps4p AAA ATPase regulates membrane association of a Vps protein complex required for normal endosome function. *EMBO J.*, 17(11), pp. 2982-2993.

Baietti, M. F. et al., 2012. Syndecan-syntenin-ALIX regulates the biogenesis of exosomes. *Nat Cell Biol.*, 14(7), pp. 677-685.

Balcaitis, S. et al., 2005. Lentiviral transduction of microglial cells. *Glia*, 50(1), pp. 48-55.

Bales, K. R. et al., 2009. Human APOE isoform-dependent effects on brain beta-amyloid levels in PDAPP transgenic mice. *J Neurosci.*, 29(21), pp. 6771-6779.

Bard, F. et al., 2000. Peripherally administered antibodies against amyloid beta-peptide enter the central nervous system and reduce pathology in a mouse model of Alzheimer disease. *Nat Med.*, 6(8), pp. 916 - 919.

Barger, S. W. & Harmon, A. D., 1997. Microglial activation by Alzheimer amyloid precursor protein and modulation by apolipoprotein E. *Nature*, 388(6645), pp. 878-881.

Becker, A. B. & Roth, R. A., 1992. An unusual active site identified in a family of zinc metalloendopeptidases. *Proc Natl Acad Sci USA.*, 89(9), pp. 3835-3839.

Bennett, R. G., Duckworth, W. C. & Hamel, F. G., 2000. Degradation of amylin by insulin-degrading enzyme. *J Biol Chem*, 275(47), pp. 36621-36625.

Bennett, R. G., Hamel, F. G. & Duckworth, W. C., 2000. Insulin inhibits the ubiquitin-dependent degrading activity of the 26S proteasome. *Endocrinology*, 141(7), pp. 2508-2517.

Benton, J. S. et al., 1982. Alzheimer's disease as a disorder of isodendritic core. *Lancet*, 319(8269), p. 456.

Benzing, W. et al., 1999. Evidence for glial-mediated inflammation in aged APP(SW) transgenic mice. *Neurobiol Aging.*, 20(6), p. 581–589.

Berg, K. A., Harvey, J. A., Spampinato, U. & Clarke, W. P., 2008. Physiological and therapeutic relevance of constitutive activity of 5-HT2A and 5-HT2C receptors for the treatment of depression. *Prog Brain Res.*, Volume 172, p. 287–305.

Bernimoulin, M. et al., 2009. Differential stimulation of monocytic cells results in distinct populations of microparticles. *J Thromb Haemost.*, 7(6), p. 1019–1028.

Bertram, L. et al., 2000. Evidence for genetic linkage of Alzheimer's disease to chromosome 10q. *Science*, 290(5500), pp. 2302-2303.

Bianchi, M. E., 2007. DAMPs, PAMPs and alarmins: all we need to know about danger. *J Leukoc Biol.*, 81(1), pp. 1-5.

Bian, L. et al., 2004. Insulin-degrading enzyme and Alzheimer disease: a genetic association study in the Han Chinese. *Neurology*, 63(2), pp. 241-245.

Biber, K., Neumann, H., Inoue, K. & Boddeke, H. W., 2007. Neuronal 'On' and 'Off' signals control microglia. *Trends Neurosci.*, 30(11), pp. 596-602.

Bickel, P. E. et al., 1997. Flotillin and epidermal surface antigen define a new family of caveolae-associated integral membrane proteins. *J Biol Chem.*, 272(21), pp. 13793-13802.

Bishop, N. & Woodman, P., 2000. ATPase-defective mammalian VPS4 localizes to aberrant endosomes and impairs cholesterol trafficking. *Mol Biol Cell.*, 11(1), pp. 227-239.

Björk, B. F. et al., 2007. Positive association between risk for late-onset Alzheimer disease and genetic variation in IDE. *Neurobiol Aging.*, 28(9), p. 1374–1380.

Blacker, D. et al., 2003. Results of a high-resolution genome screen of 437 Alzheimer's disease families. *Hum Mol Genet.*, 12(1), pp. 23-32.

Bobrie, A. et al., 2012. Diverse subpopulations of vesicles secreted by different intracellular mechanisms are present in exosome preparations obtained by differential ultracentrifugation. *J Extracell Vesicles*, Volume 1, p. 10.3402/jev.v1i0.18397.

Bockaert, J. et al., 2006. Neuronal 5-HT metabotropic receptors: fine-tuning of their structure, signaling, and roles in synaptic modulation. *Cell Tissue Res.*, 326(2), pp. 553-572.

Bohm, C. et al., 2015. Current and future implications of basic and translational research on amyloid-β peptide production and removal pathways. *Mol Cell Neurosci.*, 66(Pt A), pp. 3-11.

Bonhaus, D. W. et al., 1999. RS-127445: a selective, high affinity, orally bioavailable 5-HT2B receptor antagonist. *Br J Pharmacol.*, 127(5), pp. 1075-1082.

Boussaha, M. et al., 2002. Polymorphisms of insulin degrading enzyme gene are not associated with Alzheimer's disease. *Neurosci Lett.*, 329(1), p. 121–123.

Brockhaus, J., Ilschner, S., Banati, R. & Kettenmann, H., 1993. Membrane properties of ameboid microglial cells in the corpus callosum slice from early postnatal mice. *J Neurosci.*, 13(10), pp. 4412-4421.

Broderick, C. et al., 2002. Constitutive Retinal CD200 Expression Regulates Resident Microglia and Activation State of Inflammatory Cells during Experimental Autoimmune Uveoretinitis. *Am J Pathol.*, 161(5), p. 1669–1677.

Broh-Kahn, R. & Mirsky, I., 1949. The inactivation of insulin by tissue extracts; the effect of fasting on the insulinase content of rat liver. *Arch Biochem.*, 20(1), pp. 10-4.

Bruns, C. et al., 2011. Biogenesis of a novel compartment for autophagosome-mediated unconventional protein secretion. *J Cell Biol.*, 195(6), pp. 979-992.

Bulloj, A. et al., 2008. Detergent resistant membrane-associated IDE in brain tissue and cultured cells: Relevance to Abeta and insulin degradation. *Mol Neurodegener*, Volume 3:22.

Bulloj, A. et al., 2010. Insulin-degrading enzyme sorting in exosomes: a secretory pathway for a key brain amyloid-beta degrading protease.. *J Alzheimers Dis.*, 19(1), pp. 79-95.

Burke, B., Sumner, S., Maitland, N. & Lewis, C. E., 2002. Macrophages in gene therapy: cellular delivery vehicles and in vivo targets. *J Leukoc Biol.*, 72(3), pp. 417-428.

Burns, D. L., 1988. Subunit structure and enzymic activity of pertussis toxin. *Microbiol Sci.*, 5(9), pp. 285-287.

Burnstock, G., Krügel, U., Abbracchio, M. P. & Illes, P., 2011. Purinergic signalling: from normal behaviour to pathological brain function. *Prog Neurobiol.*, 95(2), p. 229–274.

Buschow, S. I. et al., 2009. MHC II in dendritic cells is targeted to lysosomes or T cell-induced exosomes via distinct multivesicular body pathways. *Traffic*, 10(10), p. 1528–1542.

Caccamo, A. et al., 2005. Age- and region-dependent alterations in Abeta-degrading enzymes: implications for Abeta-induced disorders. *Neurobiol Aging.*, 26(5), pp. 645-654.

Candeias, E. et al., 2012. The impairment of insulin signaling in Alzheimer's disease. *IUBMB Life*, 64(12), p. 951–957.

Carantoni, M. et al., 2000. Alzheimer disease and vascular dementia: relationships with fasting glucose and insulin levels. *Dement Geriatr Cogn Disord.*, 11(3), p. 176–180.

Cawley, N. X. et al., 2012. New roles of carboxypeptidase E in endocrine and neural function and cancer. *Endocr Rev.*, 33(2), pp. 216-253.

Chen, P., Sapperstein, S. K., Choi, J. D. & Michaelis, S., 1997. Biogenesis of the Saccharomyces cerevisiae Mating Pheromone a-Factor. *J Cell Biol.*, 136(2), p. 251–269.

Chen, T., Koga, K., Li, X.-Y. & Zhuo, M., 2010. Spinal microglial motility is independent of neuronal activity and plasticity in adult mice. *Mol Pain*, Volume 6, p. 19.

Chidiac, P. et al., 1994. Inverse agonist activity of beta-adrenergic antagonists. *Mol Pharmacol.*, 45(3), pp. 490-499.

Chien, C., Bartel, P., Sternglanz, R. & Fields, S., 1991. The two-hybrid system: A method to identify and clone genes for proteins that interact with a protein of interest. *Proc Natl Acad Sci U S A.*, 88(21), pp. 9578-9582.

Chou, Y.-H.et al., 2009. Structural changes in intermediate filament networks alter the activity of insulin-degrading enzyme. *FASEB J.*, 23(11), pp. 3734-3742.

Christ, L. et al., 2016. ALIX and ESCRT-I/II function as parallel ESCRT-III recruiters in cytokinetic abscission. *J Cell Biol.*, 212(5), pp. 499-513.

Chung, H., Brazil, M. I., Soe, T. T. & Maxfield, F. R., 1999. Uptake, degradation, and release of fibrillar and soluble forms of Alzheimer's amyloid beta-peptide by microglial cells. *J Biol Chem.*, 274(45), pp. 32301-32308.

Chung, H.-Y.et al., 2008. NEDD4L Overexpression Rescues the Release and Infectivity of Human Immunodeficiency Virus Type 1 Constructs Lacking PTAP and YPXL Late Domains. *J Virol.*, 82(10), p. 4884–4897.

Ciaccio, C. et al., 2009. Somatostatin: a novel substrate and a modulator of insulin-degrading enzyme activity. *J Mol Biol*, Volume 5, pp. 1556-67.

Cirrito, J. R. et al., 2011. Serotonin signaling is associated with lower amyloid-β levels and plaques in transgenic mice and humans. *PNAS*, 108(36), p. 14968–14973.

Claeysen, S. et al., 2000. Pharmacological properties of 5-Hydroxytryptamine(4) receptor antagonists on constitutively active wild-type and mutated receptors. *Mol Pharmacol.*, 58(1), pp. 136-144.

Cochet, M. et al., 2013. 5-HT4 ReceptorsConstitutively Promote the Non-Amyloidogenic Pathway of APP Cleavage and Interact with ADAM10. *ACS Chem Neurosci.*, 4(1), p. 130–140.

Cocucci, E. & Meldolesi, J., 2015. Ectosomes and exosomes: shedding the confusion between extracellular vesicles. *Trends Cell Biol.*, 25(6), p. 364–372.

Cocucci, E., Racchetti, G. & Meldolesi, J., 2009. Shedding microvesicles: artefacts no more. *Trends Cell Biol.*, 19(2), p. 43–51.

Colombo, M. et al., 2013. Analysis of ESCRT functions in exosome biogenesis, composition and secretion highlights the heterogeneity of extracellular vesicles. *J Cell Sci.*, 126(Pt 24), pp. 5553-5565.

Combs, C. K., Karlo, J. C., Kao, S.-C. & Landreth, G. E., 2001. beta-Amyloid stimulation of microglia and monocytes results in TNFalpha-dependent expression of inducible nitric oxide synthase and neuronal apoptosis. *J Neurosci.*, 21(4), pp. 1179-1188.

Cook, D. G. et al., 2003. Reduced hippocampal insulin-degrading enzyme in late-onset Alzheimer's disease is associated with the apolipoprotein E-epsilon4 allele. *Am J Pathol.*, 162(1), pp. 313-319.

Costes, S. & Butler, P. C., 2015. Insulin Degrading Enzyme inhibition, a novel therapy for type 2 diabetes? *Cell Metab.*, 20(2), p. 201–203.

Cross, A. J., 1990. Serotonin in Alzheimer-type Dementia and Other Dementing Illnesses. *Ann N Y Acad Sci.*, Volume 600, p. 405–415.

Davalos, D. et al., 2005. ATP mediates rapid microglial response to local brain injury in vivo. *Nat Neurosci.*, 8(6), pp. 752 - 758.

d'Azzo, A., Bongiovanni, A. & Nastasi, T., 2005. E3 ubiquitin ligases as regulators of membrane protein trafficking and degradation. *Traffic*, 6(6), pp. 429-441.

De Felice, F. G. & Ferreira, S. T., 2014. Inflammation, defective insulin signaling, and mitochondrial dysfunction as common molecular denominators connecting type 2 diabetes to Alzheimer disease. *Diabetes*, 63(7), pp. 2262-2272.

De Giorgio, L. A. et al., 2002. APP knockout attenuates microglial activation and enhances neuron survival in substantia nigra compacta after axotomy. *Glia*, 38(2), p. 174–178.

de Rooij, J. et al., 1998. Epac is a Rap1 guanine-nucleotide-exchange factor directly activated by cyclic AMP. *Nature*, 396(6710), pp. 474-477.

De Strooper, B. et al., 1998. Deficiency of presenilin-1 inhibits the normal cleavage of amyloid precursor protein. *Nature*, 391(6665), pp. 387-390.

Dinkel, H. et al., 2014. The eukaryotic linear motif resource ELM: 10 years and counting. *Nucleic Acids Res.*, 42(Database issue), pp. D259-266.

Dinkins, M. B. et al., 2014. Exosome reduction in vivo is associated with lower amyloid plaque load in the 5XFAD mouse model of Alzheimer's disease. *Neurobiol Aging*, 35(8), pp. 1792-1800.

Donaldson, J. G., Cassel, D., Kahn, R. A. & Klausner, R. D., 1992. ADP-ribosylation factor, a small GTP-binding protein, is required for binding of the coatomer protein beta-COP to Golgi membranes. *Proc Natl Acad Sci USA.*, 89(14), pp. 6408-6412.

Donaldson, J. G., Finazzi, D. & Klausner, R. D., 1992. Brefeldin A inhibits Golgi membrane-catalysed exchange of guanine nucleotide onto ARF protein. *Nature*, 360(6402), pp. 350 - 352.

Dores, M. R. et al., 2015. The α-arrestin ARRDC3 mediates ALIX ubiquitination and G protein–coupled receptor lysosomal sorting. *Mol Biol Cell.*, 26(25), p. 4660–4673.

Dreses-Werringloer, U. et al., 2008. A polymorphism in CALHM1 influences Ca2+ homeostasis, Aβlevels, and Alzheimer's disease risk. *Cell*, 133(7), p. 1149–1161.

Duckworth, W. C., Bennett, R. G. & Hamel, F. G., 1998. Insulin degradation: progress and potential. *Endocr Rev*, 19(5), pp. 608-624.

Dueck, H., Eberwine, J. & Kim, J., 2016. Variation is function: Are single cell differences functionally important?. *Bioessays*, 38(2), p. 172–180.

Eckel, R. H. et al., 2011. Obesity and Type 2 Diabetes: What Can Be Unified and What Needs to Be Individualized?. *Diabetes Care*, 34(6), pp. 1424-1430.

Edbauer, D. et al., 2002. Insulin-degrading enzyme rapidly removes the beta-amyloid precursor protein intracellular domain (AICD). *J Biol Chem.*, 277(16), pp. 13389-13393.

Edland, S. D., Slager, S. & Farrer, M., 2004. Genetic association studies in Alzheimer's disease research: challenges and opportunities. *Stat Med.*, 23(2), p. 169–178.

Edland, S. et al., 2003. Insulin degrading enzyme (IDE) genetic variants and risk of Alzheimer's disease: evidence of effect modification by apolipoprotein E (APOE). *Neurosci Lett.*, 345(1), p. 21–24.

Emmanouilidou, E. et al., 2010. Cell-produced alpha-synuclein is secreted in a calcium-dependent manner by exosomes and impacts neuronal survival. *J Neurosci.*, 30(20), pp. 6838-6851.

Ertekin-Taner, N. et al., 2004. Genetic variants in a haplotype block spanning IDE are significantly associated with plasma Abeta42 levels and risk for Alzheimer disease. *Hum Mutat.*, 23(4), p. 334–342.

Ertekin-Taner, N. et al., 2000. Linkage of plasma Abeta42 to a quantitative locus on chromosome 10 in late-onset Alzheimer's disease pedigrees. *Science*, 290(5500), pp. 2303-2304.

Escribano, L. et al., 2010. Rosiglitazone rescues memory impairment in Alzheimer's transgenic mice: mechanisms involving a reduced amyloid and tau pathology. *Neuropsychopharmacology*, 35(7), p. 1593–1604.

Eyo, U. B. & Wu, L.-J., 2013. Bidirectional microglia-neuron communication in the healthy brain. *Neural Plast.*, 2013(2013).

Fader, C. M. & Colombo, M. I., 2009. Autophagy and multivesicular bodies: two closely related partners. *Cell Death Differ.*, 16(1), p. 70–78.

Fagni, L., Dumuis, A., Sebben, M. & Bockaert, J., 1992. The 5-HT4 receptor subtype inhibits K+ current in colliculi neurones via activation of a cyclic AMP-dependent protein kinase. *Br J Pharmacol.*, 105(4), pp. 973-979.

Farris, W. et al., 2003. Insulin-degrading enzyme regulates the levels of insulin, amyloid beta-protein, and the beta-amyloid precursor protein intracellular domain in vivo. *Proc Natl Acad Sci USA.*, 100(7), pp. 4162-4167.

Farris, W. et al., 2004. Partial Loss-of-Function Mutations in Insulin-Degrading Enzyme that Induce Diabetes also Impair Degradation of Amyloid β-Protein. *Am J Pathol.*, 164(4), p. 1425–1434.

Fawcett, J., Permana, P. A., Levy, J. L. & Duckworth, W. C., 2007. Regulation of protein degradation by insulin-degrading enzyme: analysis by small interfering RNA-mediated gene silencing. *Arch Biochem Biophys.*, 468(1), p. 128–133.

Fields, R. D. & Burnstock, G., 2006. Purinergic signalling in neuron–glia interactions. *Nat Rev Neurosci.*, 7(6), p. 423–436.

Fields, S. & Song, O.-k., 1989. A novel genetic system to detect protein-protein interactions. *Nature*, 340(6230), pp. 245-246.

Fontainhas, A. M. et al., 2011. Microglial morphology and dynamic behavior is regulated by ionotropic glutamatergic and GABAergic neurotransmission. *PLoS One.*, 6(1), p. e15973.

Fujisawa, Y., Sasaki, K. & Akiyama, K., 1991. Increased insulin levels after OGTT load in peripheral blood and cerebrospinal fluid of patients with dementia of Alzheimer type. *Biol Psychiatry*, 30(12), pp. 1219-1228.

Fujita, A. et al., 1994. A yeast gene necessary for bud-site selection encodes a protein similar to insulin-degrading enzymes. *Nature*, 372(6506), pp. 567-570.

Fujita, H. et al., 2003. A dominant negative form of the AAA ATPase SKD1/VPS4 impairs membrane trafficking out of endosomal/lysosomal compartments: class E vps phenotype in mammalian cells. *J Cell Sci.*, 116(Pt 2), pp. 401-414.

Funk, K. E., Mrak, R. E. & Kuret, J., 2011. Granulovacuolar Degeneration Bodies of Alzheimer's Disease Resemble Late-stage Autophagic Organelles. *Neuropathol Appl Neurobiol.*, 37(3), p. 295–306.

Gandy, S., 2005. The role of cerebral amyloid β accumulation in common forms of Alzheimer disease. *J Clin Invest.*, 115(5), p. 1121–1129.

Gan, X. & Gould, S. J., 2011. Identification of an inhibitory budding signal that blocks the release of HIV particles and exosome/microvesicle proteins. *Mol Biol Cell*, 22(6), pp. 817-830.

Gao, X.-D.et al., 2007. Sequential and Distinct Roles of the Cadherin Domain-containing Protein Axl2p in Cell Polarization in Yeast Cell Cycle. *Mol Biol Cell.*, 18(7), p. 2542–2560.

Garrus, J. E. et al., 2001. Tsg101 and the vacuolar protein sorting pathway are essential for HIV-1 budding. *Cell*, 107(1), p. 55–65.

Geldenhuys, W. J. & Schyf, C. J. V. d., 2011. Role of serotonin in Alzheimer's disease: a new therapeutic target? *CNS Drugs*, 25(9), pp. 765-781.

Géminard, C., Gassart, A. d., Blanc, L. & Vidal, M., 2004. Degradation of AP2 during reticulocyte maturation enhances binding of hsc70 and Alix to a common site on TFR for sorting into exosomes. *Traffic*, 5(3), pp. 181-193.

Gemma, C., Bachstetter, A. D. & Bickford, P. C., 2010. Neuron-Microglia Dialogue and Hippocampal Neurogenesis in the Aged Brain. *Aging Dis.*, 1(3), pp. 232-244.

Ghering, A. B. & Davidson, W. S., 2006. Ceramide structural features required to stimulate ABCA1-mediated cholesterol efflux to apolipoprotein A-I. *J Lipid Res.*, 47(12), pp. 2781-2788.

Ginhoux, F. et al., 2013. Origin and differentiation of microglia. *Front Cell Neurosci.*, Volume 7, p. 45.

Giunta, B. et al., 2008. HIV-1 TAT Inhibits Microglial Phagocytosis of Aβ Peptide. *Int J Clin Exp Pathol.*, 1(3), p. 260–275.

Glebov, K. et al., 2015. Serotonin stimulates secretion of exosomes from microglia cells. *GLIA*, pp. 626-634.

Glebov, K., Schütze, S. & Walter, J., 2011. Functional relevance of a novel SlyX motif in non-conventional secretion of insulin-degrading enzyme. *JBC*, pp. 22711-22715.

Glebov, K. & Walter, J., 2012. Statins in unconventional secretion of insulin-degrading enzyme and degradation of the amyloid-β peptide. *Neurodegener Dis.*, 10(1-4), pp. 309-312.

Gluzman, Y., 1981. SV40-transformed simian cells support the replication of early SV40 mutants. *Cell*, 23(1), pp. 175-182.

Greasley, P. J. & Clapham, J. C., 2006. Inverse agonism or neutral antagonism at G-protein coupled receptors: a medicinal chemistry challenge worth pursuing? *Eur J Pharmacol.*, 553(1-3), p. 1–9.

Griffiths, G., Quinn, P. & Warren, G., 1983. Dissection of the Golgi complex. I. Monensin inhibits the transport of viral membrane proteins from medial to trans Golgi cisternae in baby hamster kidney cells infected with Semliki Forest virus. *J Cell Biol.*, 96(3), pp. 935-850.

Grodstein, F., Chen, J., Wilson, R. S. & Manson, J. E., 2001. Type 2 diabetes and cognitive function in community-dwelling elderly women. *Diabetes Care*, 24(6), pp. 1060-1065.

Gruenberg, J. & Stenmark, H., 2004. The biogenesis of multivesicular endosomes. *Nature Rev. Mol. Cell Biol.*, Volume 5, p. 317–323.

Grundke-Iqbal, I. et al., 1986. Microtubule-associated protein tau. A component of Alzheimer paired helical filaments. *J Biol Chem.*, 261(13), pp. 6084-6089.

Gudala, K., Bansal, D., Schifano, F. & Bhansali, A., 2013. Diabetes mellitus and risk of dementia: A meta-analysis of prospective observational studies. *J Diabetes Investig.*, 4(6), p. 640–650.

Guo, Q. et al., 2010. Molecular basis for the recognition and cleavages of IGF-II, TGF-alpha, and amylin by human insulin-degrading enzyme. *J Mol Biol.*, 395(2), pp. 430-443.

Haag, M. D. M. et al., 2009. Statins are associated with a reduced risk of Alzheimer disease regardless of lipophilicity. The Rotterdam Study. *J Neurol Neurosurg Psychiatry.*, 80(1), pp. 13-17.

Haas, S., Brockhaus, J., Verkhratsky, A. & Kettenmann, H., 1996. ATP-induced membrane currents in ameboid microglia acutely isolated from mouse brain slices. *Neuroscience*, 75(1), p. 257–261.

Haass, C. & Steiner, H., 2002. Alzheimer disease gamma-secretase: a complex story of GxGD-type presenilin proteases. *Trends Cell Biol.*, 12(12), pp. 556-562.

Haberlandt, C. et al., 2011. Gray Matter NG2 Cells Display Multiple Ca2+-Signaling Pathways and Highly Motile Processes. *PLoS One*, 6(3), p. e:17575.

Hamel, F. G., Mahoney, M. J. & Duckworth, W. C., 1991. Degradation of intraendosomal insulin by insulin-degrading enzyme without acidification. *Diabetes*, 40(4), pp. 436-443.

Hamel, F. G. et al., 1988. Isolation of insulin degradation products from endosomes derived from intact rat liver. *J Biol Chem.*, 263(14), pp. 6703-6708.

Hanson, P. I. & Cashikar, A., 2012. Multivesicular Body Morphogenesis. *Annu Rev Cell Dev Biol.*, Volume 28, pp. 337-362.

Haque, R. & Nazir, A., 2014. Insulin-degrading enzyme: a link between Alzheimer's and type 2 diabetes mellitus. *CNS Neurol Disord Drug Targets*, 13(2), pp. 259-264.

Hardy, J. A. & Higgins, G. A., 1992. Alzheimer's Disease: The Amyloid Cascade Hypothesis. *Science*, 256(5054), pp. 184-185.

Harris-White, M. E. et al., 2004. Role of LRP in TGFbeta2-mediated neuronal uptake of Abeta and effects on memory. *J Neurosci Res.*, 77(2), p. 217–228.

Hashimoto, G. et al., 2012. 5-HT_4 receptor stimulation leads to soluble AβPPα production through MMP-9 upregulation. *J Alzheimers Dis.*, 32(2), pp. 437-445.

Heinrichs, A., 2008. Membrane trafficking: Ceramide buds in. *Nat Rev Mol Cell Biol.*, Volume 9.

Heneka, M. T. et al., 2010. Locus ceruleus controls Alzheimer's disease pathology by modulating microglial functions through norepinephrine. *Proc Natl Acad Sci U S A.*, 107(13), p. 6058–6063.

Hickman, S. E., Allison, E. K. & Khoury, J. E., 2008. Microglial dysfunction and defective β-amyloid clearance pathways in aging Alzheimer's disease mice. *J Neurosci.*, 28(33), p. 8354–8360.

Hislop, J. N., Marley, A. & Zastrow, M. v., 2004. Role of mammalian vacuolar protein-sorting proteins in endocytic trafficking of a non-ubiquitinated G protein-coupled receptor to lysosomes. *J Biol Chem.*, 279(21), pp. 22522-22531.

Hsiao, K. et al., 1996. Correlative memory deficits, Abeta elevation, and amyloid plaques in transgenic mice. *Science*, 274(5284), pp. 99-103.

Hurley, J. H. & Odorizzi, G., 2012. Get on the exosome bus with ALIX. *Nat Cell Biol.*, 14(7), p. 654–655.

Im, H. et al., 2007. Structure of substrate-free human insulin-degrading enzyme (IDE) and biophysical analysis of ATP-induced conformational switch of IDE. *J Biol Chem.*, 282(35), pp. 25453-25463.

Jiang, H. et al., 1994. beta-Amyloid activates complement by binding to a specific region of the collagen-like domain of the C1q A chain. *J Immunol.*, 152(10), pp. 5050-5059.

Jiang, Q. et al., 2008. ApoE promotes the proteolytic degradation of Abeta. *Neuron*, 58(5), p. 681–693.

Johnstone, R. M. et al., 1987. Vesicle formation during reticulocyte maturation. Association of plasma membrane activities with released vesicles (exosomes). *J. Biol. Chem.*, Volume 262, pp. 9412-9420.

Karran, E., Mercken, M. & Strooper, B. D., 2011. The amyloid cascade hypothesis for Alzheimer's disease: an appraisal for the development of therapeutics. *Nat Rev Drug Discov.*, 10(9), pp. 698-712.

Katzmann, D. J., Odorizzi, G. & Emr, S. D., 2002. Receptor downregulation and multivesicular-body sorting.. *Nature Rev. Mol. Cell Biol.*, Volume 3, p. 893–905.

Kettenmann, H., 2011. Physiology of microglia. *Physiol Rev.*, 91(2), pp. 461-553.

Kielar, D. et al., 2003. Adenosine triphosphate binding cassette (ABC) transporters are expressed and regulated during terminal keratinocyte differentiation: a potential role for ABCA7 in epidermal lipid reorganization. *J Invest Dermatol.*, 121(3), p. 465–474.

Kierdorf, K. & Prinz, M., 2013. Factors regulating microglia activation. *Front. Cell. Neurosci.*, Volume 7, p. 44.

Kim, H. Y., Park, S. J., Joe, E.-h. & Jou, I., 2006. Raft-mediated Src homology 2 domain-containing proteintyrosine phosphatase 2 (SHP-2) regulation in microglia. *J Biol Chem.*, 281(17), pp. 11872-11878.

Koenigsknecht-Talboo, J. & Landreth, G. E., 2005. Microglial phagocytosis induced by fibrillar beta-amyloid and IgGs are differentially regulated by proinflammatory cytokines. *J Neurosci.*, 25(36), pp. 8240-8249.

Krabbe, G. et al., 2012. Activation of serotonin receptors promotes microglial injury-induced motility but attenuates phagocytic activity. *Brain Behav Immunol*, 26(3), pp. 419-428.

Kunadt, M. et al., 2015. Extracellular vesicle sorting of α-Synuclein is regulated by sumoylation. *Acta Neuropathol.*, 129(5), pp. 695-713.

Kuo, W.-L., Gehm, B. D. & Rosner, M. R., 1990. Cloning and expression of the cDNA for a Drosophila insulin-degrading enzyme. *Mol Endocrinol*, 4(10), pp. 1580-1591.

Kuo, W. L., Montag, A. G. & Rosner, M. R., 1993. Insulin-degrading enzyme is differentially expressed and developmentally regulated in various rat tissues. *Endocrinology*, 132(2), pp. 604-611.

Kupfer, S. R., Wilson, E. M. & French, F. S., 1994. Androgen and glucocorticoid receptors interact with insulin degrading enzyme. *J Biol Chem.*, 269(32), pp. 20622-20628.

Kurochkin, I. & Goto, S., 1994. Alzheimer's beta-amyloid peptide specifically interacts with and is degraded by insulin degrading enzyme. *FEBS Lett*, 345(1), pp. 33-37.

Kurochkin, I. V., 2001. Insulin-degrading enzyme: embarking on amyloid destruction. *Trends Biochem Sci.*, 26(7), pp. 421-425.

Kutner, R., Zhang, X.-Y. & Reiser, J., 2009. Production, concentration and titration of pseudotyped HIV-1-based lentiviral vectors. *Nat Protoc*, 4(4), pp. 495-505.

Kuusisto, J. et al., 1997. Association between features of the insulin resistance syndrome and Alzheimer's disease independently of apolipoprotein E4 phenotype: cross sectional population based study. *BMJ*, Volume 315, p. 1045.

Laakso, M., 1993. How good a marker is insulin level for insulin resistance? *Am J Epidemiol.*, 137(9), pp. 959-965.

Lancaster, G. I. & Febbraio, M. A., 2005. Exosome-dependent trafficking of HSP70: a novel secretory pathway for cellular stress proteins. *J Biol Chem.*, 280(24), pp. 23349-23355.

Laulagniera, K. et al., 2005. Characterization of exosome subpopulations from RBL-2H3 cells using fluorescent lipids. *Blood Cells Mol Dis.*, 35(2), p. 116–121.

Lau, T. et al., 2010. Somatodendritic serotonin release and re-uptake in mouse embryonic stem cell-derived serotonergic neurons. *Neurochem Int 57*, pp. 969-978.

Leal, M. C. et al., 2006. Plaque-associated overexpression of insulin-degrading enzyme in the cerebral cortex of aged transgenic tg2576 mice with Alzheimer pathology. *J Neuropathol Exp Neurol*, 65(10), pp. 976-987.

Lee, C. Y. D. & Landreth, G. E., 2010. The role of microglia in amyloid clearance from the AD brain. *J Neural Transm (Vienna)*, 117(8), p. 949–96.

Lee, J.-A. & Gao, F.-B., 2012. Neuronal Functions of ESCRTs. *Exp Neurobiol.*, 21(1), p. 9–15.

Lee, S., Sato, Y. & Nixon, R. A., 2011. Lysosomal proteolysis inhibition selectively disrupts axonal transport of degradative organelles and causes an Alzheimer's-like axonal dystrophy. *J Neurosci.*, 31(21), p. 7817–7830.

Leibson, C. et al., 1997. Risk of dementia among persons with diabetes mellitus: a population-based cohort study. *Am J Epidemiol.*, 145(4), pp. 301-308.

Leissring, M. A. et al., 2004. Alternative translation initiation generates a novel isoform of insulin-degrading enzyme targeted to mitochondria. *Biochem J.*, 383(Pt.3), pp. 439-446.

Lezoualc'h, F. & Robert, S. J., 2003. The serotonin 5-HT4 receptor and the amyloid precursor protein processing. *Exp Gerontol.*, 38(1-2), p. 159–166.

Lin, H. H. et al., 2012. Identification of an AAA ATPase VPS4B-dependent pathway that modulates epidermal growth factor receptor abundance and signaling during hypoxia. *Mol Cell Biol.*, 32(6), pp. 1124-1138.

Linnartz, B. & Neumann, H., 2013. Microglial activatory (immunoreceptor tyrosine-based activation motif)- and inhibitory (immunoreceptor tyrosine-based inhibition motif)-signaling receptors for recognition of the neuronal glycocalyx. *Glia*, 61(1), p. 37–46.

Li, P. et al., 2006. The C-terminal domain of human insulin degrading enzyme is required for dimerization and substrate recognition. *Biochem Biophys Res Commun.*, 343(4), pp. 1032-1037.

Lippincott-Schwartz, J. et al., 1991. Brefeldin A's effects on endosomes, lysosomes, and the TGN suggest a general mechanism for regulating organelle structure and membrane traffic. *Cell*, 67(3), pp. 601-616.

Li, Y. et al., 2012. Reciprocal regulation between resting microglial dynamics and neuronal activity in vivo. *Dev Cell.*, 23(6), p. 1189–1202.

Li, Y.-J.et al., 2002. Age at onset in two common neurodegenerative diseases is genetically controlled. *Am J Hum Genet.*, 70(4), p. 985–993.

Lodish, H. et al., 2000. *Molecular Cell Biology.* 4th edition ed. New York: W. H. Freeman.

Lynch, J. A. et al., 2006. Insulin degrading enzyme is localized predominantly at the cell surface of polarized and unpolarized human cerebrovascular endothelial cell cultures. *J Neurosci Res.*, 83(7), pp. 1262-1270.

Lyons, A. et al., 2009. Fractalkine-induced activation of the phosphatidylinositol-3 kinase pathway attentuates microglial activation in vivo and in vitro. *J Neurochem.*, 110(5), p. 1547–1556.

Lytton, J., Westlin, M. & Hanley, M. R., 1991. Thapsigargin inhibits the sarcoplasmic or endoplasmic reticulum Ca-ATPase family of calcium pumps. *J Biol Chem.*, 266(26), pp. 17067-17071.

Maillet, M. et al., 2003. Crosstalk between Rap1 and Rac regulates secretion of sAPPalpha. *Nat Cell Biol.*, 5(7), pp. 633 - 639.

Majumdar, A. et al., 2011. Degradation of Alzheimer's amyloid fibrils by microglia requires delivery of ClC-7 to lysosomes. *Mol Biol Cell.*, 22(10), p. 1664–1676.

Majumdar, A. et al., 2007. Activation of microglia acidifies lysosomes and leads to degradation of Alzheimer amyloid fibrils. *Mol Biol Cell.*, 18(4), pp. 1490-1496.

Majumdar, R., Tameh, A. T. & Parent, C. A., 2016. Exosomes Mediate LTB4 Release during Neutrophil Chemotaxis. *PLoS Biol.*, 14(1), p. e1002336.

Malhotra, V., 2013. Unconventional protein secretion: an evolving mechanism. *EMBO J.*, 32(12), p. 1660–1664.

Malito, E. et al., 2008. Molecular bases for the recognition of short peptide substrates and cysteine-directed modifications of human insulin-degrading enzyme. *Biochemistry*, 47(48), pp. 12822-12834.

Mandrekar, S. et al., 2009. Microglia mediate the clearance of soluble Abeta through fluid phase macropinocytosis. *J Neurosci.*, 29(13), pp. 4252-4262.

Martin-Serano, J. & Neil, S. J., 2011. Host factors involved in retroviral budding and release. *Nat Rev Microbiol.*, 9(7), pp. 519-531.

Marzec, M., Eletto, D. & Argon, Y., 2012. GRP94: An HSP90-like protein specialized for protein folding and quality control in the endoplasmic reticulum. *Biochim Biophys Acta*, 1823(3), p. 774–787.

Matsuoka, Y. et al., 2001. Inflammatory responses to amyloidosis in a transgenic mouse model of Alzheimer's disease. *Am J Pathol.*, 158(4), p. 1345–1354.

Mawuenyega, K. G. et al., 2010. Decreased clearance of CNS beta-amyloid in Alzheimer's disease. *Science*, 330(6012), p. 1774.

Ma, Z. et al., 2012. Calcium homeostasis modulator 1 (CALHM1) is the pore-forming subunit of an ion channel that mediates extracellular Ca2+ regulation of neuronal excitability. *Proc Natl Acad Sci U S A*, 109(28), p. E1963–E1971.

McCready, J., Sims, J. D., Chan, D. & Jay, D. G., 2010. Secretion of extracellular hsp90α via exosomes increases cancer cell motility: a role for plasminogen activation. *BMC Cancer*, Volume 10, p. 294.

McGeer, P. L., Schulzer, M. & McGeer, E. G., 1996. Arthritis and anti-inflammatory agents as possible protective factors for Alzheimer's disease: a review of 17 epidemiologic studies.. *Neurology*, 47(2), pp. 425-432.

Meister, M. & Tikkanen, R., 2014. Endocytic Trafficking of Membrane-Bound Cargo: A Flotillin Point of View. *Membranes (Basel)*, 4(3), pp. 356-371.

Merlini, L., Dudin, O. & Martin, S. G., 2013. Mate and fuse: how yeast cells do it. *Open Biol*, Issue 3, p. 130008.

Michaelis, S., 1993. STE6, the yeast a-factor transporter. *Semin Cell Biol.*, 4(1), pp. 17-27.

Miller, B. C. et al., 2003. Amyloid-beta peptide levels in brain are inversely correlated with insulysin activity levels in vivo. *Proc Natl Acad Sci USA.*, 100(10), pp. 6221-6226.

Miners, J. S. et al., 2008. Abeta-degrading enzymes in Alzheimer's disease. *Brain Pathol.*, 18(2), pp. 240-252.

Miners, J. S. et al., 2009. Neprilysin and Insulin-Degrading Enzyme Levels Are Increased in Alzheimer Disease in Relation to Disease Severity. *J Neuropathol Exp Neurol.*, 68(8), pp. 902-914.

Miners, J. S. et al., 2011. Aβ-degrading enzymes: potential for treatment of Alzheimer disease. *J Neuropathol Exp Neurol.*, 70(11), pp. 944-959.

Mittelbrunn, M. et al., 2011. Unidirectional transfer of microRNA-loaded exosomes from T cells to antigen-presenting cells. *Nat Commun.*, Volume 2, p. 282.

Möbius, W. et al., 2002. Immunoelectron microscopic localization of cholesterol using biotinylated and non-cytolytic perfringolysin O. *J Histochem Cytochem.*, 50(1), pp. 43-55.

Montoliu-Gaya, L. & Villegas, S., 2015. Protein structures in Alzheimer's disease: The basis for rationale therapeutic design. *Arch Biochem Biophys.*, Volume 588, pp. 1-14.

Moreira, R. O., Campos, S. C. & Soldera, A. L., 2013. Type 2 Diabetes Mellitus and Alzheimer's Disease: from physiopathology to treatment implications. *Diabetes Metab Res Rev.*, p. DOI: 10.1002/dmrr.2442.

Moreno-Gonzalo, O., Villarroya-Beltri, C. & Sánchez-Madrid, F., 2014. Post-Translational Modifications of Exosomal Proteins. *Front Immunol.*, Volume 5, p. 383.

Morita, E. et al., 2007. Human ESCRT and ALIX proteins interact with proteins of the midbody and function in cytokinesis. *EMBO J.*, 26(19), pp. 4215-4227.

Mori, Y. et al., 2008. Human herpesvirus-6 induces MVB formation, and virus egress occurs by an exosomal release pathway. *Traffic*, 9(10), p. 1728–1742.

Myers, A. et al., 2000. Susceptibility locus for Alzheimer's disease on chromosome 10. *Science*, 290(5500), pp. 2304-2305.

Nabhan, J. F. et al., 2012. Formation and release of arrestin domain-containing protein 1-mediated microvesicles (ARMMs) at plasma membrane by recruitment of TSG101 protein. *PNAS*, 109(11), pp. 4146-4151.

Nabhan, J. F. et al., 2012. Formation and release of arrestin domain-containing protein 1-mediated microvesicles (ARMMs) at plasma membrane by recruitment of TSG101 protein. *PNAS*, 109(11), pp. 4146-4151.

Näslund, J. et al., 2000. Correlation between elevated levels of amyloid beta-peptide in the brain and cognitive decline. *JAMA*, 283(12), pp. 1571-1577.

Nickel, W. & Rabouille, C., 2009. Mechanisms of regulated unconventional protein secretion. *Nat Rev Mol Cell Biol.*, 10(2), pp. 148-155.

Nimmerjahn, A., Kirchhoff, F. & Helmchen, F., 2005. Resting microglial cells are highly dynamic surveillants of brain parenchyma in vivo. *Science*, 308(5726), pp. 1314-1318.

Nitsch, R. M., Deng, M., Growdon, J. H. & Wurtman, R. J., 1996. Serotonin 5-HT2a and 5-HT2c receptors stimulate amyloid precursor protein ectodomain secretion. *J Biol Chem.*, 271(8), pp. 4188-4194.

Nixon, R. A. & Yang, D.-S., 2012. Autophagy and Neuronal Cell Death in Neurological Disorders. *Cold Spring Harb Perspect Biol.*, 4(10), p. a008839.

Njie, e. G. et al., 2012. Ex vivo cultures of microglia from young and aged rodent brain reveal age-related changes in microglial function. *Neurobiol Aging.*, 33(1), p. 195.e1–195.e12.

Nowotny, P. et al., 2005. Association studies between risk for late-onset Alzheimer's disease and variants in insulin degrading enzyme. *Am J Med Genet B Neuropsychiatr Genet.*, 136B(1), p. 62–68.

Odorizzi, G., 2006. The multiple personalities of Alix. *J Cell Sci.*, 119(Pt 15), pp. 3025-3032.

Oestreich, E. A. et al., 2007. Epac-mediated activation of phospholipase C(epsilon) plays a critical role in beta-adrenergic receptor-dependent enhancement of Ca2+ mobilization in cardiac myocytes. *J Biol.Chem.*, 282(8), pp. 5488-5495.

Olokoba, A. B., Obateru, O. A. & Olokoba, L. B., 2012. Type 2 Diabetes Mellitus: A Review of Current Trends. *Oman Med J.*, 27(4), p. 269–273.

Ott, A. et al., 1999. Diabetes mellitus and the risk of dementia: The Rotterdam Study. *Neurology*, 53(9), pp. 1937-1942.

Ott, A. et al., 1996. Association of diabetes mellitus and dementia: the Rotterdam Study. *Diabetologia*, 39(11), pp. 1392-1397.

Otto, G. P. & Nichols, B. J., 2011. The roles of flotillin microdomains--endocytosis and beyond. *J Cell Sci.*, 124(Pt 23), pp. 3933-3940.

Paolicelli, R. C. et al., 2011. Synaptic pruning by microglia is necessary for normal brain development. *Science*, 333(6048), pp. 1456-1458.

Paresce, D. M., Chung, H. & Maxfield, F. R., 1997. Slow degradation of aggregates of the Alzheimer's disease amyloid beta-protein by microglial cells. *J Biol Chem.*, 272(46), pp. 29390-29397.

Pedersen, W. A. et al., 2006. Rosiglitazone attenuates learning and memory deficits in Tg2576 Alzheimer mice. *Exp Neurol.*, 199(2), p. 265–273.

Peila, R., Rodriguez, B. L. & Launer, L. J., 2002. Type 2 diabetes, APOE gene, and the risk for dementia and related pathologies: The Honolulu-Asia Aging Study. *Diabetes*, 51(4), pp. 1256-1262.

Pérez, A., Morelli, L., Cresto, J. & Castaño, E., 2000. Degradation of soluble amyloid beta-peptides 1-40, 1-42, and the Dutch variant 1-40Q by insulin degrading enzyme from Alzheimer disease and control brains. *Neurochem Res.*, 25(2), pp. 247-255.

Perez-Gonzalez, R., Gauthier, S. A., Kumar, A. & Levy, E., 2012. The Exosome Secretory Pathway Transports Amyloid Precursor Protein Carboxyl-terminal Fragments from the Cell into the Brain Extracellular Space. *J Biol Chem.*, 287(51), p. 43108–43115.

Perlman, R. K. & Rosner, M. R., 1994. Identification of zinc ligands of the insulin-degrading enzyme. *J Biol Chem.*, 269(52), pp. 33140-33145.

Permanne, B. et al., 2002. Reduction of amyloid load and cerebral damage in a transgenic mouse model of Alzheimer's disease by treatment with a beta-sheet breaker peptide. *FASEB J.*, 16(8), pp. 860-862.

Peroutka, S. J., 1995. 5-HT receptors: past, present and future. *Trends Neurosci*, 18(2), pp. 68-69.

Phuyal, S. et al., 2014. Regulation of exosome release by glycosphingolipids and flotillins. *FEBS J.*, 281(9), pp. 2214-2227.

Pollard, T. D., Earnshaw, W. C. & Lippincott-Schwartz, J., 2008. *Cell Biology.* 2nd ed. Philadelphia: Elsevier Inc.

Prince, J. A. et al., 2003. Genetic variation in a haplotype block spanning IDE influences Alzheimer disease. *Hum Mutat.*, 22(5), p. 363–371.

Prinz, M. & Priller, J., 2014. Microglia and brain macrophages in the molecular age: from origin to neuropsychiatric disease. *Nat Rev Neurosci.*, 15(5), p. 300–312.

Putz, U. et al., 2008. Nedd4 family-interacting protein 1 (Ndfip1) is required for the exosomal secretion of Nedd4 family proteins. *J Biol Chem.*, 283(47), pp. 32621-32627.

Qin, J. et al., 2012. Neutral sphingomyelinase 2 deficiency increases hyaluronan synthesis by up-regulation of Hyaluronan synthase 2 through decreased ceramide production and activation of Akt. *J Biol Chem.*, 287(17), pp. 13620-13632.

Qiu, W. Q. & Folstein, M. F., 2006. Insulin, insulin-degrading enzyme and amyloid-β peptide in Alzheimer's disease: review and hypothesis. *Neurobiol Aging*, 27(2), pp. 190-198.

Qiu, W. Q. et al., 1998. Insulin-degrading enzyme regulates extracellular levels of amyloid beta-protein by degradation. *J Biol Chem.*, 273(49), pp. 32730-32738.

Qiu, W. Q. et al., 1997. Degradation of Amyloid β-Protein by a Metalloprotease Secreted by Microglia and Other Neural and Non-neural Cells. *J Biol Chem.*, 272(10), pp. 6641-6646.

Rabouille, C., Malhotra, V. & Nickel, W., 2012. Diversity in unconventional protein secretion. *J Cell Sci.*, 125(Pt 22), p. 5251–5255.

Raiborg, C. & Stenmark, H., 2009. The ESCRT machinery in endosomal sorting of ubiquitylated membrane proteins. *Nature*, Volume 458, pp. 445-452.

Rajendran, L. et al., 2006. Alzheimer's disease β-amyloid peptides are released in association with exosomes. *Proc Natl Acad Sci USA*, 103(30), p. 11172–11177.

Ralat, L. A. et al., 2011. Ubiquitin is a Novel Substrate for Human Insulin-Degrading Enzyme. *J Mol Biol.*, 406(3), p. 454–466.

Raposo, G. & Stoorvogel, W., 2013. Extracellular vesicles: Exosomes, microvesicles, and friends. *J Cell Biol.*, 200(4), pp. 373-383.

Raposo, G. et al., 1997. Accumulation of Major Histocompatibility Complex Class II Molecules in Mast Cell Secretory Granules and Their Release upon Degranulation. *Mol Biol Cell.*, 8(12), pp. 2631-2645.

Raymond, J. R. et al., 2001. Multiplicity of mechanisms of serotonin receptor signal transduction. *Pharmacol Ther.*, 92(2-3), pp. 179-212.

Razay, G. & Wilcock, G. K., 1994. Hyperinsulinaemia and Alzheimer's disease. *Age Ageing*, 23(5), pp. 396-399.

Record, M., Carayon, K., Poirot, M. & Silvente-Poirot, S., 2014. Exosomes as new vesicular lipid transporters involved in cell-cell communication and various pathophysiologies. *Biochim Biophys Acta.*, 1841(1), p. 108–120.

Reynolds, G. et al., 1995. 5-Hydroxytryptamine (5-HT)4 receptors in post mortem human brain tissue: distribution, pharmacology and effects of neurodegenerative diseases. *Br J Pharmacol.*, 114(5), p. 993–998.

Righi, M. et al., 1989. Monokine production by microglial cell clones. *Eur J Immunol.*, 19(8), pp. 1443-1448.

Rilla, K. et al., 2013. Hyaluronan production enhances shedding of plasma membrane-derived microvesicles. *Exp Cell Res.*, 319(13), p. 2006–2018.

Rius, M., Hummel-Eisenbeiss, J. & Keppler, D., 2008. ATP-dependent transport of leukotrienes B4 and C4 by the multidrug resistance protein ABCC4 (MRP4). *J Pharmacol Exp Ther.*, 324(1), pp. 86-94.

Robert, S. et al., 2005. Regulation of the amyloid precursor protein ectodomain shedding by the 5-HT4 receptor and Epac. *FEBS Lett.*, 579(5), p. 1136–1142.

Safavi, A., Miller, B. C., Cottam, L. & Hersh, L. B., 1996. Identification of gamma-endorphin-generating enzyme as insulin-degrading enzyme. *Biochemistry*, 35(45), pp. 14318-14325.

Saijo, K. & Glass, C. K., 2011. Microglial cell origin and phenotypes in health and disease. *Nat Rev Immunol.*, 11(11), pp. 775-787.

Saini, H. K. et al., 2003. Attenuation of the serotonin-induced increase in intracellular calcium in rat aortic smooth muscle cells by sarpogrelate. *Can J Physiol Pharmacol.*, 81(11), pp. 1056-1063.

Saksena, S. et al., 2009. Functional reconstitution of ESCRT-III assembly and disassembly. *Cell*, 136(1), p. 97–109.

Saric, T., Müller, D., Seitzc, H.-J. & Pavelic, K., 2003. Non-covalent interaction of ubiquitin with insulin-degrading enzyme. *Mol Cell Endocrinol.*, 204(1-2), pp. 11-20.

Sastre, M. & Gentleman, S. M., 2010. NSAIDs: How they Work and their Prospects as Therapeutics in Alzheimer's Disease. *Front Aging Neurosci.*, Volume 2, p. 20.

Sastre, M., Klockgether, T. & Heneka, M. T., 2006. Contribution of inflammatory processes to Alzheimer's disease: molecular mechanisms. *Int J Dev Neurosci.*, 24(2-3), p. 167–176.

Sastre, M. et al., 2001. Presenilin-dependent γ-secretase processing of β-amyloid precursor protein at a site corresponding to the S3 cleavage of Notch. *EMBO Rep.*, 2(9), pp. 835-841.

Savina, A., Fader, C. M., Damiani, M. T. & Colombo, M. I., 2005. Rab11 promotes docking and fusion of multivesicular bodies in a calcium-dependent manner. *Traffic*, 6(2), p. 131–143.

Savina, A., Furlán, M., Vidal, M. & Colombo, M. I., 2003. Exosome release is regulated by a calcium-dependent mechanism in K562 cells. *J Biol Chem.*, 278(22), pp. 20083-20090.

Sbardella, D. et al., 2015. Proteasome Activity Is Affected by Fluctuations in Insulin-Degrading Enzyme Distribution. *PLoS One.*, 10(7), p. e0132455.

Schafer, D. P. et al., 2012. Microglia sculpt postnatal neural circuits in an activity and complement-dependent manner. *Neuron*, 74(4), p. 691–705.

Schekman, R. & Orci, L., 1996. Coat proteins and vesicle budding. *Science*, 271(5255), pp. 1526-1533.

Scheuring, D. et al., 2011. Multivesicular Bodies Mature from the Trans-Golgi Network/Early Endosome in Arabidopsis. *Plant Cell*, 23(9), p. 3463–3481.

Scheuring, S. et al., 2001. Mammalian Cells Express Two VPS4 Proteins Both of. *J Mol Biol.*, 312(3), p. 469–480.

Schmidt, M. et al., 2001. A new phospholipase-C-calcium signalling pathway mediated by cyclic AMP and a Rap GTPase. *Nat Cell Biol.*, 3(11), pp. 1020-1024.

Schmuck, K., Ullmer, C., Engels, P. & Lübbert, H., 1994. Cloning and functional characterization of the human 5-HT2B serotonin receptor. *FEBS Lett.*, 342(1), pp. 85-90.

Schulz, T., Schumacher, U. & Prehm, P., 2007. Hyaluronan export by the ABC transporter MRP5 and its modulation by intracellular cGMP. *J Biol Chem.*, 282(29), pp. 20999-21004.

Sciaky, N. et al., 1997. Golgi tubule traffic and the effects of brefeldin A visualized in living cells. *J Cell Biol.*, 139(5), pp. 1137-1155.

Scott, A. et al., 2005. Structural and mechanistic studies of VPS4 proteins. *EMBO J.*, 24(20), pp. 3658-3669.

Seifert, R. et al., 2005. *G Protein-Coupled Receptors as Drug Targets: Analysis of Activation and Constitutive Activity.* Weinheim: Wiley-VCH Verlag GmbH & Co.

Selkoe, D. J., 2001. Alzheimer's disease: genes, proteins, and therapy. *Physiol Rev.*, 81(2), pp. 741-766.

Seta, K. A. & Roth, R. A., 1997. Overexpression of insulin degrading enzyme: cellular localization and effects on insulin signaling. *Biochem Biophys Res Commun.*, 231(1), p. 167–171.

Sette, P. et al., 2010. The ESCRT-associated protein Alix recruits the ubiquitin ligase Nedd4-1 to facilitate HIV-1 release through the LYPXnL L domain motif. *J Virol.*, 84(16), p. 8181–8192.

Shanik, M. H. et al., 2008. Insulin resistance and hyperinsulinemia: is hyperinsulinemia the cart or the horse? *Diabetes Care*, Volume 31 Suppl 2, pp. S262-S268.

Shen, Y., Joachimiak, A., Rosner, M. R. & Tang, W.-J., 2006. Structures of human insulin-degrading enzyme reveal a new substrate recognition mechanism. *Nature*, 443(7113), pp. 870-874.

Sheridan, G. K. & Murphy, K. J., 2013. Neuron-glia crosstalk in health and disease: fractalkine and CX3CR1 take centre stage. *Open Biol.*, 3(12).

Shimizu, E. et al., 2008. IL-4-induced selective clearance of oligomeric beta-amyloid peptide(1-42) by rat primary type 2 microglia. *J Immunol.*, 181(9), pp. 6503-6513.

Shoham, T. et al., 2006. Building of the Tetraspanin Web: Distinct Structural Domains of CD81 Function in Different Cellular Compartments. *Mol Cell Biol.*, 26(4), p. 1373–1385.

Simard, A. R. et al., 2006. Bone marrow-derived microglia play a critical role in restricting senile plaque formation in Alzheimer's disease. *Neuron*, 49(4), p. 489–502.

Simons, M. & Raposo, G., 2009. Exosomes - vesicular carriers for intercellular communication. *Curr. Opin Cell. Biol.*, Volume 21, pp. 575-581.

Smolny, M. et al., 2014. Development of non-viral vehicles for targeted gene transfer into microglia via the integrin receptor CD11b. *Front Mol Neurosci..*

Solito, E. & Sastre, M., 2012. Microglia function in Alzheimer's disease. *Front. Pharmacol.*, Volume 3, p. 14.

Song, E.-S., Juliano, M. A., Juliano, L. & Hersh, L. B., 2003. Substrate activation of insulin-degrading enzyme (insulysin). A potential target for drug developmen. *J Biol Chem.*, 278(50), pp. 49789-49794.

Son, S. M., Kang, S., Choi, H. & Mook-Jung, I., 2015. Statins induce insulin-degrading enzyme secretion from astrocytes via an autophagy-based unconventional secretory pathway. *Mol Neurodegener*, Volume 10:56.

Spencer, N. J., 2015. Constitutively Active 5-HT Receptors: An Explanation of How 5-HT Antagonists Inhibit Gut Motility in Species Where 5-HT is Not an Enteric Neurotransmitter? *Front Cell Neurosci.*, Volume 9, p. 487.

Spiliotis, E. T. & Nelson, W. J., 2003. Spatial control of exocytosis. *Curr Opin Cell Biol.*, 15(4), p. 430–437.

Stansley, B., Post, J. & Hensley, K., 2012. A comparative review of cell culture systems for the study of microglial biology in Alzheimer's disease. *J Neuroinflammation*, Volume 9.

Steringer, J. P. et al., 2012. Phosphatidylinositol 4,5-bisphosphate (PI(4,5)P2)-dependent oligomerization of fibroblast growth factor 2 (FGF2) triggers the formation of a lipidic membrane pore implicated in unconventional secretion. 287(33), pp. 27659-27669.

Stewart, R. & Liolitsa, D., 1999. Type 2 diabetes mellitus, cognitive impairment and dementia. *Diabet Med.*, 16(2), p. 93–112.

Streit, W., Miller, K., Lopes, K. & Njie, E., 2008. Microglial degeneration in the aging brain--bad news for neurons? *Front Biosci.*, Volume 13, pp. 3423-3438.

Suzumura, A., 2013. Neuron-microglia interaction in neuroinflammation. *Curr Protein Pept Sci.*, 14(1), pp. 16-20.

Tamai, K. et al., 2010. Exosome secretion of dendritic cells is regulated by Hrs, an ESCRT-0 protein. *Biochem Biophys Res Commun.*, 399(3), p. 384–390.

Tamboli, I. et al., 2010. Statins promote the degradation of extracellular amyloid {beta}-peptide by microglia via stimulation of exosome-associated insulin-degrading enzyme (IDE) secretion.. *JBC*, pp. 37405-37414.

Tang, D. et al., 2012. PAMPs and DAMPs: Signal 0s that Spur Autophagy and Immunity. *Immunol Rev.*, 249(1), p. 158–175.

Tang, W.-J., 2015. Targeting Insulin-Degrading Enzyme to Treat Type 2 Diabetes Mellitus. *Cell*, 27(1), p. 24–34.

Tanzi, R. E., 2012. The genetics of Alzheimer disease. *Cold Spring Harb Perspect Med.*, 2(10).

Temmerman, K. et al., 2008. A direct role for phosphatidylinositol-4,5-bisphosphate in unconventional secretion of fibroblast growth factor 2. *Traffic*, 9(7), p. 1204–1217.

Terwel, D. et al., 2011. Critical role of astroglial apolipoprotein E and liver X receptor-α expression for microglial Aβ phagocytosis. *J Neurosci.*, 31(19), pp. 7049-7059.

Tesseur, I. et al., 2013. Chronic 5-HT4 receptor activation decreases Aβ production and deposition in hAPP/PS1 mice. *Neurobiol Aging*, 34(7), p. 1779–1789.

Théry, C., Amigorean, S., Raposo, G. & Clayton, A., 2006. Isolation and Characterization of Exosomes from Cell Culture Supernatants and Biological Fluids. *Curr Protoc Cell Biol*, pp. 3.22.1-3.22.29.

Théry, C. et al., 2001. Proteomic Analysis of Dendritic Cell-Derived Exosomes: A Secreted Subcellular Compartment Distinct from Apoptotic Vesicles. *J Immunol.*, 166(12), pp. 7309-7318.

Trajkovic, K. et al., 2008. Ceramide triggers budding of exosome vesicles into multivesicular endosomes. *Science*, 319(5867), pp. 1244-1247.

Tremblay, M.-È., Lowery, R. L. & Majewska, A. K., 2010. Microglial Interactions with Synapses Are Modulated by Visual Experience. *PLoS Biol.*, 8(11), p. e1000527.

Trombetta, E. S. & Parodi, A. J., 2003. Quality control and protein folding in the secretory pathway. *Annu Rev Cell Dev Biol.*, Volume 19, pp. 649-676.

Tulapurkar, M. E., Ramarathnam, A., Hasday, J. D. & Singh, I. S., 2015. Bacterial lipopolysaccharide augments febrile-range hyperthermia-induced heat shock protein 70 expression and extracellular release in human THP1 cells. *PLoS One.*, 10(2), p. e0118010.

Tundo, G. et al., 2012. Somatostatin Modulates Insulin-Degrading-Enzyme Metabolism: Implications for the Regulation of Microglia Activity in AD. *PLoS One.*, 7(4), p. e34376.

Tundo, G. R. et al., 2013. Insulin-degrading enzyme (IDE): a novel heat shock-like protein. *J Biol Chem.*, 288(4), p. 2281–2289.

Turola, E. et al., 2012. Microglial microvesicle secretion and intercellular signaling. *Front Physiol.*, Volume 3, p. 149.

Udrisar, D. P. et al., 2005. Androgen- and estrogen-dependent regulation of insulin-degrading enzyme in subcellular fractions of rat prostate and uterus. *Exp Biol Med (Maywood)*, 230(7), pp. 479-486.

Urbanelli, L. et al., 2013. Signaling Pathways in Exosomes Biogenesis, Secretion and Fate. *Genes*, 4(2), pp. 152-170.

van Niel, G. et al., 2011. The tetraspanin CD63 regulates ESCRT-independent and -dependent endosomal sorting during melanogenesis. *Dev Cell*, 21(4), pp. 708-721.

van Uden, E. et al., 1999. A novel role for receptor-associated protein in somatostatin modulation: implications for Alzheimer's disease. *Neuroscience*, 88(3), p. 687–700.

Vassar, R. & Citron, M., 2000. Aβ-Generating Enzymes: Recent Advances in β- and γ-Secretase Research. *Neuron*, 27(3), p. 419–422.

Vekrellis, K. et al., 2000. Neurons regulate extracellular levels of amyloid beta-protein via proteolysis by insulin-degrading enzyme. *J Neurosci*, 20(5), pp. 1657-1665.

Vieira, J. S. B. C. et al., 2011. Effect of dexamethasone and testosterone treatment on the regulation of insulin-degrading enzyme and cellular changes in ventral rat prostate after castration. *Int J Exp Pathol.*, 92(4), p. 272–280.

Villarroya-Beltri, C. et al., 2014. Sorting it out: regulation of exosome loading. *Semin Cancer Biol.*, p. 3–13.

Vingtdeux, V. et al., 2015. CALHM1 ion channel elicits amyloid-β clearance by insulin-degrading enzyme in cell lines and in vivo in the mouse brain. *J Cell Sci.*, 128(13), pp. 2330-233.

von Schwedler, U. K. et al., 2003. The protein network of HIV budding. *Cell*, 114(6), p. 701–713.

Wahle, T. et al., 2005. GGA proteins regulate retrograde transport of BACE1 from endosomes to the trans-Golgi network.. *Mol Cell Neurosci*, 29(3), pp. 453-461.

Wake, H. et al., 2009. Resting microglia directly monitor the functional state of synapses in vivo and determine the fate of ischemic terminals. *J Neurosci.*, 29(13), pp. 3974-3980.

Wakselman, S. et al., 2008. Developmental neuronal death in hippocampus requires the microglial CD11b integrin and DAP12 immunoreceptor. *J Neurosci.*, 28(32), pp. 8138-8143.

Wang, D.-S., Dickson, D. W. & Malter, J. S., 2006. β-Amyloid Degradation and Alzheimer's Disease. *J Biomed Biotechnol*, 2006(3), p. 58406.

Wang, M.-J.et al., 2006. Translational event mediates differential production of tumor necrosis factor-alpha in hyaluronan-stimulated microglia and macrophages. *J Neurochem.*, 97(3), p. 857–871.

Webster, S., Bradt, B., Rogers, J. & Cooper, N., 1997. Aggregation state-dependent activation of the classical complement pathway by the amyloid beta peptide. *J Neurochem.*, 69(1), p. 388–398.

Weyer, C. et al., 2000. A high fasting plasma insulin concentration predicts type 2 diabetes independent of insulin resistance: evidence for a pathogenic role of relative hyperinsulinemia. *Diabetes*, 49(12), pp. 2094-2101.

White, I. J. et al., 2006. EGF stimulates annexin 1-dependent inward vesiculation in a multivesicular endosome subpopulation. *EMBO J.*, 25(1), pp. 1-12.

Wilcock, D. M. et al., 2003. Intracranially administered anti-Abeta antibodies reduce beta-amyloid deposition by mechanisms both independent of and associated with microglial activation. *J Neurosci.*, 23(9), pp. 3745-3751.

Wildsmith, K. R. et al., 2013. Evidence for impaired amyloid β clearance in Alzheimer's disease. *Alzheimers Res Ther.*, 5(4), p. 33.

Wilson, C. M. et al., 2014. Sortilin mediates the release and transfer of exosomes in concert with two tyrosine kinase receptors. *J Cell Sci.*, 127(Pt 18), pp. 3983-3997.

Wittig, I., Braun, H.-P. & Schägger, H., 2006. Blue native PAGE. *Nat Protoc.*, 1(1), pp. 418-428.

Wolfe, M. S. et al., 1999. Two transmembrane aspartates in presenilin-1 required for presenilin endoproteolysis and gamma-secretase activity. *Nature*, 398(6727), pp. 513-517.

Wollert, T., Wunder, C., Lippincott-Schwartz, J. & Hurley, J. H., 2009. Membrane Scission by the ESCRT-III Complex. *Nature*, 458(7235), p. 172–177.

Wong, W. T., 2013. Microglial aging in the healthy CNS: phenotypes, drivers, and rejuvenation. *Front Cell Neurosci.*, Volume 7, p. 22.

Wubbolts, R. et al., 2003. Proteomic and biochemical analyses of human B cell-derived exosomes. Potential implications for their function and multivesicular body formation. *J Biol Chem.*, 278(13), pp. 10963-10972.

Wu, L.-J. & Zhuo, M., 2008. Resting microglial motility is independent of synaptic plasticity in mammalian brain. *J Neurophysiol.*, 99(4), pp. 2026-2032.

Wyss-Coray, T. et al., 2001. TGF-beta1 promotes microglial amyloid-beta clearance and reduces plaque burden in transgenic mice. *Nat Med.*, 7(5), pp. 612 - 618.

Xu, R. et al., 2015. Highly-purified exosomes and shed microvesicles isolated from the human colon cancer cell line LIM1863 by sequential centrifugal ultrafiltration are biochemically and functionally distinct.. *Methods*.

Xu, W. et al., 2004. Diabetes mellitus and risk of dementia in the Kungsholmen project: a 6-year follow-up study. *Neurology*, 63(7), pp. 1181-1186.

Yáñez-Mó, M. et al., 2015. Biological properties of extracellular vesicles and their physiological functions. *J Extracell Vesicles*, Volume 4.

Yaso, S. et al., 1987. Possible role of cell surface insulin degrading enzyme in cultured human lymphocytes. *Diabetologia*, 30(1), pp. 27-32.

Yoshimori, T. et al., 2000. The Mouse SKD1, a Homologue of Yeast Vps4p, Is Required for Normal Endosomal Trafficking and Morphology in Mammalian Cells. *Mol Biol Cell.*, 11(2), p. 747–763.

Yuyama, K., Sun, H., Mitsutake, S. & Igarashi, Y., 2012. Sphingolipid-modulated exosome secretion promotes clearance of amyloid-β by microglia. *J Biol Chem.*, 287(14), pp. 10977-10989.

Yuyama, K. et al., 2014. Decreased Amyloid-β Pathologies by Intracerebral Loading of Glycosphingolipid-enriched Exosomes in Alzheimer Model Mice. *J Biol Chem.*, 289(35), p. 24488–24498.

Zehe, C. et al., 2006. Cell-surface heparan sulfate proteoglycans are essential components of the unconventional export machinery of FGF-2. *Proc Natl Acad Sci USA*, 130(42), p. 15479–15484.

Zhang, S. et al., 2011. CD200-CD200R dysfunction exacerbates microglial activation and dopaminergic neurodegeneration in a rat model of Parkinson's disease. *J Neuroinflammation*, Volume 8, p. 154.

Zhao, J., Li, L. & Leissring, M. A., 2009. Insulin-degrading enzyme is exported via an unconventional protein secretion pathway. *Mol Neurodegener*, Volume 4.

Zhao, L. et al., 2004. Insulin-degrading enzyme as a downstream target of insulin receptor signaling cascade: implications for Alzheimer's disease intervention. *J Neurosci.*, 24(49), pp. 11120-11126.

H Acknowledgements

Foremost, I would like to express my deep gratitude to my supervisor Prof. Dr. Jochen Walter who gave me the opportunity to carry out this study in his laboratory, for his kind supervision, advice and great support.

I am grateful to Prof. Dr. Walter Witke who kindly agreed to be the second reviewer of my dissertation. I am also thankful to Prof. Dr. Sven Burgdorf and Prof. Dr. Claus-Christian Wiegandt who spared their valuable time to take part as referees in my thesis committee.

Furthermore, I would like to thank Dr. Konstantin Glebov for his suggestions on the topic and for the funding the first two years of my dissertation, via third-party funding. In this regard, I am also particularly grateful to the dissertation scholarship from FAZIT-Stiftung, which enabled me to continue my studies. The final completion of my thesis would not have been possible without the scholarship and the kind support of Professor Jochen Walter.

My very special gratitude goes to all my dear colleagues and the members of the neurobiology group. Especially Nadja Kemmerling, Sandra Theil, Ilker Karaca, Esteban Gutierrez, Tien T. Nguyen, Patrick Wunderlich, Anna-Lena Scheithauer, Janina Gerth and Sathish Kumar who brightened up my daily lab routine. I also sincerely thank Patrick Wunderlich for his valuable advice and that he always had time and offered a helping hand. I also want to thank Nadja Kemmerling for her great help in teaching me how to generate virus particles and Dominik Piston for his wonderful and relaxed introduction to the secrets of Blue Native PAGE.

I am also indebted to all my friends, for being encouraging, interested and supportive throughout my journey. With a special mention to Florian for his ongoing great support and professional advice on writing the application for FAZIT-Stiftung. Also Lena, Christina, Martin, Thérèse and Christine, who were always there for me.

Most of all I want to thank my family – my parents and my brother Franz, who wholeheartedly supported me all these years, who gave me strength during the hard times and shared my happiness during the good ones. And I want to deeply thank Thomas for his love and patience, his everlasting understanding and incredible faith in me, which saved me more than once and always kept me encouraged and motivated.